SERVICE LIFE ASSESSMENT OF MODIFIED GRADE 91 TUBE-SHEET STRUCTURES UNDER COMBINED CREEP-FATIGUE LOADING CONDITIONS

A Thesis for Partial Completion of M.Sc. Degree

by

Md. Ala Uddin

Student No. F1018042334

Supervisor

Dr. Nazrul Islam

Associate Professor, Department of Civil Engineering

Bangladesh University of Engineering and Technology (BUET)

Department of Civil Engineering

Bangladesh University of Engineering and Technology (BUET)

July 2021

CERTIFICATE OF APPROVAL

The thesis titled **"Service Life Assessment of Modified Grade 91 Tube-sheet Structures Under Combined Creep-Fatigue Loading Conditions"** submitted by Md. Ala Uddin, Student No. 1018042334 F, Session: October-2018 has been accepted as satisfactory in partial fulfilment of the requirement for the degree of Master of Science in Civil Engineering (Structural) on 11th July 2021.
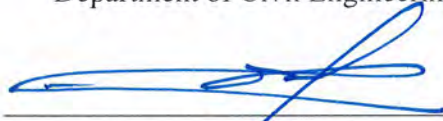
1. Dr. Nazrul Islam
    Associate Professor
    Department of Civil Engineering, BUET, Dhaka-1000.

    Chairman
    (Supervision)

2. Dr. Md. Delwar Hossain
    Professor and Head
    Department of Civil Engineering, BUET, Dhaka-1000.

    Member
    (Ex-Officio)

3. Dr. Syed Ishtiaq Ahmad
    Professor
    Department of Civil Engineering, BUET, Dhaka-1000.

    Member

4. Dr. Shohel Rana
    Associate Professor
    Department of Civil Engineering, BUET, Dhaka-1000.

    Member

5. Dr. Sushanta Roy
    Executive Engineer
    Department of Public Health Engineering, Kakrail
    Dhaka-1000.

    Member
    (External)

Dedicated

To

My Beloved Parents

Declaration

I hereby declare that the research work reported in this thesis has been performed by me, Md. Ala Uddin (F1018042334) with active assistance of my supervisor Dr. Nazrul Islam. This work has not been submitted elsewhere for any purposes. To the best of my knowledge and belief, the thesis contains no material previously published or written by any other person except when due reference is made in the text of the thesis.

I would also like to mention that this study is associated with utmost sincerity and adequate care. All the information is legit and correct. I also respectfully gainsay any responsibility regarding any kind of offense to any person, institution or organization that may occur without my knowledge and intention due to the selection of words, syllables, phrases, references or anything else associated with this thesis work.

July 2021

Md. Ala Uddin

Acknowledgement

Abstract

This study deals with the creep-fatigue strength evaluation of a tube-sheet structure made of Mod. Grade 91 steel. Such a structure is one of the components of Japan Sodium Fast Reactor (JSFR) that suffers the most severe loadings in the reactor and one of the most difficult components to design because of its complex three-dimensional semispherical shape with an arrangement of numerous holes. A test model of this component was developed by Japan Atomic Energy Agency and test was subjected to 1873 cycles of severe thermal transient loading in which elevated temperature at 600 °C and 250 °C were flowed using sodium flow repeatedly and kept at the final temperature for 2 h and 1 h, respectively. In this study, 3D finite element model of the component is developed, and heat transfer and stress analysis of this structure were performed using the temperature-dependent Mod. Grade 91 material properties for 100 cycles. Creep-fatigue life of the component is initially evaluated using the stress redistribution locus and simple elastic follow up methods. The creep-fatigue results based on these elastic analyses are compared with the inelastic analysis-based procedures that include nonlinear constitutive models e.g., bilinear and Chaboche model coupled with time hardening creep. The creep and fatigue damages using these methods are plotted in the Campbell diagram and predicted life cycles are compared to show the applicability of these methods for life prediction.

Table of Contents

List of Figures

xiv

xv

List of Tables

Lists of Abbreviations

T_{High} = Higher temperature

T_{Low} = Lower temperature

$\dfrac{Q}{t}$ = Rate of heat transfer

K= Thermal conductivity

A= Surface Area

d = Thickness of the surface

S = Specific heat

m = mass of the fluid

T_M = Melting point temperature

σ_x = Stress components along X- axis

σ_y = Stress components along Y- axis

σ_z = Stress components along Z- axis

σ_{VM} = Von Misses stress

$\sigma_1, \sigma_2, \sigma_3$ = Principal Stresses along X, Y and Z axis

τ_{max} = Maximum shear stress

Z= Elastic follow up factor

G = Elastic shear modulus

$C_1, \gamma_1, C_2, \gamma_2, C_3, \gamma_3, C_4, \gamma_4$ = Material constants.

$\mathcal{E}_o$ = Elastic peak strain

σ_o = Elastic Peak Stress

$\mathcal{E}_t$ = Total strain at time, t

σ_t = Total Stress at time, t

K = reduction factor

$\dot{\varepsilon}^c$ = Creep strain rate

$\mathcal{E}_t$ (p) = Plastic strain

$\mathcal{E}_t$ (c) = Creep strain

N_f = Fatigue failure life

N_d = Applied thermal loading cycles

D_f = Fatigue Damage

t_r = Step time

t_R = Rupture time

D_C = Creep Damage

$\Delta\mathcal{E}_{equi.,i}$ = Equivalent strain range at step, i.

$\mathcal{E}_t$ = Total strain range (mm/mm)

α_c = Time parameter for the creep rupture time

FE = Finite Element

Expt. = Experimental

Chab. = Chaboche

Chapter 1

INTRODUCTION

1.1 Background and Motivation

Global energy demand is expected to be about 30 percent higher in 2040 compared to 2010 (Alberry, 2008) , as economic output more than doubles and prosperity expands across a world whose population will grow to nearly 9 billion people. The world derives its energy from different sources: coal, gas, oil, and renewables and nuclear. Although nuclear power sector seems to be a potential source of meeting up energy consumption, competitive gas prices and government policies may result in a decline in nuclear power generation capacity in the years to come. Following the disaster at the Fukushima nuclear power plant in Japan, many governments have reviewed plans for new nuclear installations. For example, Germany has decided on a complete nuclear phase-out by 2022 followed by Thailand and others who have suspended approvals for new nuclear power plants until a safety review has been completed (Brochure, 2006).

The long-term impact of the rise in energy demands is not yet foreseeable, but it is reasonable to assume that fossil-fired power stations will continue to be the predominant form of energy generation for decades to come. However, concern has also grown in recent decades about environmental impact. Climate change, as a result of rising greenhouse gas emissions, threatens the stability of the world's climate and economy. In Australia, for example, the recently introduced "carbon tax" by Vishwanathan and Bakker (2000) is likely to impact the way. Australia produces its electricity in the future. China in particular is investing in renewable energy and plans are in place to build almost 10 times the wind capacity of Germany. But even this will not be able to keep up with demand, meaning fossil fuels will continue to make up the majority of the overall energy mix for the foreseeable future. And when it comes to fossil fuels, coal is the easy winner - it is generally easier and cheaper to mine, and easier to transport using existing infrastructure such as roads and rail, than oil or gas (Materials, 2007). If the level of electricity generation capacity is to be maintained while doing our duty towards the environment, then there is a need for new, low-emission and cost-effective fossil power plants. According to Strang and Vodarek (1996), significant reductions in CO_2 emissions can be

achieved by the use of clean coal technologies. Through the use of advanced boilers, improved turbines and gasifiers, higher temperatures and pressures, a higher efficiency can be achieved. Some of these technologies can also be used to retrofit existing (old) power stations with the introduction of supercritical and ultra-supercritical power plants (Gooch and Kimmins, 1987).

In recent years there has been a trend towards the construction of ultra-supercritical (USC) power plants, where the steam pressures can exceed 30 MPa, and where typical service temperatures are in the range of 570-630°C. Such power plants can achieve efficiencies in the vicinity of 45% which compares with a typical efficiency for a conventional fossil-fired plant, operating at -17 MPa and 560°C, of 25-30% (Ando,2014). Higher steam temperatures and pressures mean that superior materials will be required for a number of critical components. The so-called creep strength enhanced ferritic (CSEF) 9-12% Cr steels have been identified as the most promising class of materials for some of the key components in USC plants, which include the main steam pipes, headers and superheater tubing's. These steels are less costly, and they have a lower coefficient of thermal expansion and a higher thermal conductivity when compared with austenitic stainless steels, making them less susceptible to degradation through thermal fatigue. One of the first to be developed was ASTM P91 (9Cr-1Mo) steel (Cambridge, 2012) .

The earliest grades of this steel were considerably improved through small additions of V, Nb and N, and now modified P91 steel is recommended for service at temperatures up to 600°C, which compares well with allowable operating temperatures of up to 560°C for earlier grades such as P22 (2.25Cr-1Mo). Consequently, P91 steel has seen widespread application in fossil fired power plants. More recently 9-12 Cr steels, such as P92, with allowable service temperatures of up to 625°C have been developed (Coble, 1963).

Recently, majority of nuclear power plants utilize Generation III reactors, whereas next generation nuclear reactors (such as Generation IV) appear to be effective and durable, and Sodium-Cooled Fast Reactor (SFR) is one of the paradigms of them (Rajos, 2018). In SFR, Sodium is used as a coolant which carries heat with lower operating pressure and higher thermal conductivity (Ridon, 2018). In addition, SFR is cost effective, reliable and safe in regards to preservation of uranium resources with minimization of radioactive waste (Petrangeli, 2006).

Modified Grade 91 (Mod. 9Cr-1Mo) steel is an essential material for heat transferring components of the Japan's SFR (Ato et.al., 2011). However, there is no substantial evidence to uphold the structural integrity of components made of Mod. 9Cr-1Mo steel in real environment. Despite such steel being used as a structural material for fossil fired plants, the structural materials in SFRs are exposed to elevated temperatures and sodium exposure during the plant life. Therefore, it is important to understand the failure mode of structural components under actual conditions to assess their integrity (Masakazu, 2011). Since creep-fatigue damage is one of the most significant failure modes in the design of fast reactors, many methods for evaluating the creep-fatigue life have been proposed in the area of material testing (Taguchi et.al., 1993). For pure creep and pure fatigue, these code-based approaches are sufficient. However, when both creep and fatigue loading are present, these methods have fundamental limitations. In addition to that, during the long-term creep, damage assessment is more complicated in the multi-axial stress conditions than in the uniaxial loadings (Asayama and Jetter, 2008). For representing the actual behavior under such critical loading conditions, very few methods are available in the literature. This study evaluates the damage of such component subjected to creep-fatigue loading conditions using both code-based approach and advanced constitutive models which represents its behavior both in the material and component level.

1.2 Objective of the study

The objective of this study is to evaluate the service life assessment of critical structural components of steam generators subjected to high pressure and temperature in combined creep and fatigue condition. The objectives are enlisted below.

1. To estimate the service life of a Modified Grade 91 Tube-sheet structure due to creep, fatigue and combined creep-fatigue loading conditions using code-based approaches.
2. To evaluate the creep-fatigue strength and to propose service life of the Tube-sheet Structure using Advanced Constitutive Model and compare the results with code-based approach.

1.3 Scope of the study

1. This study will help understand the behavior of a structure subjected to elevated temperature and pressure and evaluate the quantitative amount of damage caused by such loads.
2. A comparatively more reliable and economic method can be determined for structures, the stress concentration at critical components due to combined creep and fatigue and the proportion of damages caused creep fatigue interaction can be determined to predict the design life of a structure.
3. This research can help differentiate the limitations of simplified code-based approaches and assist to overcome such constraints by advanced constitutive models.
4. One of the most prominent aspects of the study is to evaluate the safety factors for service life of Grade 91 tube-sheet structure in both code-based approaches and advanced models, through which individual method can be described as either conservative or non-conservative for the existing loading conditions.

1.4 Limitations

1. No experimental were conducted in conjunction with this thesis due to the lack of creep-fatigue testing facilities. Experimental data used in this work was obtained from previous research.
2. It was the target to run the model for one month continuously. However, due to the constraints of physical memory of the available computer, it was not possible to run more than two weeks continuously.

1.5 Organization of the thesis

The thesis is organized into five chapters. **Chapter 1** of this thesis contains the background and motivation of the study, the objectives, and scopes along with limitations. **Chapter 2** starts with a literature review of heat transfer analysis, creep-fatigue mechanism, and behavior of steel under uniaxial and multiaxial stress state at elevated temperature, the existing creep-fatigue models, including the code-based methods of creep-fatigue damage evaluation and advanced constitutive models. **Chapter 3** deals with description of developed finite element model, description of geometry, loading condition, properties used in the analysis, and the

parameters with value of each working models. **Chapter 4** deals with results of heat transfer analysis, stress analysis, comparison of stresses and strains among different models, Campbell diagram and predicted life cycles. **Chapter 5** includes conclusions and future study.

Chapter 2

LITERATURE REVIEW

2.1 Introduction

Heat transfer analysis and stress analysis are essential to understand the behavior of a structure subjected to elevated temperature and pressure. Due to sustained load from temperature and pressure, a structure subjects to loss in design life caused by creep and fatigue impacts. Hence, in this chapter, creep fatigue mechanism, the transient heat transfer analysis, stress analysis using both simplified and advanced constitutive models, creep fatigue damage evaluation procedures etc. will be discussed.

2.2 Background of the study

In our daily life it can be easily observed the transferring of heat in different manufacturing units such as nuclear power plant, boilers, turbines etc. and due to elevated temperature and pressure through these production units, excessive damages are occurred with the reduction of service life (Bhuvaneswari, 2019). High pressure and temperature flow cause stress concentration on the critical components of the structure and reduce yield strength leading to great significant collapse with the loss of economy and life (Edward, 2016).Therefore, it is essential to understand the structural integrity of such critical components subjected to heat and pressure to protect the manufacturing units from probable collapse (Onizawa et.al 2013).

Ucak, and Tsopelas (2008), showed new model for structural steel with capabilities to model yield plateau. They also introduced cyclic behavior using Abaqus. In this paper, they presented results through numerical data for an application in earthquake engineering. In that case, a steel bridge pier was incited with cyclic lateral load. Due to non-linear hardening region steels show a distinct yield plateau. Because of this plateau zone characteristics of the material show complication from numerical modeling point of view. In this paper application of a constitutive model for structural steels with yield plateau into Abaqus/Standard via user element subroutines (UMAT) was presented. It arrested the response of the material for monotonic and cyclic loading conditions. In this paper, authors assumed existence of a plateau region and hardening region for both monotonic and cyclic loading conditions. They also assumed that in

the plateau region the maximum saturated stress can't cross the initial yield stress. The conversion from the plateau zone to the hardening zone depends on highest loading magnitude and the acquired plastic strain.

Chaboche et. al. (1979) proposed a concept to measure loading amplitude by quadratic memory surface in plastic strain space. It was generalized by Ohno et.al. (1982)

Johnston and Gilman (1959) made a theory that the abrupt yield drop is a consequence of rapid dislocation multiplication and stress dependence of dislocation velocity. This concept was made to explain yield point phenomena for constitutive modeling. Hahn et. al (1962) proposed a uniaxial constitutive model based on this theory. After that, a multiaxial model was developed by Shioya and Shioiri (1976) and was used to find the non-uniform plastic deformation patterns in a mild steel bar.

Itoh et.al. (1992) first introduced finite element simulation to describe yield point phenomena. It was used to find out non-uniform plastic deformation arrangement in mild steel sheets under tension. Elastic–plastic Finite element computation for tension of steel sheets was done by Tsukahara and Iung (1998). For showing the yield plateau, they assumed a negative stress–strain slope in a rate-independent plasticity model. But they did not consider the upper yield point and the subsequent yield drop.

Yoshida et. al (2000) proposed a constitutive model of cyclic plasticity that allows a consideration of the yield-point phenomena. Yield-point phenomena and cyclic plasticity behavior was first explained by this model. However, it has some constraints comparing to actual material behaviors. Because it fails to produce very high upper yield point.

Yoshida (2000) Proposed an extended version of a model to describe yield-point phenomena of steels. It is developed depending on sharp yield point and the successive abrupt yield drop. This model can explain well a high upper yield point, the rate-dependent Lüders strain at the yield plateau and the consequent work hardening. Cyclic plasticity characteristics the Bauschinger effect and rate-dependent ratcheting also can be represented by this model. Finite element simulation of temper rolling process is run to ensure the effectiveness of this model. Basically, this model was prepared to remove yield point of steel sheets. In this paper, the response of upper yield point on the deformation is figured out.

Zerovnik et.al (2010) described the yield-point phenomenon in rate-independent constitutive models of cyclic plasticity. It happens at first transition from the elastic into the elastic-plastic region. They discussed response of cyclic plasticity with constitutive equations of kinematic and cyclic hardening or softening. The superiority of this model is that it needs a minimum number of material parameters for explaining the yield-point phenomenon. This model can be designated for simple uniaxial monotonous experiments. Uniaxial monotonous and uniaxial cyclic tension–compression experiments were executed for this research to find material parameters and compare response of constitutive model with the actual response.

Although a good number of researches are available regarding elastic and plastic behavior with uniaxial loading conditions, with these studies creep-fatigue interactions with cyclic loading and multiaxial loading considerations have not yet been explained to implement in real projects. Therefore, in this research an attempt has been taken to evaluate the creep-fatigue damage of Grade-91 tube-sheet structure under multi-axial loading conditions using both code-based simplified approaches and advanced constitutive models and to predict the service life in order to be aware of the probable damage of the structure.

This chapter mainly deals with the heat transfer mechanism, creep-fatigue mechanism and its impacts upon materials, and creep-fatigue damage evaluation process in different code based and advanced constitutive models.

2.3 Heat Transfer Mechanism

Heat transfer can be classified as the science that deals with the determination of the rates of energy transfer. The interested energy is heat which can be defines as the form of energy that can be transferred from one system to another as a result of temperature difference (Cengel, 2006). For heat transfer to occur, temperature difference is the basic requirement. With the knowledge of heat transfer, the rates of thermal energy transfer to or from a system can be determined, thus the times need of heating or cooling as well as the variation of temperature can be known either through experimental or theoretical method with some assumptions (Ashikin, 2010).

Heat transfer is a discipline of thermal engineering that concerns the generation, use, conversion, and exchange of thermal energy (heat) between physical systems (Sarbu and Dorca , 2019)

Heat transfer processes are classified into three types (Janna and William, 2009).

1. Conduction 2. Convection and 3. Radiation

2.3.1 Conduction

The conduction may be defined as transfer of heat which occurs through intervening matters without having bulk motion of the matter. This can be explained through **figure 2.1** which demonstrates process to understand easily.

A solid i.e., a block of metal has two surfaces, one at elevated temperature and another one is at comparatively low temperature. Here, heat from high temperature region to low temperature region is carried through conduction process. To cite an example, flow of heat through a turbine blade in a jet engine is a conduction process.

The outer side is excessively exposed to gases from combustor with higher temperature than that of inner surface with cooling air. The wall temperature with a level is critical for a turbine blade (Janna and William, 2009). The rate of conductive heat transfers through a slab of material, such as the one in the figure 2.1 below is given by the equation no.1.

$T_{High} \longrightarrow$ $\longleftarrow T_{Low}$

Heat flows to right

Solid body
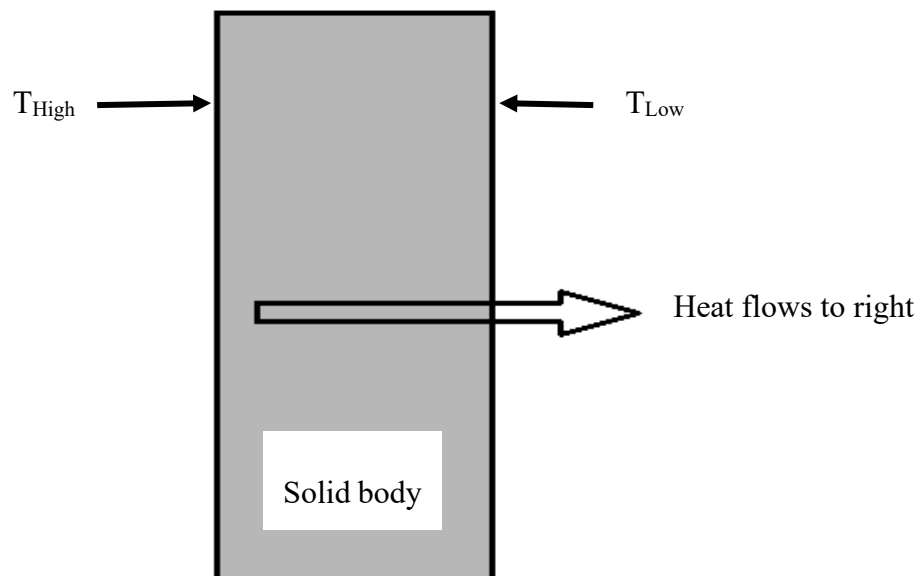
Figure 2.1 Conduction Heat Transfer (Janna and William, 2009).

$$\frac{Q}{t} = K.A.(T_1-T_2)/d \ \text{---}(1)$$

Where

$\dfrac{Q}{t}$ is the rate of heat transfer in Joules per second (Watts),

K is the thermal conductivity of the material,

A and d are its surface area and thickness, and

T_1-T_2 is the temperature difference across the slab.

Conduction heat transfer has some remarkable features (More and Hemant, 2020)
In terms of microscopic scale, conduction occurs due to rapid movement or vibration of atoms and molecules that interact with neighboring particles, and transfer some of their kinetic energy.

1. Conduction is considered as the most important pattern of heat transfer within a solid object or between solids with the presence of thermal contact.

2. Because of the space among the atoms or molecules, conduction is most prevalent in solids, and less significant through liquids or gases.

3. The rate of heat transfer due to conduction is dependent upon some factors. Among them, the most prominent ones would be -

   a) The size of the area in contact
   b) The temperature differences
   c) The thermal properties of the material(s) in contact, and
   d) The thickness of the material.

2.3.2 Convection

The transferring of heat owing to flowing of fluid is defined as convection heat transfer. The fluid may be either gas or liquid, and has pragmatic implementation in aerospace technology. In this system of heat transfer, the heat is moved through bulk movement of a non-uniform temperature fluid (More and Hemant, 2020).

Due to flow of matter in large proportion, the convection flow is expedited. In the case of the Earth, the movement of atmosphere is occurred by the circulation of hot air from tropical zones to the poles. (Note that, depending on latitude, the Earth's rotation causes huge changes in the direction of airflow.). A good example of convection is a car engine remaining cooled in the

cooling system by the flow of water, with the water pump maintaining a flow of cool water to the pistons (More and Hemant, 2020).

Since convection is generally more complex than that of conduction, we can illustrate the convection in some straightforward approaches, and perform some practical calculations of its impacts. Buoyant forces drive the natural convection. For instance, hot air rises because density decreases as temperature increases. This principle may be applied equally with any fluid. To give an example, the pot of water on the stove in is kept warm in this manner; energy from one part of the globe to another is carried by ocean currents and large-scale atmospheric circulation transfer (More, 2020).

The characteristics of convection heat transfer can be summarized as follows (More, 2020)-

1. The large-scale flow of matter in fluids causes the convection heat transfer. Solids are not viable to pass heat through convection.
2. Buoyant forces are the paramount factors for natural convection such as hot air rises as density decreases with increment of temperature. This principle is applicable equally to any sorts of fluids.
3. The heat transfer efficiency of convection process is much higher compared to that of conduction. Air in atmosphere resembles negligible conductance but good insulation, in the case, when the space is infinitesimal enough to safeguard convection.
4. Phase changes may be accompanied to convection, for example, when sweat emits from human body. This voluminous flow during convection, allows humans to cool off even if the surrounding temperature of air surmounts the body temperature.

Convection heat is given by the equation (2) as follows-

$Q = m.\ S.(T_1 - T_2)$ --(2)

Where, S is the specific heat, and m is the mass of the fluid.

2.3.3 Radiation

The transmission of energy without the presence of matter through the space may be defined as the radiation heat transfer. Radiation is regarded as the only method for heat transfer in atmosphere. Radiation can be significant even in situations in which there is an intervening

medium; a familiar example is the heat transfer from a glowing piece of metal or from a fire (Janna, 2009).

A good number of features of radiation heat transfer can be as follows (More, 2020)-

1. Wavelength is an important parameter on which the electro-magnetic energy radiation depends. For example, a smaller wavelength corresponds to a higher energy.

2. Electromagnetic energy is emitted or absorbed by all objects. Emissivity or efficacy of radiated energy relates the color of an object. To cite an example, Black is the most effective because its emissivity, e=1, whereas, white is the least effective because its emissivity, e=0.

3. A black body, more often than not, is called ideal radiator has the same color like an ideal absorber, and absorbs all the radiations that fall on it.

4. The rate of heat transfer by emitted radiation is determined by the Stefan-Boltzmann law of radiation expressed into equation no (3)-

   $Q/t = \sigma A T^4$ ---(3)

   where $\sigma = 5.67 \times 10^{-8}$ J/ (s·m^2·K$^{4)}$ is the Stefan-Boltzmann constant, A is the surface area of the object, and T is its absolute temperature in Kelvin.

5. The temperature of the object and the temperature of its surroundings have significant impacts on the net rate of heat transfer. The larger of the temperature difference between them has the higher net heat flux.

6. The emitted radiation is proportional to the fourth power of temperature. Hence, the temperature of an object is very important.

2.4 Creep

When a material is subjected to stress, a time-dependent inelastic deformation is induced in it. Such a deformation is called creep. The slow deformation can yield in permanent change in shape and size, and the rates are normally less than 1.0% per minute. Fasters rates are usually related with mechanical working such as forging and rolling (Boyer, 1988). Mathematically it can be expressed in equation no. 4 as follows-

$$\varepsilon_c = f(\delta, t, T) \text{ ---(4)}$$

Despite having the impacts of temperature upon creep, the condition during the material full effects of creep is contingent on the melting point of the corresponding material. In case of metals, such a phenomenon starts at the temperature $T > 0.4T_M$.

With a continuously slower strain rate, creep deformation is occurred at comparatively smaller temperature. On the other hand, creep usually proceeds through three several stages at higher temperature (Boyer, 1988).

2.5 Nature of creep deformation

A material i.e., metal or alloy, being subjected to a stress that is greater or equal to its yield stress, the material experiences a plastic deformation. However, when the material is exposed to comparatively high temperature, plastic deformation may be emerged, even though the induced stress is smaller than that of yield stress (Boyer, 1988).

In such a context, high temperature is defined as greater than $0.4T_M$, Where T_M is the absolute melting point. The ratio of actual temperature in Kelvin to Melting point in Kelvin is known as homologous temperature. With these temperatures, the atoms or molecules are inclined to sufficient mobilization to occur rearrangement of the structure that is dependent upon time (Sakanashi, 2013) . The classical creep deformation in metals can be categorized into three several stages, mainly-

a) Primary creep,
b) Secondary creep and,
c) Tertiary creep.

These different stages are demonstrated on a typical creep curve which is represented schematically in Figure 2.2.
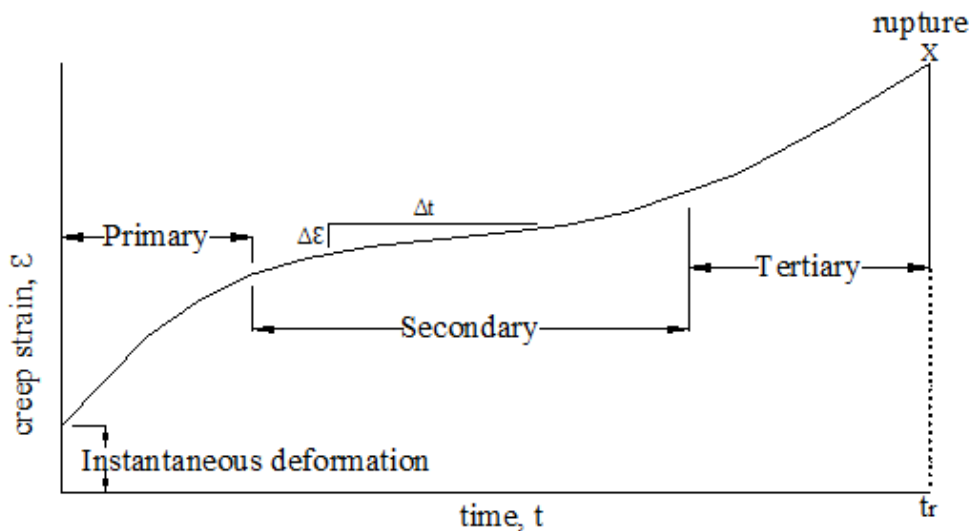
Figure 2.2 Schematic representation of a high temperature creep curve (Sakanashi, 2013)

The primary creep may be defined as the deformation that is induced after application of load. It is the initial stage of creep and creep where the creep resistance shows a surge or upward trend. Such a stage can be identified by rapid hardening of metals. In some alloys, this stage may not be present and with some types of creep, such as solute drag, an "inverted" primary appears, where the strain-rate demonstrates an incremental trend with strain (Dantec, 2015).

The secondary creep may be defined as a steady state creep due to the balance between dislocation structure and grains of a metal. In this stage of creep, there is an equilibrium between work hardening and recovery processes (The process by which deformed grains can reduce some of their stored internal strain). The material experiences large proportion of molecular changes for which existing precipitates are subjected to change chemically to form other precipitates. Dislocation structures may also witness changes for such types of creep. From Figure 2.2, it is clear that, the secondary creep sustains for longer period.

At the end, the accelerating creep rate that causes fracture in a material, may be defined as a tertiary creep. These types of creep may be limited in brittle materials and widespread in brittle materials (Sakanashi, 2013). Although different compelling factors can impact significantly to the increase in creep rate during the tertiary stage, it is usually the development of microcracks (coalescence of voids) which leads to creep fracture.

14

2.6 Creep Mechanisms

During the inducement of the secondary creep stage, creep may have occurred by two several mechanisms-

a) Diffusion creep and,
b) Dislocation creep.

These are explained in the Figure 2.3. These depend on different important factors, mainly the inter-molecular structures, proportion of the components of the materials, and the creep loading conditions (stress and temperature) (ASTM-08, 2008)
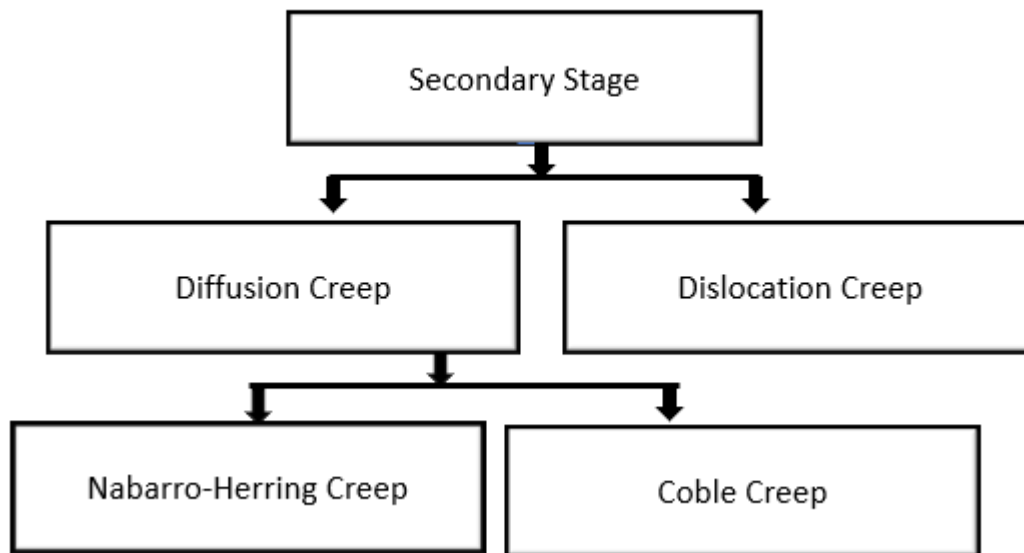
Figure 2.3 Different mechanisms occurring during secondary stage creep (ASTM-08, 2008).

2.6.1 Diffusion Creep

The creep, which is normally taken place because of the presence of vacancies within the crystal lattice and occurred by movement of materials through diffusion of molecules within the grains, may be defined as the diffusion creep. When a molecule or atom has significant thermal energy, it can shift from its original location to nearby vacancy (Sakanashi, 2013) . When a polycrystalline material is subjected to tensile forces with elevated temperature, molecules have a frequent inclination to move from those grain boundaries.

There are two types of diffusion (Shibli, 2000) creep based on the diffusion paths along the grain boundaries or within the grains themselves-

a) Coble creep and

b) Nabarro-Herring creep

During the elevated temperatures (T > O.5Tm), lattice diffusion governs the creep rate and the induced flow from such diffusion is called Nabarro-Herring creep (Fig.2.4). At minimal temperatures (T< 0.5 Tm), atomic diffusion in the crystal becomes comparatively more complex. On the contrary, atoms at grain boundaries are not more closely packed than elsewhere and vacancies exist along the boundaries which cause the grain-boundary diffusion to happen. The flow is then called Coble creep (Fig. 2.4). Since these take place on the micro-scale of each grain, the absolutely necessary diffusion distances are smaller in fine-grained alloys, which thus inclined to be subjected to more creep (ECCC, 2009).

(a)

(b)
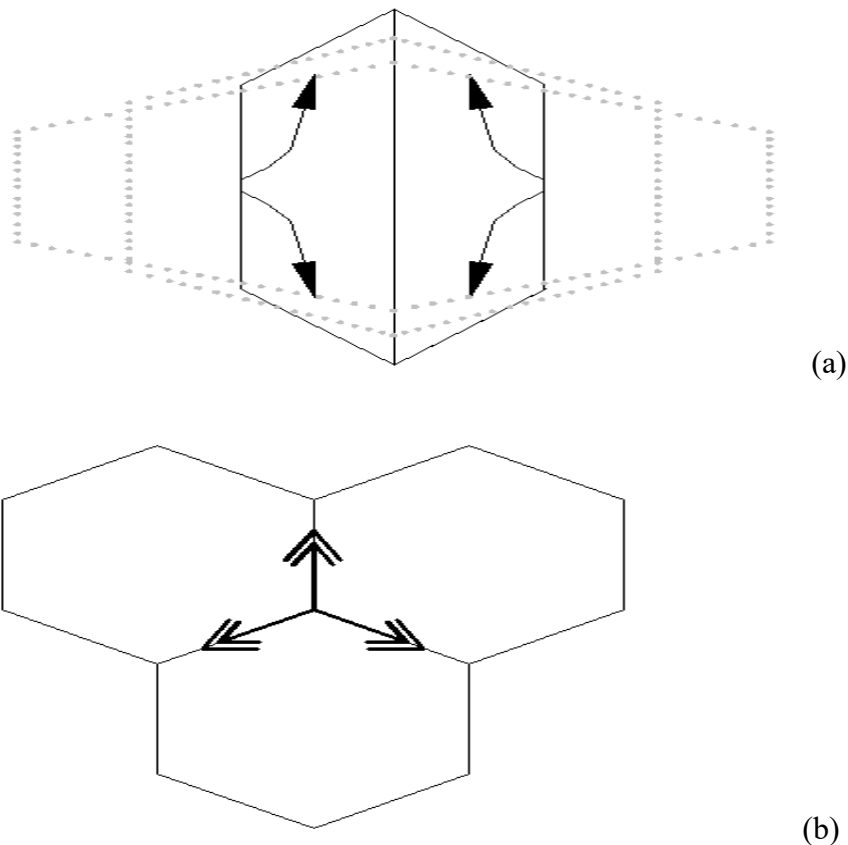
Figure 2.4 a) Nabarro-Herring creep, b) Coble creep (Haarmann et. al. 2002)

2.6.2 Dislocation Creep

Dislocation gliding and climbing explained in Fig. 2.5 illustrate that these are the fundamental factors contributing to power law creep or dislocation creep. When subjected to higher proportion of stresses, crystalline materials having dislocations are activated to glide, where, a parallel movement to Burger's vector is done by a dislocation line (Abe, 2008).

A small figure of displacement without transferring of matters may be required in such a phenomenon. The dislocation climbing assists to overcome hindrance and carry on gliding, when gliding dislocations are paused by obstruction.On the other hand, the movement which is done normal to Burgers vector may be defined as dislocation climbing. This process will usually be repeated in following time, when it encounters an obstacle (Kimura et. al., 2000).

The glide movement has significant contribution with the strain, but the strain rate is governed by the climb step. This process involves with vacancies or interstitial. Therefore, the prime rate controlling catalyst is atomic diffusion (Viswanathan, 1989) .
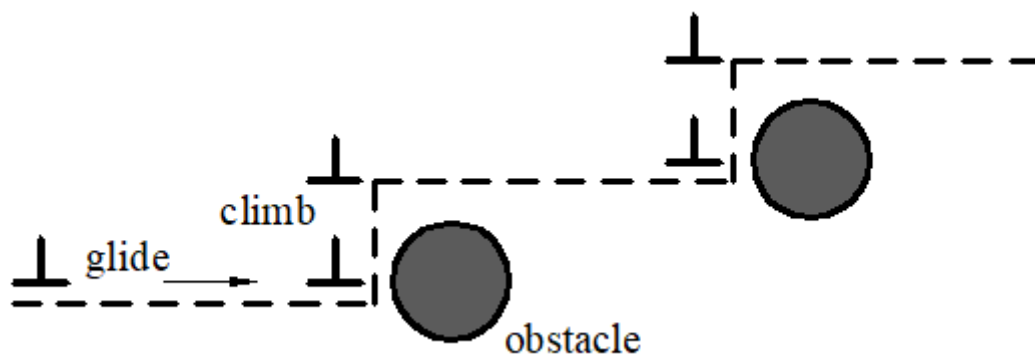
Figure 2.5 Schematic representation of dislocation glide and climb (Viswanathan, 1989) .

2.7 Effect of stress and temperature upon creep

The increase of stress and temperature ultimately lead to the increase of creep strain which is pictorially illustrated in Figure 2.6. For this reason, the rupture time will also be decreased. The behavior shown in Figure 2.6 can be explained with the following competing material reactions **(**Kimura et. al., 2000).

➢ Strain hardening.

➤ Softening processes, including recovery, recrystallization, strain softening and precipitate over-aging.

➤ Damage processes like cavitation, cracking and specimen necking.
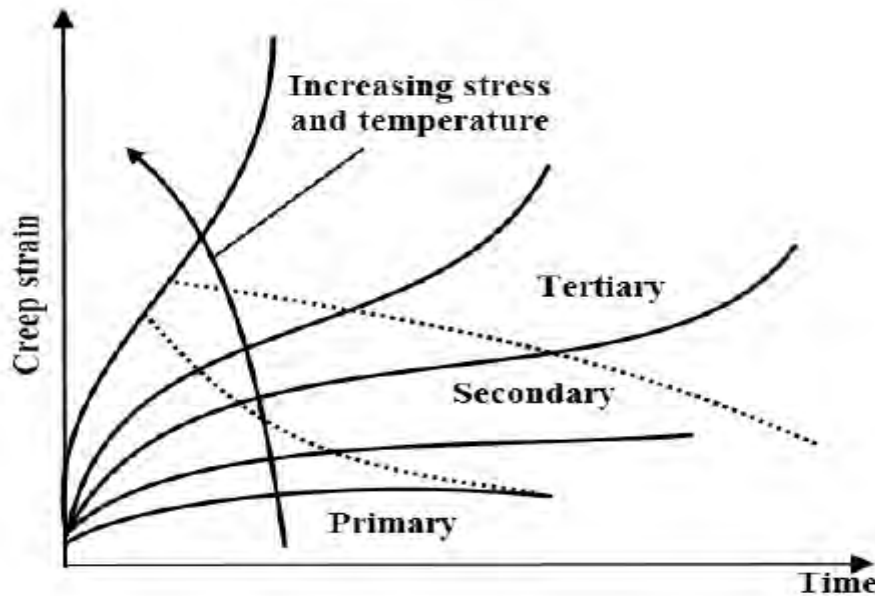
Figure 2.6 Schematic illustration of creep curve shapes for increasing stress and temperature **(**Kimura et. al., 2000).

2.7.1 Work hardening

The work hardening is an important parameter which indicates the ability of a material to prevent additional strain after it has experienced deformation. It has decreasing impact on the strain rate. In the material, thermal softening contributes to the reduction of strain hardening. The creep rate is always low at lower temperature range because recovery is thermally driven and it does not occur at lower temperature (Kimura et. al., 2000).

When hardening, recovery and damage is in equilibrium condition, the creep rate remains constant which is called the steady state creep. Strain hardening is overcome by recovery process, when incremental temperature makes the process easier. This is the prime cause for occurring the primary-secondary state transition at lower strains with the increase of temperature (Viswanathan, 1989).

The third and final stage of creep, which is called tertiary creep with expedited strain rate, is caused because of intermolecular and structural instabilities in the material such as cracks, separation of grain boundaries, cavities etc. Such type of creep causes reduction to cross-sectional area and as a result, the resistance ability of a material to load is decreased. The interaction with softening is the reason of the rapid increase in strain rate, ultimately leading to failure (Davis, 2000).

2.8 Creep under cyclic actions

In transient or primary creep, the redistributed stress finally causes the condition of steady state creep. This redistribution in terms of rate and extent depends upon creep response, temperature of metal and initial stress level of the material (Boyer, 1988). The isotropic strength variation may be termed as creep transients which is caused due to increment of dislocation density or by change in directional hardening (Penny and Marriott, 1995). The transient loading conditions are significant under cyclic loading, when huge stresses are accumulated at the initial stage of each cycle (Boyer, 1988).

2.8.1 Ratcheting

The accumulation of plastic strain under cyclic loading conditions may be defined as ratcheting. Such a phenomenon of plastic deformation occurs when cyclic stresses go beyond the yield limit.

The gross inelastic strain may be stable as demonstrated in Figure 2.7, depicting that the inelastic strains are either constant or the plastic strain may vary for each cycle (Dantec, 2015). The accumulated plastic deformation ultimately causes to failure of the structure, which is also called as incremental collapse (Gan et. al., 2006). The larger tensile strains, which cause necking may be due to ratcheting and the failure before fatigue cracks have had the possibility to form and grow (Zeman et. al. 2006). Ratcheting has significant impacts on materials which may be caused even without plastic yielding. It can alter the time-dependent response and residual stress of a material. The ratcheting can be increased because of nonlinear interaction between primary and secondary stresses. There are a good number of factors that contributes to ratcheting such as plastic slip, dislocation movement, stress ratio, loading conditions, load history, stress amplitude, stress ratio, mean stress, cell deformations etc
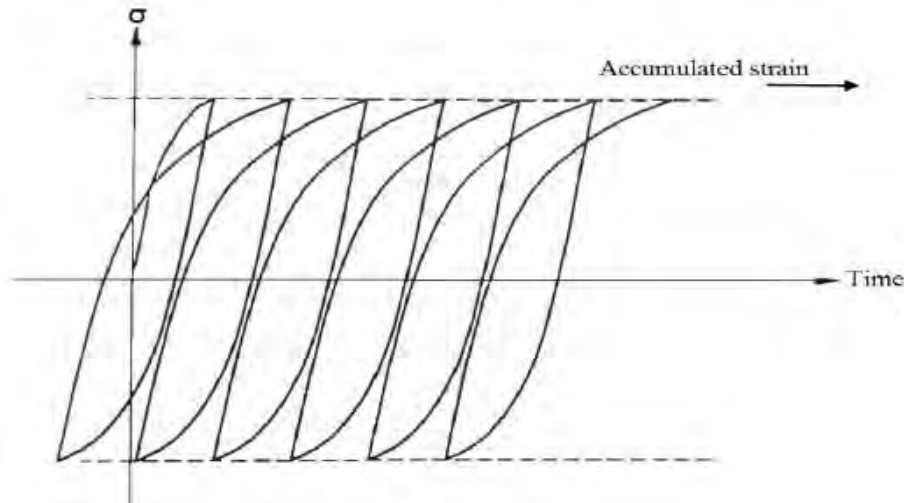
Figure 2.7 Stable strain ratcheting under load-controlled cycling (Abdollahi and Chakherlou, 2017).

2.8.2 Stress relaxation under cyclic loading

Stress relaxation due to time dependence is a sort of creep related damage that takes place because of constant fixed strain under holding time. Creep strength of the material plays a vital role in relaxation rate. To maintain the gross strain in constant, the strain within the elastic limit must show a downward trend with the decrease in stress. For instance, creep due to relaxation is an issue is for elevated -temperature bolting, where the stress progressively relaxes after the initial torque, therefore bolt retightening must be made on for example flanges to avoid leakage. Both relaxation and redistributions of stresses have large significance on the creep damage. Especially under cyclic operations. However, often appropriate relaxation data does not exist and relaxation analysis are made with constant load isothermal data (Zeman et. al. 2006).

When cyclic loads are combined with hold periods, stress relaxation has been seen to influence the low-cycle fatigue endurance. Such an example of creep-fatigue interaction with stress relaxation during hold timed is illustrated in **Figure 2.8.** Test made with steel 304SS showed that hold periods at peak tensile strain are the most damaging, while compressive hold periods did not have substantial effect, in fact it was seen that it had a healing impact for hold periods at both tensile and compressive strain. The reduced fatigue life at tensile strain holds periods got more substantial when the hold periods increased. However, the reduction rate showed to

progressively decrease for longer hold periods which indicated that that the limit of relaxation damage was reached within rather short hold times. The characteristics of the time-dependent cyclic relaxation damage varies between materials. Similar cyclic hold time relaxation tests made with material Rudiment 700 showed the complete opposite results. For the compressive strain hold periods, it had a more detrimental effect on fatigue resistance, while tensile hold periods had only a small effect. During periods of loading and unloading the accumulated creep damage during hold periods has seen to be larger than the accumulated fatigue damage **(Davis, 2000).**
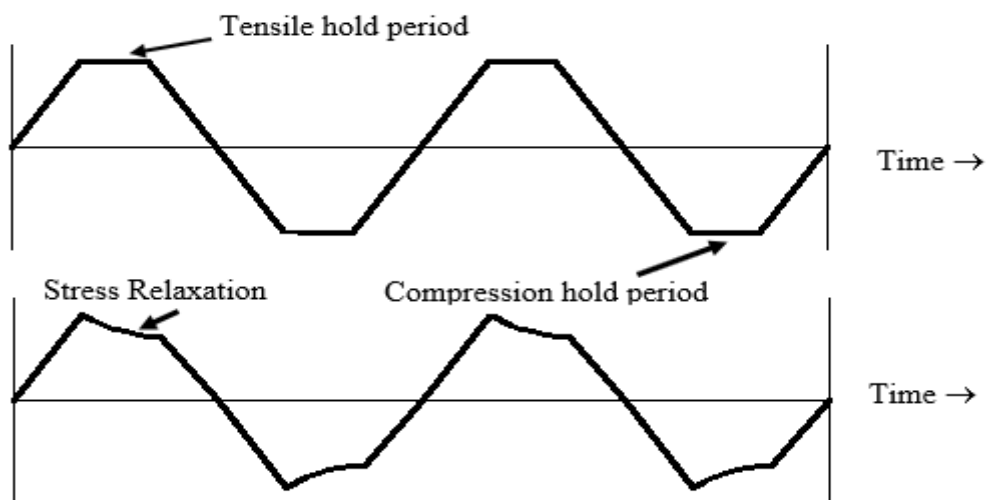
Figure 2.8 Example of creep-fatigue interaction with stress relaxation during hold periods under cyclic loading (Davis, 2000).

2.9 Creep Resistant Materials

A major contribution to the increase in power plant efficiency consisted of the development of materials with higher creep strength. The main categories of materials used are: ferritic steels, austenitic steels and nickel-based alloys. In addition to that, modified 9Cr-1Mo steel was developed jointly by Oak Ridge National Laboratory (ORNL) and Combustion Engineering, Inc. based on the 9Cr-1Mo steel (Esztergar, 1972). By optimization of the alloy with small amounts of V, Nb, and N the creep strength was considerably improved and the steel was eventually approved for tubing by ASTM as A2B, Grade T91 and by ASTM and ASME as A/SA-335, Grade P91 in 1984. Grade 91 steel variations are designated as T91 for tubing, P91 for piping, and F91 for forgings. The first large scale application of P91 steel at Ultra

21

Supercritical (USC) steam conditions occurred in the Kawagoe plants in Japan, commissioned in 1988, with operating parameters of 31 MPa at 556º C (Sikka, 1981). The chemical composition of Grade 91 steel is given in **Table 2.1** (Bakker and Viswanathan, 2000).

Table 2.1 Composition of Grade-91 Steel

Element	T/P91	
	Min	**Max**
C	0.08	0.12
M_n	0.3	0.6
P		0.02
S		0.01
Si	0.2	0.5
Cr	8	9.5
Mo	0.85	1.05
V	0.18	0.25
Nb	0.06	0.1
N	0.03	0.07
Al		0.04

2.9.1 Classical constitutive equations of creep strain analysis method

Constitutive equations were used for high chromium alloy steel P91 and its weldment could be summarized as: Norton's Law, Robinson Model, Liu and Murakami, Hill's anisotropic potential function, Kachanov-Rabotnov and Xu's formulation, based on reviewing of the previous work. The classical constitutive equations representations of primary, secondary and tertiary creep are listed in Table 2.7 (Haarmann et. al. 2002) . However, creep strain characteristics may not be acceptably modelled by certain creep constitutive equations for overall creep stages (primary, secondary and tertiary stages) of materials (Holdsworth and Merckling, 2014).

Table 2.2 Model equations for creep calculation ().

Model equation	Forms
Primary creep	
Power law	$\varepsilon_f = At^p$, $\quad \varepsilon_f = A\sigma^n.t^p$
Logarithmic	$\varepsilon_f = BLog_{10}\ (1+b.t)$
Exponential	$\varepsilon_f = C.(1-\exp(-C.t))$
sinh law	$\varepsilon_f = D.\sinh(Ct^{\frac{1}{3}})$
Secondary Creep	
Power law	$\varepsilon_{f,min} = A'.t^p$
sinh law	$\varepsilon_f = \varepsilon_o \sinh\frac{\sigma}{\sigma_o}$
Tertiary Creep	
Exponential	$\varepsilon_f = M\ (\exp(-mt)-1)$
Omega	$\varepsilon_f = \varepsilon_{fo}.\exp(\dot{\Omega}\varepsilon)$

2.9.2 Time fraction rule

The most frequently used method indicating the creep damage fraction because of primary loading loading-conditions are expressed in terms of time so that the damage is calculated by the sum of the ratio of hold times to the respective rupture time (Sanjooram, 2014).

$$D_C = \Sigma N \int \frac{dt}{t_R}\ (T, \sigma) \text{ ---(5)}$$

Where, σ_t is the stress acting during the time increment dt, at temperature, T, and ,T$_h$ (T,σ) is the rupture time associated with this level of temperature and stress. (Sanjooram, 2014)

2.9.3 Flow rule

In metal plasticity, the assumption that the plastic strain increment and deviatoric stress tensor have the same principal directions is summarized in a relation called the flow rule. Flow rule relates plastic strain increments to stress increments after onset of initial yielding (Gan et. al., 2006). The plastic strain increment (flow rule) is then determined through equation no.6 as follows-

$$d\varepsilon_p = d\lambda.\frac{\partial f}{\partial \sigma}.\Delta f \text{ ---(6)}$$

Where $d\lambda$ is a positive scalar of proportionality and also called as plastic multiplier? We define a plastic potential f, which has units of stress and is a function of stresses, f = f (σ, α, W_p). For the von Mises criterion the plastic strain increments are-

$$d\varepsilon^p = \begin{bmatrix} d\varepsilon_x^p \\ d\varepsilon_y^p \\ d\varepsilon_z^p \\ d\varepsilon_{xy}^p \\ d\varepsilon_{yz}^p \\ d\varepsilon_{zx}^p \end{bmatrix} = d\lambda \frac{1}{2\sigma_e} \begin{bmatrix} 2\sigma_x - \sigma_y - \sigma_z \\ 2\sigma_y - \sigma_z - \sigma_x \\ 2\sigma_z - \sigma_x - \sigma_y \\ 6\tau_{xy} \\ 6\tau_{yz} \\ 6\tau_{zx} \end{bmatrix}$$

where $d\lambda$ again determines the magnitude of the increment. The associated von Mises flow rule predicts that no volumetric changes occur as a result of plastic straining. In contrast, soils, concrete and other granular materials do exhibit a volumetric dilatation during plastic flow. This is reflected in the Drucker-Prager criterion (Jiang J. , 2012)where the plastic strain increments are given by-

$$d\varepsilon^p = \begin{bmatrix} d\varepsilon_x^p \\ d\varepsilon_y^p \\ d\varepsilon_z^p \\ d\varepsilon_{xy}^p \\ d\varepsilon_{yz}^p \\ d\varepsilon_{zx}^p \end{bmatrix} = d\lambda (\frac{1}{2\sigma_e} \begin{bmatrix} 2\sigma_x - \sigma_y - \sigma_z \\ 2\sigma_y - \sigma_z - \sigma_x \\ 2\sigma_z - \sigma_x - \sigma_y \\ 6\tau_{xy} \\ 6\tau_{yz} \\ 6\tau_{zx} \end{bmatrix} + \begin{bmatrix} \frac{1}{3}\alpha\sigma_x \\ \frac{1}{3}\alpha\sigma_y \\ \frac{1}{3}\alpha\sigma_z \\ 0 \\ 0 \\ 0 \end{bmatrix})$$

Here the relative change in volume can be expressed in equation no. 7 as follows-

$$\frac{\Delta V}{V} = d\varepsilon_x^p + d\varepsilon_y^p + d\varepsilon_z^p = d\lambda.\frac{1}{3}\alpha\ (\sigma_x + \sigma_y + \sigma_z)\ \text{---(7)}$$

Which is not necessarily equal to zero. For soils, however, the volumetric dilatation predicted by the associated Drucker-Prager flow rule is often somewhat larger than can be verified experimentally.

2.9.4 Strain hardening laws

Experimentally, it can be shown that if a solid is plastically deformed, then unloaded it, and after that, reloaded it in order to get more plastic flow. In that case, its resistance to plastic flow will be increased. Such a phenomenon is known as strain hardening. Definitely, strain hardening can be modelled through relating the size and shape of the yield surface to plastic strain in some appropriate ways (Li et. al. 2018).

2.9.5 Isotropic hardening

The simplest strain hardening modelling, in which the yield surface increases in size but remain with the same shape due to plastic hardening may be defined as isotropic hardening (Hakansson et. al., 2005).
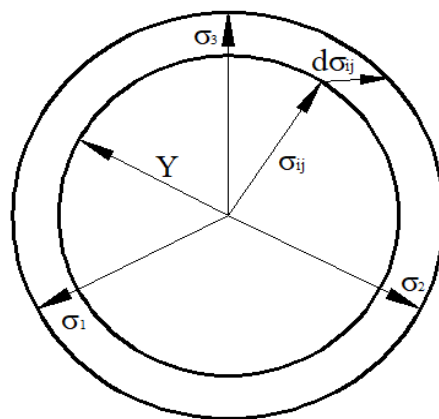
Figure 2.9 Isotropic Hardening

This means we must devise some appropriate relationship between Y and the plastic strain. To get a suitable scalar measure of plastic strain we define the accumulated plastic strain magnitude (Hakansson et. al., 2005)-

$$\varepsilon_p = \int \sqrt{\frac{2}{3} d\varepsilon_{ij}^p d\varepsilon_{ij}^p} \text{---(8)}$$

Here, the factor of $\frac{2}{3}$ is introduced so that in a uniaxial tensile test in which the specimen is stretched parallel to the direction. To see this, note that plastic strains do not change volume, so that and substitute into the formula. Then we make Y a function of. People often use power laws or piecewise linear approximations in practice. A few of the more common forms of hardening functions are-

Perfectly Plastic Solid: Y = Constant, Linear strain hardening solid: $Y = Y_o + h.\varepsilon^p$

Power law hardening material: $Y = Y_o + h.(\varepsilon^{-p})^{\frac{1}{3}}$

In these formulas, h and m are material properties. These functions are illustrated in the figures below-

Perfectly Plastic Solid   Linear Strain Hardening Solid   Power-Law Hardening Solid
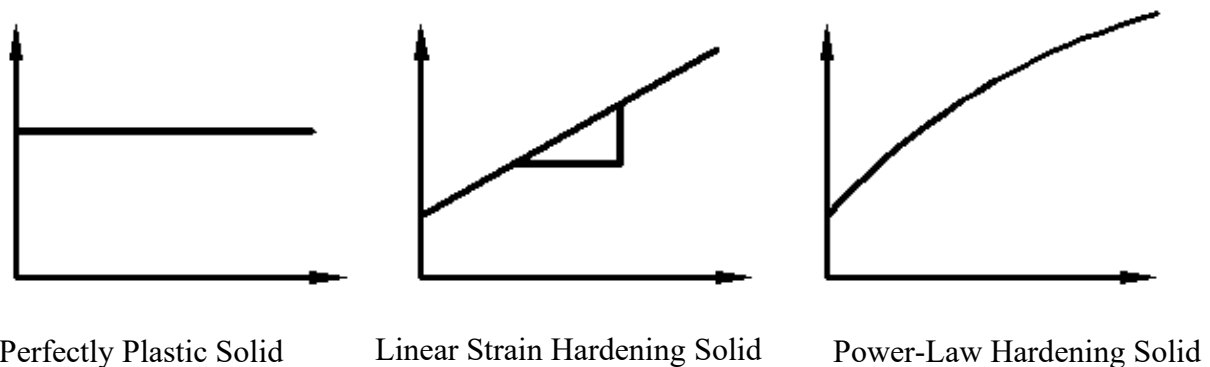
Figure 2.10 Different hardening function.

2.9.6 Kinematic hardening

An isotropic hardening law is generally not useful in situations where components are subjected to cyclic loading. It does not account for the Bauschinger effect, and so predicts that after a few cycles the solid will just harden until it responds elastically (Hakansson et. al., 2005).

To fix this, an alternative hardening law allows the yield surface to translate, without changing its shape. The idea is illustrated graphically in the picture. As you deform the material in tension, you drag the yield surface in the direction of increasing stress, thus modeling strain

hardening. This softens the material in compression, however. So, this constitutive law can model cyclic plastic deformation.

The stress-strain curves for isotropic and kinematic hardening materials are contrasted in the figure below.

(a)

(b)
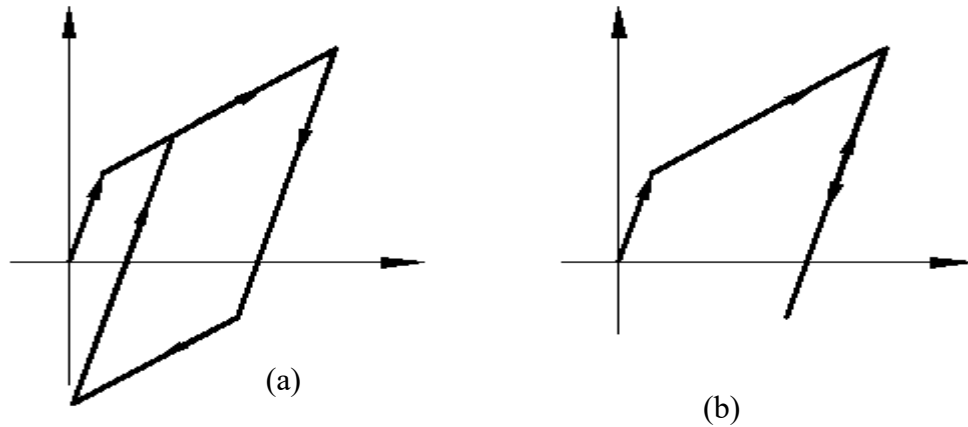
Figure 2.11 a) Isotropic and b) Kinematic hardening

To account for the fact that the centre of the yield locus is at a position in stress space, the Von-Mises yield criterion (Yang, 1980) needs to be modified as equation no. 9 follows-

$$f(\sigma_{ij}, \alpha_{ij}) = \sqrt{\frac{2}{3} (S_{ij} - \alpha_{ij})(S_{ij} - \alpha_{ij})} - \gamma \ , \ S_{ij} = \sigma_{ij} - \frac{1}{3}\sigma_{kk}.\delta_{ij} \text{------------------------------(9)}$$

$\sigma_{kk} = (\sigma_{x} + \sigma_{y} + \sigma_{z})$ and where δ_{ij} is the Kronecker delta whose value is unity when i = j and zero when i ≠ j.

Here, Y is now a constant, and hardening is modelled by the motion of the yield surface. To do so, we need to relate to the plastic strain history somehow. There are many ways to do this, which can model subtle features of the plastic response of solids under cyclic and nonproportional loading.

The simplest approach is to set-

$$\dot{\alpha}_i = \frac{2}{3} C_i \dot{\varepsilon}^{pl} \text{--(10)}$$

This hardening law of equation no. 10 predicts that the stress-plastic strain curve is a straight line with slope c. This is known as linear kinematic hardening (Muniandy et. al., 2016). A more sophisticated approach is to set in equation no. 11 as follows-

$$\dot{\alpha}_i = \frac{2}{3} C_i \dot{\varepsilon}^{pl} - \gamma_i \dot{\bar{\varepsilon}}^{pl} \alpha_i \text{ --------------------------------------(11)}$$

where c and are material constants. It's not so easy to visualize what this does it turns out that that this relation can model cyclic creep the tendency of a material to accumulate strain in the direction of mean stress under cyclic loading, as illustrated in the figure on the right. It is known as the Armstrong-Frederick hardening law (Jiang and Kurath, 1996). A contrast between linear and non-linear kinematic hardening can be shown as follows-
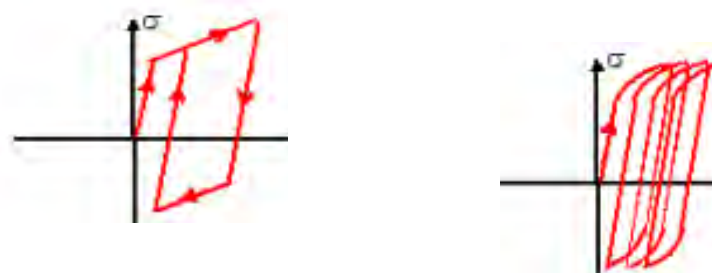
Linear Kinematic Hardening   Non-Linear Kinematic Hardening

Figure 2.12 Graphical representation of different Kinematic hardening

2.10 Influence of multiaxial stress states on creep

To describe the plastic behavior in multiaxial stress conditions, we use yield condition, flow rule and hardening rule. Any complex stress combinations with three stresses and six shear stresses can be transformed to the principal coordinate system in which no shear stresses exist. Any stress state can then be described with the principal stresses $\sigma_1 > \sigma_2 > \sigma_3$. A triaxial tress state include all three stresses, while a biaxial stress state includes only σ_1 and σ_2 and have $\sigma_3 = 0$. A uniaxial stress state is when $\sigma_1 = \sigma$ and $\sigma_2 = \sigma_3 = 0$ (Boyer, 1988).

Most material data including creep rupture data is typically based on uniaxial testing. Therefore, the fundamental idea of equivalent stress equations is to compute a corresponding

stress for complex stress states that can produce correct rupture time when applied to uniaxial creep data (Boyer, 1988).

Creep damage development is largely dependent on the stress state of a component since stress states are known to affect the ductility of a material. The stress state also determines which stress parameter is best correlated to the creep damage rate (Penny and Marriot, 1995). There are many theories on how to correlate creep damage in multiaxial stress states to uniaxial stress state creep data and the most extensively used creep-rupture strength are von Mises, Tresca and the maximum principal stress criterion (Huddleston, 1985).

2.11 Classical theories.

Von Mises criterion, also known as the octahedral shear stress criterion or the distortional energy criterion, assumes that failure by yielding occurs when the distortional strain-energy density in the material reaches the same value as for yielding by uniaxial tension or compression (Boresi and Schmidt, 2003). Von Mises in equation no.12, effective stress formula (Sica, 2017), when expressed in terms of principal stresses can be written as follows-

$$\begin{bmatrix} \sigma_{xx} & \tau_{xy} & \tau_{xz} \\ \tau_{yx} & \sigma_{yy} & \tau_{yz} \\ \tau_{zx} & \tau_{zy} & \sigma_{zz} \end{bmatrix}$$

Nominal Stress on the diagonals, and

Shear Stress off the diagonal
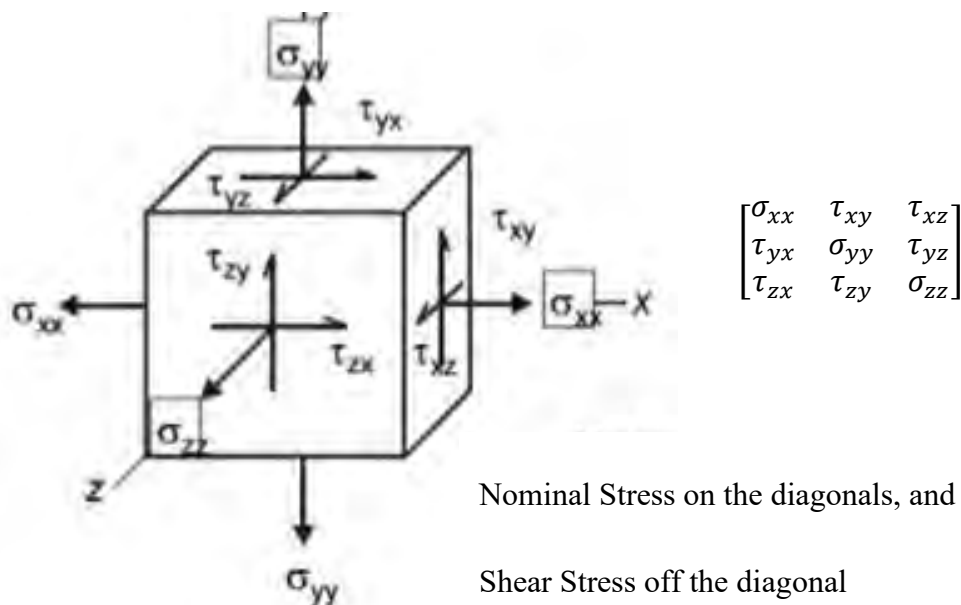
$$\sigma_{VM} = \frac{1}{\sqrt{2}} \cdot \sqrt{(\sigma_1 - \sigma_2)^2 + (\sigma_2 - \sigma_3)^2 + (\sigma_3 - \sigma_1)^2} \text{ -----------------------------------(12)}$$

The maximum shear stress criterion given by following equation also known as the Tresca criterion is based on the concept of maximum shear stress energy (Boyer, 1988). Criterion for

yielding is when the maximum shear stress of a point equals maximum shear stress at yield under uniaxial tension or compression (Abrate, 2008). For multi-axial case, the equation can be expressed as equation no.13.

$$\sigma_p^3 - (\sigma_x + \sigma_y + \sigma_z)\,\sigma_p^2 + (\sigma_x\sigma_y + \sigma_y\sigma_z + \sigma_z\sigma_x - \sigma_{yz}^2 - \sigma_{xz}^2 - \sigma_{xy}^2)\,\sigma_p - (\sigma_x\sigma_y\sigma_z + 2\sigma_{xy}\sigma_{yz}\sigma_{zx} - \sigma_x\,\sigma_{yz}^2 - \sigma_y\,\sigma_{xz}^2 - \sigma_z\,\sigma_{xy}^2) = 0 \text{ --(13)}$$

Writing it in a more precise way,

$$\sigma^3 - I_1\sigma^2 + I_2\,\sigma - I_3 = 0$$

Where,

$$I_1 = \sigma_x + \sigma_y + \sigma_z \,,\; I_2 = \sigma_x\sigma_y + \sigma_y\sigma_z + \sigma_z\sigma_x - \sigma_{yz}^2 - \sigma_{xz}^2 - \sigma_{xy}^2, \text{ and}$$

$$I_3 = \sigma_x\sigma_y\sigma_z + 2\sigma_{xy}\sigma_{yz}\sigma_{zx} - \sigma_x\,\sigma_{yz}^2 - \sigma_y\,\sigma_{xz}^2 - \sigma_z\,\sigma_{xy}^2$$

Three roots of the characteristic equation are the eigenvalues of the stress tensor σ_{ij}. Within the context of solid mechanics, such eigenvalues are known as the principal stresses.

The Von-misses stress in equation no.14 (Distortion energy) is given by (Abrate, 2008)-

$$\sigma_{VM} = \frac{1}{\sqrt{2}} \cdot \sqrt{(\sigma_1 - \sigma_2)^2 + (\sigma_2 - \sigma_3)^2 + (\sigma_3 - \sigma_1)^2} \text{ --(14)}$$

In terms of principal stress components, the yield criteria can be given as,

$$(\sigma_1 - \sigma_2)^2 + (\sigma_2 - \sigma_3)^2 + (\sigma_3 - \sigma_1)^2 = 2Y^2$$

In terms of stress components in the x, y, z coordinate system can be written as equation no. 15 as follows,

$$\sigma_{VM} = \frac{1}{\sqrt{2}} \cdot \sqrt{(\sigma_{xx} - \sigma_{yy})^2 + (\sigma_{yy} - \sigma_{zz})^2 + (\sigma_{zz} - \sigma_{xx})^2 + 6(\tau_{xy}^2 + \tau_{yz}^2 + \tau_{zx}^2)}$$

$$\text{--(15)}$$

Maximum-Shear-Stress or Tresca Criterion (Huddleston, 1985).

1. This yield criterion assumes that yielding occurs when the maximum shear stress in a complex state of stress equals the maximum shear stress at the onset of flow in uniaxial-tension.
2. From the maximum shear stress is given by equation (Zhu and Leis, 2003).

$$\tau_{max} = \frac{\sigma_1 - \sigma_3}{2}$$

Where, σ_1 is the algebraically largest and σ_3 is the algebraically smallest principal stress.

For uniaxial tension, $\sigma_1 = Y$, $\sigma_2 = \sigma_3 = 0$, and the maximum shearing yield stress τ_o is given in equation no. 16 -

$$\tau_o = \frac{Y}{2}, \text{ and hence } \tau_{max} = \frac{\sigma_1 - \sigma_3}{2} = \tau_o = \frac{Y}{2} \text{ ---(16)}$$

Therefore, the maximum shear stress criteria are given by:

$$\sigma_1 - \sigma_2 = Y \text{ --(17)}$$

The Rankine theory (Vinson and Sierakowski, 2008) base the failure criteria on the maximum principal stress (MPS) in equation no. 18. The theory states that yielding in a complex stress system occur when the maximum principal tensile stress, σ_1 reach the value of the yield stress.

$$\sigma_{MPS} = \sigma_1 \text{ --(18)}$$

Important to mention is that yielding also can occur in compression if the minimum principal stress, σ_3 reaches the yield stress before yielding is reached in tension. The theory is best suited for brittle material since failure in ductile materials occur in shear, in addition, homogenous materials can resist very high hydrostatic pressures without failure, which indicates that the maximum principal stress criteria is not valid for all stress states (Hearn, 1997).

Brittle material ruptures are generally governed by the MPS criterion while the von Mises effective stress is the controlling parameter for ductile ruptures that occurs under high stresses under short service. However, long service times in elevated temperatures can lead to a significant reduction in ductility, the rupture is then governed by either the MPS or a mixed criterion including both von Mises and MPS. Some studied has also been dedicated to finding out whether creep failure would occur at complete tensile tri-axiality $\sigma_1 = \sigma_2 = \sigma_3$, a stress state

31

for which von Mises effective stress becomes zero. It is however believed that even though no failure or deformation would occur in a short time span, long exposure time would eventually lead to a MPS controlled rupture. However, this is not easily verified due to difficulties associated with performing multiaxial testing (Boyer, 1988).

2.12 Fatigue

Fatigue life for creep fatigue is always related to the plastic strain, not the elastic strain. This is because the externally applied deformation energy at the macroscopic level is consumed in many small plastic strains at the microstructure level (Narayanasamy and Prasad, 2013). This plastic strain then breaks molecular bonds and contributes to micro cracks, hence the failure of the material. In addition, applied stress is also related to fatigue life to describe creep-fatigue behavior. This is because the stress above yield value results in unrecoverable deformation; then the accumulated damage leads to structural failure (Boresi and Schmidt, 2003). Fatigue damage occurs when a material is subjected to cyclic loading. Although the term 'fatigue' first appeared in 1854, the history of fatigue can be traced as far back as 1837, when the first fatigue test results were published by Albert (Sakanashi, 2013).

2.12.1 Fatigue Failure Mechanisms

Due to the initiation and propagation of cracks, the fatigue failure occurs under balanced cyclic loading conditions until separation of specimen takes place (Dowling, 2013). In general, nucleation occurs at a free surface, and the crack becomes enlarged in three stages (Figure 13).

Stage-I: The first stage growth begins with the extension of the initiation process (The order of the burgeoning crack length may be of 10 pm) and occurs towards a crack tip shear plane. The existence of such initiation and propagation is normally of the order of a few grain diameters.

Stage-II: The second stage growth is perpendicular to the applied stress and is governed by the continuum response of the material.

Stage-III: At the ending stage, when the local crack tip deformation is of the order of the material in static fracture, homogeneities e.g., voids growth, contributes to crack advance and leads to final failure (ASTM-08, 2008).
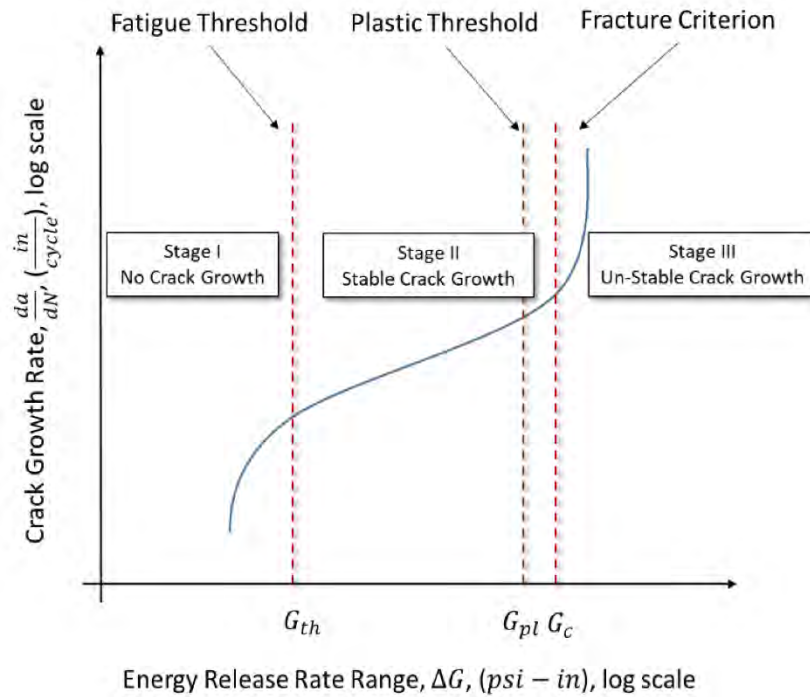
Figure 2.13 Fatigue crack growth stages (ASTM-08, 2008).

A crack in a solid can be stressed in three different modes, as illustrated in Figure 2.14 Normal stresses to give rise to the (opening mode) or mode I loading, where the displacements of the crack surfaces are perpendicular to the plane of the crack. In-plane shear results in mode II or (sliding mode) the displacement of the crack surfaces is in the plane of the crack.

Mode I: Opening   Mode II: Sliding in plane   Mode III: Sliding out of plane
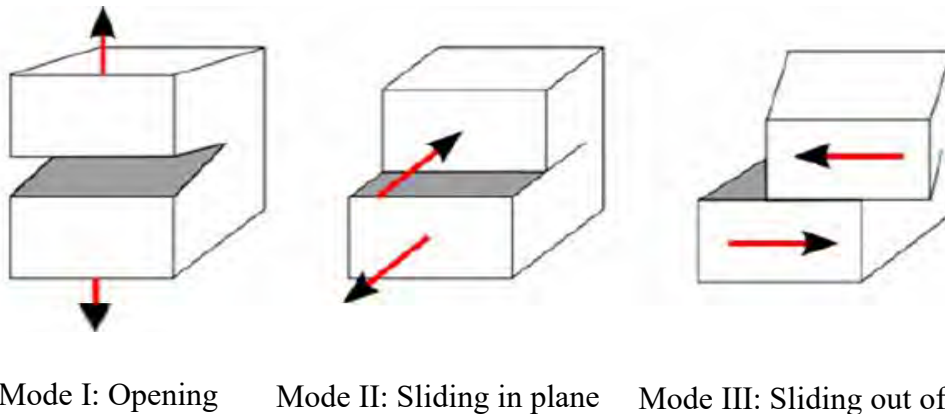
Figure 2.14 The three crack modes of loading (Shibli, 2000) .

The (tearing mode) or mode III is caused by out-of-plane shear. The superposition of the three modes describes the general case of loading and the most important mode is technically Mode I (Shibli, 2000) .

33

2.12.2 Fatigue Crack Initiation

Fatigue crack initiation in a ductile metal is a consequence of reversed plasticity within a grain on a metallurgical feature scale of 10^{-3} mm. Surface grains are weakest; they deform plastically at the lowest stress, and this leads to the production of a micro-crack within a grain (Dowling, 2013). Such micro-plasticity, due to slip within grains, can occur at stresses much lower than the tensile yield stress. The slip can take place only on certain crystallographic planes within a grain. Resistance to crack initiation depends strongly on surface roughness, residual stress and environment, all of which are difficult to control (ECCC, 2009).

2.12.3 Fatigue Crack Propagation

In the metal fatigue literature, the terms fatigue crack propagation and fatigue crack growth are both used for the increase in size of a fatigue crack (Dowling, 2013). A Stage I crack becomes a Stage II crack. When it reaches a critical length, it changes direction and propagates normal to the maximum principal tensile stress. The critical length is strongly dependent on microstructural features and on stress conditions and it varies widely. It is usually less than 0.25mm and typically, around 0.02 mm. After the transition, a Stage II crack propagates through the majority of the cross section. More descriptive terms for Stage I and II, micro-crack and macro-crack respectively, are sometimes used (ECCC, 2009).

2.12.4 Factors Affecting Fatigue Crack propagations

There are different types of factors affecting the fatigue crack propagation which can be classified into the following categories-

Microstructure of the material: The impacts of microstructure rely on certain factors such as grain structure, structural flaws and average grain size, which have paramount effects on fatigue life and growth of crack. For instance, larger grain size material shows lower fatigue life limit compared to that of smaller grain size material at an ambient temperature. However, at elevated temperature, the coarse-grained materials show better fatigue properties (Abe, 2008)**.**

Processing Techniques: Several processing techniques such as forging, rolling and extrusion yield in directional properties because of grain orientation. Due to such an impact, fatigue life

of material is increased along the oriented direction and lowest towards transverse direction. Apart from that, surface coating, cold and hot working, platting, case hardening, cladding etc. can influence fatigue life and crack growth with the residual stress production (Abe, 2008).

Load Spectrum: Because of magnitude, sign, history as well as rate of loading, the real service loading may be a difficult one, which ultimately impacts the fatigue life and subsequent crack propagation rate (Abe, 2008).

Geometry of the component: Connections, notches, welds, thickness and surface finish produce the geometric impacts, and where the crack initiation is significantly influenced by the surface smoothness. Stress concentration is caused due to holes, notches, joints etc. and hence lead to initiation of crack (Abe, 2008).

Temperature: Crack growth due to fatigue at elevated temperature is a complex phenomenon to study. The significant factor affecting the crack growth are probably being creep-fatigue simultaneous impacts, thermos-mechanical impacts, ageing effects and the environmental interaction (Kimura et. al. , 2000). The reduced grain boundary strength, slip character of the material, and accelerated oxidation are affected by elevated temperature. The simultaneous impacts of such factors is to expedite the crack propagation. Above certain temperature, the fatigue limit is considerably reduced (Viswanathan, 1989).

Inter-granular crack growth rate was studied by Bown, et al., (Davis, 2000) at particularly high temperature in a vacuum under static load, and the same behavior was reported for martensitic alloys at different temperature ranges in air.

Environment: A corrosive environment causes degradation of the material; the most common visible effect being pitted or surface roughness (etching). These notch-like regions act as stress raisers and are generally the sites of crack initiation. Thus, one needs to shorten the crack nucleation stage and to increase the crack growth rate. The increase in temperature reduces the fatigue resistance of the material; thus, increasing the crack propagation.

Oxidation: The influence of oxygen is more pronounced as the temperature is increased. A suggested mechanism is the embrittlement of grain boundaries due to oxygen penetration. This embrittlement is explained in terms of pinning the grain boundaries due to the existence of

oxides and small cavities. During cyclic loading at a high temperature, the lack of grain boundary mobility may lead to inter-granular cracking (Abe, 2008).

2.13 Different types of fatigues

2.13.1 Low Cycle Fatigue

Low cycle fatigue of metals can be defined as failure resulting from cycles of loading comparatively less than about 10^4 cycles (Boyer, 1988) and it is classified into

a) Isothermal fatigue and b) Thermal fatigue.

Low cycle fatigue phenomena began to gain attention. Until World War II little attention was paid to the low cycle range, and most of the existing fatigue results were for high cycles only. Then it was realized that for some pressure vessels, pressurized fuselages, mechanisms for extending landing gears and controlling wing flaps, missiles, spaceship launching equipment, etc. only a short fatigue life was required (Penny and Marriott, 1995).

Today many components in heat exchanger, gas and steam turbines, nuclear reactors and aircraft industries employ stresses appreciably above their yield stresses, which may be due to, for example, start-up and shut-down of the power plant, or the taking-off and landing of an aircraft. The frequency of cycling has usually different orders of magnitude and waveform depending on the experience life.

At high temperature the material deformation process is complex; it involves the addition of a number of thermally activated processes including grain boundary sliding, dislocation climb, etc. (Gan et. al., 2006) and when the time factor is combined with high temperature, creep and environmental interactions may play an important part in the failure process.

Isothermal fatigue: Isothermal fatigue (IF) is the simplest form of cyclic fatigue operating at a constant and uniform temperature. Cyclic loading may be applied externally or during operation of plant when alternative stresses due to vibration can cause fatigue. Indeed, other more complicated forms of cyclic loading sometimes referred to a single representative isothermal temperature (Deng et.al., 2019).

Many investigators have concerns regarding the isothermal fatigue which studies the behavior of the materials subjected to cyclic high temperatures. Others have used isothermal fatigue data to find out whether a relationship exists with the study of thermal shock fatigue crack growth behavior in different materials. Usually, it is assumed that maximum temperature of the thermal shock cycle is more damaging than the average temperature. Therefore, for correlate purposes, isothermal fatigue studies are normally performed at the maximum temperature of the thermal shock cycle (Kimura et. al., 2000).

Thermal Fatigue: Thermal fatigue may be defined as failure due to the rate of temperature changes and the alternating exposure at higher and lower temperatures influencing the life of a material. Thermal fatigue can be known by many different names; creep fatigue, thermal shock, craze cracking, thermal rupture, thermal strain fatigue, thermal stress fatigue and high temperature fatigue (Zeman et. al., 2006).

It can be broadly divided into two categories:

1. Stresses can that arise in the absence of thermal gradients due to the expansion and contraction of mechanically restrained structures (Davis, 2000).
2. Stresses that are produced from rapid changes in temperature; for instance, thermal gradient may cause different expansion through the section of the component

2.13.2 Thermo-mechanical Fatigue

Thermo-Mechanical Fatigue (TMF) is a variation of mechanical fatigue of materials where heating and cooling cycles are applied to test a material added to a mechanical cyclic loading. The temperature cycles have, in most cases the same frequency as the loading cycles, but different phase shifts. If the phases shift $\varphi = 0°$, the TMF tests are called In-Phase tests where the maximum mechanical strain occurs at the maximum temperature of the cycle. If the phase shift is $\varphi = 180°$, the TMF tests are called Out-of-Phase where the maximum mechanical strains coincide with the minimum temperature (Esztergar, 1972).

Thermo-mechanical fatigue also refers to the process of fatigue damage under simultaneous changes in temperature and mechanical strain. Fatigue damage at high temperatures develops as a result of inelastic deformation where the strains are no recoverable. Therefore, TMF

damage is complex, as it may accumulate over a range of temperatures and strains under both steady-state and/or transient conditions.

It can contribute to the accumulation of TMF damage in various kinds of equipment, such as jet engines, land-based turbines for power generation, heat-exchangers and pressure vessels. For example, during straight and level flight, aircraft jet engines (or steady operation of power generation turbines) have essentially constant temperatures and imposed loads, where steady-state creep (and the environment) is the primary damage mechanisms. During take-off and landing of the aircraft engine or start-up and shut-down for power generation turbines; however, the transient demand for more power output induces load and temperature changes, which thus impose fatigue damage (Deng et. al., 2019).

2.14 Accumulated creep-fatigue damage evaluation

The method for evaluating accumulated creep-fatigue (ASME, Boiler & Pressure Vessel Code, Section III, Division 1, Subsection NH - Class 1 Components in Elevated Temperature Service, 2015) is based on superposition of the Miners rule for fatigue and the time-fraction rule for creep damage. The damage due to creep and fatigue are evaluated separately and combined as follows in equation no. 19 (Nikolais, 2017):

$$\sum_{j=1}^{p}(\frac{n}{N_d})_j \; + \sum_{k=1}^{q}(\frac{\Delta t}{T_d})_k = D_f + D_c = \text{D} \text{ ---(19)}$$

Where $\frac{n}{N_d}$ is the cyclic portion of the life fraction, for which n is the number of fatigue cycles at a given strain range j, Nd is the number of allowable cycles (the fatigue life) for cycle type, j corresponding to a given strain range at the maximum temperature occurring during the cycle. The creep life fraction given by $\frac{\Delta t}{T_d}$ is time dependent, where Δt is the duration of the time interval, k, at a certain stress- and temperature-level and T_d is the rupture time at that same stress and maximum temperature for the time interval k. D is the total creep-fatigue damage factor (ASME, Boiler & Pressure Vessel Code, Section III, Division 1, Subsection NH - Class 1 Components in Elevated Temperature Service, 2015).

This linear damage approach was chosen in the 1970s, and is consistent with the other damage assessment procedures in the ASME code. The use of Miners rule is for example used for assessing fatigue damage at lower temperatures. Many methods for evaluating creep-fatigue

damage were considered, however the linear fraction approach was chosen since it was straight forward and does not require as many tests as other methods (Jetter, 2012).

Figure 2.15 shows the bilinear summation diagram used in the Subsection NH for creep-fatigue interaction. The intersection points for the permitted materials are also indicated in the figure. The lines in the envelope are conservative lower bound limits based on experimental data.

<figure>

Campbell Diagram

y-axis: $\Sigma\Delta/Tr$ (0, 0.2, 0.4, 0.6, 0.8, 1)

x-axis: $\Sigma n/N_d$ (0, 0.2, 0.4, 0.6, 0.8, 1)

(0.3,0.3)

(0.1,0.1)

</figure>
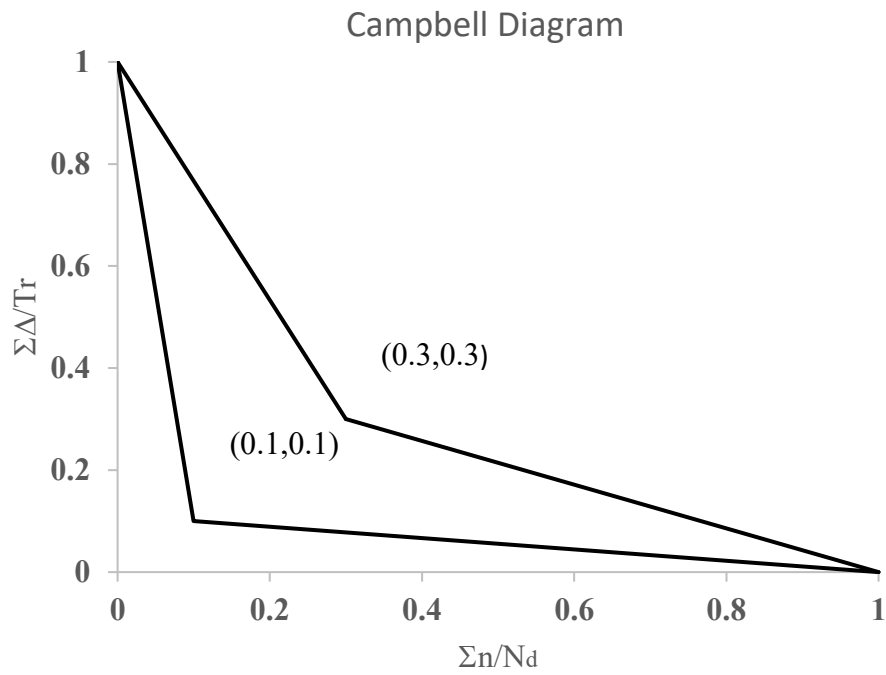
Figure 2.15 Creep-fatigue damage envelope re-plotted from ASME-NH (Nikolais, 2017).

2.15 Terms related to current study
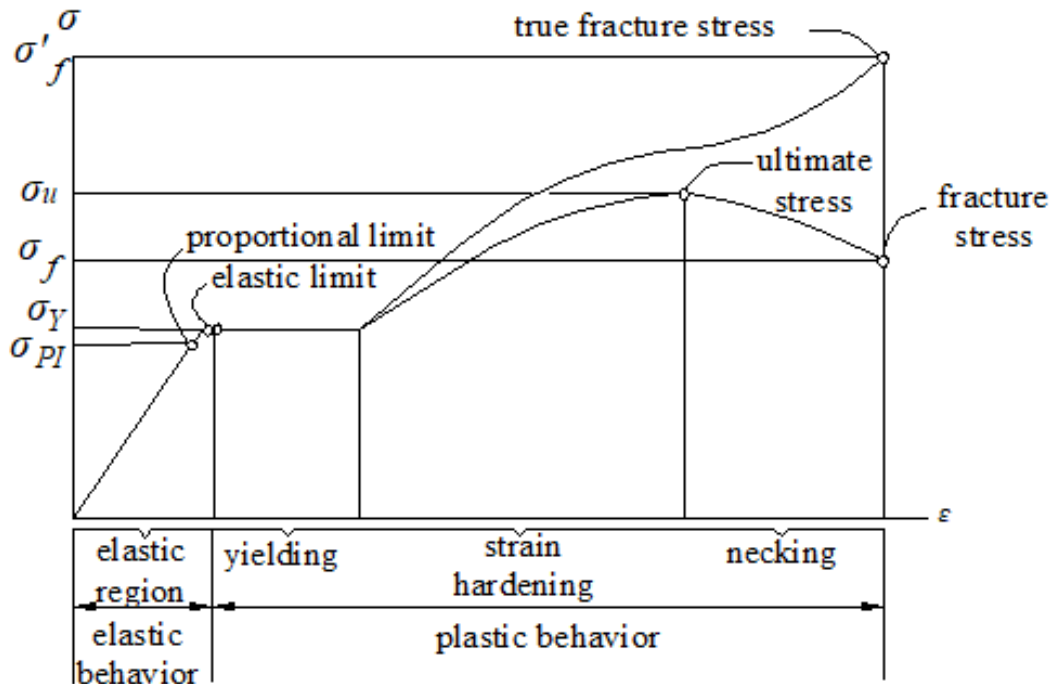
Figure 2.16 Stress vs Strain graph for mild steel (Hibbeler, 2011.)

Proportional Limit: Stress above which stress is no longer proportional to strain

Elastic Limit: The unloaded maximum stress that can be applied without resulting in permanent deformation when.

Yield Point: Stress at which there are large increases in strain with little or no increase in stress. Among common structural materials, only steel exhibits this response.

Ultimate Strength: The maximum stress the material can withstand.

2.16 Generalized constitutive model

The constitutive models used are all based on the infinitesimal strain theory. The total strain ε_{ij} is partitioned into three parts as

$$\varepsilon_{ij} = \varepsilon_{ij}^e + \varepsilon_{ij}^{in} + \varepsilon_{ij}^T \text{ ---(20)}$$

Where, $\mathcal{E}_{ij}^e$ is the elastic strain tensor; $\mathcal{E}_{ij}^{in}$ is the inelastic strain tensor and $\mathcal{E}_{ij}^T$ is the thermal strain tensor.

In non-unified visco-plasticity theories, the inelastic strain can be further divided as (Penny and Marriott, 1995)-

$$\mathcal{E}_{ij}^{in} = \mathcal{E}_{ij}^p + \mathcal{E}_{ij}^{cr} \text{---(21)}$$

where $\mathcal{E}_{ij}^p$ corresponds to the rate-independent plastic strain and $\mathcal{E}_{ij}^{cr}$ is the creep strain. For elastoplastic models, $\mathcal{E}_{ij}^{cr}=0$ and $\mathcal{E}_{ij}^{in} = \mathcal{E}_{ij}^p$ For unified visco-plasticity theories, there is no distinction between plastic and creep strains-only $\mathcal{E}_{ij}^{in}$ exists, representing the combined effect of rate-independent deformation (plastic deformation) and rate-dependent deformation (creep and relaxation).

For all models, inelastic flow is governed by the inelastic flow equation f in the stress space, expressed as-

$$f = f\left(J\left(\sigma_{ij}' - X_{ij}\right), K, R\right) \text{---(22)}$$

Where, σ_{ij}' is the stress deviator, X_{ij} is the back-stress tensor, K is the drag stress and R defines the evolution of the elastic limit. J defines an invariant function in stress space; the Von Mises invariant is typically used for isotropic material (Penny and Marriott, 1995).

2.17 Code based methods for creep-fatigue damage evaluation

The strain- and deformation-controlled limit evaluation can be performed using one of the three following analysis methods:

1. Elastic analysis

2. Simplified inelastic analysis

3. Inelastic analysis

These are arranged in the order from simplest to most difficult and least accurate to most accurate. Also, the amount of material data required for the analysis and the cost to perform

them increase for method two and three. Of all the three criteria, the elastic limits are set to be most conservative, due to difficulties of accurately predicting inelastic strain with elastic analysis. As illustrated in the following flowchart in Figure2.17, when stresses from the elastic analysis cannot satisfy the elastic limits, either the component need to be redesigned or a simplified inelastic analysis can be performed (Jawad and Jetter,2009). Similarly, if the simplified analysis does not meet the requirements for the simplified inelastic stress limits, the component must either be modified or an inelastic analysis be carried out (Jetter, 2012).
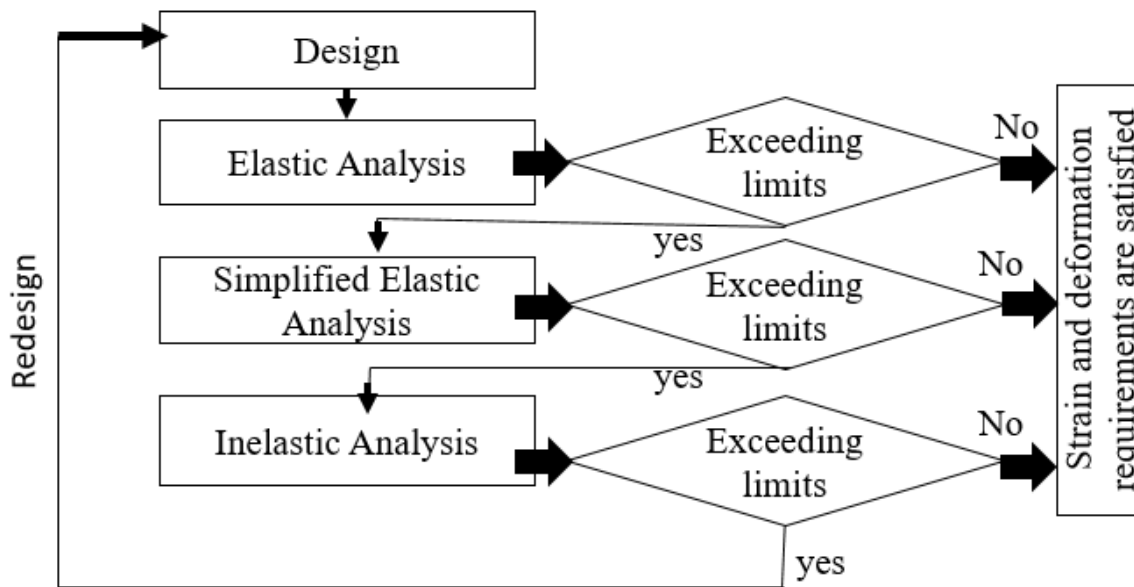
Figure 2.17 Flowchart of analysis procedure for evaluation of inelastic strain limits

2.17.1 Elastic analysis

The elastic analysis is typically preferred among engineers since it is the easiest, most convenient and least expensive analysis method. The method involves linearization to separate and categorize stresses to approximate the more accurate plastic and creep analysis. The method is appropriate to use when the combined primary and secondary stresses are below the yield strength of the material (Jawad and Jetter,2009). However, a downside with stress categorization is that it requires substantial knowledge and engineering judgement, especially for complex structures and three-dimensional stress fields (PVP, 2015). The elastic analysis is not as accurate as a plastic or creep analysis, which more accurately predicts the materials stress-strain relationship. It is, however the most conservative criteria and considered adequate for most design applications (Jawad and Jetter,2009).

2.17.2 Simplified elastic analysis

The simplified inelastic analysis also uses the results from the stress categorization made with the elastic analysis. However, these are used to calculate a strain which is compared to the allowable strain limit, thus the name simplified inelastic analysis. The method is based on the concept that the core stress remains elastic when subjected to primary and secondary stresses (obtained from stress linearization) (Jetter, 2012).

2.17.3 Stress Redistribution Locus (SRL)Method

There are various methods to estimate elastic-plastic-creep deformation and they can be categorized into inelastic FEM analyses and simplified methods with elastic FEM analyses.

Inelastic FEM analyses surpass elastic FEM analyses in accuracy of estimation. But inelastic FEM analyses need much time for calculation. Moreover, inelastic strains estimated by inelastic FEM analyses are significantly influenced by many factors such as yield condition, hardening rule, etc. Hence, they have difficulties in maintaining the unique solution. Because of that, the methods assisted by elastic FEM analyses are adopted to many codes such as JSME rules on design and constructions (JSME, 2009). The methods with elastic FEM analyses have advantages in calculation time and uniqueness of results. However, inelastic strains estimated by conventional simplified methods with elastic FEM analyses are too conservative.

As Figure 2.18, on the conventional method, a straight line is plotted from a result evaluated with elastic FEM analysis, and inelastic solution is determined as the intersection of the straight line and stress-strain curve of the material. The straight line has large conservativeness (Sato et. al., 2011).
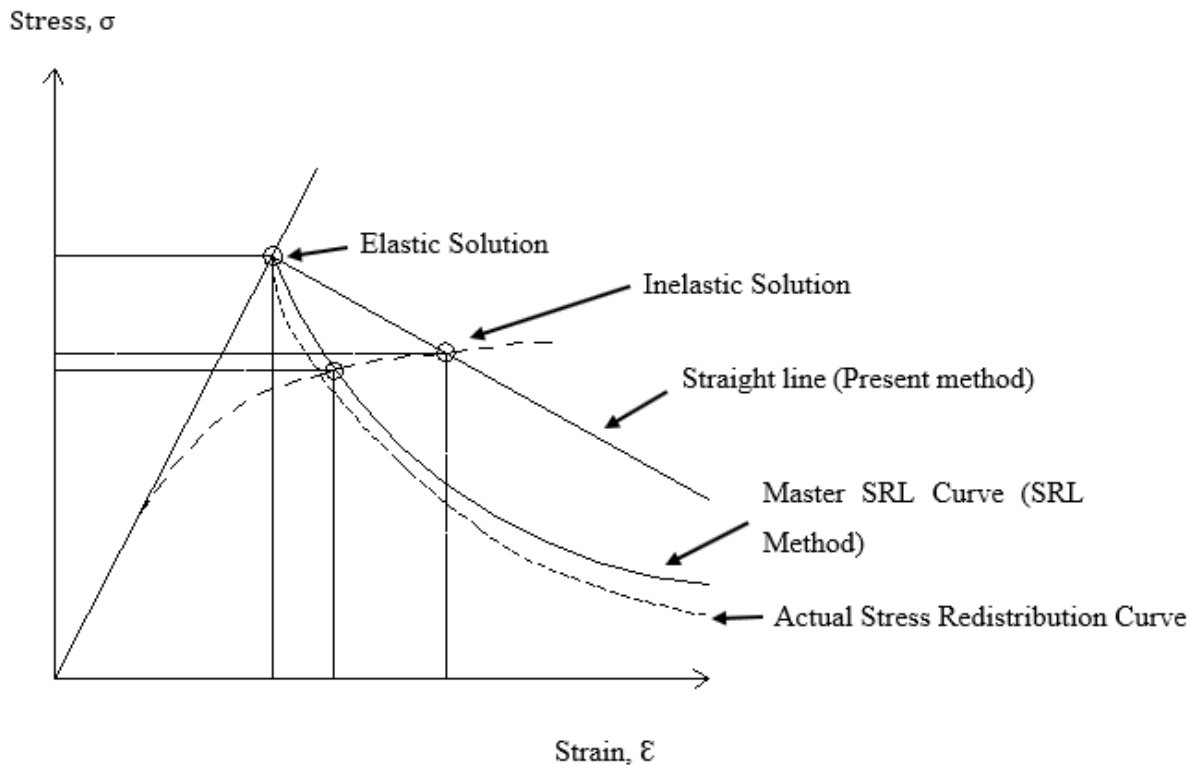
Figure 2.18 Methods to Estimate Inelastic Deformation with Elastic FEM Analyses.

2.17.4 Elastic Follow Up Method

In 1955, Robinson pointed out that a self-sprung piping system, with zero thermal expansion stress at installation temperature but operating at elevated temperature, may accumulate excessive creep strains in localized regions of high stress (Robinson, 1955). To evaluate this susceptibility to creep in different types of expansion loops, Robinson introduced the concept of "elastic follow-up." Elastic follow-up is not a failure mode. It is a concept used to underscore the importance of possible inelastic strain concentration in a piping system designed primarily using the elastic rules specified in the ASME Boiler and Pressure Vessel Code (ASME, ASME Boiler and Pressure Vessel Code ANSI/ASME BPV-III, Section III, Nuclear Power Plant Components, 1983).

The concept of EFU was introduced by Robinson (Robinson, 1955) in connection with creep stress relaxation, was later extended to describe the impact of plasticity and geometrical nonlinearities on the response of structures by Kasahara et. al., (2004).

Generalization of definition of elastic follow-up

The definition of elastic follow-up factor has been generalized. The definition of Elastic follow-up factor, Z is shown in Figure 2.19, whereas in the proposed approach Z is defined as:

$$Z = \frac{\varepsilon_{final} - \frac{\sigma_{final}}{E}}{\varepsilon_{initial} - \frac{\sigma_{final}}{E}} \text{---(23)}$$

The "initial" and "final" subscripts in this equation refer to the stress and strain before and after the structure experiences a nonlinear event. The term, $\frac{\sigma_{final}}{E}$ indicates a reference strain, i.e., the elastic strain equivalent to the final stress. The generalized definition of Z given by Eq. 23 together with the extended concept to combined nonlinearity is presented schematically in Fig. 2.19
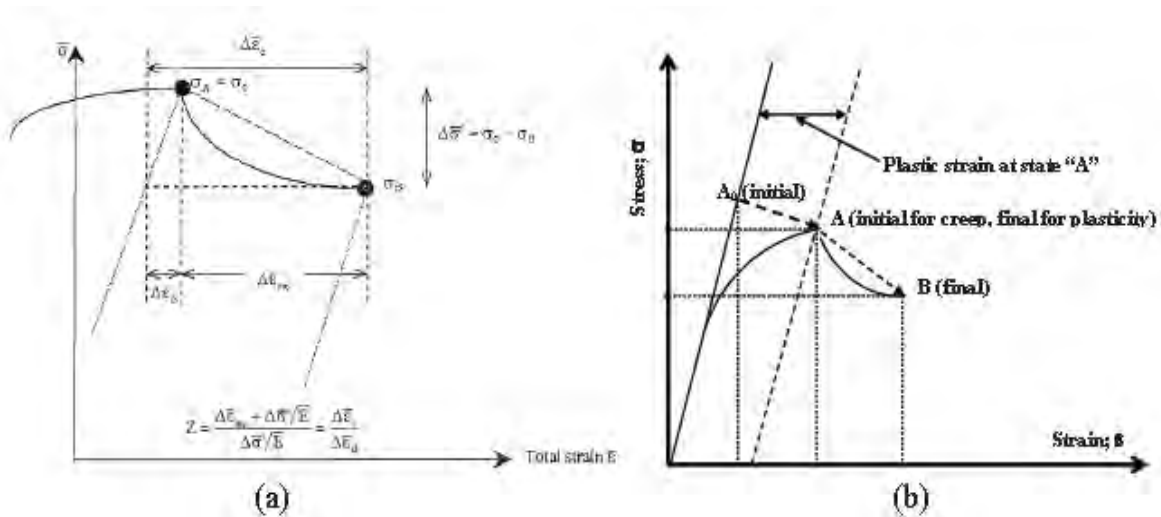
Figure 2.19 Definition of Elastic follow-up factor Z; a) as provided in R5 (*Reproduced from R5, issue 3, BEGL, UK*); b) extended definition of Z to combined plasticity and creep.

Z is the factor by which the creep strain increment exceeds the elastic strain decrease. Algebraically this is simply-

$$\varepsilon_c = -Z \cdot \Delta\varepsilon_{el} = -Z \cdot \frac{\Delta\sigma}{E} \text{--(24)}$$
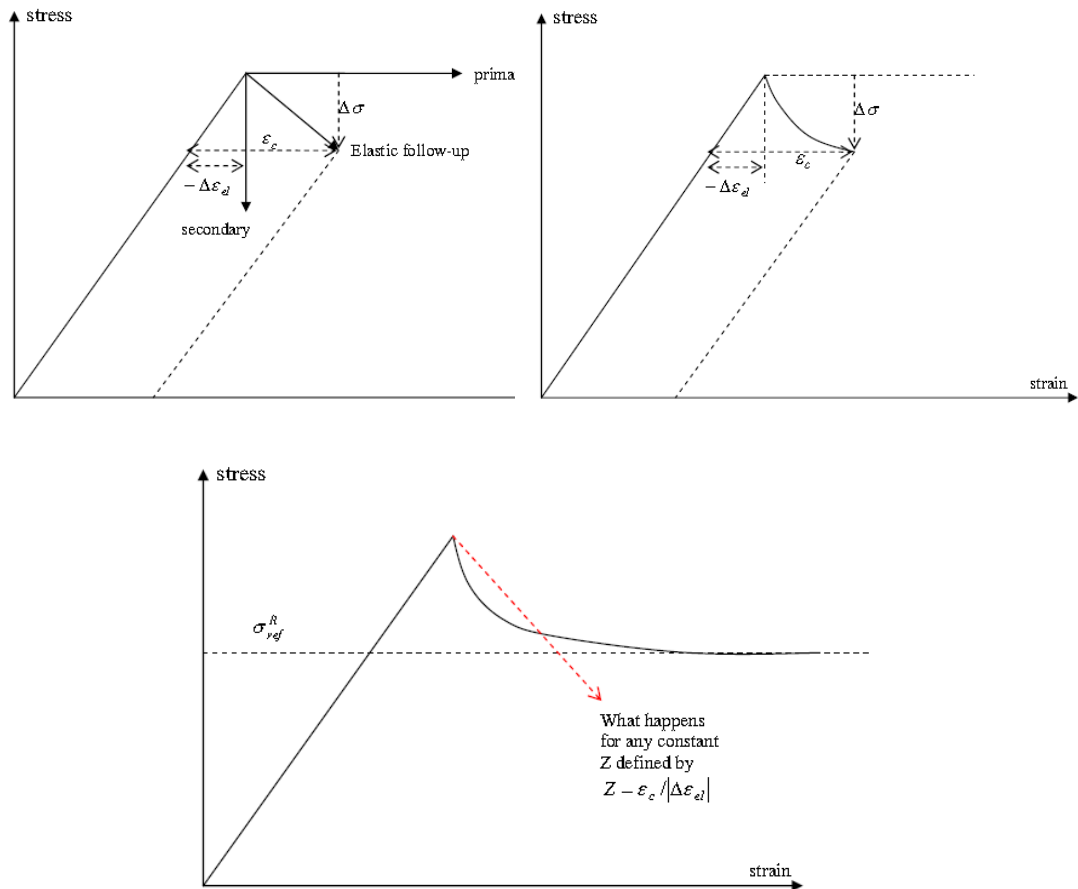
Figure 2.20 Relaxed stress for elastic follow up

To ensure that the stress cannot relax below the primary stress σ_{ref}, we must ensure that $\frac{d\sigma}{dt}$ becomes zero $\sigma \rightarrow \sigma_{ref}$ This is accomplished by replacing-

$$\frac{Z\prime}{E} \cdot \frac{d\sigma}{dt} = (\ \mathcal{E}_c(\mathcal{E}_c, \sigma, T) - (\ \mathcal{E}_c(\mathcal{E}_c, \sigma_{ref}, T) \text{ ---}(25)$$

The advantage of this interpretation is that the relaxation equation (25) can be used which ensures that the stress does not drop below the primary rupture reference stress and this is essential requirement. The factor Z has two extreme values, 1 and ∞.

2.18 Inelastic analysis

The inelastic analysis method does neither include comprehensive nor specific guidance in Subsection NH. This was an intentional decision, since material models for inelastic analysis are still under development, and it was considered that over-specific guidance would halt further progress in the field (Jetter, 2012) . With an inelastic analysis, the inelastic strains and deformation due to service loads can be obtained directly from the analysis. The analysis does however require constitutive equations that describe both time-independent and time-dependent material response. There exist many formulations of such equations, however the prediction obtained from the various equations can vary significantly.

For predictions with an inelastic analysis to be meaningful, the equation selected to model the material's response must be evaluated according to the materials load and temperature history. This typically require a large quantity of material test data which are typically not available and material testing would be required. All the above-mentioned requirements make the method both expensive and time consuming. In addition, since it is not practical to test a material for all stages of the load and temperature history, the choice of material model and the evaluation of the results therefore requires a substantial portion of engineering judgement -

(Jawad and Jetter, 2009).

2.19 Different Advanced Constitutive Plasticity models

Plasticity models have a long history of use in finite element simulations, and have also been extensively used to represent the behavior of thermoplastic materials. Using a plasticity model to predict the non-linear response can give poor predictions of the material response, particularly during cyclic loading or during unloading. There are almost five key concepts in all classical theories of plasticity-

1. The decomposition of strain into elastic and plastic
2. Yield criteria which predict whether the solid responds elastically or plastically.
3. Strain hardening rule, which control the way in which resistance to plastic flow increases with plastic straining.
4. The plastic flow rule, which determines the relationship between stress and plastic strain under multi-axial loading.

5. The plastic unloading criteria, which models the irreversible behavior of the solid

There are many different plasticity models that have been developed and that are available in finite element software. Among them, Bilinear model, Multilinear model and Chaboche model are used for this thesis. These models have also some limitations to predict response in some cases.

The different models can be divided into two groups:

A) Isotropic hardening plasticity   B) Kinematic hardening plasticity

2.19.1 Isotropic hardening Plasticity Model

It is easier to use and can provide accurate predictions all the way to failure under monotonic loading. In case of isotropic hardening for successive loading and unloading a solid, its yield stress would have increased compared to what it was in the first cycle. Isotropic hardening just means if you load something in tension past yield and when you unload it, then load it in compression, it will not yield in compression until it reaches the level past yield that you reached when loading it in tension. In other words, if the yield stress in tension increases due to hardening the compression yield stress grows the same amount even though you might not have been loading the specimen in compression. Isotropic hardening is not useful in situations where components are subjected to cyclic loading (Taherizadeh et. al., 2015).

2.19.2 Kinematic Hardening models

Kinematic hardening model often   based on non-linear equations with material parameters that need to be determined from experimental tests, and hence are often more difficult to calibrate. The kinematic hardening models often have a restriction that the tangent modulus decreases with increasing plastic strain, a restriction that is contradicting experimental behaviors of many polymers (Taherizadeh et. al., 2015).

During plastic deformation, kinematic hardening causes a shift in the yield surface in stress space. In uniaxial tension, plastic deformation causes the tensile yield stress to increase and the magnitude of the compressive yield stress to decrease. This type of hardening can model the

behavior of materials under either monotonic or cyclic loading and can be used to model phenomena such as the Bauschinger effect and plastic ratcheting (Chow and Yang, 2004).

The yield criterion has the form:

$$F(\bar{\sigma}) - \sigma_y = 0$$

Where, $\sigma_y = yield\ stress$

$$F(\bar{\sigma}) = function\ of\ relative\ stress$$

relative stress, $\bar{\sigma} = \sigma - \alpha$

back stress, α = the shift in the position of the yield surface

The general classes of kinematic hardening models are:

1) Bilinear kinematic hardening model
2) Multilinear kinematic hardening model
3) Nonlinear kinematic hardening

2.19.3 Bilinear Kinematic Model

In this model, effective stress versus effective strain curve is bilinear. This model requires three materials parameters which are user defined. The material parameters are elastic modulus, yield stress and tangent modulus. Elastic modulus defines initial slope of curve. After yield stress, plastic deformation occurs and the relationship between stress and stain is assumed linear represented by line. The slope of the line is user defined tangent modulus. Tangent modulus cannot be less than zero or greater than the elastic modulus. Bilinear plasticity model fails to produce ratcheting under cyclic loading and yields shake down phenomena (Sudula, 2020).

Back stress, $\alpha = 2G\varepsilon^{sh}$ G = elastic shear modulus

Shift strain, $d\varepsilon^{sh} = \frac{C}{2G}d\varepsilon^{pl}$

$$C = \frac{2}{3}\frac{EE_T}{E-E_T}$$

E = Young's modulus

$$E_T = \text{User defined tangent modulus}$$
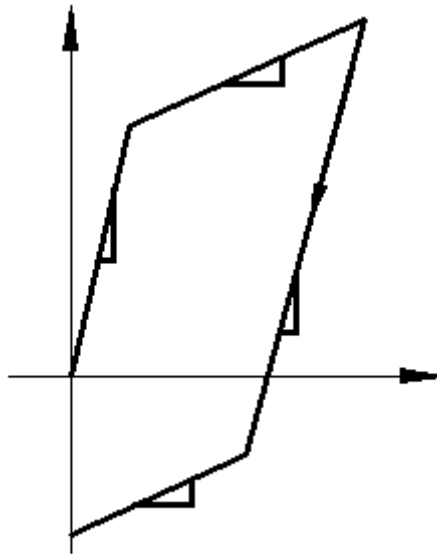
Figure 2.21 Stress vs Strain for Bilinear Kinematic Hardening (Ansys User's Guide, 1997)

2.19.4 Multi linear model

In this model, the uniaxial stress-strain response is represented by several linear segments. The effective stress versus effective strain curve is multilinear with each of the linear segments defined by a set of stress-strain points which are input by user. This model fails to produce ratcheting under uniaxial loading and predicts ratcheting under multiaxial loading

$$w_k = \frac{E - E_{TK}}{E - \frac{1-2v}{3} E_{TK}} - \sum_{i=1}^{k-1} w_i$$

$E_{Tk} = \text{tangent modulus for segment of the stress-strain curve}$

$v = \text{Poisson's ratio}$

Uniaxial yield stress, $\sigma_{yk} = \frac{1}{2(1+v)} (3E\varepsilon_k - (1 - 2v)\sigma_k)$

Total plastic strain, $d\varepsilon^{pl} = \sum_{i=1}^{N_{sv}} w_i \, d\varepsilon_i^{pl}$
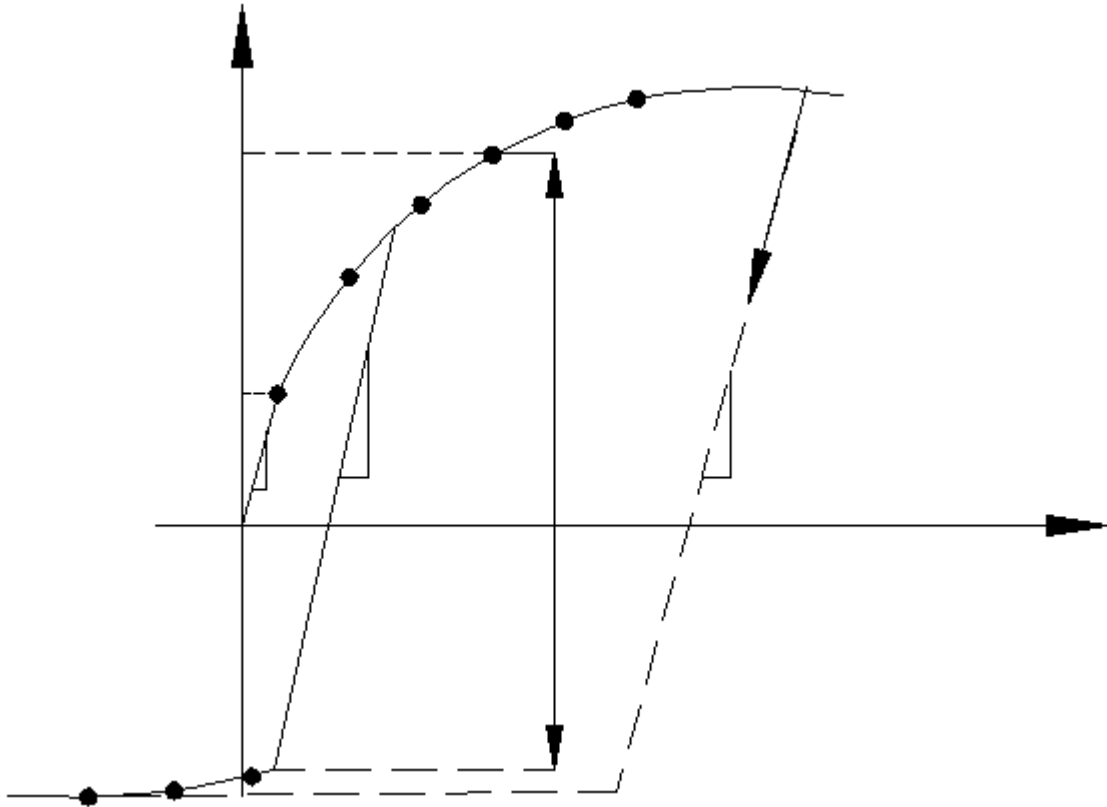
Figure 2.22 Stress vs Strain for Multilinear Kinematic Hardening (Ansys User's Guide, 1997.)

2.19.5 Chaboche Model

Chaboche proposed the nonlinear kinematic hardening model which is a rate-independent version of the kinematic hardening model. Although, this model can produce the nonlinear part of the stress-strain response reasonably well for small strain ranges, it stabilizes to a constant stress at large strain range (Chen and Jiao, 2004). The model allows the superposition of several independent back stress tensors and can be combined with any of the available isotropic hardening models. It can be useful in modeling cyclic plastic behavior such as cyclic hardening or softening and ratcheting or shakedown (Chaboche and Rousselier, 1983). This model has nine parameters ($C_1, \gamma_1, C_2, \gamma_2, C_3, \gamma_3, C_4, \gamma_4, \overline{\alpha_4}$), where $\overline{\alpha_4}$s called the threshold term. Although, with the four decomposed rules and the threshold term the Chaboche model can simulate the stress-strain and uniaxial ratcheting responses well, it still over predicts multiaxial ratcheting simulation

$$\alpha = \sum_{i=1}^{n} \alpha_i$$

$$n = \text{number of kinematic models to be supposed}$$

$$\dot{\alpha}_i = \frac{2}{3} C_i \dot{\varepsilon}^{pl} - \gamma_i \dot{\bar{\varepsilon}}^{pl} \alpha_i$$

where C_i and γ_i are user input material parameters

$$\dot{\varepsilon}^{pl} = \text{plastic strain rate}$$

$$\dot{\bar{\varepsilon}}^{pl} = \text{magnitude of plastic strain rate}$$

The elastoplastic (EP) model is time-independent; it will not reflect the strain rate effect experienced by materials at elevated temperatures. The Chaboche model needs to be fitted for different temperatures and the material parameters are then interpolated to account for the temperature effect. Chaboche explicitly accounts for isotropic hardening through means of the isotropic hardening resistance parameter (R), which describes the change in size of the yield surface. A temperature rate term is included in the Chaboche back stress formulation. The Chaboche model is fitted independently for each temperature. For Non-linear Kinematic Hardening, C is the kinematic hardening modulus, and Y is the parameter that determines the decrease of kinematic hardening. Where Y_o stands for the initial yield stress, Y_{sat} is the saturation stress, and n is the material constant that defines the change rate of the yield surface size. In order to predict the Bauschinger effect of a material subjected to cyclic loads using FE simulation, the material constitutive parameters (Y_o, Y_{sat}, n, C_i and Y_i) must be determined first.

Chapter 3

FINITE ELEMENT MODELING AND ANALYSIS OF A TUBE-SHEET STRUCTURE FOR CREEP-FATIGUE DAMAGE EVALUATION

3.1 Introduction

This chapter describes finite element modeling and analysis of a tube-sheet structure by using a commercial finite element software ABAQUS. This chapter attempts to describe the details of the geometry of the tube-sheet structure, thermal and structural loading condition, description of the thermal and material models and their associated parameters employed for analysis towards evaluating creep and fatigue damage.

3.2 Steam Generators and Geometry of its Tube-Sheet

The steam generator (SG) is one of the key components in the design of a Sodium Fast Reactor (SFR). Commercial SFRs pursued large-capacity SGs in response to the demand for economic competitiveness in its design studies. The design is complicated because of elevated-temperature effects, high pressure, and the potential for a sodium–water reaction. Therefore, adoption of a once-through sodium-heated SG with double-walled straight tube SG made of Mod. 9Cr–1Mo steel has been planned for next-generation Fast Reactors (FRs) in Japan (Ando et. al., 2014).

Among the components of SG, tube-sheets are one of the critical components which allow Sodium (Na) flow through the tubes for fast heating and cooling. Hence, a test model of the tube sheet structure was designed by JAEA considering the stress inducement mechanism in the Center Flattened Spherical Tube-Sheet (CFST). In the test model design as discussed in Ando et al (2014), particularly the stress inducement mechanism was adjusted as the superposition of the gross hoop stress and the local stress concentrated at the edges of the outer-layer holes. One of the thermal stress mechanisms in the CFST is hoop stress inducement caused by interaction between the perforated and surrounding regions of the tube-sheets. When a thermal transient occurs, the temperature of the perforated region quickly responds to the

fluid temperature through the attached numerous tubes. On the other hand, in the surrounding regions, the temperature response is slow. Consequently, the surrounding regions do not contract as much as the perforated region. Therefore, this mechanism originates from the difference in the temperature responses and induces hoop stress. The other thermal stress mechanism of tube-sheet is peak stress inducement caused by the stress concentration around the edges of the holes in the perforated region, especially located at high penetration angle. Therefore, stiffness balance of tube sheet and surrounding regions were adjusted to simulate such thermal stress inducement mechanism and the maximum penetration angle in the perforated region of the test model was limited to 300. These fundamental features are conformed to the specifications of the tube-sheets. Based on these fundamental concepts, the detailed design of the test model was defined using FEA to generate a comparable stress inducement mechanism and appropriate creep–fatigue damage in the test section of the tube sheet under the assumed thermal loading conditions. A hole diameter of 19.2 mm and a pitch of 40.0 mm with a triangle penetration pattern were also adopted in the test model design. The number of penetration layers was constrained by the maximum size of the raw material available.

Mod.9Cr–1Mo steel is a candidate material for the primary and secondary heat transport system components of the Japan sodium-cooled fast reactor (JSFR) (Aoto et. al., 2011). However, there is little hard evidence to support the structural integrity of components made of Mod.9Cr–1Mo steel under actual environments. Therefore, a thermal cyclic test was performed by Japan atomic energy agency with a tube sheet model simulating the center-flattened spherical tube sheet (CFST) (Ando et. al., 2013). The test results were summarized in the associated paper (Ando et. al., 2014), which includes the details of the tube sheet model design and the test procedure.

Geometry of such a modified Grade 91 tube-sheet structure is shown in Fig. 3.1 which test model was developed by JAEA. The experimental tube sheet component consists of tubes in which diameter of inner and outer tubes are 15.6 mm and 19 mm with thickness 1.4 mm and 1.7 mm, respectively. The center-to-center distance of tube holes are 40 mm from each other (see Fig. 3.2 and Table 3.1 for the specification). The part of the tube-sheet geometry used for FE analysis is shown in red mark in Fig. 3.1. To validate the manner of failure in the originally developed tube-sheet under cyclic thermal transients and to predict damages under combined creep and fatigue condition, the tube sheet of modified grade-91 steel is simulated in this

research. Modeling parameters, boundary and load conditions are described in the following sections.
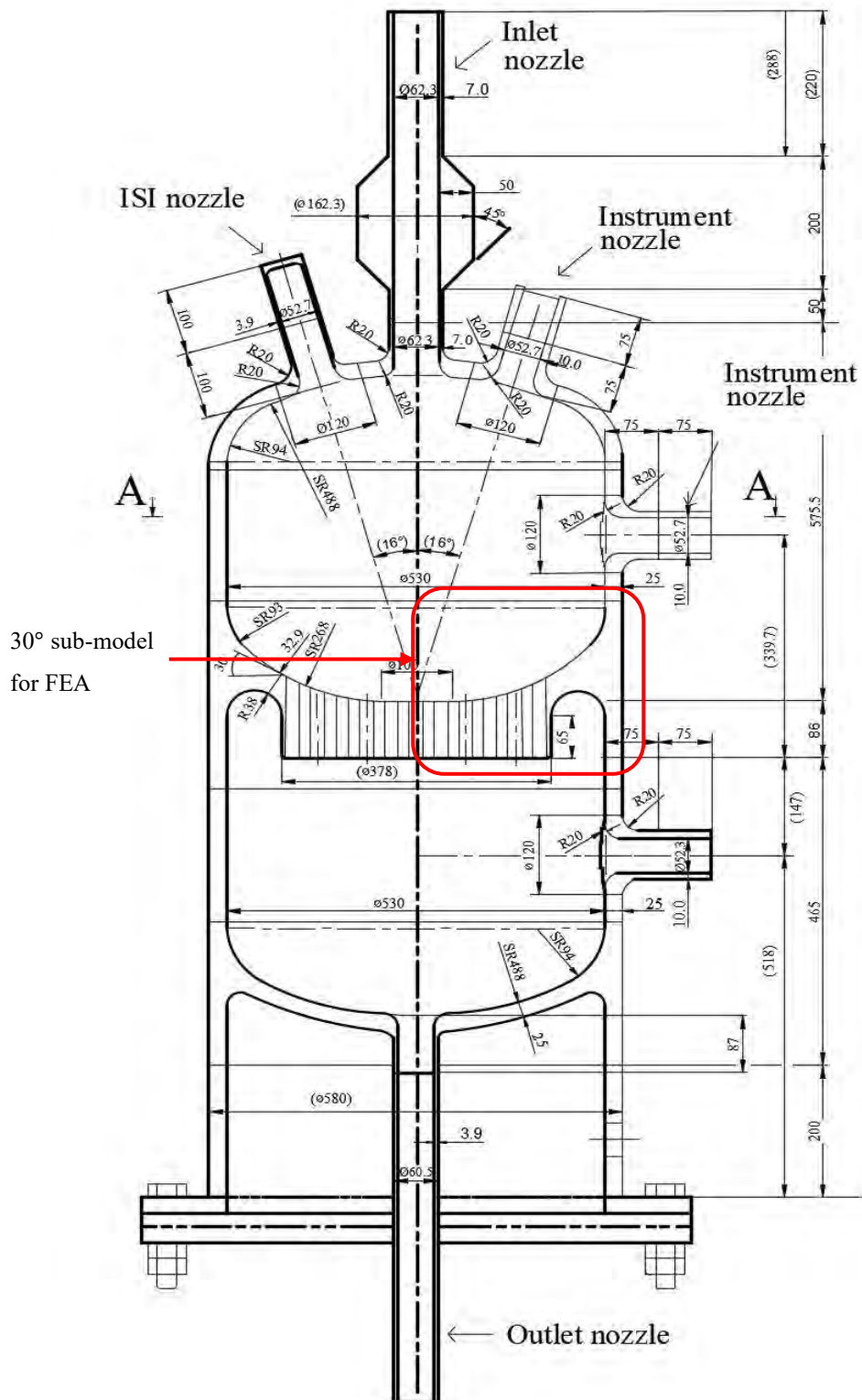
Figure 3.1 Geometry of the steam generator and its tube-sheet structure (dimensions are in mm)

(a)   (b)
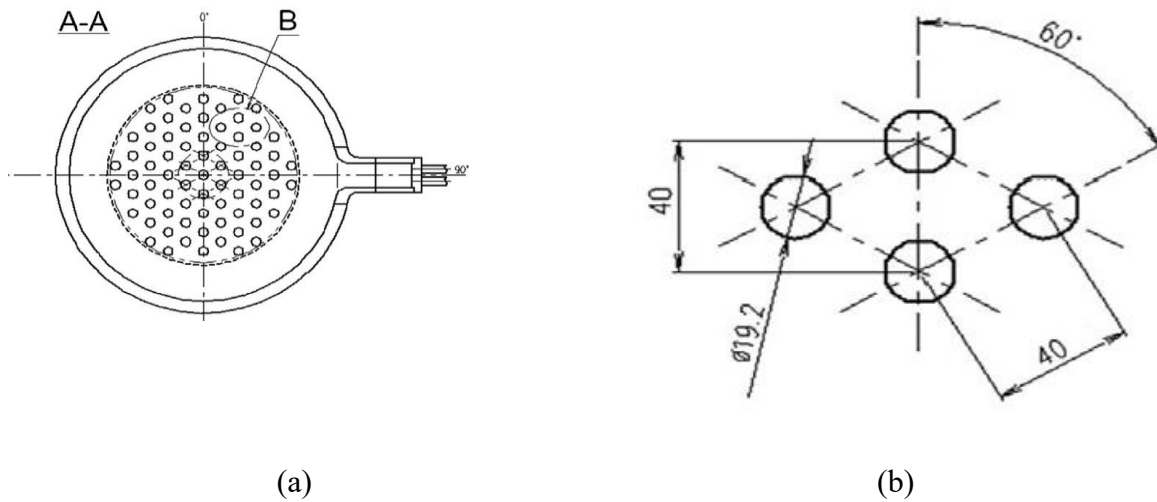
Figure 3.2 Dimensions and specifications of the holes of tube sheet

Table 3.1 Specification of CFST

Item	Unit	Value
Number of Tube		4010
Tube outer diameter (Inner tube/ outer tube)	mm	15.6/ 19.0
Tube thickness (Inner tube/ outer tube)	mm	1.4/ 1.7
Tube pitch	mm	40
Material		Mod Grade 91

3.3 Loading condition

In Heat Transfer analysis, the model has two independent loading conditions - Hot and Cold transient. For the hot transient, sodium heated to 600°C was led into the test model, and a constant sodium flow was maintained for 2 h. For the cold transient, sodium heated to 250°C was led into the test model, and a constant sodium flow was maintained for 1 h. A 2 h withhold at 600°C after the hot transient was chosen to generate creep damage due to stress relaxation (Ando et., al, 2014). A 1 h hold at 250°C after the cold transient was chosen to eliminate the temperature distributions in the test model for the following cycle. The electromagnetic pumps installed in each circuit enabled the temperature change rate of the flowing sodium to be controlled to 5°C/s (Ando et. al., 2014). As a result, it took 3 h and 140 s for a cycle. During

stress analysis, 19.6 MPa was applied. The heat transfer and stress analysis were simulated for 100 cycles with the aforementioned loading conditions.
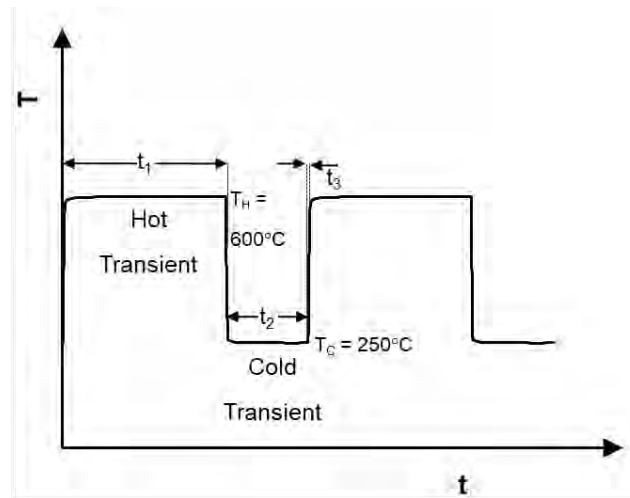
Figure 3.3 Applied thermal loading in the experiment (Na flow)

Table 3.2 Analysis cases

T_H (°C)	T_c (°C)	t_1 (sec)	t_2 (hour)	t_3 (sec) t_4(hr)		N
600	250	70	2	70	1	100

In the heat transfer analysis, the boundary condition was adiabatic on the outer surface of the test model, because the test model was covered with a thermal insulator during the test. On the inner surface, which was exposed to a heat flow due to the flowing sodium, a heat transfer element was used and the coefficient was evaluated based on the Seban–Shimazaki correlation) (Ando et. al., 2014).

3.4 Finite Element Modelling

3D FE model of the 30-degree sector of the component (red-marked location of Fig. 3.1) is developed in ABAQUS. FE mesh and boundary conditions of this test model are shown in Figs. 3.4a, 3.4b and 3.4c. Mesh optimization is performed. For heat transfer analysis, an adiabatic condition in the outer surface of the tube-sheet has been applied, and for the inner surface of the tube-sheet, thermal loads are applied following Fig. 3.3 and Table 3.2. Symmetric boundary conditions are applied in the radial surfaces for stress analysis as shown in the Fig.

57

3.4. Assuming the thermomechanical problem as sequentially coupled, heat transfer analysis is conducted first followed by the thermal stress analysis. 20-noded heat transfer element (DC3D20) and brick element with reduced integration (C3D20R) are used for the heat transfer analysis and stress analysis, respectively.

(a)

(b)   (c)
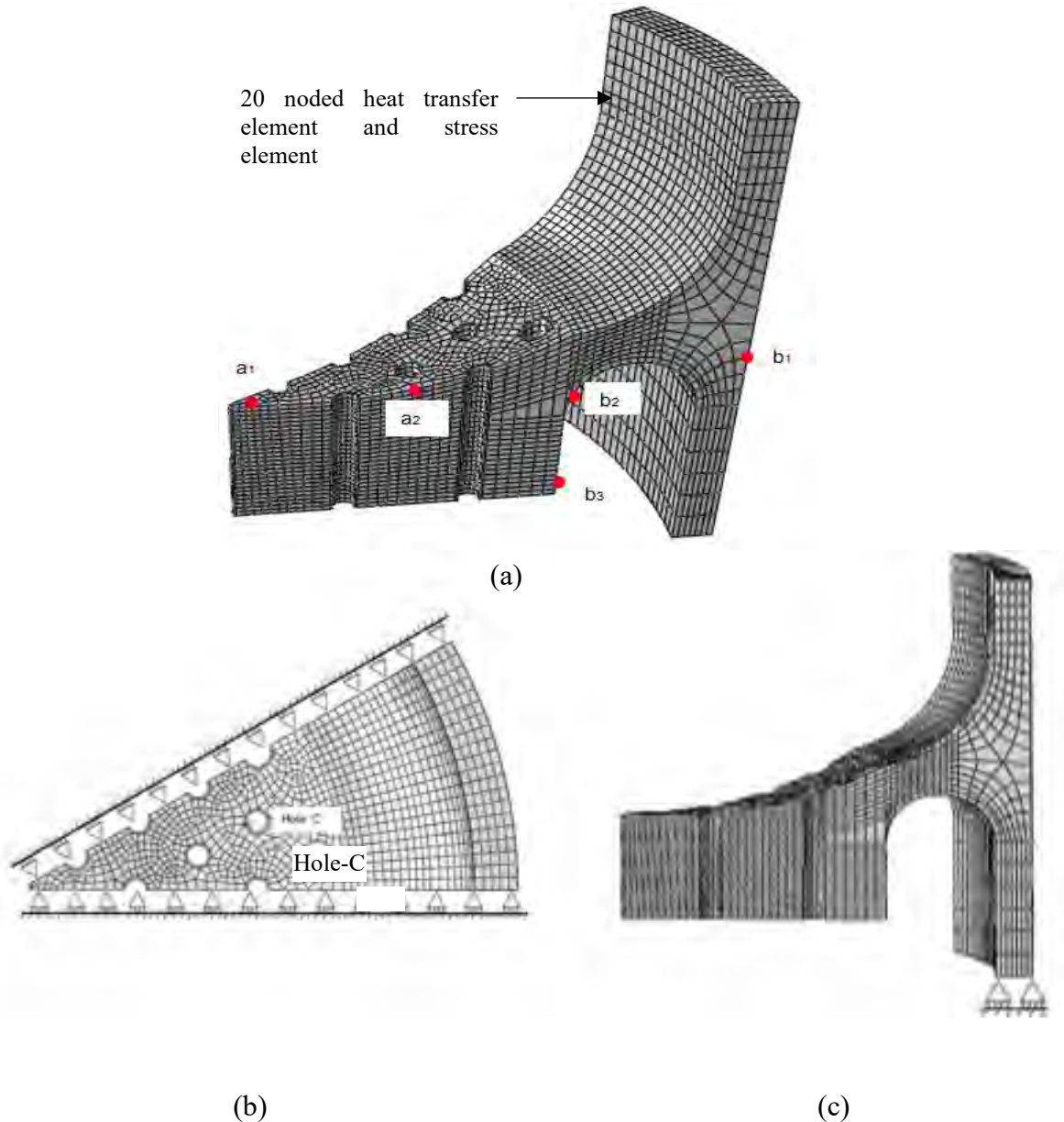
Figure 3.4 Boundary conditions and mesh for FE analysis (a) 3D FE mesh of the tube sheet, and (b and c) boundary conditions

3.5 Analysis Parameters for Heat Transfer Analysis

Finite element simulation of the thermal flow of sodium has been conducted using thermal analysis by applying the loading and boundary conditions as discussed in above section. In this

analysis procedure, thermal parameters required for are thermal film coefficient, thermal conductivity, and specific heat capacity. These parameters are described below.

3.5.1 Thermal Film Coefficient

The heat transferred by convection per unit area per degree temperature difference between the surface and the fluid is called film coefficient (Zogzas et. al., 2007). It is also called unit convection conductance or surface coefficient. The larger the coefficient, the faster heat is transferred from its source to the product being heated. Film coefficient (h) varies with temperature fluctuations and different types of coefficients were applied at different locations. In this study, these values were calculated using Eqs 3.1-3.3 for the inner holes, top surface and bottom surfaces, respectively following Seban–Shimazaki correlation (Ando et. al., 2014) where unit of h is $\frac{Kilo-Calory}{mm^2.sec.^0C}$, however, for the analysis conducted in this research, unit of h has been converted to $\frac{mW}{mm^2.K}$. Unit of T is in Degree Celsius in these equations. The film coefficients in the different regions of the tube-sheet (Fig. 3.5) are plotted in Fig. 3.6.

For inner hole: h = $8.21x10^{-13}T^2 - 3.82x\ 10^{-9}.T + 6.13x10^{-6}$ (3.1)

For top surface: h = $8.21x10^{-13}T^2 - 3.82x\ 10^{-9}.T + 2.91x10^{-6}$ (3.2)

For bottom surface: h = $8.21x10^{-13}T^2 - 3.82x\ 10^{-9}.T + 2.43x10^{-6}$ (3.3)
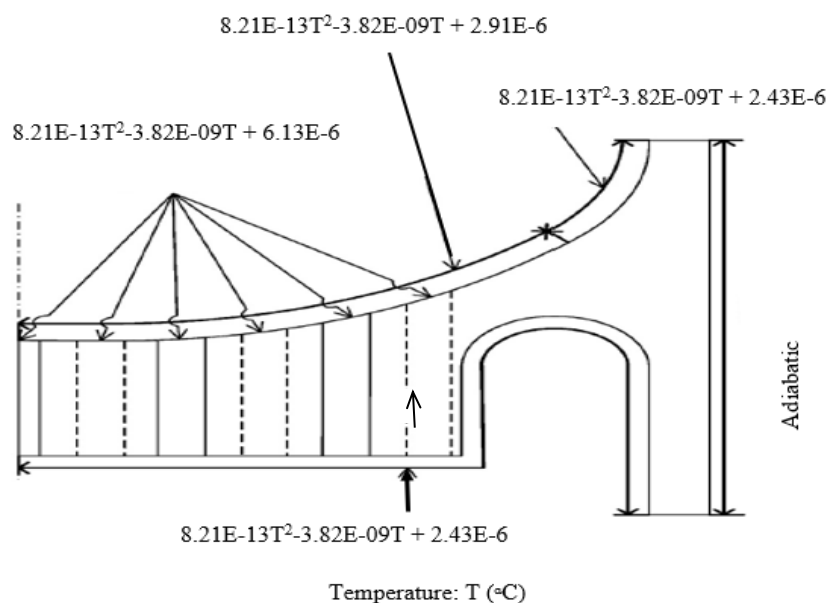
Figure 3.5 Film coefficient in the different region of the tube sheet
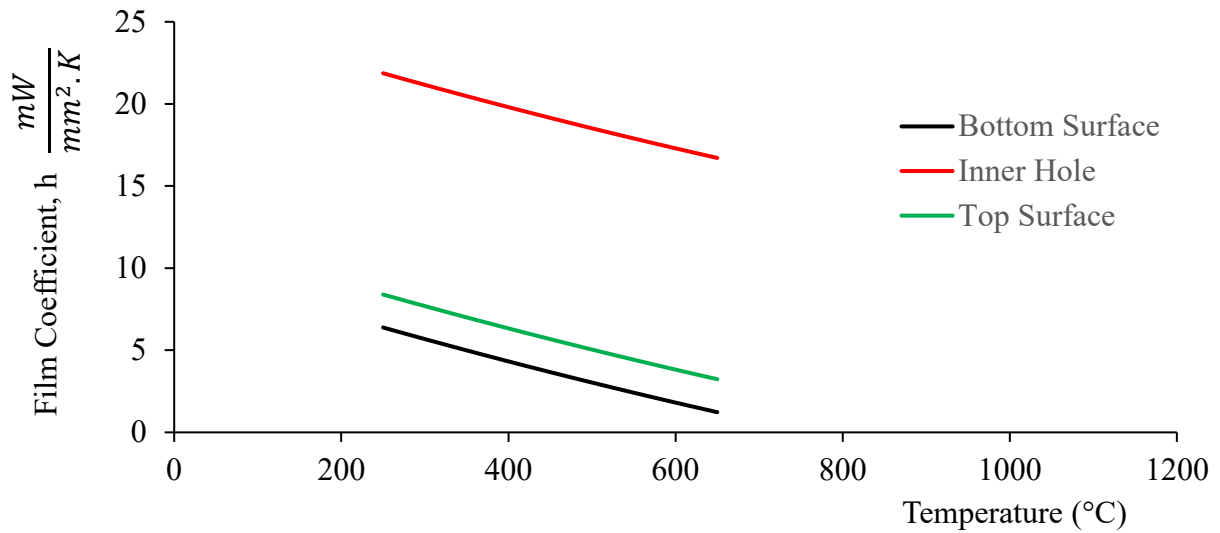
Figure 3.6 Variation of Film Coefficients with temperature in different region

3.5.2 Thermal Conductivity

The thermal conductivity of a material is a measure of its ability to conduct heat. Heat transfer occurs at a lower rate in materials of low thermal conductivity than in materials of high thermal conductivity. In this study, temperature dependent heat conductivity parameters of Grade 91 steel are collected from Ando et al., (2014), which are plotted in Fig. 3.7.
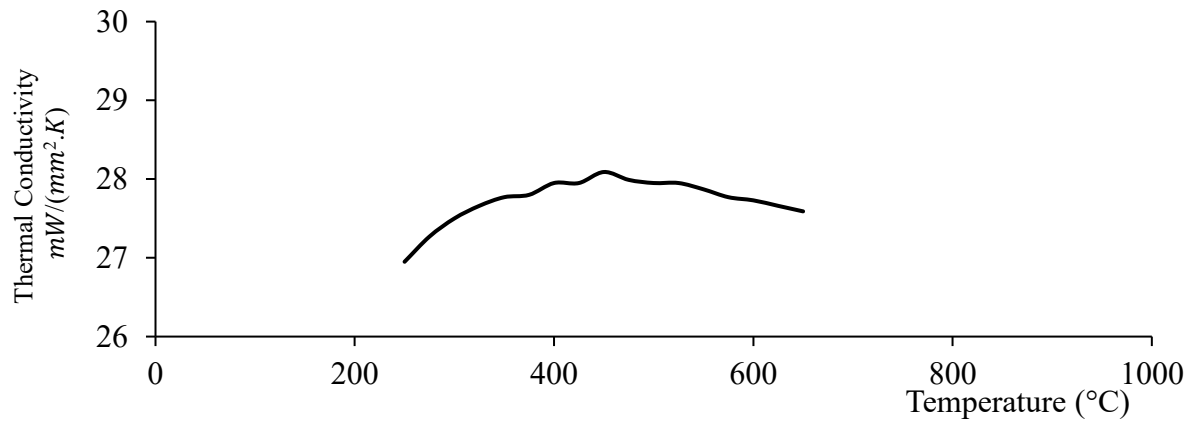
Figure 3.7 Thermal Conductivity of mod. Grade 91 steel with the variations of Temperature (Ando M. H., 2014)

3.5.3 Specific Heat

Specific heat capacity is a measure of the amount of heat energy required to change the temperature of 1 kg of a material by 1 K. Mod. Grade 91's specific heat parameters are obtained from Ando et. al., (2014) and plotted in Fig. 3.8.
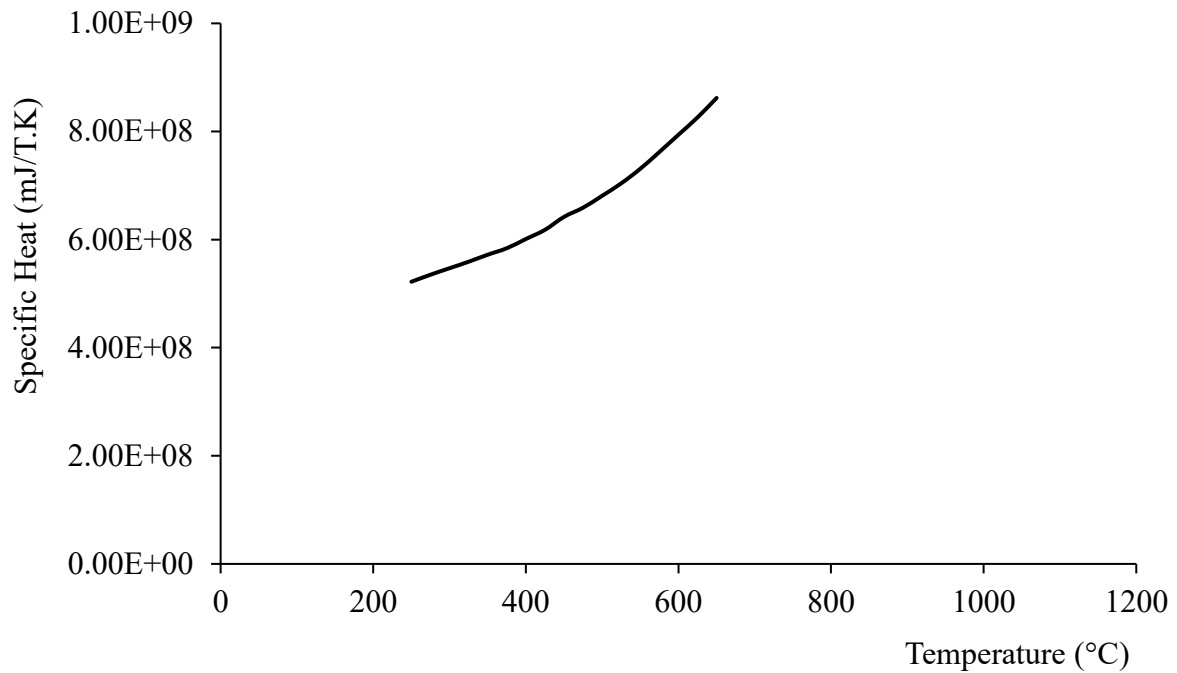
Figure 3.8 Specific Heat of mod. Grade 91 steel with the variations of Temperature) (Ando et. al., 2014)

3.6 Analysis Parameters for Stress Analysis

For the stress analysis, elastic and inelastic analysis were conducted of which material parameters are modulus of elasticity, yield stress, hardening parameters and creep parameters depending on the type of analysis. These parameters used for the stress analysis are described below.

3.6.1 Coefficient of Thermal Expansion

The coefficient of thermal expansion describes how the size of an object changes with a change in temperature. Specifically, it measures the fractional change in size per degree change

in temperature at a constant pressure, such that lower coefficients describe lower propensity for change in size. It is the tendency of matter to change its shape, area, volume, and density in response to a change in temperature, usually not including phase transitions (Ritz, 2019).

Thermal expansion generally decreases with increasing bond energy, which also has an effect on the melting point of solids, so, high melting point materials are more likely to have lower thermal expansion. In general, liquids expand slightly more than solids. The control of thermal expansion in brittle materials is a key concern for a wide range of reasons. The temperature dependent thermal expansion coefficient parameters of mod. Grade 91 steel used in this study are collected from Ando et al (2014), which are plotted in Fig. 3.9.
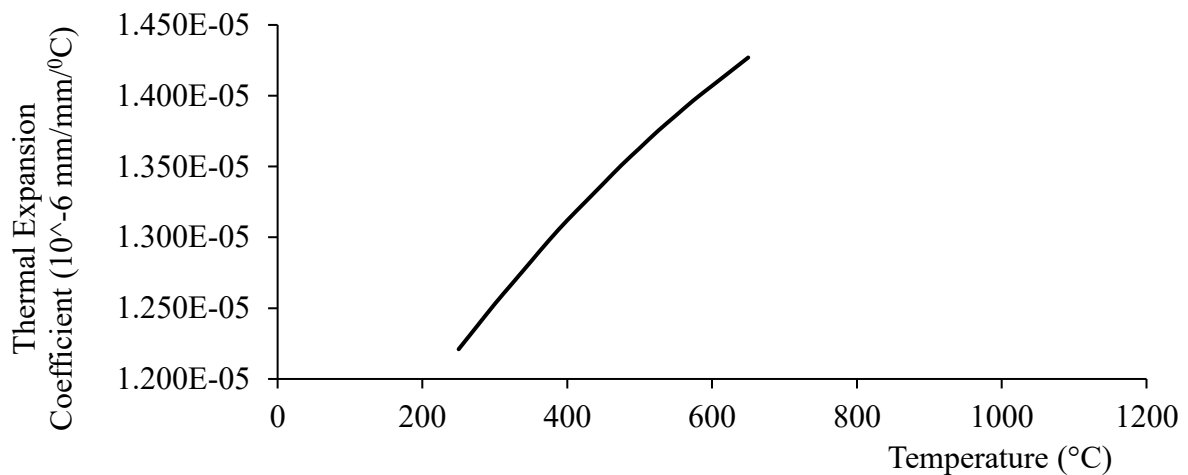
Figure 3.9 Thermal Expansion Coefficient of mod. Grade 91 steel with the variations of Temperature (Ando M. H., 2014).

3.6.2 Modulus of Elasticity

Modulus of elasticity measures the resistance of a material to elastic (recoverable) deformation under load. A stiff material has a high modulus of elasticity and changes its shape only slightly under elastic loads (e.g., diamond). A flexible material has a low modulus of elasticity and changes its shape considerably (e.g., rubbers). The temperature dependent modulus of elasticity parameters of mod. Grade 91 steel used in this study are collected from Ando et al (2014), which are plotted in Fig. 3.10.
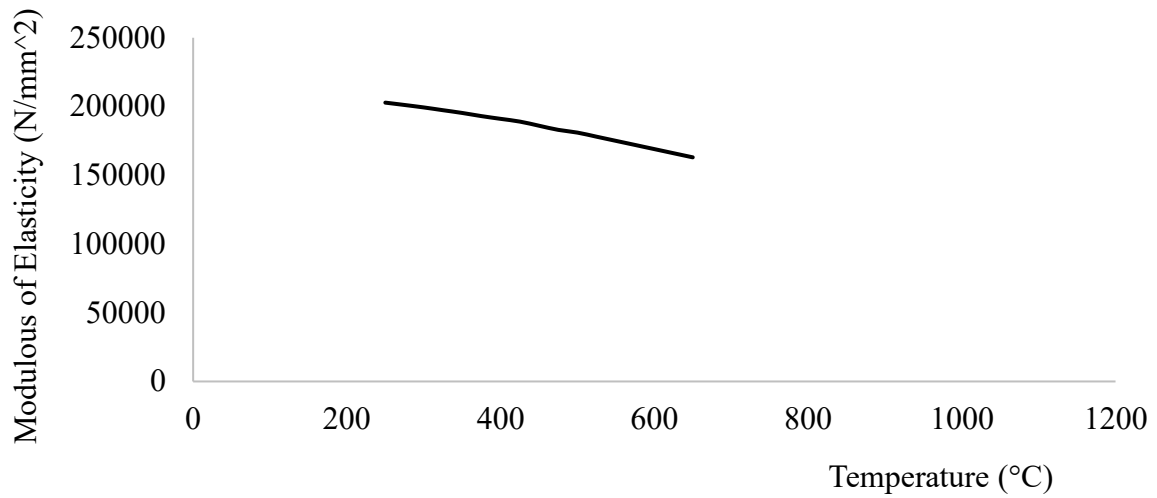
Figure 3.10 Temperature dependent Modulus of Elasticity (Ando M. H., 2014).

3.6.3 Bilinear work hardening model

The bilinear work hardening model is a constitutive model for representing plasticity which parameters are elastic modulus, tangent modulus, and the yield stress. The temperature dependent tangents with the yield stress and Poisson's ratio of mod. Grade 91 steel used in this study are listed in the Table 3.3.

Table 3.3 Bilinear Hardening Parameters (Ando et al, 2014)

Temperature (K)	Poisson's Ratio	Yield Stress (MPa)	Tangent (MPa)
523	0.300	331	20106
548	0.300	331	20106
573	0.300	331	20106
598	0.300	331	20106
623	0.300	331	20106
648	0.300	321	20333
673	0.300	310	20439
698	0.300	297	20408
723	0.300	283	20226
748	0.301	268	19879
773	0.302	252	19361
798	0.304	235	18667
823	0.306	217	17801
848	0.308	199	16771
873	0.310	181	15593
898	0.312	164	14287
923	0.314	148	12878

3.6.4 Chaboche model

The Chaboche model is a rate-independent version of nonlinear kinematic hardening model proposed by Chaboche. The model allows the superposition of several independent back stress tensors and can be combined with any of the available isotropic hardening models. The constitutive model is useful in predicting cyclic plastic behavior such as cyclic hardening, softening and ratcheting. The Chaboche kinematic hardening parameters consisting four back-stress superposition used in this study have been adopted from Islam, 2018 which are listed in Table 3.4.

Table 3.4 Chaboche kinematic hardening parameters of mod. Grade 91 steel (Islam, 2018)

Parameters	Parameters at T=250°	Parameters at T=600°
C_1(MPa)	900000	900000
C_2(MPa)	150000	120000
C_3(MPa)	90000	40000
C_4(MPa)	4500	2500
γ_1	13696	14294
γ_2	2105	1385
γ_3	602	703
γ_4	0	0
σ (MPa)	220	115
E (MPa)	185000	145000

3.6.5 Chaboche with time hardening creep parameters

Time hardening creep model parameters representing both short-term stress relaxation and long-term creep of mod. Grade 91 steel are listed in Tables 3.5 and 3.6. For Chaboche with viscous creep model, the following parameters (Table 3.5) have been used.

Table 3.5 Time hardening short-term creep-parameter (set-1)

Material Properties	Parameters at T=250°	Parameters at T=600°
Power law multiplier	$4x10^{-17}$	$1x10^{-12}$
Eq. Stress Order	3.1	3.1
Time order	-0.1	-0.1

Table 3.6 Time hardening long-term creep-parameter (set-2)

Material Properties	Parameters at T=250°	Parameters at T=600°
Power law multiplier	$4x10^{-17}$	$7x10^{-16}$
Eq. Stress Order	3.1	3.1
Time order	-0.1	-0.1

Table 3.7 Viscous Power Law Model Parameters

Material Properties	Parameters at T=250°	Parameters at T=600°
K	1100	1200
N	2	2

3.7 Methods of Creep-Fatigue Damage Analysis

For understanding creep-fatigue failure mechanism, 3D FEA of the tube-sheet structure is conducted for elastic and inelastic stress analysis using the constitutive model parameters discussed in Section 3.6. The responses from FE analyses are used for creep-fatigue interaction determination using Simple Elastic Follow-Up method (SEF), Stress Relaxation method (SRL), inelastic method incorporating Bilinear model, Chaboche model, Chaboche with time hardening creep model. Here, SEF and SRL are the simple FEM based analysis, and remaining are the inelastic FEM based analysis. Inelastic FEM analyses surpass elastic FEM analyses in accuracy of estimation. But inelastic FEM analyses need much time for calculation. Moreover, inelastic strains estimated by inelastic FEM analyses are significantly influenced by many factors such as yield condition, hardening rule, etc. Hence, they have difficulties in maintaining the unique solution. Because of that, the methods assisted by elastic FEM analyses are adopted to many codes such as JSME rules on design and constructions (Sato et al., 2011). The methods

with elastic FEM analyses have advantages in calculation time and uniqueness of results. However, inelastic strains estimated by conventional simplified methods with elastic FEM analyses are too conservative. The creep-fatigue damage simulation responses using these methods are demonstrated in Chapter 4. Procedures of these methods are discussed in this section.

3.7.1 Stress Redistribution Locus (SRL) Method

SRL means stress redistribution locus plotted from a result of elastic analysis. The SRL does not depend on constitutive equations and magnitude of loads. The stress redistribution locus method indicates a specific locus for stress concentration region through which a linkage between stress and inelastic strain can be proposed from the results of elastic Finite Element Analysis (FEA) (Maddox, 2003) . This method is expressed by following equations.

$$\mathcal{E}_t = \frac{\mathcal{E}_o}{K} \cdot [\frac{\sigma_o}{\sigma_t} + (k\text{-}1) \cdot \frac{\sigma_t}{\sigma_o}] \text{---(3.1)}$$

Where

$\mathcal{E}_o$ = Elastic peak strain, σ_o= Elastic Peak Stress

$\mathcal{E}_t$ = Total strain, σ_t= Total Stress

K= reduction factor = 1, for Neuber's hyperbola

= 1.6 for optimized case.

Again, $\mathcal{E}_t = \mathcal{E}_t$ (el) + $\mathcal{E}_t$ (p)+ $\mathcal{E}_t$ (c)

$\mathcal{E}_t$ (el) $= \frac{\sigma_t}{E}$, $\mathcal{E}_{t\,(p)}$ = Plastic strain

$$\mathcal{E}_{c(t=t')} = \dot{\varepsilon}^c \times \Delta t + \frac{\sigma_1 - \sigma_2}{E} \text{ ---(3.2)}$$

$\dot{\varepsilon}^c = A.\sigma_t^n.t^m$

Here, A=1x10^{-12}, n=3.1 and m= -0.1 for 600^{0}C (Ando et. al, 2014)

Putting the values of $\mathcal{E}_0$, σ_0, σ_t and k in Eq. 3.1, $\mathcal{E}_t$ is calculated. Using this value of $\mathcal{E}_t$ and t through trial and error, step time, Δt is calculated using equation 3.2 as follows.

$$\frac{\mathcal{E}_o}{K} \cdot [\frac{\sigma_o}{\sigma_t} + (k\text{-}1) \cdot \frac{\sigma_t}{\sigma_o}] = A.\sigma_t^n.t^m \times \Delta t + \frac{\sigma_1 - \sigma_2}{E} + \frac{\sigma_t}{E} \text{ ---(3.3)}$$

Since, a certain locus is used for predicting inelastic behavior at stress concentration region, there exists a couple of variety for applying the locus. The strain range can be calculated using the result of elastic FEA with utilization of SRL and stress-strain curve (Kaufman, 1986) with the following equation.

$$\Delta\varepsilon_t = \varepsilon_1(e) + \varepsilon_2(e) + \varepsilon_1(p) + \varepsilon_2(c)\text{--(3.4)}$$

The procedure of determination of creep-fatigue damage using the SRL method is demonstrated in Fig. 3.11. Damage calculation is shown in Chapter 4.
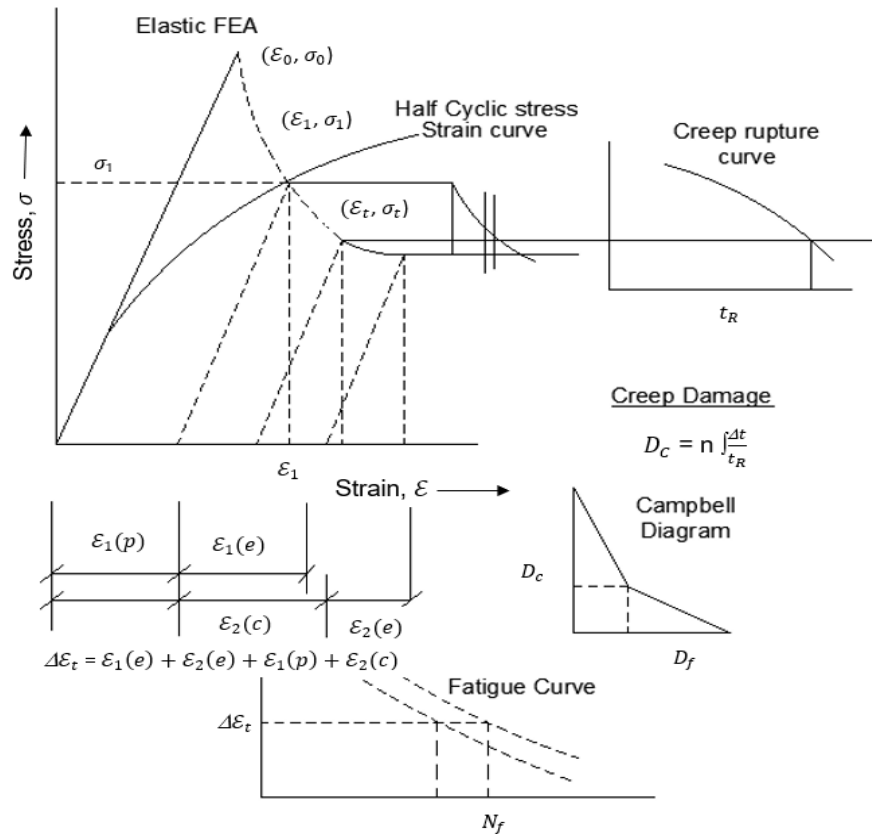
Figure 3.11 Creep and fatigue damage evaluation procedure using SRL (Ando et. al., 2014)

3.7.2 Sample Calculations in SRL Method

In the SRL Neuber method, from figure 3.12, the strain components are as follows.

$\varepsilon_1(e) = 0.2$ %, $\varepsilon_2(e) = 0.15\%$, $\varepsilon_1(p) = 0.8\%$ and $\varepsilon_2(c) = 3.25 - 0.8 = 2.45\%$

Now, using the equation no. 3.4, the total strain range in SRL- Neuber method,

$\Delta\varepsilon_t = 0.2\% + 0.15\% + 0.15\% + 2.45 = 3.6\%$

$\Delta\varepsilon_t = 3.5\%$ and for this strain range, fatigue life (N_f) is calculated as follows.

$$(Log_{10}.N_f)^{\frac{1}{2}} = A_o + A_1.Log_{10}(\Delta\varepsilon_t) + A_2\left(Log_{10}(\mathcal{E}\Delta_t)\right)^2 + A_3\left(Log_{10}(\mathcal{E}\Delta_t)\right)^3 \text{ ------------(3.5)}$$

Here,

$A_o = 1.182614 - 8.971940x10^{-10}.T^2.R^3$

$A_1 = 6.379346x10^{-1} - 3.220658x10^{-3}.R$

$A_2 = 2.065574x10^{-1} + 3.103560x10^{-11}.T^3$

$A_3 = 1.168810x10^{-2}$, R = Log_{10} ($\dot{\varepsilon}^c$)

T: Temperature in Degree Celsius (T≤650)

Figure 3.12 Strain range components in SRL- Neuber Method

Here, total strain range = 3.6% = 0.036, time, t =10940 sec, R = -5.494949278,

Temperature, T =600 degree Celsius.

A_o =1.236203527, A_1 = 0.655631952, A_2 = 0.21326109, and A_3 = - 0.0116881

Using equation no. 3.5,

$(\log_{10} N_f)^{-\frac{1}{2}}$ = 0.683086275

$\log_{10} N_f$ = 2.143131806

N_f =142.9208079 = 139 cycles (approx.)

Fatigue Damage $D_f = \frac{N_d}{N_f} = \frac{100}{139} = 0.72$ for 100 cycles

To calculate the creep damage,

$\varepsilon_o = 0.002662219$, $\sigma_o = 449.915$ MPa, stress at the beginning of inelastic range, $\sigma_1 = 220$ MPa

E= 169000 MPa at 600 degrees Celsius.

Let the stress, $\sigma_t = 219.915$ MPa,

Hence, using equation no. 3.1, total strain, $\varepsilon_t = \frac{\varepsilon_o}{K} \times [\frac{\sigma_o}{\sigma_t} + (k-1) \times \frac{\sigma_t}{\sigma_o}]$

$\varepsilon_t = \frac{0.002662219}{1} \times [\frac{449.915}{219.915} + (1-1) \times \frac{223.915}{449.915}] = 0.005446524$

Elastic strain, $\varepsilon_e = \frac{\sigma_1 - \sigma_t}{E} = \frac{220 - 219.915}{16900} = 5.02959 x 10^{-7}$

Plastic Strain, $\varepsilon_p = 0.005372$

Creep Strain, $\varepsilon_c = \varepsilon_t - \varepsilon_e - \varepsilon_p = 5.446524 x 10^{-3} - 5.02959 x 10^{-7} - 5.372 x 10^{-3}$

$$= 7.36276 x 10^{-5}$$

Using equation no. 3.3 with trial-and-error process,

$\Delta t = 1.03$ sec $= \frac{1.03}{3600} = 0.000285$ hr.

$$\log_{10}(\alpha_c. t_R) = -35.2576 + \frac{29368.9}{T+273.15} + \frac{14217.17}{T+273.15} . \log_{10} \sigma_t - \frac{5678.093}{T+273.15} . (\log_{10} \sigma_t)^2 \text{ --------(3.6)}$$

$t_R = 2.311494$ hr.

Hence, for one step, creep- damage, $D_C = \frac{t_r}{t_R} = \frac{0.000285}{2.311494} = 1.232968807 x^{-4}$

Calculation for all the steps of one cycle is attached in Appendix-A.

Calculating for all the steps of one cycle, total creep damage in SRL-Neuber method for one cycle is found as below.

$$D_c = \sum \frac{t}{t_R} = 0.00375$$

For 100 cycles, the cumulative creep damage is represented in the following figure.
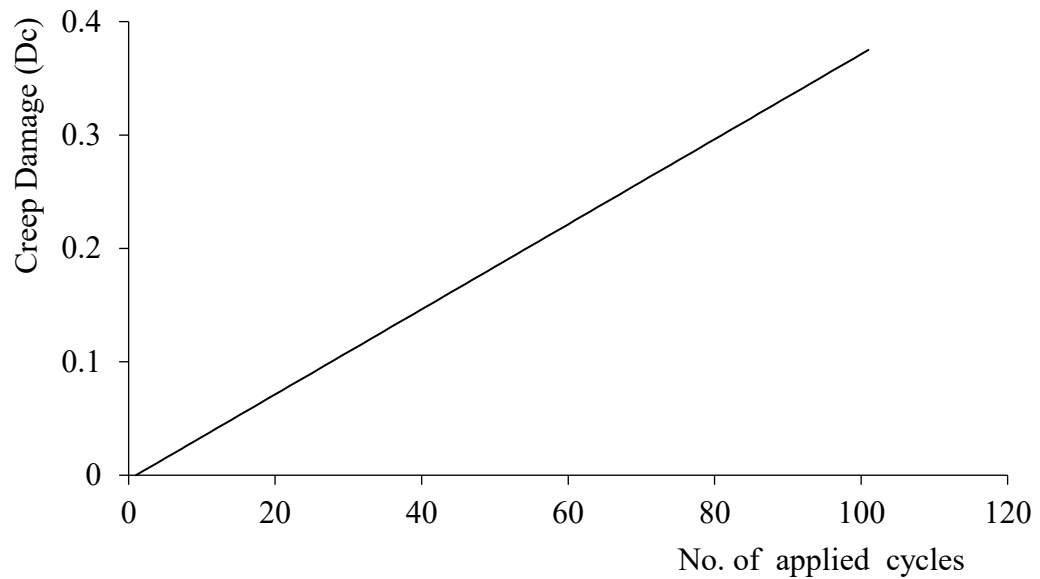
Figure 3.13 Cumulative Creep Damage of 100 Cycles in SRL Neuber method

To predict the service life, let's see the combined creep-fatigue interactions in Campbell diagram.
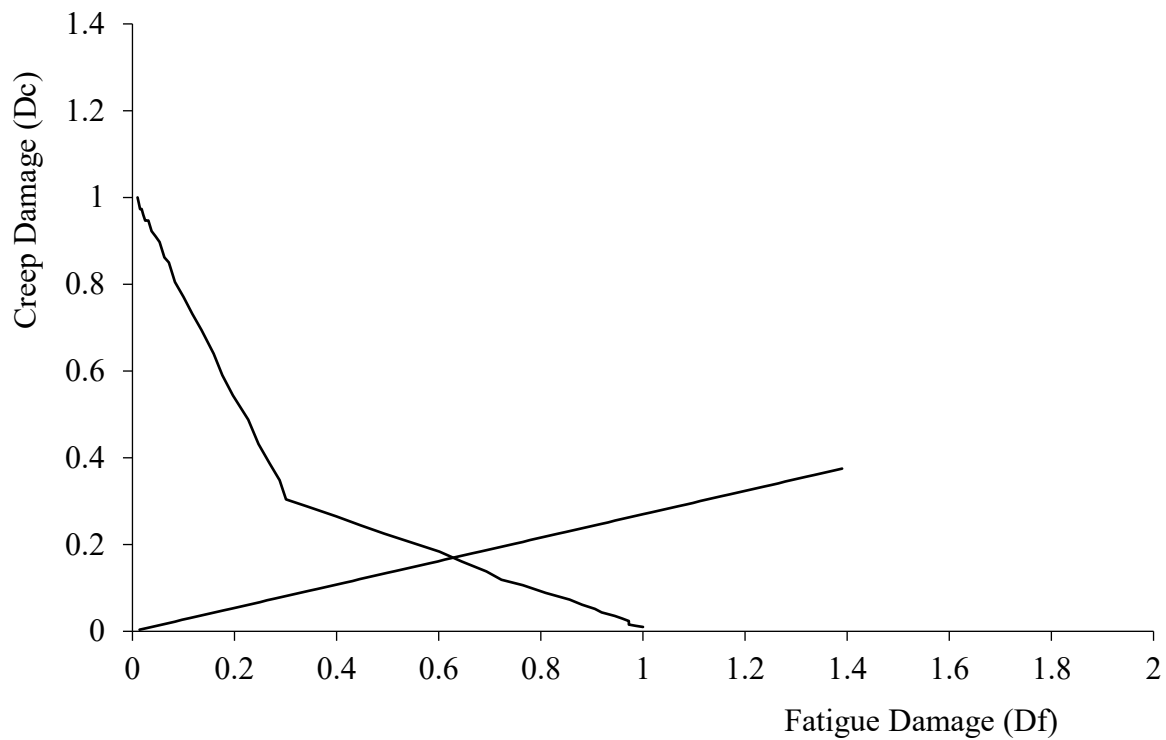
Figure 3.14 Creep-fatigue interactions of SRL-Neuber method.

From figure 3.14, the crossing point of creep-fatigue graph and Campbell diagram is found as $(D_f, D_c) = (0.6255, 0.1687)$, which indicates the damage to initiate the failure of the structure.

In this method,

Fatigue damage per cycle, $d_f = 0.0139$

Creep damage per cycle, $d_c = 0.00375$

Total damage per cycle, $d_f + d_c = 0.0177$

D-limit calculations:

If $d_c > d_f$, D limit $= \dfrac{3 \times \frac{d_c}{d_f} + 3}{7 \times \frac{d_c}{d_f} + 3}$

If $d_f > d_c$, D limit $= \dfrac{3 \times \frac{d_f}{d_c} + 3}{7 \times \frac{d_f}{d_c} + 3}$

Since, $d_f > d_c$, D-limit $= \dfrac{3 \times \frac{d_f}{d_c} + 3}{7 \times \frac{d_f}{d_c} + 3} = 0.779249448$

Therefore, predicted crossing cycles = $\frac{D-limit}{d_f + d_c}$ = 44

In the **SRL optimized case**, from figure 3.14, the strain components are as follows.

$\varepsilon_1(e) = 0.2\ \%,\ \ \varepsilon_2(e) = 0.15\%,\ \varepsilon_1(p) = 0.6\%$ and $\varepsilon_2(c) = 2.8 - 0.6 = 2.2\%$

Now, using the equation no. 3.4, the total strain range in SRL- Neuber method,

$\Delta\varepsilon_t = 0.2\% + 0.15\% + 0.6\% + 2.2 = 3.15\%$

$\Delta\varepsilon_t = 3.15\%$ and for this strain range, fatigue life (N_f) is calculated as follows.

$$(Log_{10}.N_f)^{\frac{1}{2}} = A_o + A_1.Log_{10}(\Delta\varepsilon_t) + A_2\ (Log_{10}(\mathcal{E}\Delta_t))^2 + A_3\ (Log_{10}(\mathcal{E}\Delta_t))^3 \text{---------------(3.5)}$$

Here,

$A_o = 1.182614 - 8.971940x10^{-10}.T^2.R^3$

$A_1 = 6.379346x10^{-1} - 3.220658x10^{-3}.R$

$A_2 = 2.065574x10^{-1} + 3.103560x10^{-11}.T^3$

$A_3 = 1.168810x10^{-2}, R = Log_{10}\ (\dot{\varepsilon}^\circ)$

T: Temperature in Degree Celsius (T≤650)
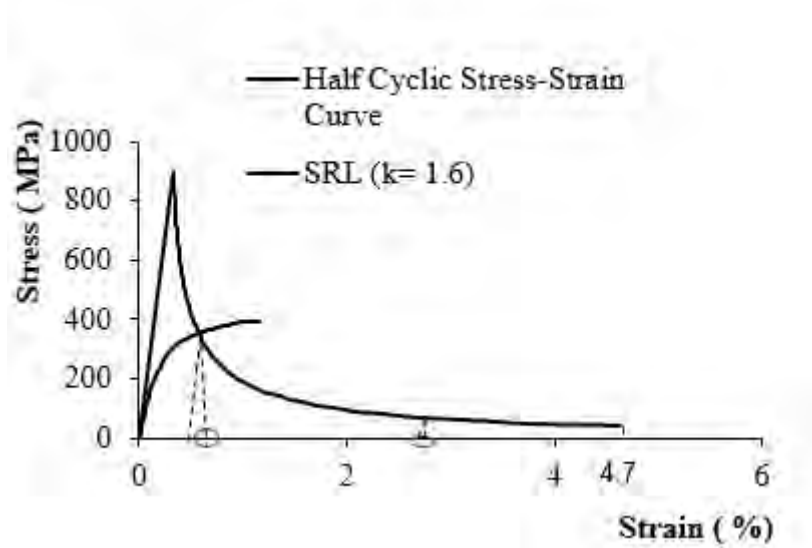
Figure 3.15 Strain range components in SRL- Optimized case.

Here, total strain range = 3.15% = 0.0315, time, t =10940 sec, R = -5.494949278,

Temperature, T =600   degree Celsius.

A_o =1.236203527, A_1 = 0.655631952, A_2 = 0.21326109, and A_3 = - 0.0116881

Using equation no. 3.5,

$(\log_{10} N_f)^{-\frac{1}{2}}$ = 0.674257477

$\log_{10} N_f$ = 2.199624043

N_f =158.3521788 = 159 cycles (approx.)

Fatigue Damage $D_f = \dfrac{N_d}{N_f} = \dfrac{100}{159} = 0.63$ for 100 cycles

To calculate the **creep damage**,

$\mathcal{E}_o$ = 0.002662219, σ_o = 449.915 MPa, stress at the beginning of inelastic range, σ_1 = 220 MPa

E= 169000 MPa at 600 degrees Celsius and K= 1.6

Let the stress, σ_t= 219.915 MPa,

Hence, using equation no. 3.1, total strain, $\mathcal{E}_t = \dfrac{\mathcal{E}_o}{K}$ x $[\dfrac{\sigma_o}{\sigma_t}$ +(k-1) x $\dfrac{\sigma_t}{\sigma_o}]$

$\mathcal{E}_t = \dfrac{0.002662219}{1}$ x $[\dfrac{449.915}{219.915}$ +(1-1) x $\dfrac{223.915}{449.915}]$ = 0.003404077

Elastic strain, $\mathcal{E}_e = \dfrac{\sigma_1 - \sigma_t}{E} = \dfrac{220 - 219.915}{16900} = 5.02959 x 10^{-7}$

Plastic Strain, $\mathcal{E}_p$ = 0.003366

Creep Strain, $\mathcal{E}_c = \mathcal{E}_t - \mathcal{E}_e - \mathcal{E}_p = 3.404077 x 10^{-3} - 5.02959 x 10^{-7} - 3.366 x 10^{-3}$

$= 3.71415 x 10^{-5}$

Using equation no. 3.3 with trial-and-error process,

Δt = 0.483 sec = $\dfrac{0.483}{3600}$ = 0.000134 hr.

$\log_{10}(\alpha_c. t_R) = -35.2576 + \dfrac{29368.9}{T+273.15} + \dfrac{14217.17}{T+273.15}.\log_{10} \sigma_t - \dfrac{5678.093}{T+273.15}.(\log_{10} \sigma_t)^2$--------(3.6)

t_R = 2.311494 hr.

Hence, for one step, creep- damage, $D_C = \dfrac{t_r}{t_R} = \dfrac{0.000134}{2.311494} = 5.79711 x^{-5}$

Calculation for all the steps of one cycle is attached in Appendix-B.

73

Calculating for all the steps of one cycle, total creep damage in SRL-Neuber method for one cycle is found as below.

$$D_c = \sum \frac{t}{t_R} = 0.002$$

For 100 cycles, the cumulative creep damage of SRL Optimized case is represented in the following figure.
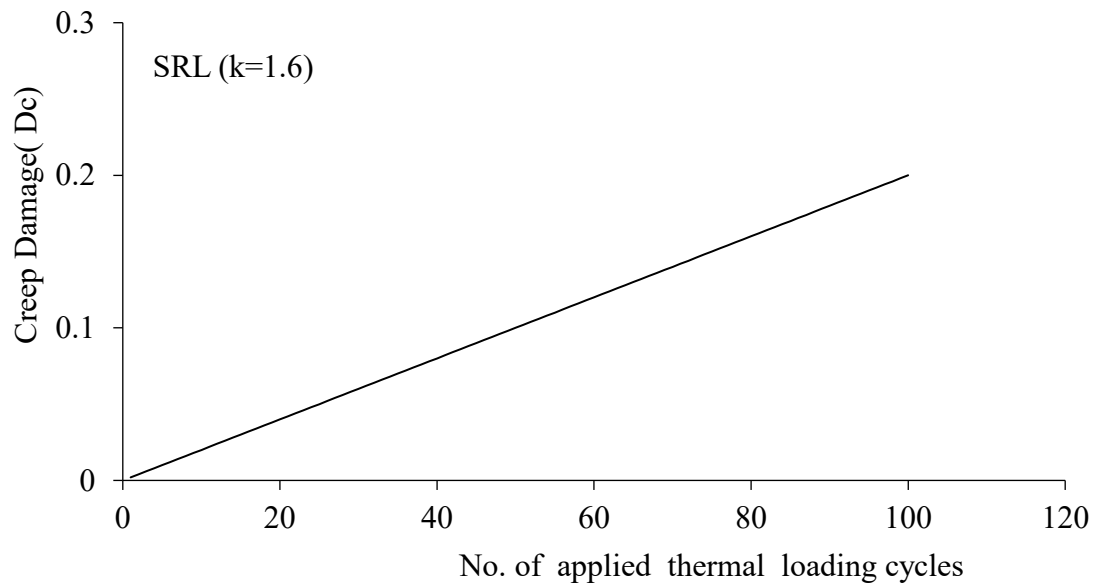
Figure 3.16 Strain range components in SRL- Optimized case.

The service life prediction using this method from combined creep-fatigue interactions is shown below in Campbell diagram.

Figure 3.17 Creep-fatigue interactions of SRL-Optimized case.

From figure 3.17, the crossing point of creep-fatigue graph and Campbell diagram is found as $(D_f, D_c) = (0.72, 0.13)$, which indicates the damage to initiate the failure of the structure.

In this method,

Fatigue damage per cycle, $d_f = 0.011$

Creep damage per cycle, $d_c = 0.00194$

Total damage per cycle, $d_f + d_c = 0.0129$

D-limit calculations:

If $d_c > d_f$, D limit $= \dfrac{3 \times \frac{d_c}{d_f} + 3}{7 \times \frac{d_c}{d_f} + 3}$

If $d_f > d_c$, D limit $= \dfrac{3 \times \frac{d_f}{d_c} + 3}{7 \times \frac{d_f}{d_c} + 3}$

Since, $d_f > d_c$,   D-limit $= \dfrac{3 \text{ x} \frac{d_f}{d_c} + 3}{7 \text{x} \frac{d_f}{d_c} + 3} = 0.833404895$

Therefore, predicted crossing cycles $= \dfrac{D-limit}{d_f + d_c} = 64$

3.7.3 Simple Elastic Follow-Up (SRL) method

The SEF method assumes that a certain ratio between the elastic strain gradient and inelastic strain gradient is available at the stress concentration region. Based on this concept, the stress and inelastic strain can be estimated from the results of elastic FEA and a stress strain curve. This concept is incorporated in the current JSME FRs code (Ando M. , 2014). The JSME FRs code applies same value of elastic follow up coefficient for estimating the strain range and creep relaxation. To put it plainly, elastic follow up coefficient applied for estimating the strain range is expressed in q_p of Eq. 3.3 and that applied for estimating the stress relaxation during the creep is expressed q_c of Eq. 3.4.

Initial stress for stress relaxation can be estimated from the result of elastic FEA using the both elastics follow up coefficient and a stress-strain curve. The stress and inelastic strain can be calculated from the crossing point of the elastic follow up line and a stress-strain curve (Dhalla, 1986,). These are expressed as follows.

$\varepsilon_t = \varepsilon_o + (1-q_p) . \dfrac{\Delta\sigma}{E}$ and $q_p = \dfrac{\Delta\varepsilon_p}{\frac{\Delta\sigma}{E}}$ ---(3.3)

In the JSME FRs code, a value of $q_p = 3$ is applied as conservative estimation for a general structure in FR components and applied an elastic perfectly plastic body with an elastic limit of 1.5 times of the design allowable stress intensity, Sm as a stress strain curve. In this study, ½ cyclic stress-strain curve was applied for a stress-strain curve (Ando et. al., 2014).

For estimating the creep damage, the stress relaxation behavior can be estimated from the equation of the creep-strain ratio using elastic follow up coefficient. It is expressed in Eq. 3.4.

$\dfrac{\Delta\sigma}{\Delta t} = \dfrac{E\varepsilon_c}{q_c}$ --(3.4)

When the method is applied to strain range controlled uniaxial creep-fatigue test, elastic follow up coefficient, q_c is equal to 1, because there is any different stiffness in gauge region. The JSME FRs code defined the elastic follow up coefficient equal to 3 for considering the different stiffness and triaxiality effect. In actual components, a structure has its own elastic follow up coefficients q_p and q_c, which depend on the component configurations and stress conditions. In this study, a certain value $q_p = q_c = 3$ was applied to the SEF (Ando et. al., 2014). Damage calculation is shown in Chapter 4.

3.7.4 Sample Calculations in SEF Method

With the procedure of the figure 3.11 and equation no. 3.4, the strain range is calculated below using the figure 3.18.
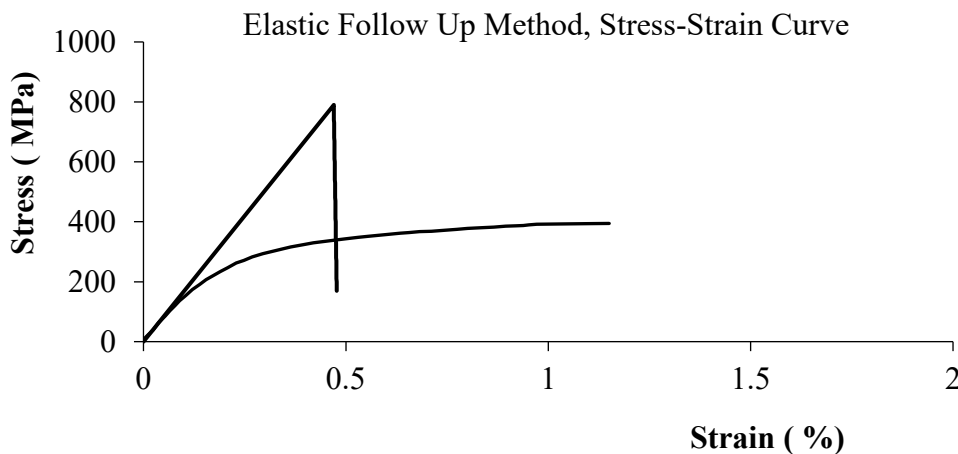
Figure 3.18 Stress Strain relation in SEF method

$\Delta\varepsilon_t = 0.49\% + 0.49\% = 0.98\%$

$\Delta\varepsilon_t = 0.98\ \%$ and for this strain range, fatigue life (N_f) is calculated as follows.

$$(Log_{10}.N_f)^{\frac{1}{2}} = A_o + A_1.Log_{10}(\Delta\varepsilon_t) + A_2\ (Log_{10}(\varepsilon\Delta_t))^2 + A_3\ (Log_{10}(\varepsilon\Delta_t))^3 \text{ ------------(3.5)}$$

Here,

$A_o = 1.182614 - 8.971940x10^{-10}.T^2.R^3$

$A_1 = 6.379346x10^{-1} - 3.220658x10^{-3}.R$

$A_2 = 2.065574x10^{-1} + 3.103560x10^{-11}. T^3$

$A_3 = 1.168810x10^{-2}$, R $= Log_{10}(\dot{\varepsilon}^c)$

T: Temperature in Degree Celsius (T≤650)

Here, total strain range = 0.98% = 0.0098, time, t =10940 sec, R = -5.494949278,

Temperature, T =600 degree Celsius.

A_o =1.236203527, A_1 = 0.655631952, A_2 = 0.21326109, and A_3 = - 0.0116881

$(\log_{10} N_f)^{-\frac{1}{2}}$ = 0.603699644

$\log_{10} N_f$ = 2.743836072

N_f = 554.4164039 = 555 cycles (approx.)

Fatigue Damage $D_f = \dfrac{N_d}{N_f} = \dfrac{100}{555}$ = 0.18 for 100 cycles

To calculate the creep damage,

Here, σ_{t1} = 302.075 MPa

Let, step time-1 = 0.00011 and step time-2 = 0.00013.

Therefore, Δt = 0.00013 - 0.00011 = $2.0x10^{-5}$ sec.

$\dfrac{\Delta\sigma}{\Delta t}$ = E $\dot{\varepsilon}^c$ /q = E x Axσ_t^n/q, Hence, $\Delta\sigma$ = Δt x E x Axσ_1^n/q = $2.0x10^{-5}$ x 169000 x $302.075^{12.4}$

Stress in the next point, σ_{t2} = σ_1 - $\Delta\sigma$

$$= 449.915 - 2.0x10^{-5} \text{ x } 169000 \text{ x } 302.075^{12.4}$$

$$= 301.9301877 \text{ MPa}$$

t_R = A' x $\sigma_{t2}^{-n'}$ = $2.0x10^{26}$ x $301.93^{-10.7}$ = 0.568898339 hr.

D_C = d(tr)/T$_R$ = $\dfrac{0.00013-0.00011}{0.568898}$ = 0.000027

Creep damage for all the steps of one cycle is attached in **Appendix-C.**

Total creep damage for one cycle is 0.0367.

Cumulative creep damage for 100 cycle is presented in figure 3.19
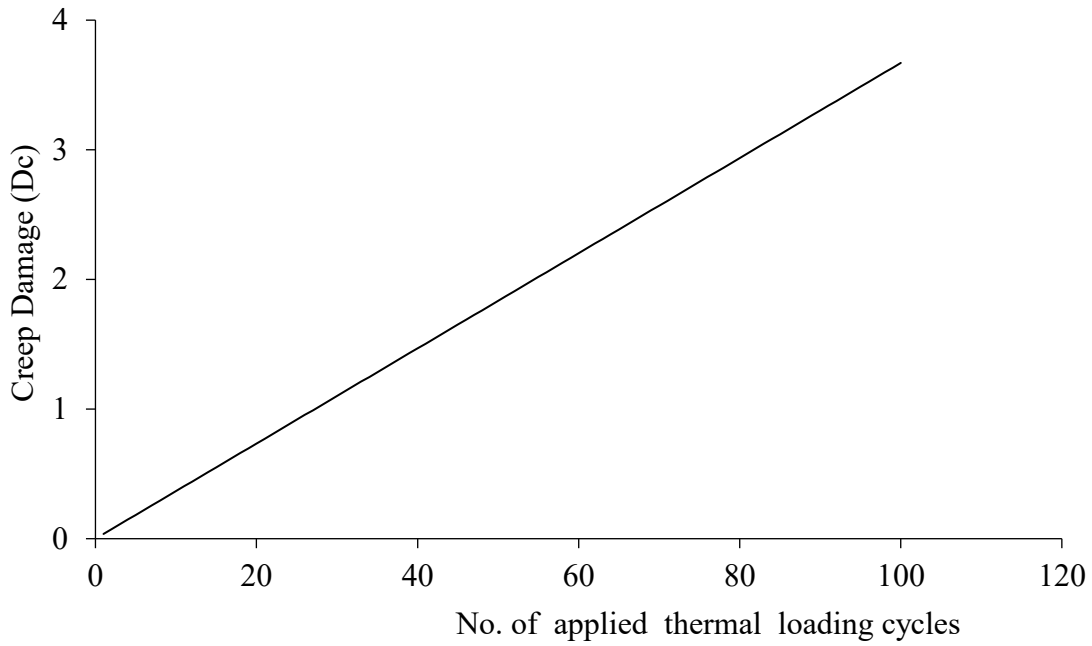
Figure 3.19 Cumulative creep damage for 100 cycles in SEF method

The service life prediction using this method from combined creep-fatigue interactions is shown below in Campbell diagram.
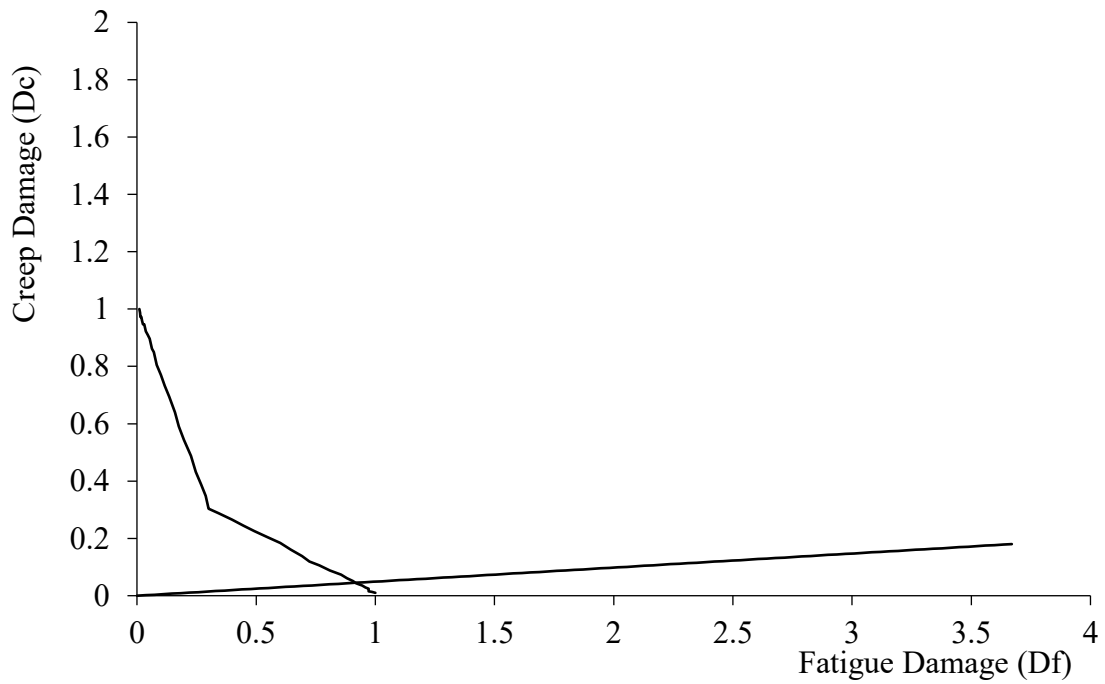
Figure 3.20 Creep-fatigue interactions of SEF method.

79

From figure 3.20, the crossing point of creep-fatigue graph and Campbell diagram is found as $(D_f, D_c) = (0.954, 0.0468)$, which indicates the damage to initiate the failure of the structure. In this method,

Fatigue damage per cycle, $d_f = 0.0367$

Creep damage per cycle, $d_c = 0.0018$

Total damage per cycle, $d_f + d_c = 0.0385$

D-limit calculations:

If $d_c > d_f$, D limit $= \dfrac{3 \times \frac{d_c}{d_f} + 3}{7 \times \frac{d_c}{d_f} + 3}$

If $d_f > d_c$, D limit $= \dfrac{3 \times \frac{d_f}{d_c} + 3}{7 \times \frac{d_f}{d_c} + 3}$

Since, $d_f > d_c$, D-limit $= \dfrac{3 \times \frac{d_f}{d_c} + 3}{7 \times \frac{d_f}{d_c} + 3} = 0.941320293$

Therefore, predicted crossing cycles $= \dfrac{D-limit}{d_f + d_c} = 24$

3.7.5 Inelastic Analysis

The modeling of mechanical properties of materials and structures is a complex and wide-ranging subject. In some applications, it is sufficient to assume that the material remains elastic, i.e., that the deformation process is fully reversible and the stress is a unique function of strain. However, such a simplified assumption is appropriate only within a limited range, and in general must be replaced by a more realistic approach that considers the inelastic processes such as plastic yielding or cracking (Jirásek and Bazant, 2002). In such cases, inelastic analysis should be carried out for predicting more realistic component behavior. In this study, creep-fatigue damage evaluation is carried out by employing inelastic stress analysis. Strain data from the analysis is used for fatigue damage prediction. This strain is calculated using the following steps (Koo, 2014).

Step 1: Calculate all strain components for each point, i, in time for entire design lifetime.

Step 2: Select a point when conditions are at an extreme for the cycle, either maximum or minimum. Refer to this time point by a subscript o.

Step 3: Calculate the history of the change in strain components by subtracting the values at the time, o, from the corresponding components at each point in time, *i,* during entire deign life time.

$\Delta\mathcal{E}_{xi} = \mathcal{E}_{xi} - \mathcal{E}_{xo}$, $\Delta\mathcal{E}_{yi} = \mathcal{E}_{yi} - \mathcal{E}_{yo}$, $\Delta\mathcal{E}_{zi} = \mathcal{E}_{zi} - \mathcal{E}_{zo}$ etc.

Step 4: Calculate the equivalent strain range for each point in time as:

$$\Delta\mathcal{E}_{equi.,i} = \frac{\sqrt{2}}{2(1+\upsilon)} \cdot \sqrt{[(\Delta\mathcal{E}_{xi} - \Delta\mathcal{E}_{yi})^2 + (\Delta\mathcal{E}_{yi} - \Delta\mathcal{E}_{zi})^2 + (\Delta\mathcal{E}_{zi} - \Delta\mathcal{E}_{xi})^2 + \frac{3}{2}(\Delta\gamma_{xyi}^2 + \Delta\gamma_{yzi}^2 + \Delta\gamma_{zxi}^2]} ----(3.5)$$

Where, $v = 0.3$ for Elastic Analysis,

$= 0.5$ for Inelastic Analysis.

Step 5: Define, $\Delta\mathcal{E}_{max}$ = Maximum of $(\Delta\mathcal{E}_{equi.,i})$

Step 6: Find allowable number of cycles, N_f from the following procedures (Onizawa et.al, 2013).

$$(Log_{10}.N_f)^{\frac{1}{2}} = A_o + A_1.Log_{10}(\Delta\mathcal{E}_t) + A_2 (Log_{10}(\mathcal{E}\Delta_t))^2 + A_3 (Log_{10}(\mathcal{E}\Delta_t))^3 --------------(3.6)$$

Here,

$A_o = 1.182614 - 8.971940x10^{-10}.T^2.R^3$

$A_1 = 6.379346x10^{-1} - 3.220658x10^{-3}.R$

$A_2 = 2.065574x10^{-1} + 3.103560x10^{-11}.T^3$

$A_3 = 1.168810x10^{-2}$, $R = Log_{10}(\dot{\varepsilon}^c)$

T: Temperature in Degree Celsius (T≤650)

$\mathcal{E}_t$: Total strain range (mm/mm)

N_f = Cycles to cause fatigue failure.

Finally, fatigue damage is determined from $\boldsymbol{D_f} = \frac{N_d}{N_f}$, where N_d = Applied cycles, $\boldsymbol{N_f}$ = Number of cycles to cause failure.

To determine the creep damage, creep-rupture time is evaluated. For short region time, creep rupture time is calculated from the following equation (Onizawa, 2013).

$$\log_{10}(\alpha_c.t_R) = -35.2576 + \frac{29368.9}{T+273.15} + \frac{14217.17}{T+273.15}.\log_{10}\sigma_t - \frac{5678.093}{T+273.15}.(\log_{10}\sigma_t)^2 \text{ -------(3.7)}$$

Where α_c = Time parameter for the creep rupture time=3, t_R= Rupture time.

Time fraction rule is applied to determine creep damage (Ando et. al., 2014), from the Eq. 3.8.

$$D_c = \sum \frac{t}{t_R}. \text{ --(3.8)}$$

3.7.6 Sample Calculations in Bilinear Method

$\Delta\varepsilon_{xi} = \varepsilon_{xi} - \varepsilon_{xo} = 0.00000629612 - 0 = 0.00000629612$

$\Delta\varepsilon_{yi} = \varepsilon_{yi} - \varepsilon_{yo} = -0.00000284317 - 0 = -0.00000284317$

$\Delta\varepsilon_{zi} = \varepsilon_{zi} - \varepsilon_{zo} = -0.00000107561 - 0 = -0.00000107561$

$\Delta\gamma_{xyi} = 2 \text{ x } (-0.0000016687)$

$\Delta\gamma_{yzi} = 2 \text{ x } (-0.0000000301125)$

$\Delta\gamma_{zxi} = 2 \text{ x } (-0.00000158661)$

Using equation no. 3.5, the equivalent strain is found as below.

$\Delta\varepsilon_{equi.,i} = 0.0000062$

Following the similar procedure and calculating the equivalent strains for all the steps, the maximum equivalent strains is taken to get the strain range. In this process, the strain range,

$\Delta\varepsilon_t = \Delta\varepsilon_{max} = $ Maximum of $(\Delta\varepsilon_{equi.,i}) = 0.007342$

Now using the equation no. 3.6, the fatigue failure life is calculated as below.

$A_o = 1.236203527$, $A_1 = 0.655631952$, $A_2 = 0.21326109$, and $A_3 = -0.0116881$

$(\log_{10} N_f)^{-\frac{1}{2}} = 0.583569629$

$\log_{10} N_f = 2.93639609$

$N_f = 863.7659697 = 864$ cycles (approx.)

Fatigue damage, $D_f = \frac{N_d}{N_f} = \frac{1}{864} = 0.001157721$ for 1cycle

Similarly calculating the fatigue damage for all the 100 cycles and adding them, the total fatigue damage, $D_f = 0.057178813$

The cumulative fatigue damage for all the 100 cycles can be represented as follows.
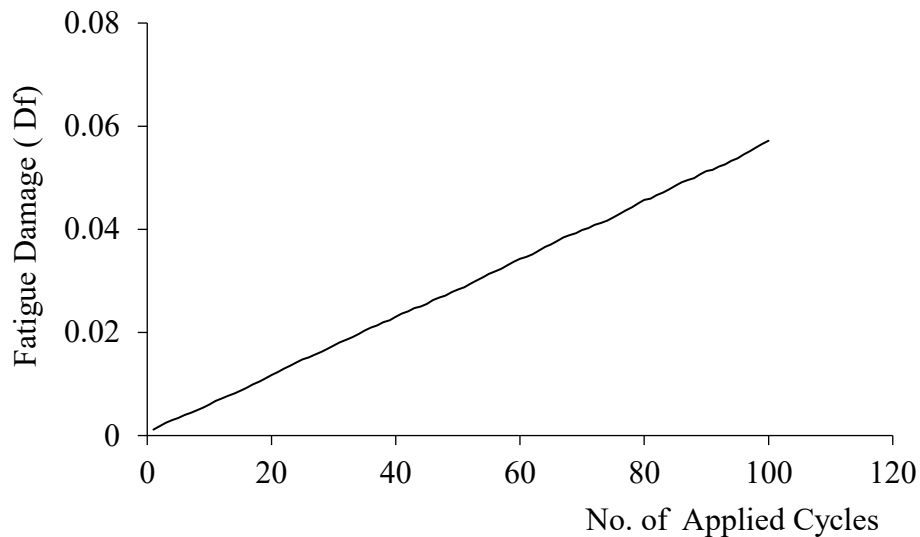
Figure 3.21 Cumulative fatigue damage for 100 cycles in Bilinear method

To calculate the creep damage,

Let step time, $t_r = 0.0874788$ sec. $= 2.42997x10^{-5}$ hr.

For this step, Von Misses stress, $\sigma_t = 237.131$ MPa

Using equation no. 3.7, the creep rupture time is calculated below.

$t_R = 51.52$ hr.

By applying equation no. 3.8, the creep damage for this step is found as follows.

$$D_c = \frac{t}{t_R} = \frac{2.42997x10^{-5}}{51.52} = 4.71655x10^{-7}$$

Applying this time fraction formula, the creep damage for all the steps of the 1st cycle is 0.00904774

Calculation of total creep damage for one cycle is attached in **Appendix-D.**

The cumulative creep damage for 100 cycles is 0.767172, which is represented in the figure 3.22.

Figure 3.22 Cumulative creep damage for 100 cycles in Bilinear method

The service life prediction using this method from combined creep-fatigue interactions is shown below in Campbell diagram.
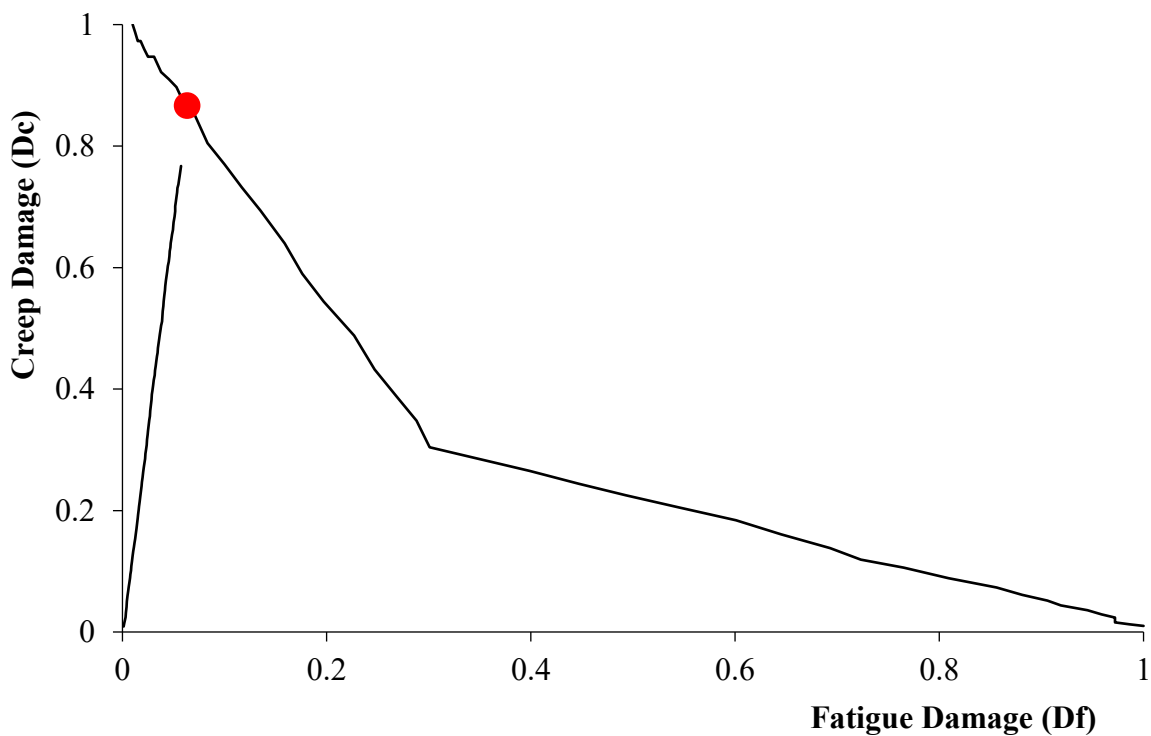
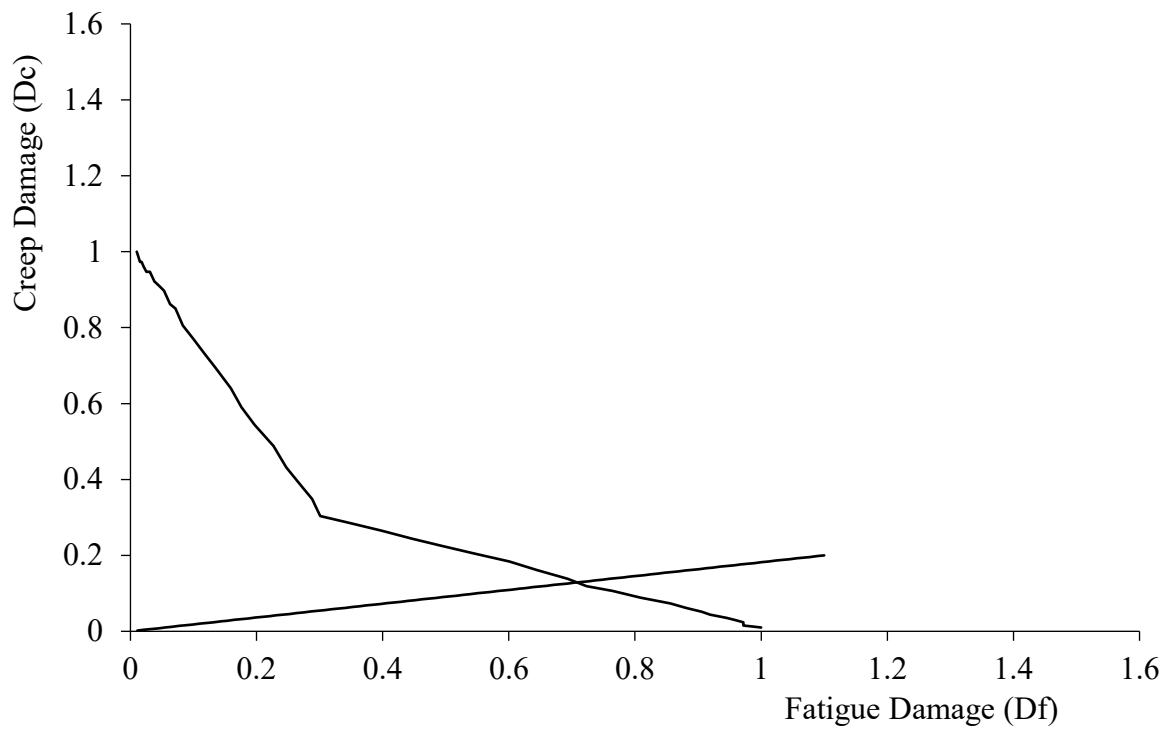**Figure 3.23** Creep-fatigue interactions of Bilinear method in the Campbell diagram

From figure 3.23, the crossing point of creep-fatigue graph and Campbell diagram is found as $(D_f, D_c) = (0.0715, 0.85)$, which indicates the damage to initiate the failure of the structure. In this method,

Fatigue damage per cycle, $d_f = 0.0005740279$

Creep damage per cycle, $d_c = 0.00767171517$.

Total damage per cycle, $d_f + d_c = 0.00825$

D-limit calculations:

If $d_c > d_f$, D limit $= \dfrac{3 \times \frac{d_c}{d_f} + 3}{7 \times \frac{d_c}{d_f} + 3}$

If $d_f > d_c$, D limit $= \dfrac{3 \times \frac{d_f}{d_c} + 3}{7 \times \frac{d_f}{d_c} + 3}$

Since, $d_c > d_f$, D- limit $= \dfrac{3 \times \frac{d_c}{d_f} + 3}{7 \times \frac{d_c}{d_f} + 3} = 0.915063713$

Therefore, predicted crossing cycles $= \dfrac{D-limit}{d_f + d_c} = 110$

3.7.7 Sample Calculations in Chaboche Model

$\Delta \varepsilon_{xi} = \varepsilon_{xi} - \varepsilon_{xo} = 0.0000117426 - 0 = 0.0000117426$

$\Delta \varepsilon_{yi} = \varepsilon_{yi} - \varepsilon_{yo} = 0.00000179167 - 0 = 0.00000179167$

$\Delta \varepsilon_{zi} = \varepsilon_{zi} - \varepsilon_{zo} = -0.00000044016 - 0 = -0.00000044016$

$\Delta \gamma_{xyi} = 2 \times (-0.00000113149)$

$\Delta \gamma_{yzi} = 2 \times (-0.00000137816)$

$\Delta \gamma_{zxi} = 2 \times (0.0000103513)$

Using equation no. 3.5, the equivalent strain is found as below.

$\Delta \varepsilon_{equi.,i} = 0.0000149$

Following the similar procedure and calculating the equivalent strains for all the steps, the maximum equivalent strains is taken to get the strain range. In this process, the strain range for one cycle,

$\Delta \mathcal{E}_t = \Delta \mathcal{E}_{max}$ =Maximum of $(\Delta \mathcal{E}_{equi.,i})$ =0.009028

Now using the equation no. 3.6, the fatigue failure life is calculated as below.

A_o =1.236203527, A_1 = 0.655631952, A_2 = 0.21326109, and A_3 = - 0.0116881

$(\log_{10} N_f)^{-\frac{1}{2}}$ = 0.598241492

$\log_{10} N_f$ = 2.79413212

N_f = 622.4896288 = 823 cycles (approx.)

Fatigue damage, $D_f = \frac{N_d}{N_f} = \frac{1}{623}$ = 0.001606452 for 1cycle

Similarly calculating the fatigue damage for all the 100 cycles and adding them, the total fatigue damage, D_f = 0.076674

The cumulative fatigue damage for all the 100 cycles can be represented as follows.
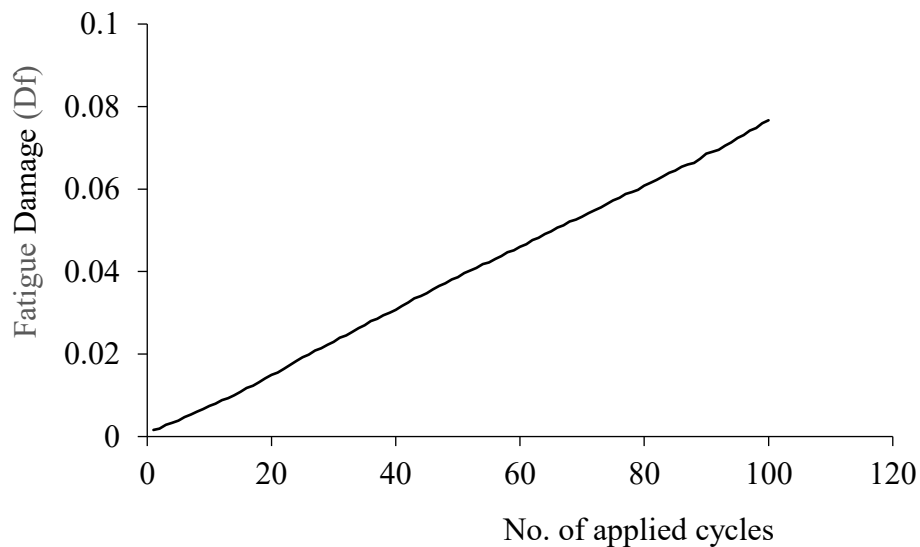
Figure 3.24 Cumulative fatigue damage for 100 cycles in Chaboche Model

To calculate the creep damage,

Let step time, t_r = 0.0258493 sec. = $7.18 x 10^{-6}$ hr.

86

For this step, Von Misses stress, σ_t = 220.094 MPa

Using equation no. 3.7, the creep rupture time is calculated below.

t_R = 83.068 hr.

By applying equation no. 3.8, the creep damage for this step is found as follows.

$$D_c = \frac{t}{t_R} = \frac{7.18x10^{-6}}{83.068} = 8.64x10^{-8}$$

Applying this time fraction formula, the creep damage for all the steps of the 1st cycle is 0.087127108

Calculation of total creep damage for one cycle is attached in **Appendix-E.**

The cumulative creep damage for 100 cycles is 1.450672, which is represented in the figure 3.25.
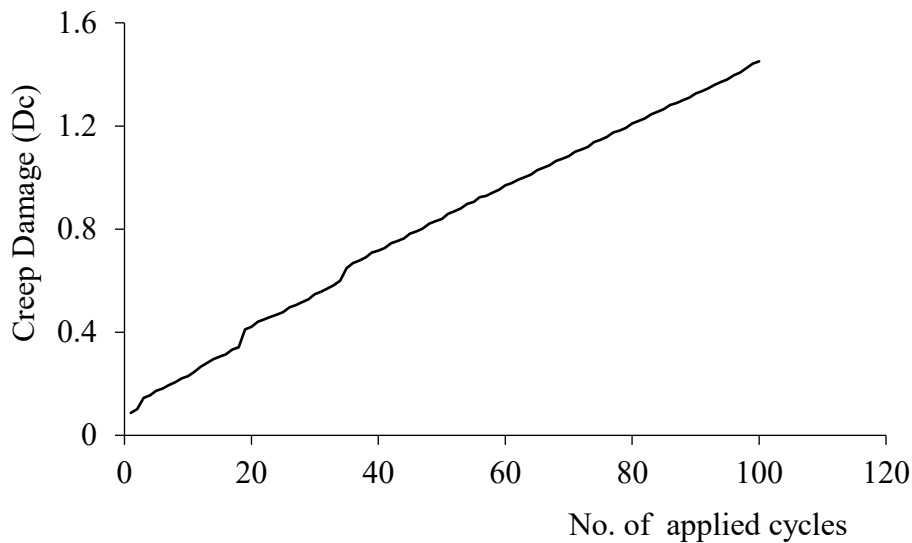
Figure 3.25 Cumulative creep damage for 100 cycles in Bilinear method

The service life, let's see the combined creep-fatigue interactions in Campbell diagram.
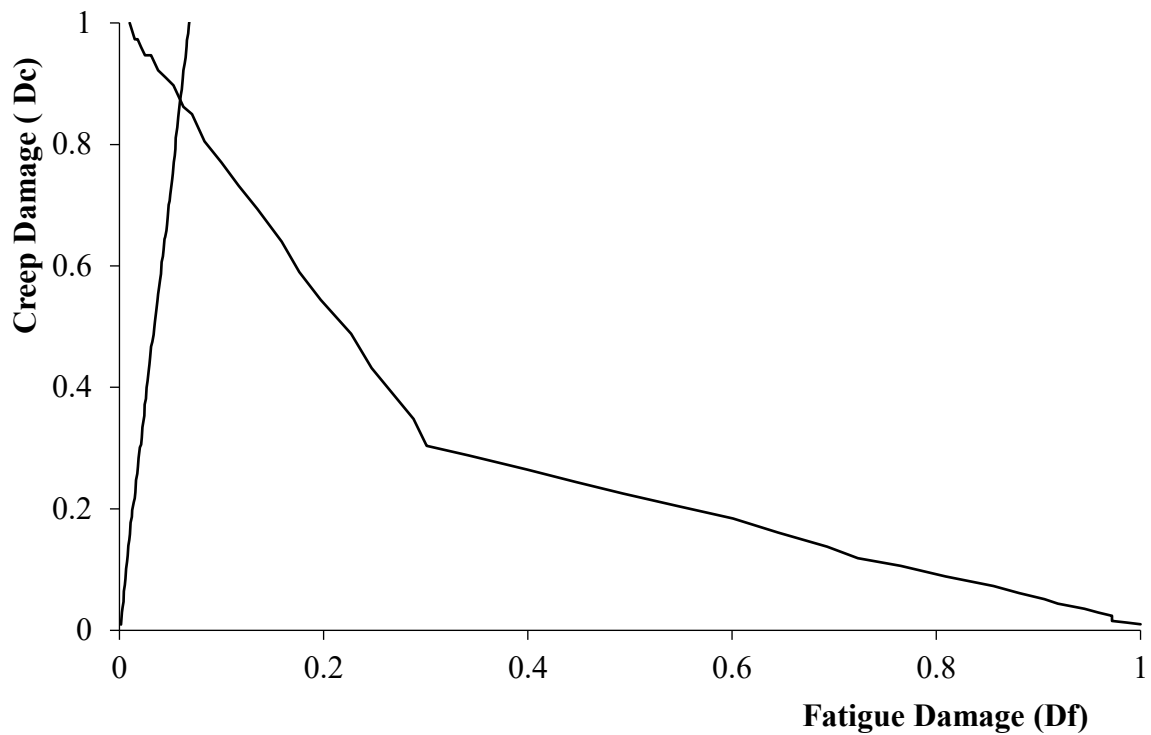
Figure 3.26 Creep-fatigue interactions of Bilinear method in the Chaboche Model.

From figure 3.26, the crossing point of creep-fatigue graph and Campbell diagram is found as $(D_f, D_c) = (0.059, 0.87)$, which indicates the damage to initiate the failure of the structure.
In this method,

Fatigue damage per cycle, $d_f = 0.0007667408$

Creep damage per cycle, $d_c = 0.013369893$

Total damage per cycle, $d_f + d_c = 0.014$

D-limit calculations:

If $d_c > d_f$, D limit $= \dfrac{3 \times \frac{d_c}{d_f} + 3}{7 \times \frac{d_c}{d_f} + 3}$

If $d_f > d_c$, D limit $= \dfrac{3 \times \frac{d_f}{d_c} + 3}{7 \times \frac{d_f}{d_c} + 3}$

Since, $d_c > d_f$, D- limit $= \dfrac{3 \times \frac{d_c}{d_f} + 3}{7 \times \frac{d_c}{d_f} + 3} = 0.932559924$

Therefore, predicted crossing cycles $= \frac{D-limit}{d_f + d_c} = 65$

3.7.8 Sample Calculations in Chaboche with short time hardening creep

$\Delta\varepsilon_{xi} = \varepsilon_{xi} - \varepsilon_{xo} = 0.0000117426 - 0 = 0.0000117426$

$\Delta\varepsilon_{yi} = \varepsilon_{yi} - \varepsilon_{yo} = 0.00000179167 - 0 = 0.00000179167$

$\Delta\varepsilon_{zi} = \varepsilon_{zi} - \varepsilon_{zo} = -0.00000044016 - 0 = -0.00000044016$

$\Delta\gamma_{xyi} = 2 \times (-0.00000113149)$

$\Delta\gamma_{yzi} = 2 \times (-0.00000137816)$

$\Delta\gamma_{zxi} = 2 \times (0.0000103513)$

Using equation no. 3.5, the equivalent strain is found as below.

$\Delta\varepsilon_{equi.,i} = 0.0000149$

Following the similar procedure and calculating the equivalent strains for all the steps, the maximum equivalent strains is taken to get the strain range. In this process, the strain range for one cycle,

$\Delta\varepsilon_t = \Delta\varepsilon_{max} = $ Maximum of $(\Delta\varepsilon_{equi.,i}) = 0.009028$

Now using the equation no. 3.6, the fatigue failure life is calculated as below.

$A_o = 1.236203527$, $A_1 = 0.655631952$, $A_2 = 0.21326109$, and $A_3 = -0.0116881$

$(\log_{10} N_f)^{-\frac{1}{2}} = 0.598241492$

$\log_{10} N_f = 2.79413212$

$N_f = 622.4896288 = 623$ cycles (approx.)

Fatigue damage, $D_f = \frac{N_d}{N_f} = \frac{1}{623} = 0.001606452$ for 1cycle

Similarly calculating the fatigue damage for all the 100 cycles and adding them, the total fatigue damage, $D_f = 0.082606$

The cumulative fatigue damage for all the 100 cycles can be represented as follows.
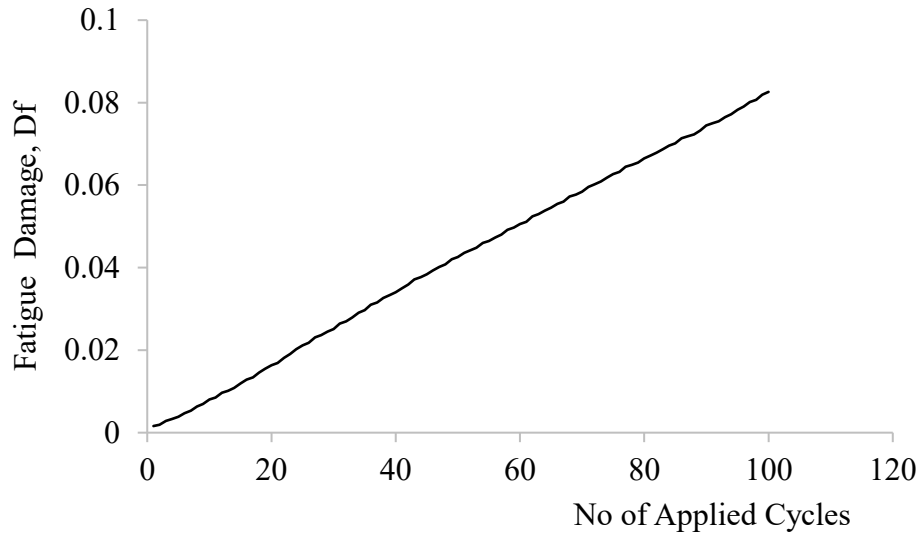
Figure 3.27 Cumulative fatigue damage for 100 cycles in Chaboche with short time hardening creep

To calculate the creep damage,

Let step time, $t_r = 0.058286$ sec. $= 1.619x10^{-5}$ hr.

For this step, Von Misses stress, $\sigma_t = 260.845$ MPa

Using equation no. 3.7, the creep rupture time is calculated below.

$t_R = 27.68$ hr.

By applying equation no. 3.8, the creep damage for this step is found as follows.

$$D_c = \frac{t}{t_R} = \frac{1.619x10^{-5}}{27.68} = 5.84x10^{-7}$$

Applying this time fraction formula, the creep damage for all the steps of the 1st cycle is 0.087127108

Calculation of total creep damage for one cycle is attached in **Appendix-E.**

The cumulative creep damage for 100 cycles is 1.450672, which is represented in the figure 3.28.
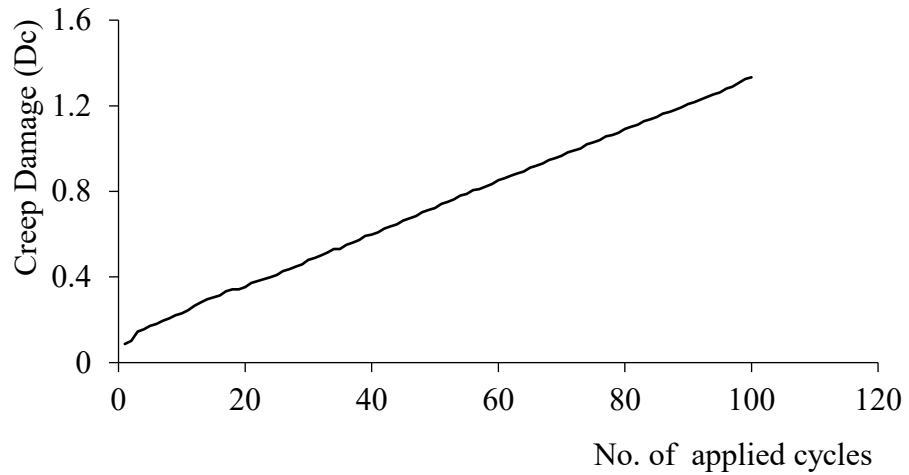
Figure 3.28 Cumulative creep damage for 100 cycles in Chaboche with short time hardening creep

The service life prediction using this method from combined creep-fatigue interactions is shown below in Campbell diagram.
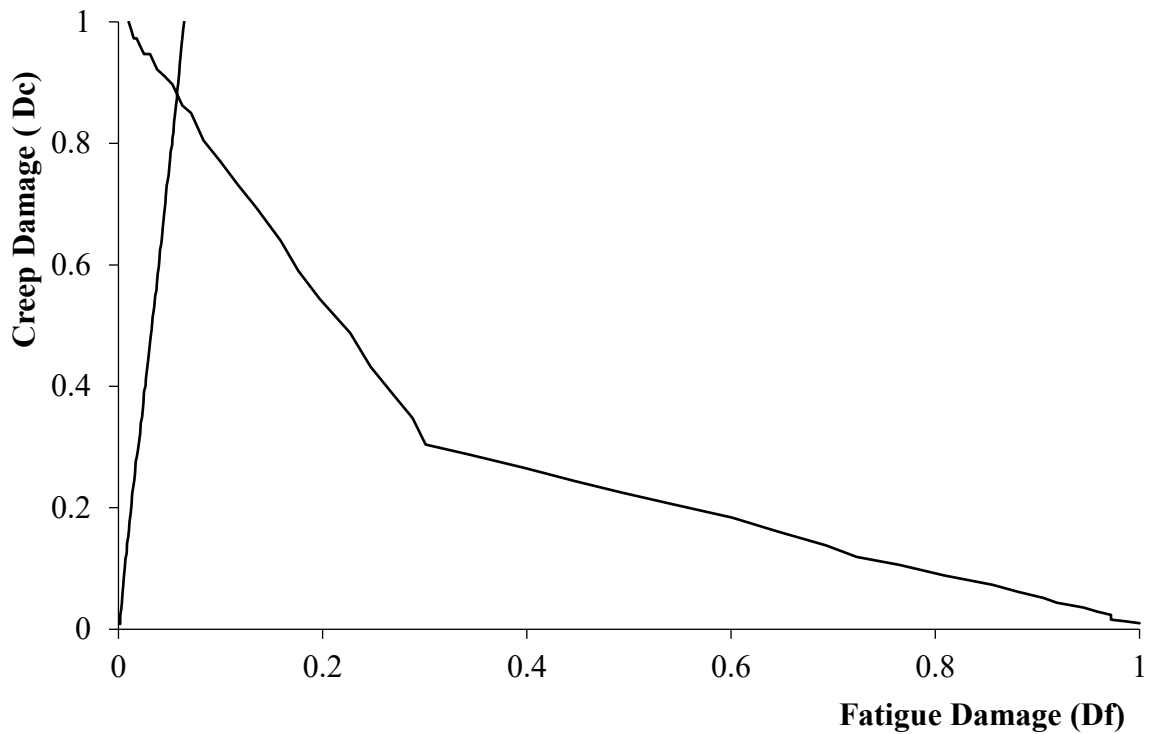
Figure 3.29 Creep-fatigue interactions of Bilinear method in the Chaboche with short time hardening creep

From figure 3.29, the crossing point of creep-fatigue graph and Campbell diagram is found as (D_f, D_c) = (0.057, 0.87), which indicates the damage to initiate the failure of the structure.

In this method,

Fatigue damage per cycle, $d_f = 0.000826060$

Creep damage per cycle, $d_c = 0.01370038$

Total damage per cycle, $d_f + d_c = 0.0145$

D-limit calculations:

If $d_c > d_f$, D limit $= \dfrac{3 \times \frac{d_c}{d_f} + 3}{7 \times \frac{d_c}{d_f} + 3}$

If $d_f > d_c$, D limit $= \dfrac{3 \times \frac{d_f}{d_c} + 3}{7 \times \frac{d_f}{d_c} + 3}$

Since, $d_c > d_f$, D- limit $= \dfrac{3 \times \frac{d_c}{d_f} + 3}{7 \times \frac{d_c}{d_f} + 3} = 0.929522389$

Therefore, predicted crossing cycles $= \dfrac{D-limit}{d_f + d_c} = 63$

3.7.9 Sample Calculations in Chaboche with long time hardening creep

$\Delta\mathcal{E}_{xi} = \mathcal{E}_{xi} - \mathcal{E}_{xo} = 0.0000117426 - 0 = 0.0000117426$

$\Delta\mathcal{E}_{yi} = \mathcal{E}_{yi} - \mathcal{E}_{yo} = 0.00000179167 - 0 = 0.00000179167$

$\Delta\mathcal{E}_{zi} = \mathcal{E}_{zi} - \mathcal{E}_{zo} = -0.00000044016 - 0 = -0.00000044016$

$\Delta\gamma_{xyi} = 2 \times (-0.00000113149)$

$\Delta\gamma_{yzi} = 2 \times (-0.00000137816)$

$\Delta\gamma_{zxi} = 2 \times (0.0000103513)$

Using equation no. 3.5, the equivalent strain is found as below.

$\Delta\mathcal{E}_{equi.,i} = 0.0000149$

Following the similar procedure and calculating the equivalent strains for all the steps, the maximum equivalent strains is taken to get the strain range. In this process, the strain range for one cycle,

$\Delta\mathcal{E}_t = \Delta\mathcal{E}_{max} =$ Maximum of $(\Delta\mathcal{E}_{equi.,i}) = 0.009028$

Now using the equation no. 3.6, the fatigue failure life is calculated as below.

A_o =1.236203527, A_1 = 0.655631952, A_2 = 0.21326109, and A_3 = - 0.0116881

$(\log_{10} N_f)^{-\frac{1}{2}}$ = 0.598241492

$\log_{10} N_f$ = 2.79413212

N_f = 622.4896288 = 623 cycles (approx.)

Fatigue damage, $D_f = \dfrac{N_d}{N_f} = \dfrac{1}{623}$ = 0.001606452 for 1cycle

Similarly calculating the fatigue damage for all the 100 cycles and adding them, the total fatigue damage, D_f = 0.080457

The cumulative fatigue damage for all the 100 cycles can be represented as follows.
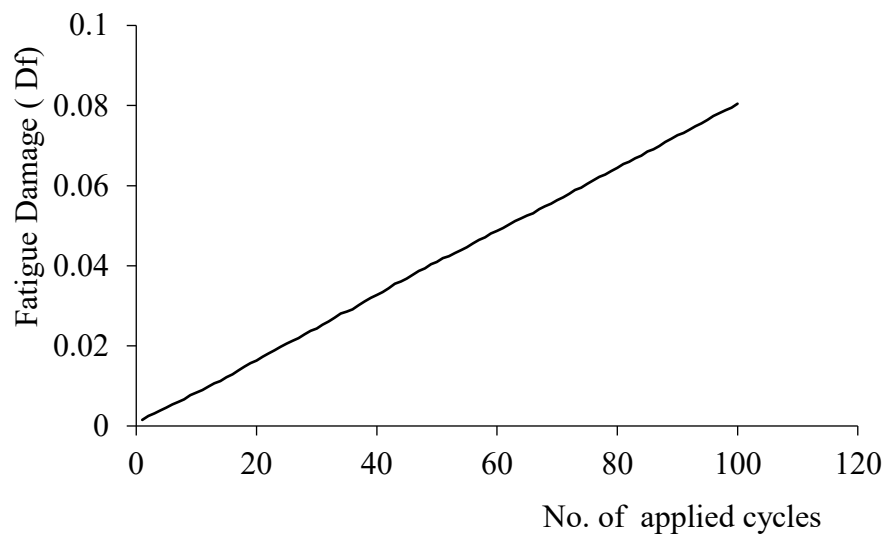
Figure 3.30 Cumulative fatigue damage for 100 cycles in Chaboche with long time hardening creep

To calculate the creep damage,

Let step time, t_r = 7.87909 sec. = 0.002188636 hr.

For this step, Von Misses stress, σ_t = 494.502 MPa

Using equation no. 3.7, the creep rupture time is calculated below.

t_R = 0.311046939 hr.

By applying equation no. 3.8, the creep damage for this step is found as follows.

$D_c = \dfrac{t}{t_R} = \dfrac{2.188636 x 10^{-3}}{0.31104693} = 7.036 x 10^{-3}$

Applying this time fraction formula, the creep damage for all the steps of the 1st cycle is 0.095558042

Calculation of total creep damage for one cycle is attached in **Appendix-F.**

The cumulative creep damage for 100 cycles is 1.336989, which is represented in the figure 3.31.
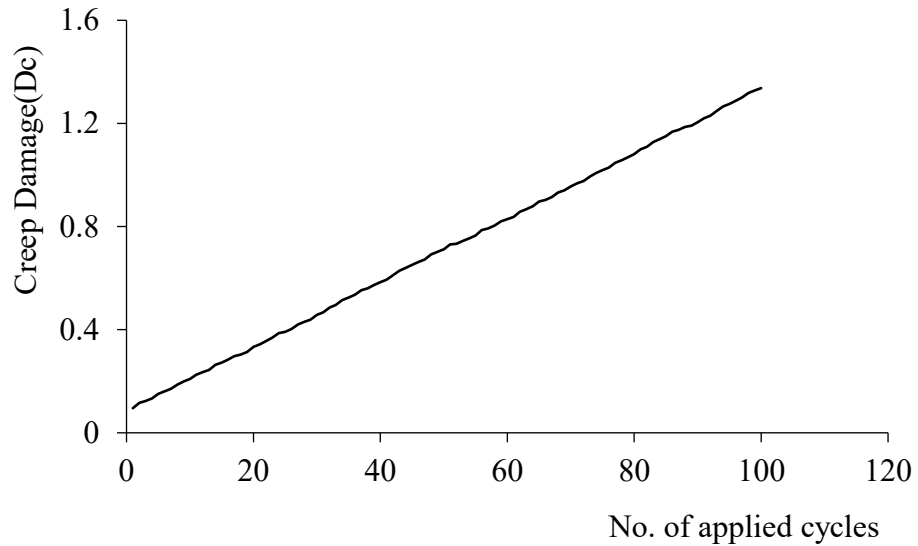
Figure 3.31 Cumulative creep damage for 100 cycles in Chaboche with long time hardening creep

The service life prediction using this method from combined creep-fatigue interactions is shown below in Campbell diagram.
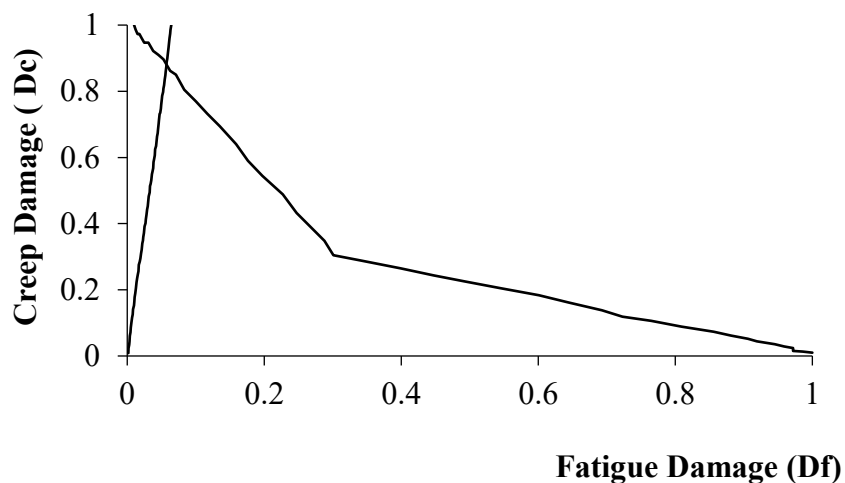
Figure 3.32 Creep-fatigue interactions of Bilinear method in the Chaboche with short time hardening creep

From figure 3.32, the crossing point of creep-fatigue graph and Campbell diagram is found as $(D_f, D_c) = (0.057, 0.87)$, which indicates the damage to initiate the failure of the structure. In this method,

Fatigue damage per cycle, $d_f = 0.0008045652$

Creep damage per cycle, $d_c = 0.01459183$

Total damage per cycle, $d_f + d_c = 0.0154$

D-limit calculations:

If $d_c > d_f$, D limit $= \dfrac{3 \times \frac{d_c}{d_f} + 3}{7 \times \frac{d_c}{d_f} + 3}$

If $d_f > d_c$, D limit $= \dfrac{3 \times \frac{d_f}{d_c} + 3}{7 \times \frac{d_f}{d_c} + 3}$

Since, $d_c > d_f$, D- limit $= \dfrac{3 \times \frac{d_c}{d_f} + 3}{7 \times \frac{d_c}{d_f} + 3} = 0.934862871$

Therefore, predicted crossing cycles $= \dfrac{D - limit}{d_f + d_c} = 60$

3.7.10 Sample Calculations in Chaboche with viscous creep

$\Delta\varepsilon_{xi} = \varepsilon_{xi} - \varepsilon_{xo} = 0.000117451 - 0 = 0.000117451$

$\Delta\varepsilon_{yi} = \varepsilon_{yi} - \varepsilon_{yo} = -0.0000179209 - 0 = -0.0000179209$

$\Delta\varepsilon_{zi} = \varepsilon_{zi} - \varepsilon_{zo} = -0.00000439836 - 0 = -0.00000439836$

$\Delta\gamma_{xyi} = 2 \times (-0.0000350981)$

$\Delta\gamma_{yzi} = 2 \times (-0.0000137993)$

$\Delta\gamma_{zxi} = 2 \times (0.000103522)$

Using equation no. 3.5, the equivalent strain is found as below.

$\Delta\varepsilon_{equi.,i} = 0.000154$

Following the similar procedure and calculating the equivalent strains for all the steps, the maximum equivalent strains is taken to get the strain range. In this process, the strain range for one cycle,

$\Delta \mathcal{E}_t = \Delta \mathcal{E}_{max}$ =Maximum of $(\Delta \mathcal{E}_{equi.,i}) = 0.008681$

Now using the equation no. 3.6, the fatigue failure life is calculated as below.

$A_o = 1.236203527$, $A_1 = 0.655631952$, $A_2 = 0.21326109$, and $A_3 = -0.0116881$

$(\log_{10} N_f)^{-\frac{1}{2}} = 0.595570543$

$\log_{10} N_f = 2.819249952$

$N_f = 659.5533823 = 660$ cycles (approx.)

Fatigue damage, $D_f = \dfrac{N_d}{N_f} = \dfrac{1}{660} = 0.001516178$ for 1cycle

Similarly calculating the fatigue damage for all the 100 cycles and adding them, the total fatigue damage, $D_f = 0.085099179$

The cumulative fatigue damage for all the 100 cycles can be represented as follows.
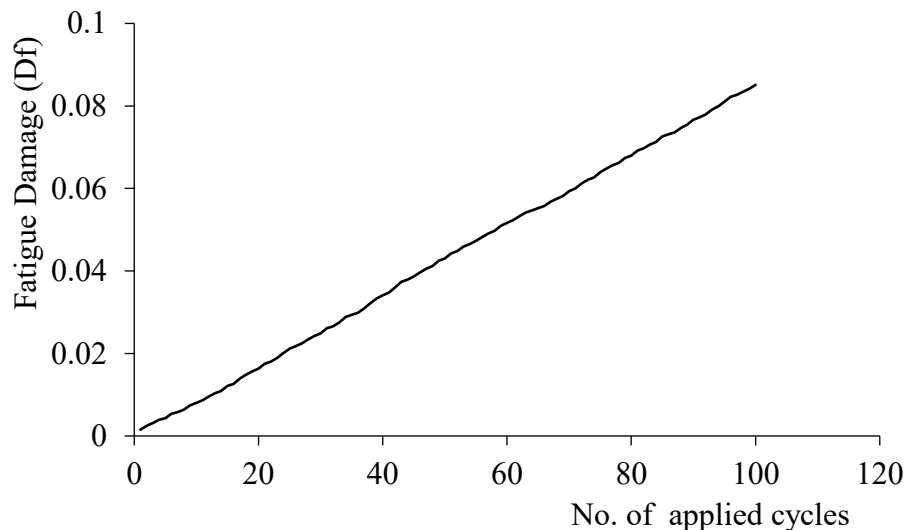
Figure 3.33 Cumulative fatigue damage for 100 cycles in Chaboche with viscous creep

To calculate the creep damage,

Let step time, $t_r = 0.202031$ sec. $= 5.611x10^{-5}$ hr.

For this step, Von Misses stress, $\sigma_t = 418.174$ MPa

Using equation no. 3.7, the creep rupture time is calculated below.

$t_R = 1.064118$ hr.

By applying equation no. 3.8, the creep damage for this step is found as follows.

96

$$D_c = \frac{t}{t_R} = \frac{5.611x10^{-5}}{1.064118} = 5.27x10^{-5}$$

Applying this time fraction formula, the creep damage for all the steps of the 1st cycle is 0.095558042

Calculation of total creep damage for one cycle is attached in **Appendix-G.**

The cumulative creep damage for 100 cycles is 1.337, which is represented in the figure 3.34.
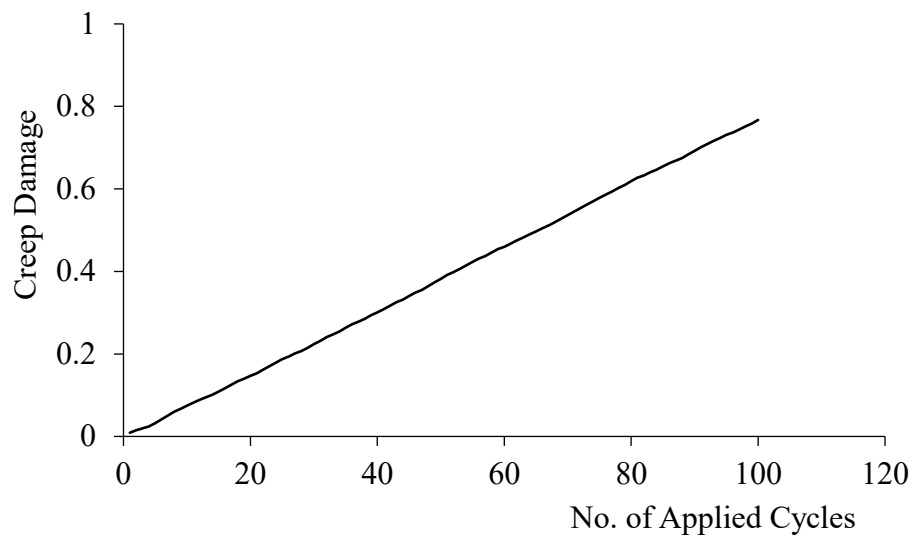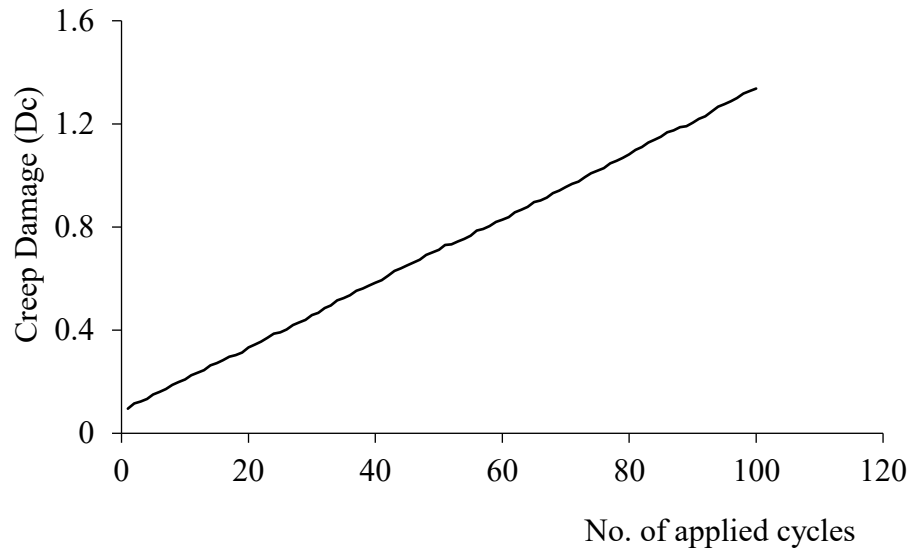

Figure 3.34 Cumulative creep damage for 100 cycles in Chaboche with viscous creep

The service life prediction using this method from combined creep-fatigue interactions is shown below in Campbell diagram.
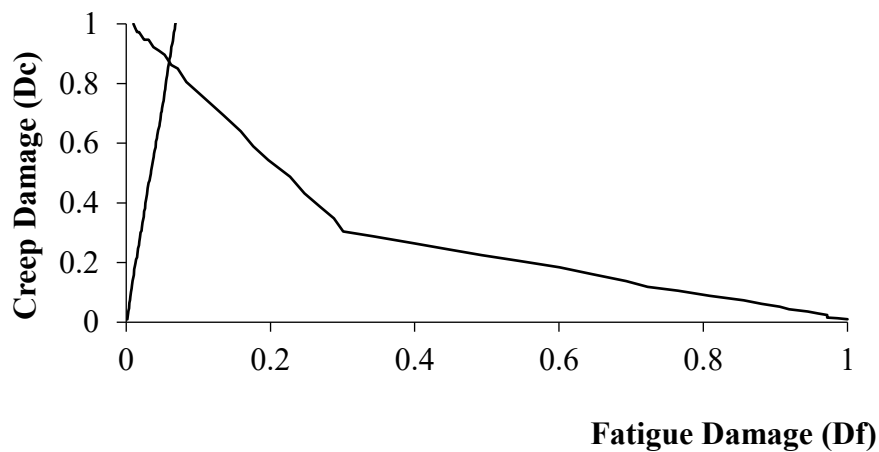
Figure 3.35 Creep-fatigue interactions of Bilinear method in the Chaboche with viscous creep

From figure 3.36, the crossing point of creep-fatigue graph and Campbell diagram is found as $(D_f, D_c) = (0.059, 0.86)$, which indicates the damage to initiate the failure of the structure.

In this method,

Fatigue damage per cycle, $d_f = 0.00085099$

Creep damage per cycle, $d_c = 0.01364989$

Total damage per cycle, $d_f + d_c = 0.0145$

D-limit calculations:

If $d_c > d_f$, D limit $= \dfrac{3 \times \frac{d_c}{d_f} + 3}{7 \times \frac{d_c}{d_f} + 3}$

If $d_f > d_c$, D limit $= \dfrac{3 \times \frac{d_f}{d_c} + 3}{7 \times \frac{d_f}{d_c} + 3}$

Since, $d_c > d_f$, D- limit $= \dfrac{3 \times \frac{d_c}{d_f} + 3}{7 \times \frac{d_c}{d_f} + 3} = 0.927430989$

Therefore, predicted crossing cycles $= \dfrac{D - limit}{d_f + d_c} = 63$

Chapter 4

ANALYSIS AND RESULTS

4.1 Introduction

In this study, sequentially coupled thermo-mechanical analysis has been performed through FE simulation, and the thermal results have been compared with the experimental responses of Japan Atomic Energy Agency (JAEA). Results of thermal analysis have been utilized in stress analysis. Then creep-fatigue damage was evaluated using both elastic and inelastic FEM based approaches. To evaluate the creep-fatigue strength and service life, SRL (K=1, Neuber), SRL Optimized case (K=1.6), and Simple Elastic Follow-Up (SEF) methods were used in elastic analysis. In addition, inelastic FEM based procedure based on Bilinear, Chaboche model and Chaboche with time hardening short-term creep (set 1) and long-term creep (set 2) is used in the inelastic analysis. Using these methods, the creep-fatigue damages are compared in Campbell diagram. The service life cycles based on combined creep-fatigue damage interaction are plotted to demonstrate the conservativeness of these methods.

4.2 Heat Transfer Analysis

During the transient heat transfer analysis, the temperature data is applied to the inner surface of the holes and inner side of the tube sheet, considering the boundary condition is adiabatic on the outer surface of the tube-sheet. The mod. Grade 91 thermal properties demonstrated in Chapter 3 are used in heat transfer analysis for determining the temperature distribution. At 110 sec. of hot transient, the upper surface of the tube-sheet and the inner surface of the penetration holes experience a greater amount of temperature than that of the inside surface during the hot transient (Figure 4.1a). Whereas tube-sheet center faces less proportion of temperatures compared to the outer side from 110 sec. of cold transient (Figure 4.1b).

NT11
+8.717e+02
+8.464e+02
+8.211e+02
+7.958e+02
+7.704e+02
+7.451e+02
+7.198e+02
+6.945e+02
+6.692e+02
+6.438e+02
+6.185e+02
+5.932e+02
+5.679e+02

NT11
+8.531e+02
+8.256e+02
+7.980e+02
+7.705e+02
+7.430e+02
+7.154e+02
+6.879e+02
+6.604e+02
+6.328e+02
+6.053e+02
+5.778e+02
+5.502e+02
+5.227e+02

(a)   (b)
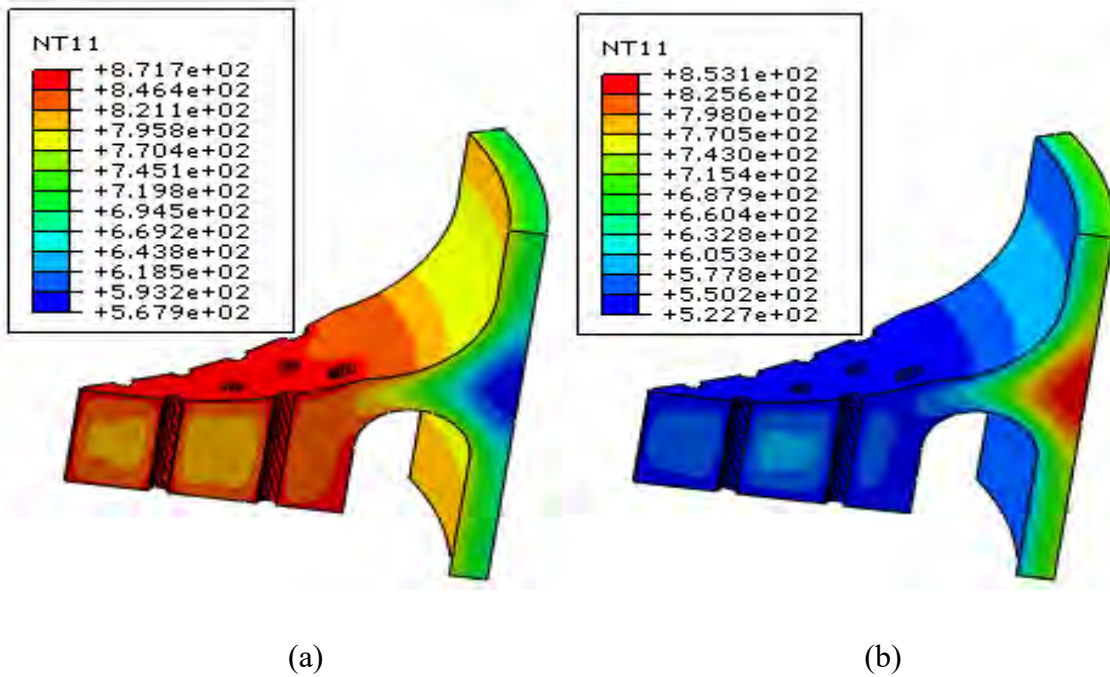
Figure 4.1 Simulated thermal distribution at 110 sec of N = 1: (a) for hot transient, and (b) Cold Transient.

Experimental temperature distribution and simulated responses at different locations (a1, a2, b1, b2, b3 as shown in Figure 3.4a) of the tube-sheet structure for the hot and cold transient loading are compared in Figures 4.2a and 4.2b, respectively which illustrate the simulated temperature distribution as acceptable but not in an incredibly good agreement.
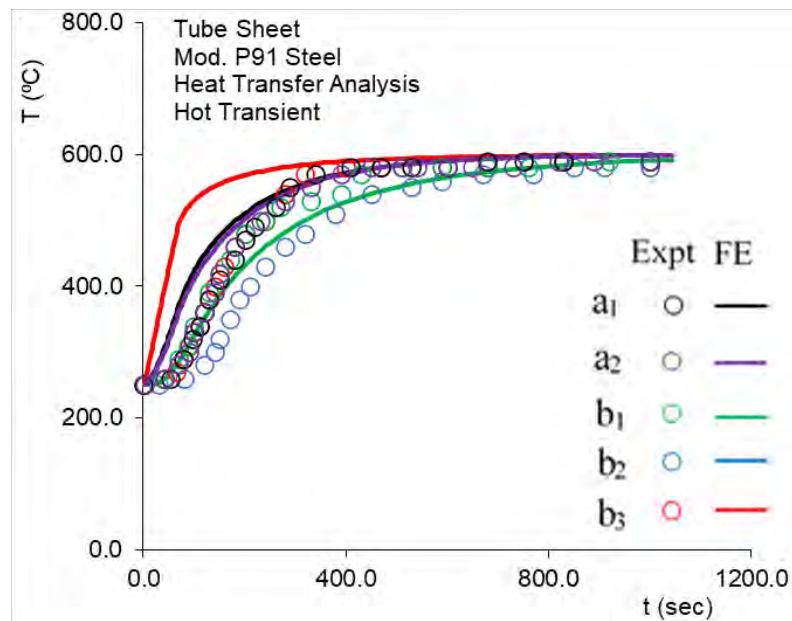
(a)
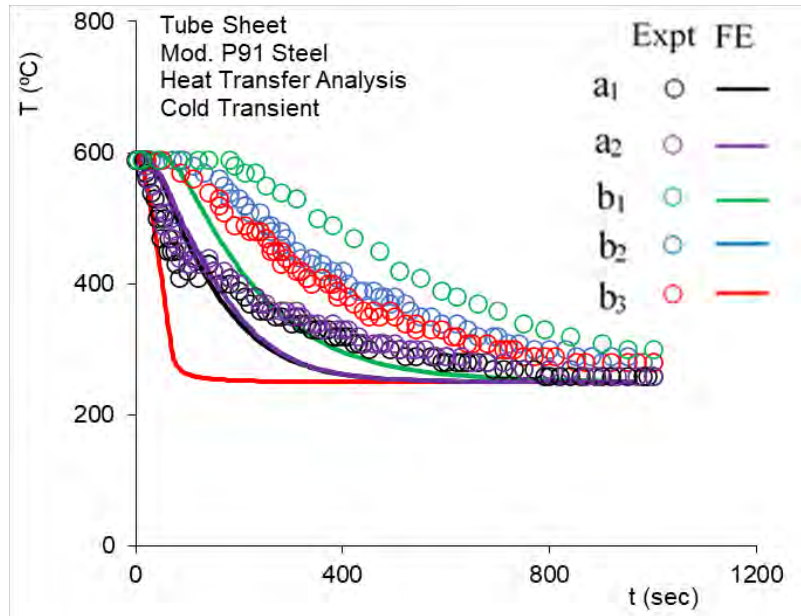
(b)

Figure 4.2 Experimental and simulated thermal responses in a1, a2, b1, b2, b3 (shown in Fig. 3.4a) during (a) hot transient loading, and (b) cold transient loading

4.3 Stress Analysis

Thermal distribution simulated from the heat transfer analysis are used in simulating the thermomechanical responses of the tube-sheet structure. The structural analysis is performed using the elastic, plastic, and inelastic creep-based models. Temperature dependent elastic modulus and poison's ratio as discussed in chapter 3 are used in the elastic analysis and bilinear material parameters are used in the inelastic analysis. In addition, Chaboche model with time hardening creep is utilized for inelastic analysis of the structure. The Chaboche parameters are obtained from cyclic stress-strain relationship of mod. P91 steel and time hardening creep parameters are obtained from the stress relaxation data (Islam, 2018). Readers are referred to Islam, 2018 for details of these material parameters. In this paper, analysis results of elastic model parameter, bilinear parameter, Chaboche model, Chaboche with viscoplastic model parameter, Chaboche with time hardening short-term creep and Chaboche with time hardening long-term creep parameters are illustrated as 'Elastic', 'Bilinear, Chaboche, Chaboche-Visco, 'Chaboche-Time1' and 'Chaboche-Time2', respectively.

4.3.1 Elastic Analysis

The von-Mises stress and equivalent strain histories (N = 1) for the upper surface and inner edge of hole C at $\theta = 180°$ (Fig. 3.4b) are shown in Figure 4.3a and Figure 4.3b, respectively for the elastic analysis.

Mod. P91 steel, Upper Surface, inner edge of hole 'C', $\Theta=180^0$ (Local Axis), N=2, t=10940 sec.

—Elastic-Stress

(a)

Mod. P91 steel, Upper Surface, inner edge of hole 'C', $\Theta=180^0$ (Local Axis) N=2, t=10940 sec.
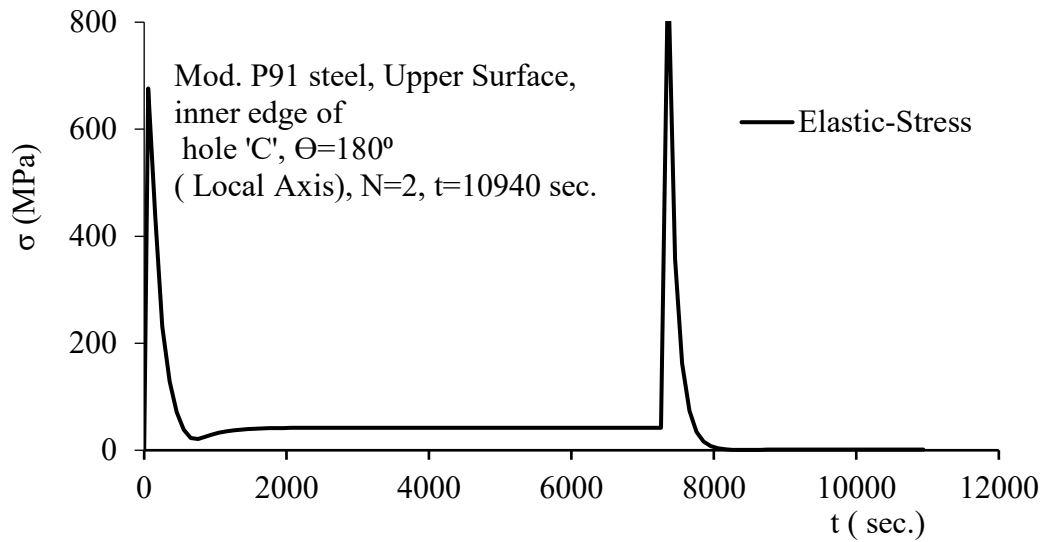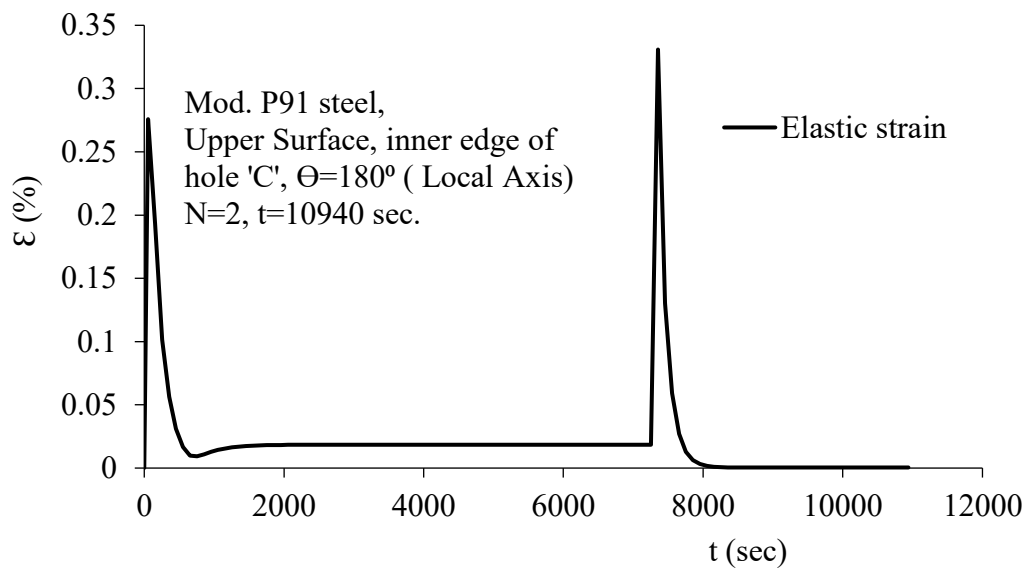
—Elastic strain

(b)

Figure 4.3 Elastic analysis (a) Von Misses Stress Vs. Time, and (b) Strain Vs. Time.

4.3.2 Stress Redistribution Locus Method (SRL)

In the SRL Neuber method (k = 1), following procedure in chapter 3, strain range is found to be, ε_t = 1+ 2.6 = 3.6 % from Fig. 4.4a which leads to 139 nos. of cycles to cause fatigue failure. Hence, the fatigue damage, Df = 0.72. The creep damage for 100 cycles is 0.375. This (Df, Dc) = (0.72, 0.375) remains within the bilinear curve of Campbell diagram (Figure 4.14). For optimized case (k = 1.6) of SRL method, strain range is 3.5 % from Fig. 4.4b that corresponds to 143 nos. of cycles to cause fatigue failure. This process yields in fatigue damage Df = 0.69 and creep damage Dc = 0.2 for 100 cycles.
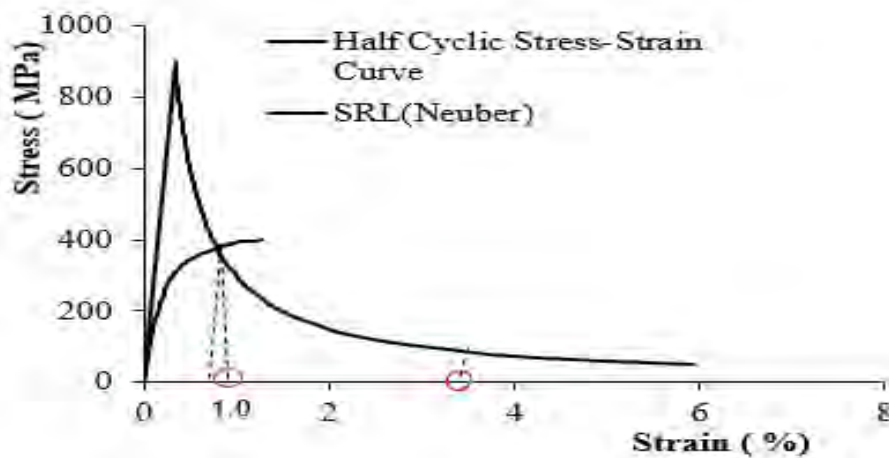
(a)
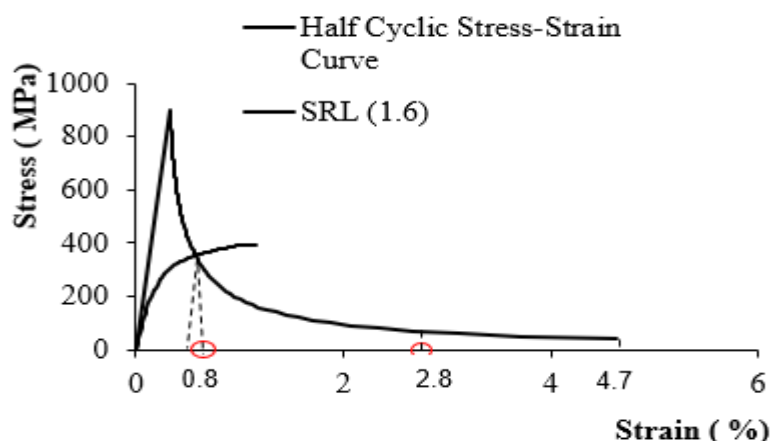
(b)

Figure 4.4 Stress vs. strain graph for (a) SRL-Neuber (K=1) and (b) SRL K=1.6

103

4.3.3 Elastic Follow Up Method

In the Elastic Follow Up method, strain range is found to be 0.98% following procedure discussed in chapter 3 and from Fig. 4.5 which leads to 554 nos. of cycles to cause fatigue failure. Hence, the fatigue damage, Df=0.18. The creep damage for 100 cycles is 3.67. This (Df, Dc) = (0.18, 3.67) remains outside the bilinear curve of Campbell diagram (Figure 4.14). During the inelastic solution, the strain increment is very insignificant in this method for which, after elastic solution, the graph (Fig. 4.5) remains almost vertically downward.
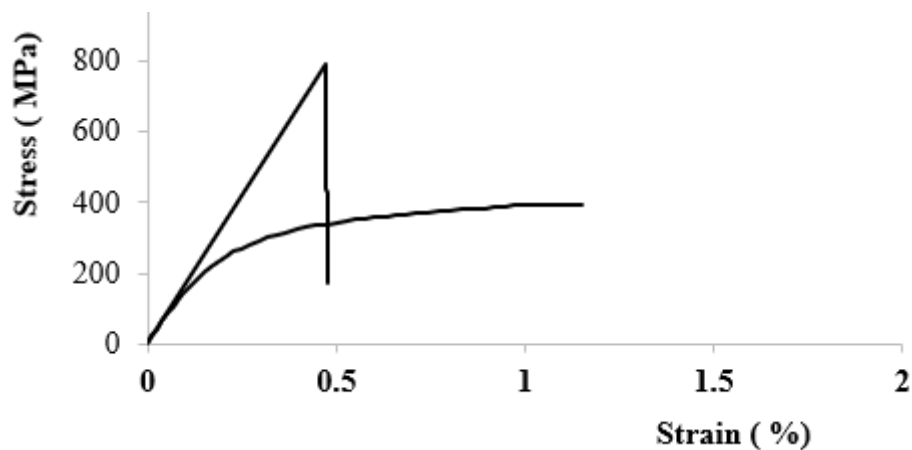
Figure 4.5 Stress vs. strain graph for SEF

4.3.4 Bilinear Model for FEA

Maximum equivalent stress simulated using bilinear material parameters are shown Figs. 4.6a and 4.6b, respectively for the hot and cold transients of T = 100 sec, N = 1. The von-Mises stress and equivalent strain histories (N = 1) for the upper surface and inner edge of hole C at θ = 180° (Fig. 3.4b) are shown in Figure 4.7a and Figure 4.7b, respectively for the bilinear model parameters.

From these analysis responses, it can be illustrated that, during the hot transient loading, the larger stress exists at the edges of hole a, c, and d (Figure 4.6). In the outermost hole 'd', greater amount of stress developed at center side of hole edge.
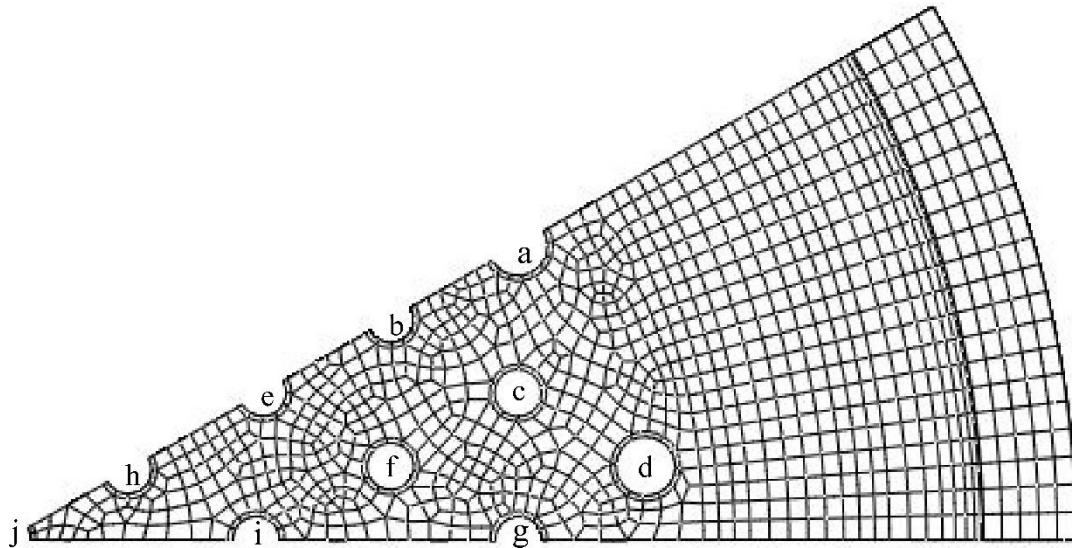
Figure 4.6 Locations of holes in the tube-sheet

While on the other hand, hole 'c' and 'a' experienced larger proportion of stress both in center and outer sides of hole edges. Concerning with the cold transient loading, it can be demonstrated that, larger stresses developed at center of hole a and d. Whereas for hole c, maximum stress was at outer side of edge.

(a)

105
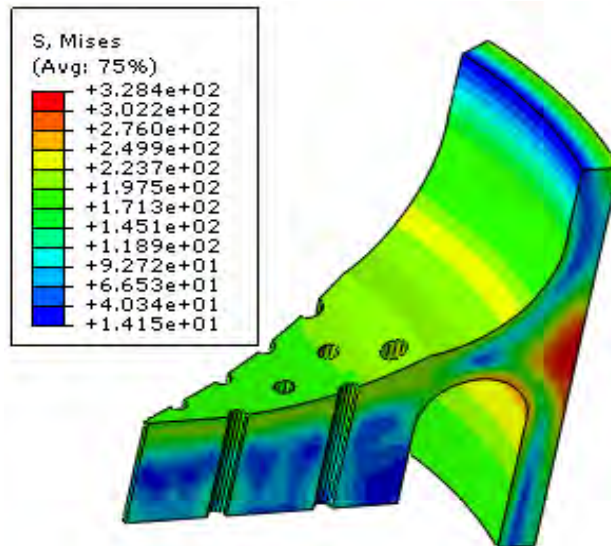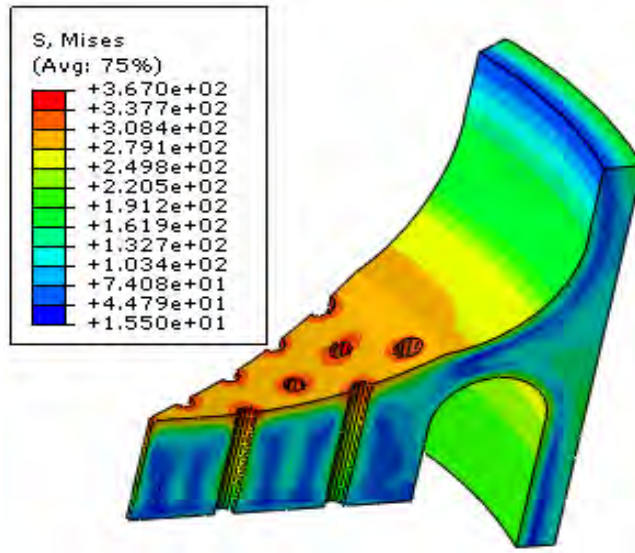
(b)

Figure 4.6 Stress contour from bilinear analysis at t = 100 sec, N = 1 of (a) hot transient, and (b) cold transient loading.

From the Bilinear analysis, it is observed that maximum stress is achieved as 386.48 MPa, while minimum stress is 42.95 MPa (Figure 4.7). In addition, the highest strain is 0.844% and the lowest strain is 0.18%.
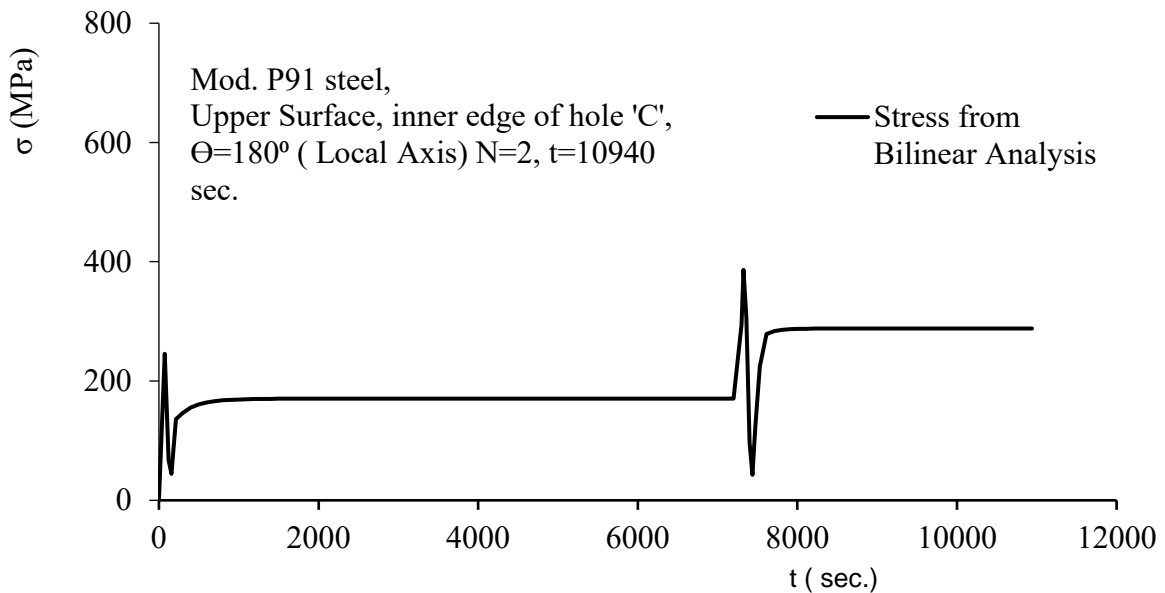
(a)
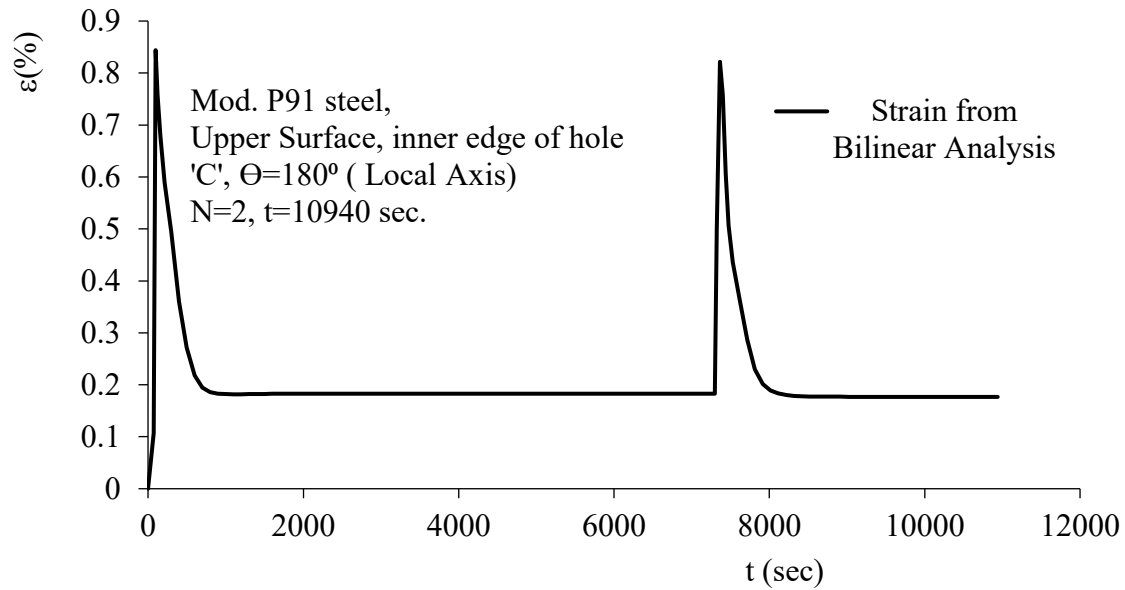
(b)

Figure 4.7 Bilinear analysis (a) Stress vs. time (b) Strain Vs. time

Using maximum equivalent strain range 0.84%, the fatigue life is found as 1943 and the fatigue damage is 0.051. Then following procedures discussed in chapter 3, creep damage for 100 cycles was calculated. Creep damage for one cycle is 0.0075. Total creep damage for 100 cycles is 0.75. Here, (Df, Dc) = (0.051, 0.75) which is within the points, (1,0), (0.3,0.3) and (0,1) of Campbell diagram (Fig. 14).

4.3.5 Chaboche Model

In the Chaboche model, it is observed that the maximum stress is 379.95 MPa, while the minimum stress belongs to approximately 25.29 MPa only (Figure 4.8a). In addition, this analysis shows the highest strain as 0.46%, and the lowest strain is 0.039% (Figure 4.8b).

In the Chaboche Model, strain range is 0.46% which leads to 2441 nos. of cycles to cause fatigue failure. Hence, the fatigue damage, Df = 0.076. The creep damage for 100 cycles is 1.33. This (Df, Dc) = (0.076, 1.33) remains outside the bilinear curve of Campbell diagram (Figure 4.14).
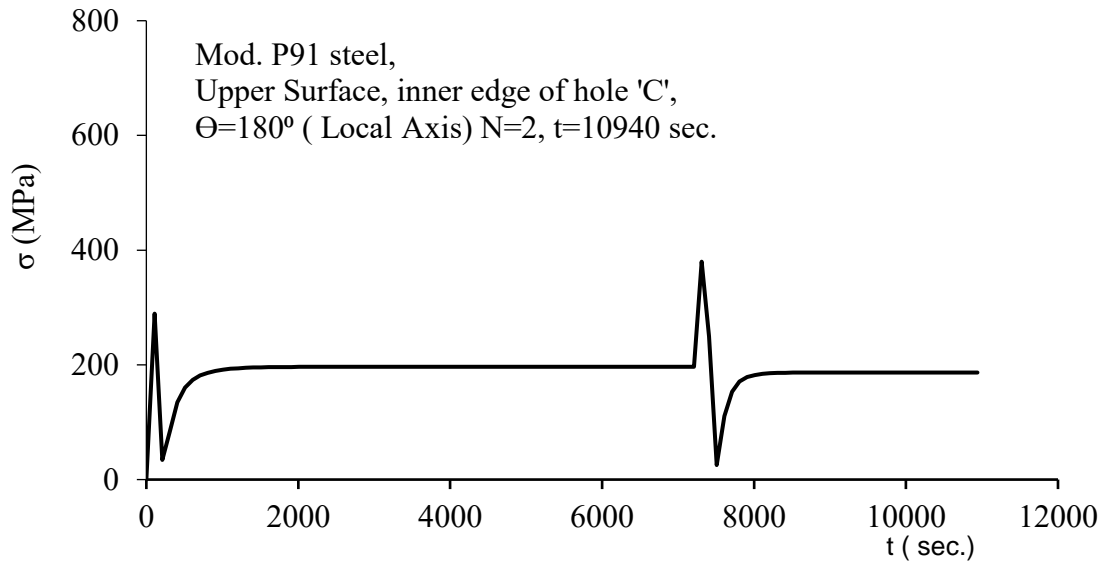
(a)
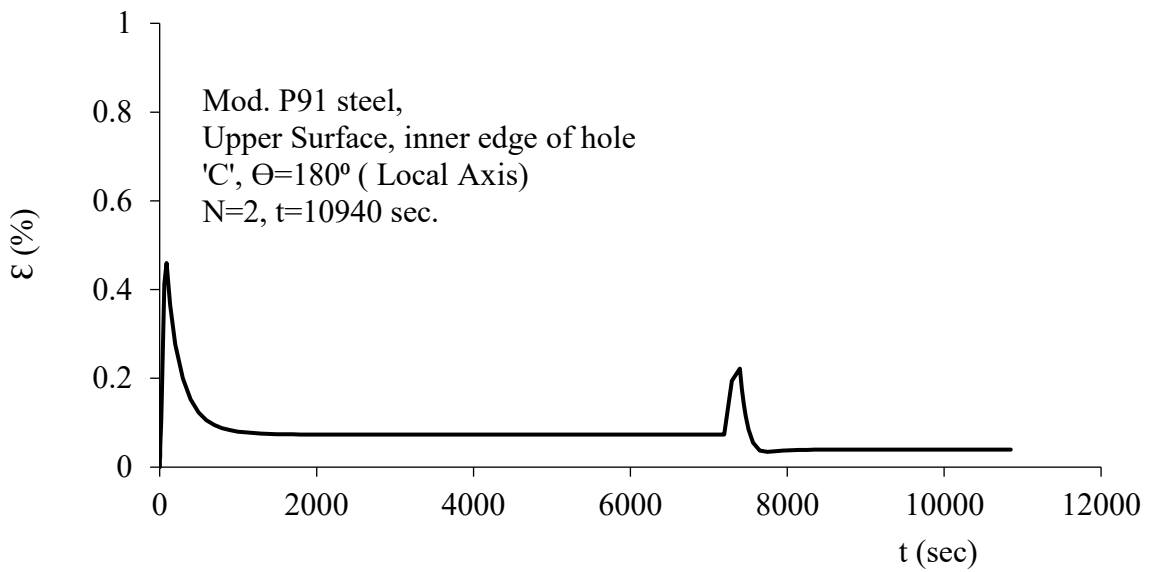
(b)

Figure 4.8 Chaboche model responses (a) Equivalent Stress vs. Time and (b) Equivalent Strain vs. Time.

4.3.6 Chaboche with Time Hardening Creep

Figure 4.9 shows that the result from Chaboche model and Chaboche Model with time hardening creep is far different. In the analysis of Chaboche with creep model (set-1), the

maximum stress concentration is 470.75 MPa and minimum stress is 32.68 MPa. In case of strain, the highest strain is 0.46%, while lowest value is 0.039%.

In the Chaboche with creep model (set-1), strain range is 0.46% which leads to 2441 nos. of cycles to cause fatigue failure. Hence, the fatigue damage, Df=0.082. The creep damage for 100 cycles is 1.37. This (Df, Dc) = (0.082, 1.37) remains outside the bilinear curve of Campbell diagram (Figure 4.14). In the similar process, by the Chaboche with creep model (set-2), fatigue and creep damage are, (Df, Dc) = (0.080, 1.45).
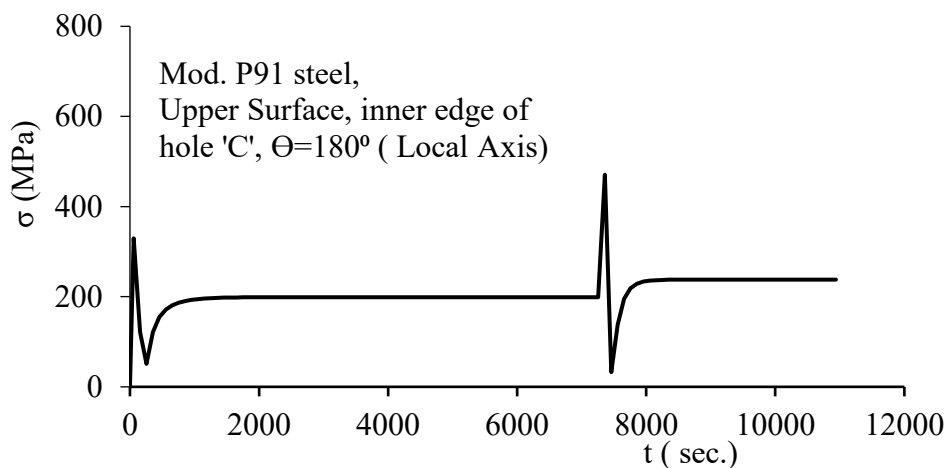
(a)
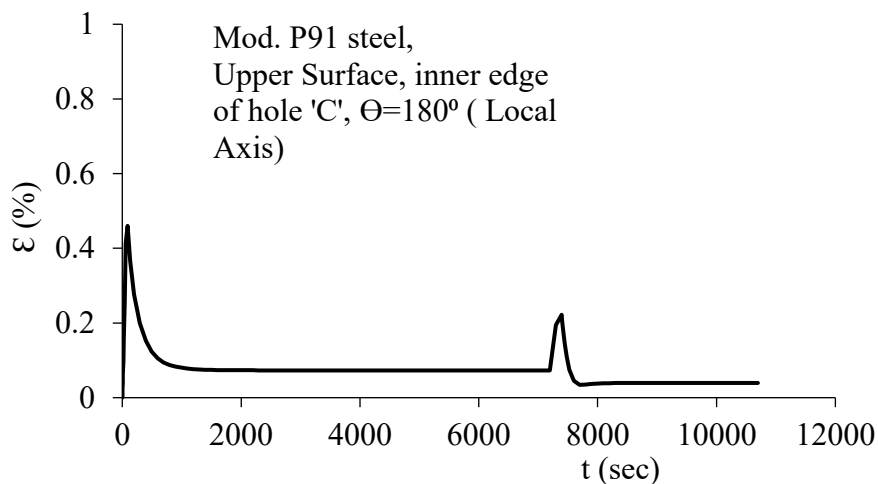
(b)

Figure 4.9 Chaboche model with time hardening creep (a) Stress vs. Time and (b) Strain vs. Time

109

4.3.7 Chaboche with Isotropic Hardening and Viscous Creep

The maximum stress concentration after adopting the Chaboche model with isotropic hardening coupled with viscous creep is 470.756 MPa and minimum stress is 32.68 MPa. In case of strain, the highest strain is 0.46%, while the lowest value is 0.039%.

In the Chaboche Model with viscous creep, strain range is 0.46% which leads to 2441 nos. of cycles to cause fatigue failure. Hence, the fatigue damage, Df=0.085. The creep damage for 100 cycles is 1.36. This (Df, Dc) = (0.085, 1.36) remains outside the bilinear curve of Campbell diagram (Figure 4.14).

4.4 Comparison of stresses of different Models

From the analysis in different methods, it is clear that the maximum stresses are found in elastic analysis which is 899.83 MPa, whereas the minimum peak stresses are found in Chaboche model as 370.945 MPa. The highest stresses in other methods exist in between theses stresses and that is approximately 470 MPa. The peak stress in elastic stress is more than the two times than that of Chaboche model. In each of the graphs (Figure 4.10), there are two peak values. However, overall, the elastic stress is the maximum while the Chaboche model demonstrates the minimum peak values. In each method, there is a smooth stress relaxation which can be observed but after 7000 sec. of analysis, although other methods show upward trend, the elastic analysis provides a downward trend leading to zero at the end.
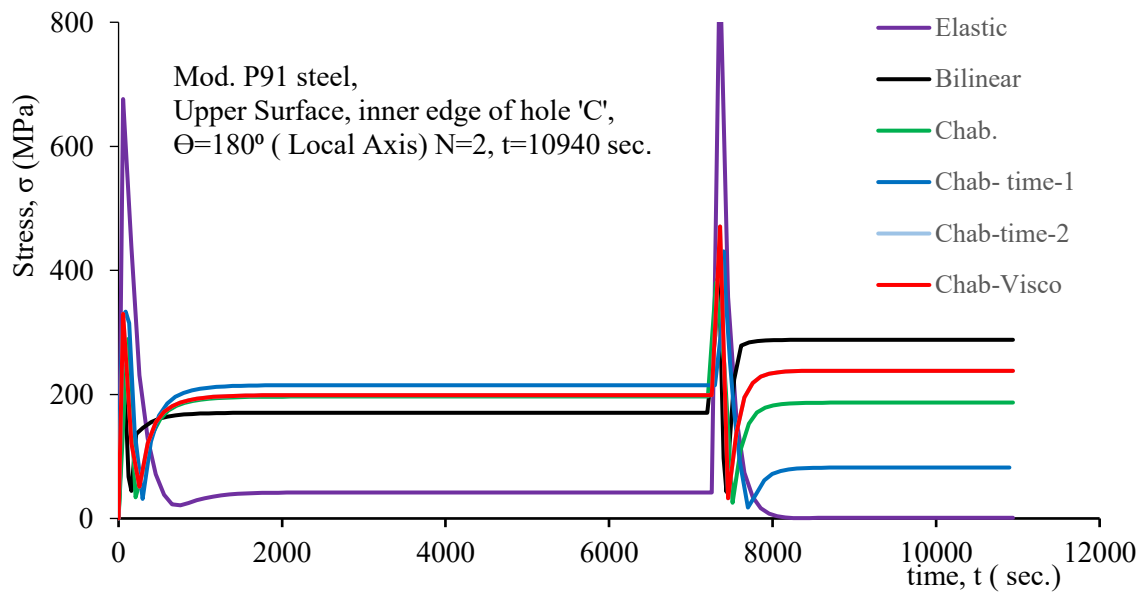
Figure 4.10 Comparison of equivalent stresses in different methods

4.5 Comparison of Strains of different Models

Among the strains in different methods, the highest peak strain is found from Bilinear analysis that is almost 0.84%. On the contrary, the lowest peak value is derived from elastic analysis. Similar to the stresses, here also exists two peak values (Figure 4.11) in each method following a downward trend of strains after reaching its peak. The proportion of steady strains are 0.18% for Bilinear analysis, 0.073% for Chaboche with Hardening and 0.018% for elastic analysis. Steady strains from Chaboche with Creep and Hardening are similar to that of Chaboche with Hardening model. The lower peak value in bilinear analysis is 0.82%. Whereas, these values are 0.33% and 0.21% for elastic analysis and Chaboche with Hardening model, respectively.
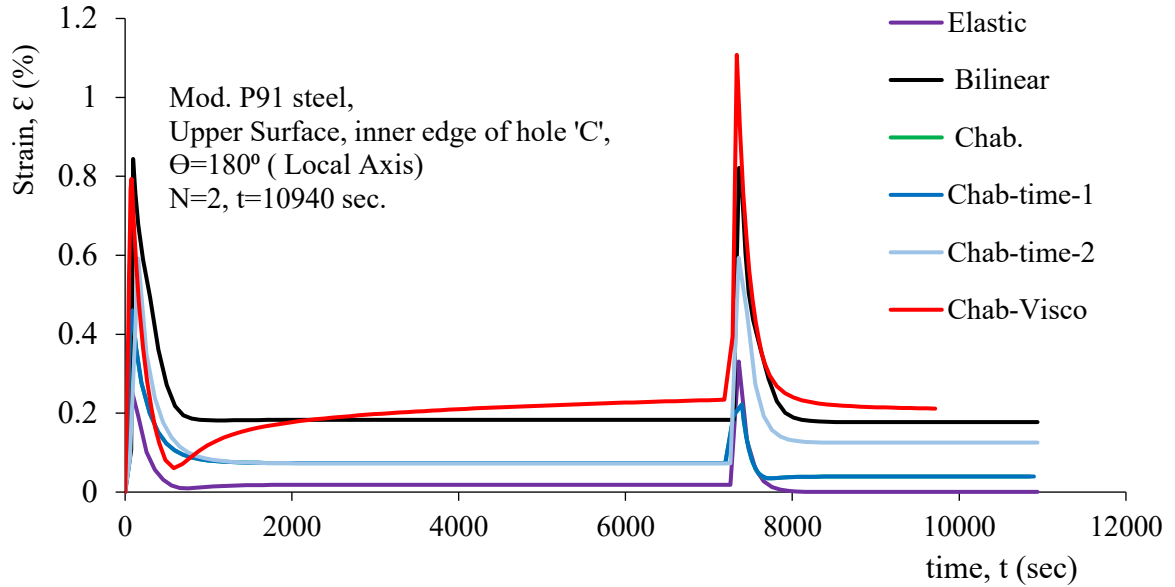
Figure 4.11 Comparison of strains in different methods

4.6 Comparison of creep damages of different Models

The creep damages calculated in simplified methods i.e., SEF, SRL etc. seem to be very lower compared to that of advanced methods calculated from the cycles of maximum peak stress. The highest creep damage is found in Chaboche model with hardening set-2 which is 2.3 for 100 cycles (Figure 4.13 a), while the lowest damage is found in Stress Redistribution Locus Neuber methods with 0.196 (Figure 4.12a). The second highest creep value is found from the Chaboche with Hardening set-1 which is 1.45 and Chaboche model shows this value as 1.29. The Chaboche with viscous creep shows almost similar value with bilinear method. The SEF, SRL (k=1.6) and SRL (k=1) demonstrate the creep value as 0.367, 0.194 and 0.375, respectively. Figure 4.12a estimated creep damage based single peak creep damage multiplied by the number of cycles.

Figure 4.12b represents creep damages where creep damages are estimated by cumulative sum of creep damages. The creep damage calculated from the cumulative results of 100 cycles resembles a larger variation in different Chaboche models and Bilinear method. The creep damages in Chaboche model, Chaboche with hardening set-1, Chaboche with hardening set-2 and Chaboche with viscous creep are 1.337, 1.37, 1.459 and 1.365, respectively.
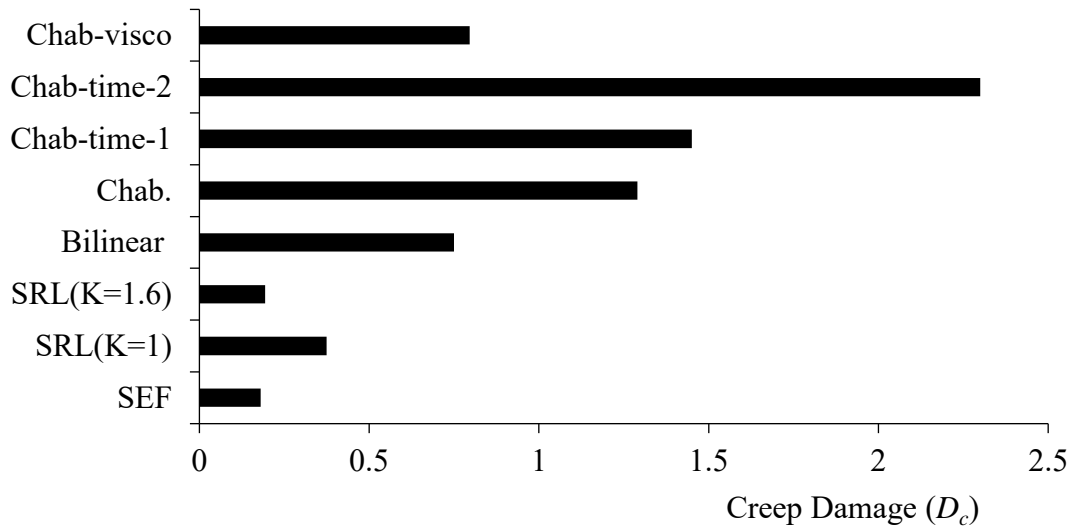
(a)
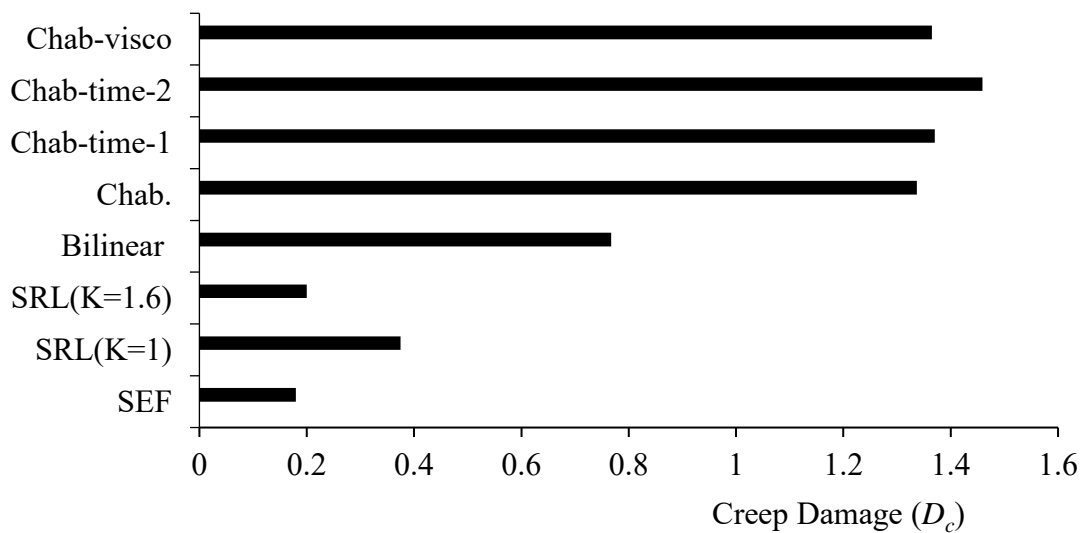
(b)

Figure 4.12 Comparison of creep damages in different methods for 100 cycles with (a) maximum creep damage of single cycle multiplied by number of cycles, (b) cumulative creep damage of 100 cycles.

Fatigue damages are plotted in Figures 4.13a and 4.13b for single peak fatigue damages multiplied by the number of cycles and for cumulative fatigue damages, respectively. From the analysis, it is observed that, the higher proportion of fatigue damage is found from simplified

methods than that of advanced models. The highest fatigue damage is found from Stress Redistribution Locus - Neuber method and the value is 0.72 for the cycle of maximum peak stress multiplied by 100. In optimum case, SRL (K=1.6) also shows a considerable fatigue damage of 0.69. Chaboche with hardening set-1, Chaboche model and bilinear method provide very insignificant fatigue damage. Chaboche with hardening set-2, Chaboche with viscous creep and SEF provide the damage as 0.115, 0.133, and 0.18, respectively. The fatigue damage is found more than 5.4 times in SRL Neuber method than that of Chaboche with viscous creep and 4 times compared to SEF method. Bilinear method demonstrates 3.5 times lower values in contrast to Simplified Elastic method.
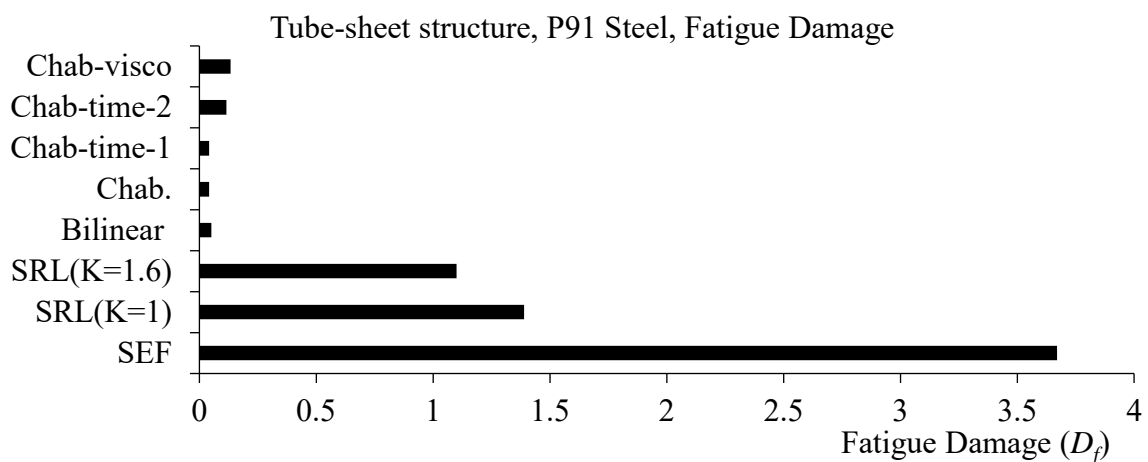
(a)
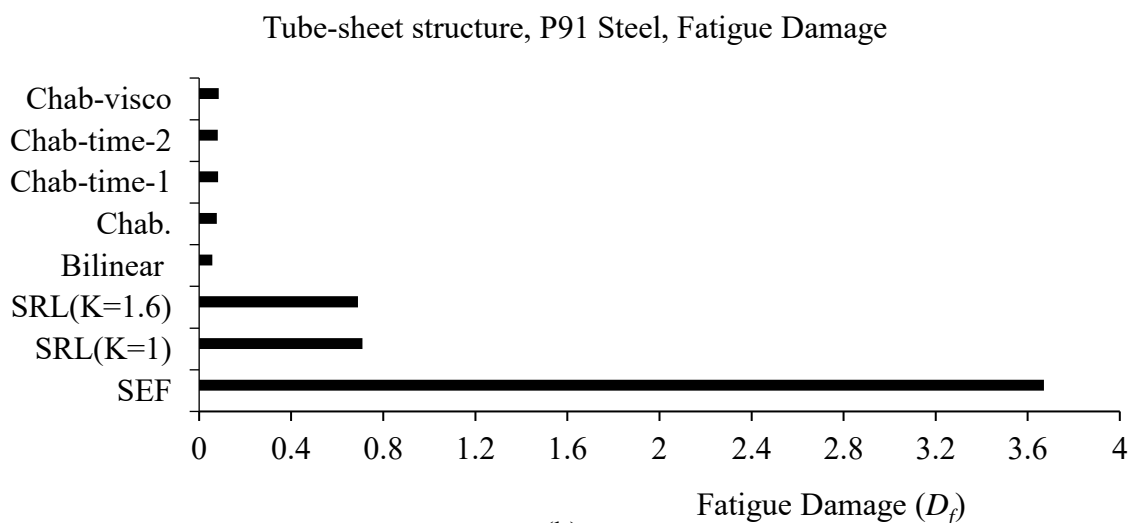
(b)

Figure 4.13 Comparison of fatigue damages in different methods for 100 cycles with (a)

maximum fatigue damage of single cycle multiplied by number of cycles, (b) cumulative fatigue damage of 100 cycles.

It is also observed that, the SRL methods provide largest proportion of fatigue damage (0.72, 0.69) in contrast to SEF and Chaboche models when cumulative fatigue damage of 100 cycles is considered. The Chaboche models have almost similar damages, and these are less than SEF method. The lowest damage is shown in Bilinear method with only 0.057.

4.7 Campbell Diagram

From the Campbell diagram (Figure 4.14a), it has been illustrated that, creep damages are dominant in Bilinear and advanced Chaboche models, where fatigue damages are dominant in the SEF and SRL methods. All the advanced methods and SRL demonstrate the creep-fatigue interactions that crosses the interaction curve. The maximum creep damage is found in Chaboche with time hardening creep model (set-2) and the minimum Creep damage is obtained in SEF and SRL-Neuber (K=1) method. In contrast, the highest fatigue damage is achieved in SEF, and lowest fatigue damages are obtained in inelastic based Bilinear and Chaboche with time hardening creep models. Creep-fatigue damage interactions for inelastic based analysis are also dependent on how the damage calculations are performed. Figure 4.14a shows the creep-fatigue damages which are estimated based on maximum damage of single cycle multiplied by number of cycles and figure 4.14b shows cumulative damages. Other than bilinear and elastic FEM based approaches, inelastic FEM damage estimation are different in two cases.
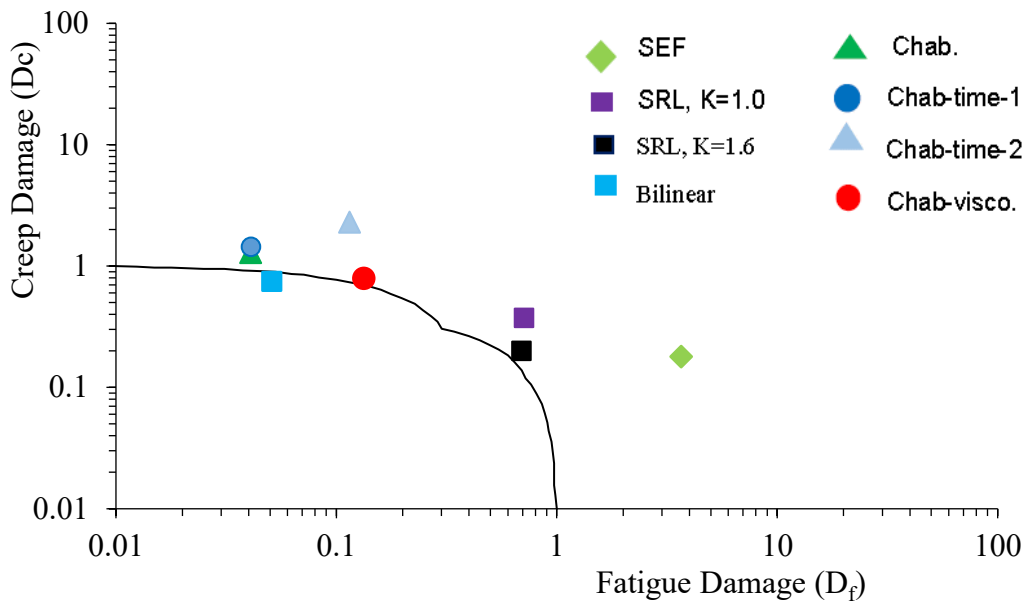
(a)
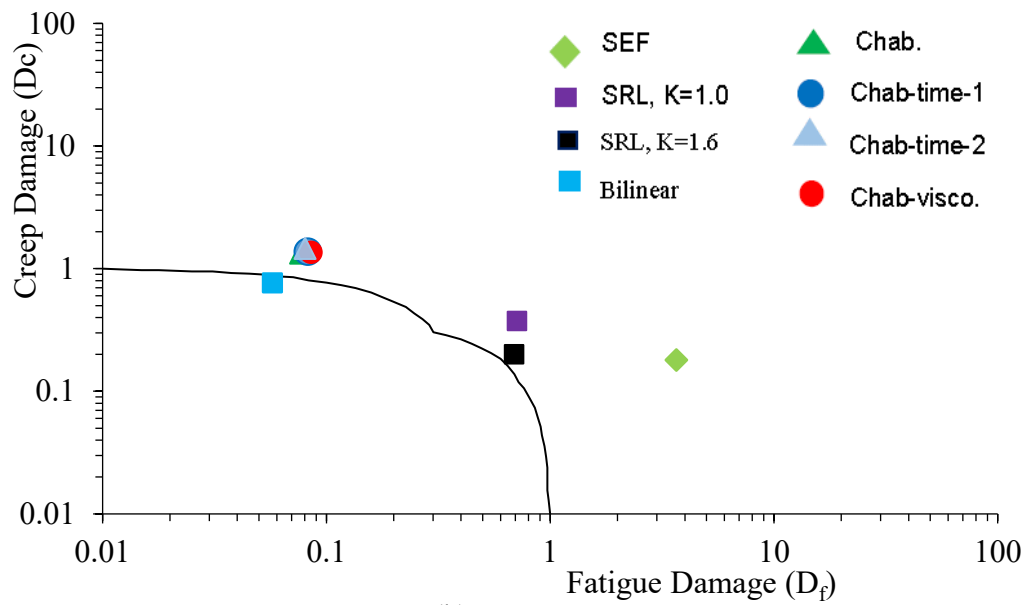
(b)

Figure 4.14 Comparison of creep and fatigue interactions in Campbell diagram for (a) maximum damage of single cycle multiplied by number of cycles, (b) cumulative damage of 100 cycles.

4.8 Predicted thermal cycles with combined creep-fatigue interactions

When both creep and fatigue damages are considered for life prediction and damages are evaluated based on maximum damage of single cycle multiplied by number of cycles, the

Chaboche model, the Chaboche with time hardening set-1 and set-2, Chaboche with viscous creep, SEF, SRL (K=1), and SRL (K=1.6) method show the predicted life cycles as **71, 64, 38, 90, 62 and 87** respectively. In contrast, the Bilinear method showed unconservative side with a factor of 1.15. See Fig. 6.17.

From the cumulative calculation of 100 cycles due to creep fatigue interactions, the Chaboche with hardening set-1 and set-2, Chaboche with viscous creep, SEF, SRL (k=1), and SRL (K=1.6) method show the predicted life cycles as **65, 63, 60, 63, 62 and 87** respectively. In contrast, the Bilinear method showed unconservative side with a factor of 1.10. See Fig. 4.18.
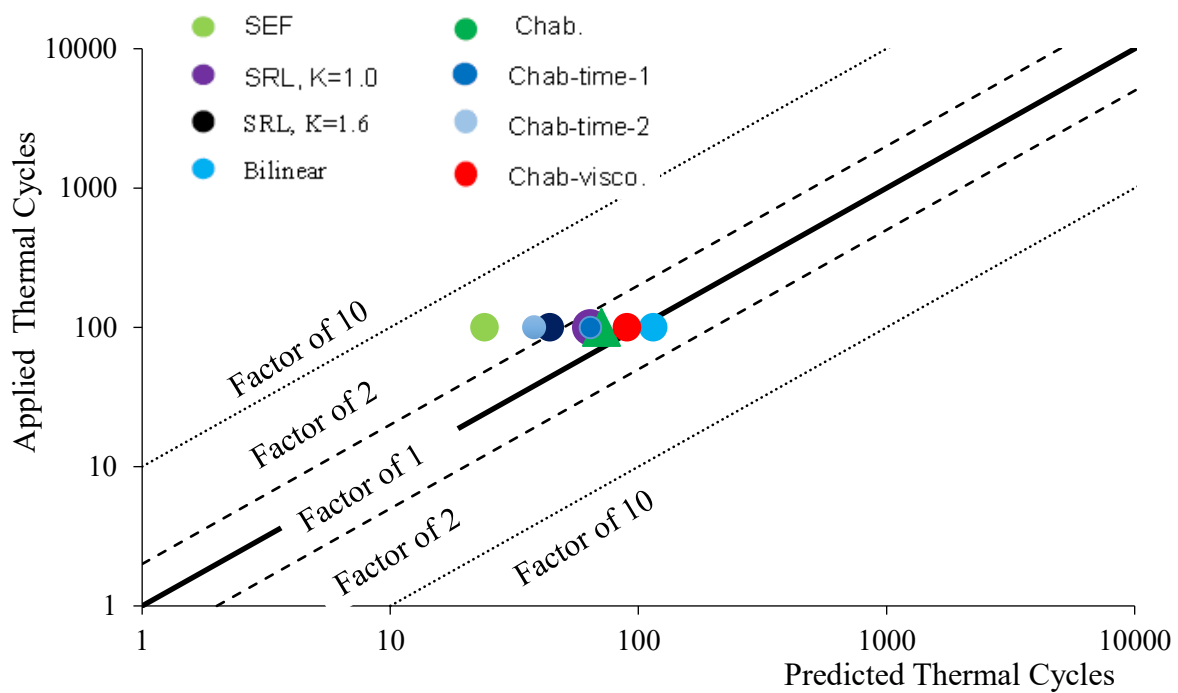
Figure 4.15 Comparison of predicted life in different methods with both creep-fatigue damage (maximum damage of single cycle multiplied by number of cycles)
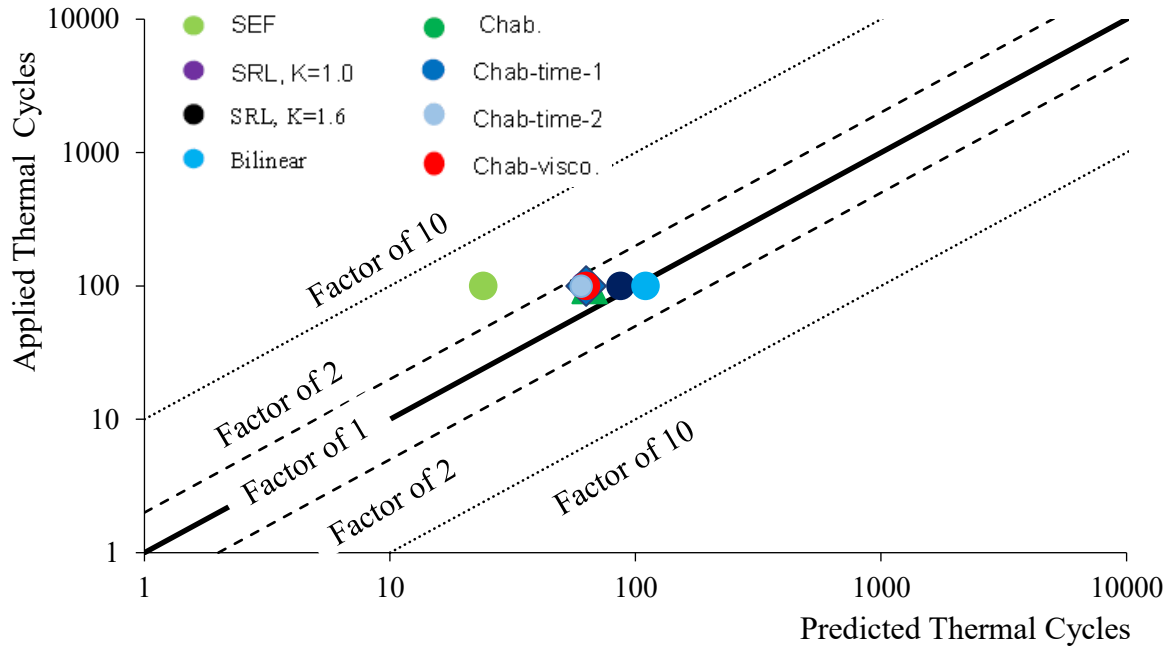
Figure 4.16 Comparison of predicted life in different methods with both creep-fatigue damage (cumulative damage for the number of cycles)

Chapter 5

CONCLUSIONS AND RECOMMENDATIONS

5.1 Introduction

This research evaluates the creep, fatigue and simultaneous creep and fatigue interaction of mod. Grade 91 tube-sheet structures due to elevated temperature and pressure using finite element analysis. Such a structure is paramount in Nuclear Fast Reactor for its excellent resistance capacity, when subjected to heat and pressure. A sample of test was conducted by Japan Atomic Energy Agency between the temperature 600° C for 2 hours and 250°C for 1 hour together with a pressure of 19.2 MPa. To conduct the finite element analysis, the sequentially coupled thermo-mechanical analysis was conducted to utilize the thermal results in stress analysis and hence to determine the creep and fatigue damage through Stress Redistribution Locus (SRL) Neuber method, Stress-Redistribution optimized case, Simple Elastic Follow up (SEF) method, Bilinear method, Chaboche Model, Chaboche with time hardening short-term creep, Chaboche with time hardening long-term creep and Chaboche with viscous creep models. Finally, the damages were compared in Campbell diagram and a comparison was made among the predicted cycles. From the analysis responses, it has been found that SEF method is more conservative than SRL method for damage estimation. Elastic analysis based SRL and SEF methods predict higher fatigue damages, and inelastic analysis based bilinear and Chaboche model with creep parameters estimate more creep damages. Based on these results, a life prediction chart is presented which shows elastic procedure predicts life in higher safety factor in comparison to inelastic based procedures.

5.2 Discussions

The study develops a 3D FE model of Tube-Sheet Structure of Steam Generators for evaluating life of the critical component at very high temperature and pressure under combined cyclic and load hold condition. A comparative study of elastic and inelastic FEM based approaches has been presented for life estimation, namely Simple Elastic Follow-Up Method (Elastic), Stress Relaxation Locus Method (Elastic), Inelastic Method with Bilinear Kinematic Hardening,

Chaboche Kinematic Hardening, Chaboche model with Short-Term Stress Relaxation, Chaboche Model with Long-Term Creep and Chaboche Model with Viscous Power Law model. The stress and strain responses in different models are represented in the following figures.
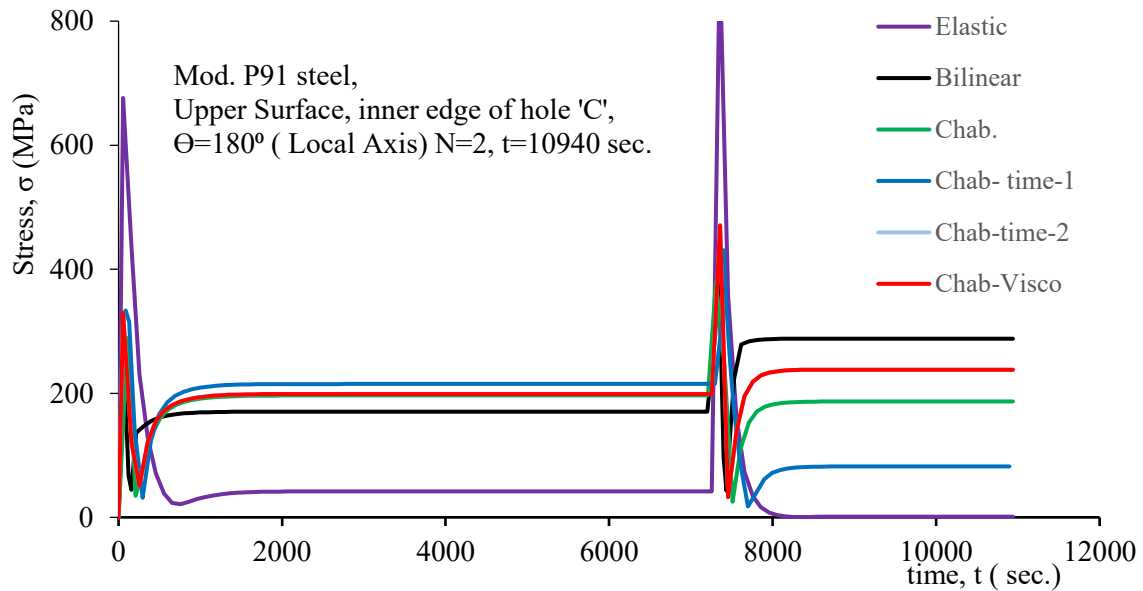
Figure 5.1 Stress vs. time response in different models.
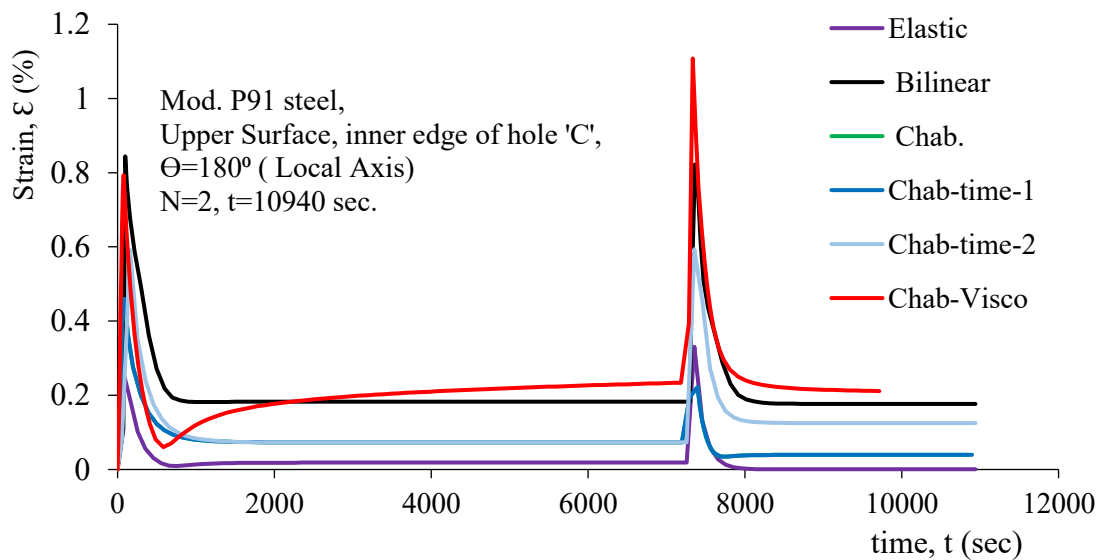
Figure 5.2 Strain vs. time response in different models.

As the simplified elastic FEM based approaches have limitations to evaluate the creep damages and stress relaxation in these approaches is approximated based on non-linear empirical formula, $\varepsilon_t = \frac{\varepsilon_o}{K} . [\frac{\sigma_o}{\sigma_t} + (k-1). \frac{\sigma_t}{\sigma_o}]$ for SRL method, which do not have the capability to simulate material level responses, hence creep damage was determined using advanced constitutive models having stress relaxation phenomenon which provide much higher creep damage. To conduct elastic analysis, the results of thermal analysis was used, and modulus of elasticity (E) and density are utilized as input parameter. In the SRL Neuber (K=1), D_c and D_f are 0.375 and 0.72, respectively. In SRL optimized case (k=1.6), $(D_c, D_f) = (0.2, 0.69)$. For SEF method, stress relaxation is assumed as linear which is provided by the equation, $\varepsilon_t = \varepsilon_o + (1-q_p). \frac{\Delta\sigma}{E}$. Here, (D_c, D_f) is equal to (0.18, 3.67).

Bilinear method is one of the inelastic approaches in which temperature dependent bilinear hardening parameters such as poisons ratio, yield stress and tangent modulus were used coupled with the parameters used in elastic analysis. In this method creep and fatigue damages are 0.75 and 0.051, respectively.

For the Chaboche model, $C_1, \gamma_1, C_2, \gamma_2, C_3, \gamma_3, C_4, \gamma_4$, E and σ were provided as input parameters at both 250°C and 600°C. The output of creep-fatigue interactions is D_c= 1.33 and D_f = 0.076 for 100 applied thermal loading cycles.

For the Chaboche with short time stress relaxation model, the temperature dependent time hardening short-term creep-parameters such as power law multiplier, eq. stress order and time order were used at both 250°C and 600°C. In this inelastic advanced constitutive model, the creep and fatigue damages are found as 1.37 and 0.082, respectively.

For the Chaboche with long time stress relaxation model, the temperature dependent time hardening long-term creep-parameters such as power law multiplier, eq. stress order and time order were used at both 250°C and 600°C. The outcome of simultaneous creep-fatigue effects is D_c= 1.45 and D_f = 0.080 for 100 applied thermal loading cycles.

In the Chaboche with viscous creep model, the multiplier (k) and power(N) are provided depending upon temperature at both 250°C and 600°C. Here, (D_c, D_f) is equal to (0.085, 1.36).

5.3 Conclusions

In this research, both elastic and inelastic FEM analysis are performed and the study proposes to use advanced inelastic analysis-based methods with Chaboche model, uncoupled long-term creep, short-term stress relaxation and viscous power law creep for evaluating life of the component which can predict wide variety of material responses. In short, two conclusions have been made from this study as listed below.

i)   The study shows that simplified elastic FEM based procedure predicts conservative life under combined creep-fatigue loading condition; the models use artificial procedures for stress relaxation and have fundamental limitations for predicting material behavior.

ii)   Though Inelastic FEM based on advanced constitutive models are not also used in the PVP industries, this research focused on how advanced inelastic FEM based creep fatigue damage prediction help understand component failure. The finding proposes that advanced inelastic FEM based approaches can estimate higher component life which also simultaneously predicts wide variety of material responses, hence component can be designed with more accuracy, safety and confidence.

5.4 Recommendations for future studies

For better understanding of the critical components for steam generation of power plants which are subjected to very-high temperature and high pressure, this research can be further advanced for the future studies listed below.

i)   Advanced CDM based Damage Coupled Viscoplastic models can be used for life estimation of the tube-sheet structure where creep and fatigue damages can be evaluated directly from the model.

ii)   In this study, thermal responses are not exactly simulated, hence film coefficient for thermal simulation needs further investigation for better prediction of thermal cycles and hence the creep-fatigue interaction.

References

Abdollahi, E. and Chakherlou, T. N. (2017), "Numerical and experimental study of ratcheting in cold expanded plate of Al-alloy 2024-T3 in double shear lap joints", Fatigue & Fracture of Engineering Materials & Structures, Vol. 41(1), 41-56.

Abe, F. (2008), " Introduction to Creep-resistant steels. England: Woodland Publishing Limited", England.

Abrate, S. (2008), "Criteria for Yielding or Failure of Cellular Materials", Journal of Sandwitch Structures and Materials, Vol. 10.

Abu-Eishah, S. (2001), " Correlations for the Thermal Conductivity of Metals as a Function of Temperature", International Journal of Thermophysics, Vol. 22(6), 1855-1868,

Alberry, P. (2008), " Power Generation Materials-EGTM70", Swansea.

Ando, M. (2014), " Comparison and Assessment of the Creep-Fatigue Evaluation Methods with Notched Specimen Made of Mod.9Cr-1Mo Steel", Journal of Pressure vessel Technology, Vol. 136, 041406 (1-8).

Ando, M. Hasebe, S. Kobayashi, S. Kasahara, N. Toyoshi, A. Ohmae, T. Enuma, Y. (2014), "Thermal transient test and strength evaluation of a tubesheet structure made of Mod. 9Cr-1Mo steel. Part I: Test model design and experimental results", Journal of Neuclear Engineering and Design, Vol. 275, 408-421.

Ando, M. Hasebe, S. Kobayashi, S. Kasahara, N. Toyoshi, A. Ohmae, T. Enuma, Y. (2013), "Thermal transient test and strength evaluation of a thick cylinder modelmade of. Mod.9Cr–1Mo steel", Journal of Neuclear Engineering Design, Vol. 255, 296–309.

Ando, M. Hasebe, S. Kobayashi, S. Kasahara, N. Tovoshi, A. Ohmae, T. Enuma, Y. (2014), "Thermal transient test and strength evaluation of a tubesheet structuremade of Mod.9Cr–1Mo steel. Part I: Test model design and experimental results", Journal of Neuclear Engineering Design, Vol. 275, 408-421.

Ando, M., Hasebea, S., Kobayashia, S., Kasaharaa, N., Toyoshib, A., Ohmaeb, T.,Enumac, Y., "Thermal transient test and strength evaluation of a tubesheetstructure made of Mod.9Cr–1Mo steel. Part II: Creep-fatiguestrength evaluation," Journal of Nuclear Engineering and Design, Vol. 275, 422–432, 2014.

Ando, M. T. (2013), " Stress mitigation designof tubesheets with consideration of thermal stress inducement mechanism", J.Pressure Vessel Technol., 135 (6), 061207-1–061207-10.

Aoto, K. Uto, N. Sakamoto, Y. Ito, T. Toda, M. Kotake, S. (2011), "Design Study and R&D progress on Japan Sodium-Cooled Fast Reactor", Journal of Nuclear Engineering Science, , Vol. 48, 643-471.

Asayama, T. and Jetter, R. (2008), " An overview of creep-fatigue damage evaluation methods and an alternative approach", Proceedings of ASME Pressure Vessel and Piping Conference, ASME PVP2008-61820.

Ashikin, N. (2010), " Experimental Study of Heat Transfer Coefficient for Nano-fluid with Inserted Tape", Universiti malaysia pahang.

ASME. (1983), ASME Boiler and Pressure Vessel Code ANSI/ASME BPV-III, Section III, Nuclear Power Plant Components. New York.

ASME. (2015), Boiler & Pressure Vessel Code, Section III, Division 1, Subsection NH - Class 1 Components in Elevated Temperature Service.

ASTM-08.(2008), ASTM E8/E8M-08: Standard Test Methods for Tension Testing of Metallic Materials. USA: ASTM International.

Bakker, W. T.Viswanathan, R. (2000), " Materials for Ultra Supercritical Fossil Power Plants", Palo Alto.

Bhuvaneswari, S. E. (2019), "A Study of the Literature Review on Heat Transfer in A Helically Coiled Heat Exchanger", International journal of engineering research & technology (ijert), vol. 7.

Boresi, A. P. and Schmidt, R. J. (2003), "Advanced mechanics of materials", 6th ed. New York: Wiley.

Boyer, H. E. (1988), "Atlas of creep and stress-rupture curves", Ohio, Metals Park: ASM International.

Brochure (2006), " Advanced Power Plant Using High Efficiency Boiler / Turbine", Carbon Abatement Technologies Programme, Vol.BPB010.

Cambridge University, (2012), "Creep deformation of metals," Retrieved from http://www.doitpoms.ac.uk/tlplib/creep/index.php.

Cengel, Y.A. and Boles, M. A. (2006), " Thermodynamics: An Engineering Approach," New York, McGraw Hill.

Chaboche, J. L. and Rousselier, G. (1983), "On the Plastic and Viscoplastic Constitutive Equations—Part I: Rules Developed With Internal Variable Concept", j.Pressure Vessel Technol., Vol. 105(2), 153-158.

Chaboche, J. (1989), " Constitutive Equations for Cyclic Plasticity and Cyclic Viscoplasticity", International Journal of Plasticity, Vol.5(3), 247-302.

Chaboche, J. L. Dang-Van, K. Cordier, G. (1979), "Modelization of Strain Memory Effect on Cyclic Hardening of 316 Stainless Steel", Transections of the 5th International Conference on Structural Mechanics Reactor Technology, Vol. 11(3), 555-563,

Chen, X., Jiao (2004), " Modified kinematic hardening rule for multiaxial", International Journal of Plasticity, Vol. 20, 871-891.

Chikazawa, Y. (2012) "Evaluation of JSFR key technologies", Neuclear Technology, Vol. 179(3), 360-373.

Chow, C. L. and Yang, X. J. (2004), " A Generalized Mixed Isotropic-Kinematic Hardening Plastic Model Coupled with Anisotropic Damage for Sheet Metal Forming", International Journal of Damage Mechanics, Vol.13.

Coble, R.(1963), "A Model for Boundary Diffusion-Controlled Creep in Pollycrystalline Materials", Journal of Apllied Physics, Vol. 34, 1679-1684.

Dantec, D.(2015), "Correlated Solutions : Retrieved from Principle of Digital Image Correlation", http://www.correlatedsolutions.com/index.php/principle-of-digital-imagecorrelation.

Davis, J. R. (2000), " Mechanical testing and evaluation," 10th ed., Ohio, Materials Park:ASM International.

Deng, W. Xu, J. Hu, Y. Huang, Z. Jiang, L. (2019), " Isothermal and thermomechanical fatigue behavior of Inconel 718", Materials Science & Engineering, pp. 813-819.

Dhalla, A. K. (1986), " Verification of an Elastic Procedure," Journal of Pressure Vessel Technology, Vol. 108.

Dowling, N. E. (2013), "Mechanical Behavior of Materials," Pearson.

ECCC.(2009), ECCC data sheet, Steel Grade 91 (X10CrMoVNb9-1).

Edward, A. A. (2016), " Design Modellling and Performance Optimization of a marine Boiler", World Journal of Engineering Research and Technology, Vol.2,44-58 .

Esztergar, E. P. (1972), " Creep-Fatigue Interaction and Cumulative Damage Evaluations for Type 304 Stainless Steel: Hold-Time Fatigue Test Program and Review of Multiaxial Fatigue", Retrieved from Oak Ridge National Laboratory Oak Ridge, TennesseeORNL-4757 1972:https://www.iaea.org/inis/collection/NCLCollectionStore/_Public/04/038/40384 40.pdf, 1972.

Gan, W. Zhang, P. Wagoner, R. H. Daehn, G. S. (2006), " Effect of load redistribution in transient plastic flow," Metallurgical and Materials Transactions, Vol. 37 (7), 2097-2106.

Gooch, D. J. and Kimmins, S. T. "A study of Type IV Cracking in 0.S%CrMoV/2.2SCrMo Weldments", 3rd International Conference on Creep and Fracture of Engineering Materials and Structures, 698-703.

Haarmann, K. Vaillant, J. C. Vandenberghe, B. Bendick, W. Arbab, A. (2002), " The T91/P91 book, 2nd ed. Vallourec & Mannesmann Tubes".

Hakansson, P. Wallin, M. Ristinmaa, M. (2005), " Comparison of isotropic hardening and kinematic hardening in thermoplasticity," International Journal of Plasticity, Vol. 21(7), 1435-1460.

Hearn, E. J. (1997), "An Introduction to the Mechanics of Elastic and Plastic Deformation of Solids and Structural Material", 3rd ed. Oxford: Butterworth-Heinemann, Vol. 5, 401-429.

Huddleston, R. L. (1985), " An Improved Multiaxial Creep-Rupture Strength Criterion", Journal of Pressure Vessel Technology, Vol. 107, 421-429, 1985.

Islam, N. and Hassan, T. (2018), " Uniaxial Fatigue, Creep and Ratcheting Response Simulations of Alloy 617 Using Damage Coupled Viscoplastic Model", Proceedings of the ASME 2018 Pressure Vessels and Piping Conference, PVP2018-84756.

Itoh, M. Yoshida, F. Yamashita, Y. Ohmori, M. (1992), " FEM analysis for nonuniform yielding processes in mild steel plates under stretching," JSME International Journal, Vol. 135, 70-77.

Jawad, M. H. and Jetter, R. I. (2009), "Design and analysis of boiler and pressure vessel components ithe creep range", New York: ASME Press.

Janna, S. and William, (2009), " Engineering Transfer" Toledo, Ohio, CRC Press.

Jetter, R. I. (2012), "Subsection NH-Class 1 Components in Elevated Temperature Service, " in Companion Guide to the ASME Boiler and Pressure Vessel Code, vol. Vol. 1, K. R. Rao, Ed. 4th ed., New York: ASME Press.

Jiang, J. F. and Wu, Y. F. (2012), "Identification of material parameters for Drucker–Prager plasticity model for FRP confined circular concrete columns", International Journal of Solids and Structures, Vol. 49(3-4), 445-456.

Jiang, Y. and Kurath, P. (1996), "Characteristics of the Armstrong-Frederick Type Plasticity Models", International Journal of Plasticity, Vol. 12(3), 387-415.

127

Jirásek, M. and Bazant, Z. (2002), " Inelastic Analysis of Structures", John Wiley & Sons Ltd.,Illinois,USA..

Johnston, W. G. and Gilman, J. L. (1959), "Dislocation velocities, dislocation densities and plastic flow in lithium floride crystals," Journal of Applied Physics, Vol. 30, pp. 129.

JSME. (2009), Codes for Nuclear Power Generation Facilities – Rules on Design and Construction for Nuclear Power Plants.

Kasahara, N. (2001), "Strain concentration at structural discontinuities and its prediction based on characteristics of compliance change in structures", JSME, International Journal Series A, Vol.144, pp. 354-361.

Kasahara, N. Nagata, T. Chapuliot, S. (2004), "Nuclear Engineering and Design,".

Kaufman, A. and Hwang, S. Y. (1986), "Cyclic Creep Analysis from Finite Element Solutions", In the proceedings of 1986 Southern Conference on Theoretical and Applied Mechanics, . University of Southern California, 1986.

Kimura, K. Kushima, H. Abe, F. (2000), "Heterogeneous changes in microstructure and degradation behavior of 9Cr-1Mo-V-Nb steel during long term creep", Key Engineering Materials, vol. 171-174, 483-490.

Koo, G. (2014), "Creep-Fatigue Evaluations by KAERI Inelastic Analysis Model", Korea Atomic Energy Research Institute.

Li, B. Ren, F.C. Tang, X. Y. (2018), " The Effect of Strain Hardening on Mechanical Properties of S30408 Austenitic Stainless Steel: A Fundamental Research for the Quality Evaluation of Strain Strengthened Pressure Vessel", Material Science and Engineering, Vol. 382, IOP Conference Series.

Maddox, S .J. (2003), "Review of fatigue assessment procedures for welded aluminium structures", International Journal of Fatigue, Vol. 25 , 1359–1378.

Masakazu, I. (2011), " The Status of Generation IV Sodium-Cooled Fast Reactor Technology Development and its Future Project" ,Science Direct, Vol. 7, 79-87.

Materials, (2007), "Fossil-Fuelled Power Generation", UK, Materials UK Energy Review.

More, and Hemant, (2020), "Nuclear Physics. Retrieved from The fact factor," https://thefactfactor.com/category/facts/pure_science/physics/.

Muniandy, N. Siswanto, W. A. Tobi, A. l. M. (2016), "The influence of Linear Kinematic Hardening and Non-linear Combined Isotropic-kinematic Hardening Plasticity Model on Sliding Contact", International Journal of Mechanics and Mechatronics Engineering, Vol. 16(04), 83-88.

Narayanasamy, R. and Prasad, S. (2013) " Mechanical behavior of materials : engineering methods for deformation, fracture, and fatigue", Pearson, Pearson Education.

Nikolais, A. J. R. (2017), "Evaluation of a nonlinear cumulative creep damage model for design applications", Master's Thesis,University of Stavanger.

Ohno, N. (1982), " A Constitutive Model of Cyclic Plasticity with a Nonhardening Strain Region", Journal of Applied Mechanics, ASME, Vol. 104, 721-727.

Onizawa, T. (2013), "Development of 2012 Edition of JSME Code for Design and Construction of Fast Reactors(3) and Development of the Material Strength Standard of Modified 9Cr.-1 Mo. Steel", Proceedings of the ASME 2013 Pressure Vessels and Piping Conference. Paris, France: PVP2013.

Penny, R. K. and Marriott, D. L. (1995), " Design for creep," 2nd ed., London: Chapman & Hall.

Petrangeli, G. (2006), " Safety of Specific Plants and of Other Activities", Nuclear Safety, Vol. 25(5), 229-236.

ASME, (2015), "ASME:Boiler & Pressure Vessel Code, Section VIII, Division 2 - Rules for construction of pressure vessels:Alternative rules".

Rajos, A. (2018), " Sodium-Cooled Fast Reactors as a Generation IV Nuclear Reactor," Stanford University, PH241.

Rasaq, B. T.(2018), " Determination of Thermal Conductivities of Some", Physical Science International Journal, Vol. 19(3), 1-8.

Ridon, K. M. (2018), " Nuclear Energy Development in Bangladesh: A Study of Opportunities and Challenges", Energies, Vol. 1672(11), 02-15.

Ritz, E. T. Sabrina J. Benedek, N. A. (2019), "Thermal expansion in insulating solids from first principles", Journal of Applied Physics, Vol. 126 (17).

Robinson, E. L. (1955), " Steam Piping Design to Minimize Creep Concentrations", ASME, Vol. 77, 1147-1158.

Holdsworth, S. R. and Merckling, G. (2014), "ECCC Developments in the Assessment of Creep-Rupture Properties," http://www.ommi.co.uk/etd/eccc/advancedcreep/SRHGMpap1.pdf.

Sakanashi, Y. (2013), "Measurement of Creep Deformation in Weldments," UK: Ph.D. Thesis, The Open University.

Sanjooram, P. (2014), "Stress and Creep Damage Evolution in Materials for Ultra Supercritical power Plants," PhD Thesis, The Open University.

Sarbu, L. and Dorca, A. (2019), "Review on heat transfer analysis in thermal energy storage using latent heat", International Journal of Energy Research, Vol. 43(1), 29-64.

Sato, M. Kikuchi, H. Kashahara, N. (2011), "Study On Mechanism Of Stress-Strain Redistribution By Elasticplastic", Proceedings of the ASME 2011 Pressure Vessels & Piping Division Conference, Baltimore, Maryland, USA: PVP2011.

Sekhar, R. and Sharma, K.V. (2013) "Study of viscosity and specific heat capacity characteristics of water- based Al2O3 nanofluids at low particle concentrations," Journal of Experimental Nanoscience, Vol. 10, 86-102.

Sham, T. A. (2017), " Assessment of Creep Damage Evaluation Methods for Grade 91 Steel in the. FR17," Lemont, Illinois, USA.

Shibli, I. A. (2000), " Overview of the HIDA project", 2nd International HIDA Conference on Advances in Defect Assessment in High Temperature Plant.

Shioya, T. Shioiri, J. (1976), " Elastic–plastic analysis of the yield process in mild steel", Journal of the Mechanics and Physics of Solids, Vol. 24, 187-204.

Sica, L. U. R. (2017), " An experimental study of the validity of the von Mises yielding criterion for elasto-viscoplastic materials," Rio de Janeiro: PhD thesis in Mechanical Engineering.

Sikka, V. K. Ward, C. T. Thomas, K. C. (1981), " Modified 9Cr-1Mo steel," Conference on ferritic Steels for High Temperature Applications, 65-84.

Strang, A. and Vodarek,V. (1996), "Z Phase Formation in Martensitic 12CrMoVNb Steel", Materials Science and Technology, Vol.12, 552-556.

Sudula, V. S. P. (2020), "Bilinear Isotropic and Bilinear Kinematic Hardening of AZ31 Magnesium Alloy",International Journal of Advanced Research in Engineering and Technology, Vol. 11(8), 518-531.

Taguchi, K. U. (1993), "Creep-fatigue life prediction for modified 9Cr-1mo steel," Proceedings of ASME Pressure Vessel and Piping Conference, Vol. 262, 175-180.

Taherizadeh, A. Daniel, E. G. Yoon, J. W. (2015), " A non-associated plasticity model with anisotropic and nonlinear kinematic hardening for simulation of sheet metal forming," International Journal Solids and Structures, Vol. 69-70, 370-382.

Takahashi, Y. (1999), " Further evaluation of creep-fatigue life prediction methods for low-carbon nitrogen-added 316 stainless steel," Journal of Pressure Vessel Technology, Vol. 121, 142-148.

Tsukahara, H. Iung, T. (1998), "Finite element simulation of the Piobert–Lüders behavior in a uniaxial tensile test", Materials Science and Engineering, 304-308.

Ucak, A. and Tsopelas, P.(2008), "Realistic Modeling of Structural Steels with Yield Plateau Using Abaqus/Standard," Proceedings of the 2008 Abaqus Users Conference. Newport, RI.

Vinson, J. R. and Sierakowski, R. L.(2008), "The Behavior of Structures Composed of Composite Materials (Solid Mechanics and Its Applications", Kluwer academic publishers.

Vishwanathan, R. and Bakker, W.T. (2000), "Materials for Ultra Supercritical Fossil Power Plants", Palo Alto.

Viswanathan, R. (1989), "Damage mechanisms and life assessment of high-temperature components", Ohio, Metals Park : ASM International.

Yamano, H. Kubo, S. Shimakawa,Y. Fujita, K. Suzuki,T. Kuriska, K. (2012),"Safety Design and Evaluation in a Large-Scale Japan Sodium-Cooled Fast Reactor", Science and Technology of Neuclear Installations, Vol. 14.

Yang, W. (1980), "A Generalized von Mises Criterion for Yield and Fracture. Journal of Applied Mechanics", Journal of Applied Mechanics, Vol. 47(2), 297-300.

Yoshida, F. (2000), " A constitutive model of cyclic plasticity", International Journal of Plasticity, Vol. 16, 359-380.

Zeman, J. L. Rauscher, F. Schindler, S. (2006), " Pressure Vessel Design: The Direct Route (Advances in Structural Integrity)", Burlington: Elsevier Science.

Zerovnik, A. Kunc, R. Prebil, I. (2010), "Yield-point phenomenon in constitutive models of cyclic plasticity", Computational Material Science, Vol. 49(3), 473-482.

Zhu, X. K. Leis, B. N. (2003), " Strength Criteria and Analytic Predictions," Proceedings of the Thirteenth(2003) International Offshore and Polar Engineering Conference, pp. ISSN 1098-6189, Hawaii,USA: International Society of Offshore and Polar Engineers.

Zogzas, N. P. Krokida, M. K. Michailidis, P. A. Maroulis, Z., B. (2007), " Literature data of heat transfer coefficients in food processing," International Journal of Food Properties, Vol. 5(2) ,2002-2012 .

Appendix-A

Creep damage calculation steps in SRL-Neuber method is shown below.

σ_t	ε_t	ε_e	ε_p	ε_c	Δt	t_r	t_r (hr.)	t_R (hr.)	Creep damage
223.9	0.00535	-2E-05	0.0054	0					
222.9	0.00537	-2E-05	0.0054	1.8E-05	1	1	0.0003	1.9063	0.0001457
221.9	0.0054	-1E-05	0.0054	3.6E-05	9.75E-01	1.98E+00	0.0005	2.03243	1.33E-04
220.9	0.00542	-5E-06	0.0054	5.5E-05	9.98E-01	2.97E+00	0.0008	2.16729	1.28E-04
219.9	0.00545	5E-07	0.0054	7.4E-05	1.03E+00	4.00E+00	0.0011	2.31149	1.23E-04
218.9	0.00547	6E-06	0.0054	9.3E-05	1.06E+00	5.06E+00	0.0014	2.46573	1.19E-04
217.9	0.0055	1E-05	0.0054	0.00011	1.09E+00	6.15E+00	0.0017	2.63073	1.15E-04
216.9	0.00552	2E-05	0.0054	0.00013	1.12E+00	7.27E+00	0.002	2.80727	1.11E-04
215.9	0.00555	2E-05	0.0054	0.00015	1.15E+00	8.42E+00	0.0023	2.9962	1.07E-04
214.9	0.00557	3E-05	0.0054	0.00017	1.19E+00	9.61E+00	0.0027	3.19842	1.03E-04
213.9	0.0056	4E-05	0.0054	0.00019	1.22E+00	1.08E+01	0.003	3.41491	9.96E-05
212.9	0.00563	4E-05	0.0054	0.00021	1.26E+00	1.21E+01	0.0034	3.64672	9.60E-05
211.9	0.00565	5E-05	0.0054	0.00023	1.30E+00	1.34E+01	0.0037	3.89498	9.26E-05
210.9	0.00568	5E-05	0.0054	0.00025	1.34E+00	1.47E+01	0.0041	4.16092	8.93E-05
209.9	0.00571	6E-05	0.0054	0.00027	1.38E+00	1.61E+01	0.0045	4.44584	8.61E-05
208.9	0.00573	7E-05	0.0054	0.0003	1.42E+00	1.75E+01	0.0049	4.75117	8.30E-05
207.9	0.00576	7E-05	0.0054	0.00032	1.46E+00	1.90E+01	0.0053	5.07842	8.01E-05
206.9	0.00579	8E-05	0.0054	0.00034	1.51E+00	2.05E+01	0.0057	5.42925	7.72E-05
205.9	0.00582	8E-05	0.0054	0.00036	1.55E+00	2.21E+01	0.0061	5.80542	7.44E-05

204.9	0.00585	9E-05	0.0054	0.00038	1.60E+00	2.37E+01	0.0066	6.20885	7.17E-05
203.9	0.00587	1E-04	0.0054	0.00041	1.65E+00	2.53E+01	0.007	6.64161	6.91E-05
202.9	0.0059	0.0001	0.0054	0.00043	1.70E+00	2.70E+01	0.0075	7.10591	6.66E-05
201.9	0.00593	0.0001	0.0054	0.00045	1.76E+00	2.88E+01	0.008	7.60417	6.42E-05
200.9	0.00596	0.0001	0.0054	0.00048	1.81E+00	3.06E+01	0.0085	8.13897	6.18E-05
199.9	0.00599	0.0001	0.0054	0.0005	1.87E+00	3.25E+01	0.009	8.71312	5.96E-05
198.9	0.00602	0.0001	0.0054	0.00052	1.93E+00	3.44E+01	0.0096	9.32963	5.74E-05
197.9	0.00605	0.0001	0.0054	0.00055	1.99E+00	3.64E+01	0.0101	9.99178	5.53E-05
196.9	0.00608	0.0001	0.0054	0.00057	2.05E+00	3.84E+01	0.0107	10.7031	5.33E-05
195.9	0.00611	0.0001	0.0054	0.0006	2.12E+00	4.05E+01	0.0113	11.4674	5.13E-05
194.9	0.00615	0.0001	0.0054	0.00062	2.19E+00	4.27E+01	0.0119	12.2888	4.94E-05
193.9	0.00618	0.0002	0.0054	0.00065	2.26E+00	4.50E+01	0.0125	13.1717	4.76E-05
192.9	0.00621	0.0002	0.0054	0.00068	2.33E+00	4.73E+01	0.0131	14.121	4.58E-05
191.9	0.00624	0.0002	0.0054	0.0007	2.41E+00	4.97E+01	0.0138	15.142	4.41E-05
190.9	0.00627	0.0002	0.0054	0.00073	2.48E+00	5.22E+01	0.0145	16.2401	4.25E-05
189.9	0.00631	0.0002	0.0054	0.00076	2.57E+00	5.48E+01	0.0152	17.4216	4.09E-05
188.9	0.00634	0.0002	0.0054	0.00078	2.65E+00	5.74E+01	0.016	18.6931	3.94E-05
187.9	0.00637	0.0002	0.0054	0.00081	2.74E+00	6.02E+01	0.0167	20.0616	3.79E-05
186.9	0.00641	0.0002	0.0054	0.00084	2.83E+00	6.30E+01	0.0175	21.535	3.65E-05
185.9	0.00644	0.0002	0.0054	0.00087	2.92E+00	6.59E+01	0.0183	23.1217	3.51E-05
184.9	0.00648	0.0002	0.0054	0.0009	3.02E+00	6.89E+01	0.0191	24.8307	3.38E-05
183.9	0.00651	0.0002	0.0054	0.00093	3.12E+00	7.21E+01	0.02	26.6719	3.25E-05
182.9	0.00655	0.0002	0.0054	0.00096	3.23E+00	7.53E+01	0.0209	28.6561	3.13E-05
181.9	0.00658	0.0002	0.0054	0.00099	3.34E+00	7.86E+01	0.0218	30.7947	3.01E-05
180.9	0.00662	0.0002	0.0054	0.00102	3.45E+00	8.21E+01	0.0228	33.1004	2.90E-05

179.9	0.00666	0.0002	0.0054	0.00105	3.57E+00	8.56E+01	0.0238	35.5869	2.79E-05
178.9	0.00669	0.0002	0.0054	0.00108	3.69E+00	8.93E+01	0.0248	38.2688	2.68E-05
177.9	0.00673	0.0002	0.0054	0.00111	3.82E+00	9.32E+01	0.0259	41.1624	2.58E-05
176.9	0.00677	0.0003	0.0054	0.00114	3.96E+00	9.71E+01	0.027	44.285	2.48E-05
175.9	0.00681	0.0003	0.0054	0.00118	4.09E+00	1.01E+02	0.0281	47.6556	2.39E-05
174.9	0.00685	0.0003	0.0054	0.00121	4.24E+00	1.05E+02	0.0293	51.2949	2.29E-05
173.9	0.00689	0.0003	0.0054	0.00124	4.39E+00	1.10E+02	0.0305	55.2251	2.21E-05
172.9	0.00693	0.0003	0.0054	0.00128	4.54E+00	1.14E+02	0.0318	59.4706	2.12E-05
171.9	0.00697	0.0003	0.0054	0.00131	4.70E+00	1.19E+02	0.0331	64.0578	2.04E-05
170.9	0.00701	0.0003	0.0054	0.00135	4.87E+00	1.24E+02	0.0344	69.0156	1.96E-05
169.9	0.00705	0.0003	0.0054	0.00138	5.05E+00	1.29E+02	0.0358	74.3753	1.89E-05
168.9	0.00709	0.0003	0.0054	0.00142	5.23E+00	1.34E+02	0.0373	80.1707	1.81E-05
167.9	0.00713	0.0003	0.0054	0.00145	5.42E+00	1.40E+02	0.0388	86.4392	1.74E-05
166.9	0.00718	0.0003	0.0054	0.00149	5.62E+00	1.45E+02	0.0404	93.2209	1.67E-05
165.9	0.00722	0.0003	0.0054	0.00153	5.83E+00	1.51E+02	0.042	100.56	1.61E-05
164.9	0.00726	0.0003	0.0054	0.00156	6.04E+00	1.57E+02	0.0437	108.504	1.55E-05
163.9	0.00731	0.0003	0.0054	0.0016	6.27E+00	1.63E+02	0.0454	117.105	1.49E-05
162.9	0.00735	0.0003	0.0054	0.00164	6.50E+00	1.70E+02	0.0472	126.421	1.43E-05
161.9	0.0074	0.0003	0.0054	0.00168	6.75E+00	1.77E+02	0.0491	136.513	1.37E-05
160.9	0.00744	0.0003	0.0054	0.00172	7.00E+00	1.84E+02	0.051	147.449	1.32E-05
159.9	0.00749	0.0004	0.0054	0.00176	7.27E+00	1.91E+02	0.053	159.302	1.27E-05
158.9	0.00754	0.0004	0.0054	0.0018	7.54E+00	1.98E+02	0.0551	172.154	1.22E-05
157.9	0.00758	0.0004	0.0054	0.00185	7.83E+00	2.06E+02	0.0573	186.092	1.17E-05
156.9	0.00763	0.0004	0.0054	0.00189	8.14E+00	2.14E+02	0.0596	201.212	1.12E-05
155.9	0.00768	0.0004	0.0054	0.00193	8.45E+00	2.23E+02	0.0619	217.62	1.08E-05

154.9	0.00773	0.0004	0.0054	0.00197	8.78E+00	2.32E+02	0.0644	235.429	1.04E-05
153.9	0.00778	0.0004	0.0054	0.00202	9.13E+00	2.41E+02	0.0669	254.765	9.95E-06
152.9	0.00783	0.0004	0.0054	0.00206	9.49E+00	2.50E+02	0.0695	275.765	9.56E-06
151.9	0.00788	0.0004	0.0054	0.00211	9.87E+00	2.60E+02	0.0723	298.579	9.18E-06
150.9	0.00794	0.0004	0.0054	0.00216	1.03E+01	2.70E+02	0.0751	323.37	8.81E-06
149.9	0.00799	0.0004	0.0054	0.0022	1.07E+01	2.81E+02	0.0781	350.319	8.46E-06
148.9	0.00804	0.0004	0.0054	0.00225	1.11E+01	2.92E+02	0.0812	379.621	8.13E-06
147.9	0.0081	0.0004	0.0054	0.0023	1.16E+01	3.04E+02	0.0844	411.492	7.80E-06
146.9	0.00815	0.0004	0.0054	0.00235	1.20E+01	3.16E+02	0.0877	446.166	7.49E-06
145.9	0.00821	0.0004	0.0054	0.0024	1.25E+01	3.28E+02	0.0912	483.903	7.19E-06
144.9	0.00827	0.0004	0.0054	0.00245	1.30E+01	3.41E+02	0.0948	524.985	6.90E-06
143.9	0.00832	0.0005	0.0054	0.0025	1.36E+01	3.55E+02	0.0986	569.722	6.63E-06
142.9	0.00838	0.0005	0.0054	0.00255	1.42E+01	3.69E+02	0.1025	618.455	6.36E-06
141.9	0.00844	0.0005	0.0054	0.00261	1.48E+01	3.84E+02	0.1066	671.556	6.11E-06
140.9	0.0085	0.0005	0.0054	0.00266	1.54E+01	3.99E+02	0.1109	729.437	5.86E-06
139.9	0.00856	0.0005	0.0054	0.00271	1.61E+01	4.15E+02	0.1154	792.547	5.63E-06
138.9	0.00862	0.0005	0.0054	0.00277	1.67E+01	4.32E+02	0.12	861.38	5.40E-06
137.9	0.00868	0.0005	0.0054	0.00283	1.75E+01	4.50E+02	0.1249	936.48	5.18E-06
136.9	0.00875	0.0005	0.0054	0.00288	1.82E+01	4.68E+02	0.1299	1018.44	4.97E-06
135.9	0.00881	0.0005	0.0054	0.00294	1.90E+01	4.87E+02	0.1352	1107.93	4.77E-06
134.9	0.00888	0.0005	0.0054	0.003	1.99E+01	5.07E+02	0.1408	1205.65	4.58E-06
133.9	0.00894	0.0005	0.0054	0.00306	2.08E+01	5.28E+02	0.1465	1312.41	4.40E-06
132.9	0.00901	0.0005	0.0054	0.00312	2.17E+01	5.49E+02	0.1526	1429.08	4.22E-06
131.9	0.00908	0.0005	0.0054	0.00319	2.27E+01	5.72E+02	0.1589	1556.63	4.05E-06
130.9	0.00915	0.0005	0.0054	0.00325	2.37E+01	5.96E+02	0.1655	1696.11	3.89E-06

136

129.9	0.00922	0.0005	0.0054	0.00331	2.48E+01	6.20E+02	0.1724	1848.69	3.73E-06
128.9	0.00929	0.0005	0.0054	0.00338	2.60E+01	6.46E+02	0.1796	2015.66	3.58E-06
127.9	0.00936	0.0005	0.0054	0.00345	2.72E+01	6.74E+02	0.1871	2198.45	3.43E-06
126.9	0.00944	0.0006	0.0054	0.00351	2.85E+01	7.02E+02	0.195	2398.61	3.30E-06
125.9	0.00951	0.0006	0.0054	0.00358	2.98E+01	7.32E+02	0.2033	2617.87	3.16E-06
124.9	0.00959	0.0006	0.0054	0.00365	3.12E+01	7.63E+02	0.212	2858.16	3.03E-06
123.9	0.00967	0.0006	0.0054	0.00373	3.27E+01	7.96E+02	0.2211	3121.56	2.91E-06
122.9	0.00974	0.0006	0.0054	0.0038	3.43E+01	8.30E+02	0.2306	3410.42	2.79E-06
121.9	0.00982	0.0006	0.0054	0.00387	3.60E+01	8.66E+02	0.2406	3727.3	2.68E-06
120.9	0.00991	0.0006	0.0054	0.00395	3.78E+01	9.04E+02	0.2511	4075.05	2.57E-06
119.9	0.00999	0.0006	0.0054	0.00402	3.96E+01	9.43E+02	0.2621	4456.81	2.47E-06
118.9	0.01007	0.0006	0.0054	0.0041	4.16E+01	9.85E+02	0.2736	4876.08	2.37E-06
117.9	0.01016	0.0006	0.0054	0.00418	4.37E+01	1.03E+03	0.2858	5336.69	2.27E-06
116.9	0.01024	0.0006	0.0054	0.00426	4.59E+01	1.07E+03	0.2985	5842.93	2.18E-06
115.9	0.01033	0.0006	0.0054	0.00434	4.83E+01	1.12E+03	0.3119	6399.51	2.09E-06
114.9	0.01042	0.0006	0.0054	0.00443	5.08E+01	1.17E+03	0.326	7011.68	2.01E-06
113.9	0.01051	0.0006	0.0054	0.00451	5.34E+01	1.23E+03	0.3409	7685.23	1.93E-06
112.9	0.01061	0.0006	0.0054	0.0046	5.62E+01	1.28E+03	0.3565	8426.63	1.85E-06
111.9	0.0107	0.0006	0.0054	0.00469	5.92E+01	1.34E+03	0.3729	9243	1.78E-06
110.9	0.0108	0.0006	0.0054	0.00478	6.23E+01	1.40E+03	0.3902	10142.3	1.71E-06
109.9	0.0109	0.0007	0.0054	0.00487	6.57E+01	1.47E+03	0.4085	11133.3	1.64E-06
108.9	0.011	0.0007	0.0054	0.00497	6.93E+01	1.54E+03	0.4277	12225.8	1.57E-06
107.9	0.0111	0.0007	0.0054	0.00506	7.31E+01	1.61E+03	0.448	13430.7	1.51E-06
106.9	0.0112	0.0007	0.0054	0.00516	7.71E+01	1.69E+03	0.4694	14760	1.45E-06
105.9	0.01131	0.0007	0.0054	0.00526	8.14E+01	1.77E+03	0.4921	16227.3	1.39E-06

137

104.9	0.01142	0.0007	0.0054	0.00536	8.60E+01	1.86E+03	0.5159	17847.4	1.34E-06
103.9	0.01153	0.0007	0.0054	0.00547	9.09E+01	1.95E+03	0.5412	19637.1	1.29E-06
102.9	0.01164	0.0007	0.0054	0.00557	9.61E+01	2.04E+03	0.5679	21614.8	1.24E-06
101.9	0.01175	0.0007	0.0054	0.00568	1.02E+02	2.15E+03	0.5961	23801.2	1.19E-06
100.9	0.01187	0.0007	0.0054	0.00579	1.08E+02	2.25E+03	0.626	26219.4	1.14E-06
99.92	0.01199	0.0007	0.0054	0.0059	1.14E+02	2.37E+03	0.6577	28895	1.10E-06
98.92	0.01211	0.0007	0.0054	0.00602	1.21E+02	2.49E+03	0.6913	31856.7	1.05E-06
97.92	0.01223	0.0007	0.0054	0.00614	1.28E+02	2.62E+03	0.7269	35136.4	1.01E-06
96.92	0.01236	0.0007	0.0054	0.00626	1.36E+02	2.75E+03	0.7646	38769.7	9.74E-07
95.92	0.01249	0.0007	0.0054	0.00638	1.44E+02	2.90E+03	0.8047	42796.6	9.36E-07
94.92	0.01262	0.0007	0.0054	0.00651	1.53E+02	3.05E+03	0.8472	47261.4	9.01E-07
93.92	0.01275	0.0007	0.0054	0.00664	1.63E+02	3.21E+03	0.8925	52214.1	8.66E-07
92.92	0.01289	0.0008	0.0054	0.00677	1.73E+02	3.39E+03	0.9406	57710.1	8.34E-07
91.92	0.01303	0.0008	0.0054	0.0069	1.84E+02	3.57E+03	0.9918	63811.8	8.02E-07
90.92	0.01317	0.0008	0.0054	0.00704	1.96E+02	3.77E+03	1.0463	70588.8	7.72E-07
89.92	0.01332	0.0008	0.0054	0.00718	2.09E+02	3.98E+03	1.1044	78118.9	7.44E-07
88.92	0.01347	0.0008	0.0054	0.00732	2.23E+02	4.20E+03	1.1663	86489.7	7.16E-07
87.92	0.01362	0.0008	0.0054	0.00747	2.38E+02	4.44E+03	1.2324	95798.8	6.90E-07
86.92	0.01378	0.0008	0.0054	0.00762	2.54E+02	4.69E+03	1.303	106156	6.65E-07
85.92	0.01394	0.0008	0.0054	0.00778	2.71E+02	4.96E+03	1.3784	117684	6.41E-07
84.92	0.01411	0.0008	0.0054	0.00793	2.90E+02	5.25E+03	1.4591	130521	6.18E-07
83.92	0.01427	0.0008	0.0054	0.0081	3.11E+02	5.56E+03	1.5454	144822	5.96E-07
82.92	0.01445	0.0008	0.0054	0.00826	3.33E+02	5.90E+03	1.6378	160761	5.75E-07
81.92	0.01462	0.0008	0.0054	0.00843	3.57E+02	6.25E+03	1.7369	178532	5.55E-07
80.92	0.0148	0.0008	0.0054	0.00861	3.83E+02	6.64E+03	1.8432	198355	5.36E-07

138

79.92	0.01499	0.0008	0.0054	0.00879	4.11E+02	7.05E+03	1.9574	220477	5.18E-07
78.92	0.01518	0.0008	0.0054	0.00897	4.42E+02	7.49E+03	2.08	245173	5.00E-07
77.92	0.01537	0.0008	0.0054	0.00916	4.75E+02	7.96E+03	2.212	272757	4.84E-07
76.92	0.01557	0.0008	0.0054	0.00935	5.11E+02	8.47E+03	2.354	303577	4.68E-07
75.92	0.01578	0.0009	0.0054	0.00955	5.51E+02	9.03E+03	2.5071	338028	4.53E-07
74.92	0.01599	0.0009	0.0054	0.00976	5.94E+02	9.62E+03	2.6722	376554	4.38E-07
73.92	0.0162	0.0009	0.0054	0.00997	6.42E+02	1.03E+04	2.8505	419655	4.25E-07
72.92	0.01643	0.0009	0.0054	0.01018	6.94E+02	1.10E+04	3.0431	467892	4.12E-07
					Total Creep Damage				**0.0037537**

Appendix-B

Creep damage calculation steps in SRL-Optimized is shown below.

σ_t	ε_t	ε_e	ε_p	ε_c	$\Deltaت$	t_r			Creep
223.9	0.00334	-2E-05	0.0034	0					
222.9	0.00336	-2E-05	0.0034	9.1E-06	1	1	0.0003	1.9063	0.000146
221.9	0.00337	-1E-05	0.0034	1.8E-05	4.91E-01	1.49E+00	0.0004	2.03243	6.71E-05
220.9	0.00339	-5E-06	0.0034	2.8E-05	4.71E-01	1.96E+00	0.0005	2.16729	6.04E-05
219.9	0.0034	5E-07	0.0034	3.7E-05	4.83E-01	2.44E+00	0.0007	2.31149	5.80E-05
218.9	0.00342	6E-06	0.0034	4.7E-05	4.98E-01	2.94E+00	0.0008	2.46573	5.61E-05
217.9	0.00344	1E-05	0.0034	5.7E-05	5.14E-01	3.46E+00	0.001	2.63073	5.43E-05
216.9	0.00345	2E-05	0.0034	6.6E-05	5.31E-01	3.99E+00	0.0011	2.80727	5.25E-05
215.9	0.00347	2E-05	0.0034	7.7E-05	5.48E-01	4.54E+00	0.0013	2.9962	5.08E-05
214.9	0.00348	3E-05	0.0034	8.7E-05	5.66E-01	5.10E+00	0.0014	3.19842	4.92E-05
213.9	0.0035	4E-05	0.0034	9.7E-05	5.85E-01	5.69E+00	0.0016	3.41491	4.76E-05
212.9	0.00352	4E-05	0.0034	0.00011	6.04E-01	6.29E+00	0.0017	3.64672	4.60E-05
211.9	0.00353	5E-05	0.0034	0.00012	6.24E-01	6.92E+00	0.0019	3.89498	4.45E-05
210.9	0.00355	5E-05	0.0034	0.00013	6.45E-01	7.56E+00	0.0021	4.16092	4.31E-05
209.9	0.00357	6E-05	0.0034	0.00014	6.66E-01	8.23E+00	0.0023	4.44584	4.16E-05
208.9	0.00358	7E-05	0.0034	0.00015	6.88E-01	8.92E+00	0.0025	4.75117	4.02E-05
207.9	0.0036	7E-05	0.0034	0.00016	7.11E-01	9.63E+00	0.0027	5.07842	3.89E-05
206.9	0.00362	8E-05	0.0034	0.00017	7.35E-01	1.04E+01	0.0029	5.42925	3.76E-05
205.9	0.00364	8E-05	0.0034	0.00019	7.60E-01	1.11E+01	0.0031	5.80542	3.63E-05
204.9	0.00365	9E-05	0.0034	0.0002	7.85E-01	1.19E+01	0.0033	6.20885	3.51E-05
203.9	0.00367	1E-04	0.0034	0.00021	8.12E-01	1.27E+01	0.0035	6.64161	3.39E-05
202.9	0.00369	0.0001	0.0034	0.00022	8.39E-01	1.36E+01	0.0038	7.10591	3.28E-05
201.9	0.00371	0.0001	0.0034	0.00023	8.67E-01	1.44E+01	0.004	7.60417	3.17E-05
200.9	0.00373	0.0001	0.0034	0.00025	8.97E-01	1.53E+01	0.0043	8.13897	3.06E-05
199.9	0.00374	0.0001	0.0034	0.00026	9.27E-01	1.62E+01	0.0045	8.71312	2.96E-05
198.9	0.00376	0.0001	0.0034	0.00027	9.59E-01	1.72E+01	0.0048	9.32963	2.85E-05
197.9	0.00378	0.0001	0.0034	0.00029	9.92E-01	1.82E+01	0.0051	9.99178	2.76E-05
196.9	0.0038	0.0001	0.0034	0.0003	1.03E+00	1.92E+01	0.0053	10.7031	2.66E-05
195.9	0.00382	0.0001	0.0034	0.00031	1.06E+00	2.03E+01	0.0056	11.4674	2.57E-05
194.9	0.00384	0.0001	0.0034	0.00033	1.10E+00	2.14E+01	0.0059	12.2888	2.48E-05
193.9	0.00386	0.0002	0.0034	0.00034	1.14E+00	2.25E+01	0.0063	13.1717	2.39E-05
192.9	0.00388	0.0002	0.0034	0.00035	1.17E+00	2.37E+01	0.0066	14.121	2.31E-05
191.9	0.0039	0.0002	0.0034	0.00037	1.22E+00	2.49E+01	0.0069	15.142	2.23E-05
190.9	0.00392	0.0002	0.0034	0.00038	1.26E+00	2.62E+01	0.0073	16.2401	2.15E-05
189.9	0.00394	0.0002	0.0034	0.0004	1.30E+00	2.75E+01	0.0076	17.4216	2.08E-05
188.9	0.00396	0.0002	0.0034	0.00041	1.35E+00	2.88E+01	0.008	18.6931	2.00E-05
187.9	0.00398	0.0002	0.0034	0.00043	1.40E+00	3.02E+01	0.0084	20.0616	1.93E-05

186.9	0.00401	0.0002	0.0034	0.00044	1.44E+00	3.17E+01	0.0088	21.535	1.86E-05
185.9	0.00403	0.0002	0.0034	0.00046	1.50E+00	3.32E+01	0.0092	23.1217	1.80E-05
184.9	0.00405	0.0002	0.0034	0.00047	1.55E+00	3.47E+01	0.0096	24.8307	1.73E-05
183.9	0.00407	0.0002	0.0034	0.00049	1.60E+00	3.63E+01	0.0101	26.6719	1.67E-05
182.9	0.00409	0.0002	0.0034	0.00051	1.66E+00	3.80E+01	0.0105	28.6561	1.61E-05
181.9	0.00412	0.0002	0.0034	0.00052	1.72E+00	3.97E+01	0.011	30.7947	1.55E-05
180.9	0.00414	0.0002	0.0034	0.00054	1.78E+00	4.15E+01	0.0115	33.1004	1.50E-05
179.9	0.00416	0.0002	0.0034	0.00056	1.85E+00	4.33E+01	0.012	35.5869	1.44E-05
178.9	0.00418	0.0002	0.0034	0.00057	1.92E+00	4.52E+01	0.0126	38.2688	1.39E-05
177.9	0.00421	0.0002	0.0034	0.00059	1.99E+00	4.72E+01	0.0131	41.1624	1.34E-05
176.9	0.00423	0.0003	0.0034	0.00061	2.06E+00	4.93E+01	0.0137	44.285	1.29E-05
175.9	0.00426	0.0003	0.0034	0.00063	2.14E+00	5.14E+01	0.0143	47.6556	1.24E-05
174.9	0.00428	0.0003	0.0034	0.00065	2.21E+00	5.36E+01	0.0149	51.2949	1.20E-05
173.9	0.0043	0.0003	0.0034	0.00067	2.30E+00	5.59E+01	0.0155	55.2251	1.16E-05
172.9	0.00433	0.0003	0.0034	0.00068	2.38E+00	5.83E+01	0.0162	59.4706	1.11E-05
171.9	0.00435	0.0003	0.0034	0.0007	2.47E+00	6.08E+01	0.0169	64.0578	1.07E-05
170.9	0.00438	0.0003	0.0034	0.00072	2.56E+00	6.34E+01	0.0176	69.0156	1.03E-05
169.9	0.00441	0.0003	0.0034	0.00074	2.66E+00	6.60E+01	0.0183	74.3753	9.94E-06
168.9	0.00443	0.0003	0.0034	0.00076	2.76E+00	6.88E+01	0.0191	80.1707	9.57E-06
167.9	0.00446	0.0003	0.0034	0.00078	2.87E+00	7.16E+01	0.0199	86.4392	9.22E-06
166.9	0.00448	0.0003	0.0034	0.0008	2.98E+00	7.46E+01	0.0207	93.2209	8.87E-06
165.9	0.00451	0.0003	0.0034	0.00083	3.09E+00	7.77E+01	0.0216	100.56	8.54E-06
164.9	0.00454	0.0003	0.0034	0.00085	3.21E+00	8.09E+01	0.0225	108.504	8.22E-06
163.9	0.00457	0.0003	0.0034	0.00087	3.34E+00	8.43E+01	0.0234	117.105	7.92E-06
162.9	0.0046	0.0003	0.0034	0.00089	3.47E+00	8.77E+01	0.0244	126.421	7.62E-06
161.9	0.00462	0.0003	0.0034	0.00091	3.60E+00	9.13E+01	0.0254	136.513	7.33E-06
160.9	0.00465	0.0003	0.0034	0.00094	3.74E+00	9.51E+01	0.0264	147.449	7.05E-06
159.9	0.00468	0.0004	0.0034	0.00096	3.89E+00	9.90E+01	0.0275	159.302	6.79E-06
158.9	0.00471	0.0004	0.0034	0.00098	4.05E+00	1.03E+02	0.0286	172.154	6.53E-06
157.9	0.00474	0.0004	0.0034	0.00101	4.21E+00	1.07E+02	0.0298	186.092	6.28E-06
156.9	0.00477	0.0004	0.0034	0.00103	4.38E+00	1.12E+02	0.031	201.212	6.05E-06
155.9	0.0048	0.0004	0.0034	0.00106	4.56E+00	1.16E+02	0.0323	217.62	5.82E-06
154.9	0.00483	0.0004	0.0034	0.00108	4.74E+00	1.21E+02	0.0336	235.429	5.59E-06
153.9	0.00486	0.0004	0.0034	0.00111	4.93E+00	1.26E+02	0.035	254.765	5.38E-06
152.9	0.0049	0.0004	0.0034	0.00113	5.14E+00	1.31E+02	0.0364	275.765	5.17E-06
151.9	0.00493	0.0004	0.0034	0.00116	5.35E+00	1.36E+02	0.0379	298.579	4.98E-06
150.9	0.00496	0.0004	0.0034	0.00119	5.57E+00	1.42E+02	0.0394	323.37	4.78E-06
149.9	0.00499	0.0004	0.0034	0.00121	5.80E+00	1.48E+02	0.041	350.319	4.60E-06
148.9	0.00503	0.0004	0.0034	0.00124	6.05E+00	1.54E+02	0.0427	379.621	4.42E-06
147.9	0.00506	0.0004	0.0034	0.00127	6.30E+00	1.60E+02	0.0445	411.492	4.25E-06
146.9	0.0051	0.0004	0.0034	0.0013	6.57E+00	1.67E+02	0.0463	446.166	4.09E-06
145.9	0.00513	0.0004	0.0034	0.00133	6.85E+00	1.73E+02	0.0482	483.903	3.93E-06
144.9	0.00517	0.0004	0.0034	0.00136	7.14E+00	1.81E+02	0.0502	524.985	3.78E-06
143.9	0.0052	0.0005	0.0034	0.00139	7.45E+00	1.88E+02	0.0522	569.722	3.63E-06
142.9	0.00524	0.0005	0.0034	0.00142	7.77E+00	1.96E+02	0.0544	618.455	3.49E-06
141.9	0.00528	0.0005	0.0034	0.00145	8.11E+00	2.04E+02	0.0566	671.556	3.35E-06
140.9	0.00531	0.0005	0.0034	0.00148	8.47E+00	2.12E+02	0.059	729.437	3.22E-06

141

139.9	0.00535	0.0005	0.0034	0.00151	8.84E+00	2.21E+02	0.0615	792.547	3.10E-06
138.9	0.00539	0.0005	0.0034	0.00154	9.23E+00	2.30E+02	0.064	861.38	2.98E-06
137.9	0.00543	0.0005	0.0034	0.00158	9.65E+00	2.40E+02	0.0667	936.48	2.86E-06
136.9	0.00547	0.0005	0.0034	0.00161	1.01E+01	2.50E+02	0.0695	1018.44	2.75E-06
135.9	0.00551	0.0005	0.0034	0.00164	1.05E+01	2.61E+02	0.0724	1107.93	2.64E-06
134.9	0.00555	0.0005	0.0034	0.00168	1.10E+01	2.72E+02	0.0755	1205.65	2.54E-06
133.9	0.00559	0.0005	0.0034	0.00171	1.15E+01	2.83E+02	0.0787	1312.41	2.44E-06
132.9	0.00563	0.0005	0.0034	0.00175	1.21E+01	2.95E+02	0.082	1429.08	2.34E-06
131.9	0.00567	0.0005	0.0034	0.00179	1.26E+01	3.08E+02	0.0855	1556.63	2.25E-06
130.9	0.00572	0.0005	0.0034	0.00182	1.32E+01	3.21E+02	0.0892	1696.11	2.16E-06
129.9	0.00576	0.0005	0.0034	0.00186	1.38E+01	3.35E+02	0.093	1848.69	2.08E-06
128.9	0.00581	0.0005	0.0034	0.0019	1.45E+01	3.49E+02	0.0971	2015.66	2.00E-06
127.9	0.00585	0.0005	0.0034	0.00194	1.52E+01	3.65E+02	0.1013	2198.45	1.92E-06
126.9	0.0059	0.0006	0.0034	0.00198	1.59E+01	3.80E+02	0.1057	2398.61	1.84E-06
125.9	0.00595	0.0006	0.0034	0.00202	1.67E+01	3.97E+02	0.1103	2617.87	1.77E-06
124.9	0.00599	0.0006	0.0034	0.00206	1.75E+01	4.15E+02	0.1152	2858.16	1.70E-06
123.9	0.00604	0.0006	0.0034	0.00211	1.83E+01	4.33E+02	0.1203	3121.56	1.63E-06
122.9	0.00609	0.0006	0.0034	0.00215	1.92E+01	4.52E+02	0.1256	3410.42	1.57E-06
121.9	0.00614	0.0006	0.0034	0.00219	2.02E+01	4.72E+02	0.1312	3727.3	1.51E-06
120.9	0.00619	0.0006	0.0034	0.00224	2.12E+01	4.94E+02	0.1371	4075.05	1.45E-06
119.9	0.00624	0.0006	0.0034	0.00228	2.23E+01	5.16E+02	0.1433	4456.81	1.39E-06
118.9	0.0063	0.0006	0.0034	0.00233	2.34E+01	5.39E+02	0.1498	4876.08	1.33E-06
117.9	0.00635	0.0006	0.0034	0.00238	2.46E+01	5.64E+02	0.1567	5336.69	1.28E-06
116.9	0.0064	0.0006	0.0034	0.00243	2.59E+01	5.90E+02	0.1639	5842.93	1.23E-06
115.9	0.00646	0.0006	0.0034	0.00248	2.73E+01	6.17E+02	0.1714	6399.51	1.18E-06
114.9	0.00651	0.0006	0.0034	0.00253	2.87E+01	6.46E+02	0.1794	7011.68	1.14E-06
113.9	0.00657	0.0006	0.0034	0.00258	3.02E+01	6.76E+02	0.1878	7685.23	1.09E-06
112.9	0.00663	0.0006	0.0034	0.00263	3.18E+01	7.08E+02	0.1967	8426.63	1.05E-06
111.9	0.00669	0.0006	0.0034	0.00268	3.35E+01	7.41E+02	0.206	9243	1.01E-06
110.9	0.00675	0.0006	0.0034	0.00274	3.54E+01	7.77E+02	0.2158	10142.3	9.69E-07
109.9	0.00681	0.0007	0.0034	0.00279	3.73E+01	8.14E+02	0.2262	11133.3	9.31E-07
108.9	0.00687	0.0007	0.0034	0.00285	3.94E+01	8.54E+02	0.2371	12225.8	8.94E-07
107.9	0.00694	0.0007	0.0034	0.00291	4.16E+01	8.95E+02	0.2486	13430.7	8.60E-07
106.9	0.007	0.0007	0.0034	0.00297	4.39E+01	9.39E+02	0.2608	14760	8.26E-07
105.9	0.00707	0.0007	0.0034	0.00303	4.64E+01	9.85E+02	0.2737	16227.3	7.94E-07
104.9	0.00714	0.0007	0.0034	0.00309	4.90E+01	1.03E+03	0.2873	17847.4	7.63E-07
103.9	0.0072	0.0007	0.0034	0.00315	5.19E+01	1.09E+03	0.3018	19637.1	7.34E-07
102.9	0.00727	0.0007	0.0034	0.00321	5.49E+01	1.14E+03	0.317	21614.8	7.06E-07
101.9	0.00735	0.0007	0.0034	0.00328	5.81E+01	1.20E+03	0.3331	23801.2	6.78E-07
100.9	0.00742	0.0007	0.0034	0.00335	6.16E+01	1.26E+03	0.3503	26219.4	6.52E-07
99.92	0.00749	0.0007	0.0034	0.00342	6.53E+01	1.33E+03	0.3684	28895	6.27E-07
98.92	0.00757	0.0007	0.0034	0.00349	6.92E+01	1.40E+03	0.3876	31856.7	6.04E-07
97.92	0.00765	0.0007	0.0034	0.00356	7.34E+01	1.47E+03	0.408	35136.4	5.81E-07
96.92	0.00772	0.0007	0.0034	0.00363	7.80E+01	1.55E+03	0.4297	38769.7	5.59E-07
95.92	0.0078	0.0007	0.0034	0.0037	8.28E+01	1.63E+03	0.4527	42796.6	5.38E-07
94.92	0.00789	0.0007	0.0034	0.00378	8.80E+01	1.72E+03	0.4771	47261.4	5.17E-07
93.92	0.00797	0.0007	0.0034	0.00386	9.36E+01	1.81E+03	0.5031	52214.1	4.98E-07

92.92	0.00806	0.0008	0.0034	0.00394	9.96E+01	1.91E+03	0.5308	57710.1	4.80E-07
91.92	0.00814	0.0008	0.0034	0.00402	1.06E+02	2.02E+03	0.5603	63811.8	4.62E-07
90.92	0.00823	0.0008	0.0034	0.0041	1.13E+02	2.13E+03	0.5917	70588.8	4.45E-07
89.92	0.00833	0.0008	0.0034	0.00419	1.21E+02	2.25E+03	0.6252	78118.9	4.29E-07
88.92	0.00842	0.0008	0.0034	0.00428	1.29E+02	2.38E+03	0.6609	86489.7	4.13E-07
87.92	0.00852	0.0008	0.0034	0.00437	1.37E+02	2.52E+03	0.6991	95798.8	3.98E-07
86.92	0.00861	0.0008	0.0034	0.00446	1.47E+02	2.66E+03	0.7399	106156	3.84E-07
85.92	0.00871	0.0008	0.0034	0.00455	1.57E+02	2.82E+03	0.7834	117684	3.70E-07
84.92	0.00882	0.0008	0.0034	0.00465	1.68E+02	2.99E+03	0.8301	130521	3.57E-07
83.92	0.00892	0.0008	0.0034	0.00475	1.80E+02	3.17E+03	0.88	144822	3.45E-07
82.92	0.00903	0.0008	0.0034	0.00485	1.93E+02	3.36E+03	0.9336	160761	3.33E-07
81.92	0.00914	0.0008	0.0034	0.00496	2.07E+02	3.57E+03	0.991	178532	3.22E-07
80.92	0.00925	0.0008	0.0034	0.00506	2.22E+02	3.79E+03	1.0526	198355	3.11E-07
79.92	0.00937	0.0008	0.0034	0.00517	2.38E+02	4.03E+03	1.1189	220477	3.00E-07
78.92	0.00949	0.0008	0.0034	0.00528	2.56E+02	4.28E+03	1.1901	245173	2.90E-07
77.92	0.00961	0.0008	0.0034	0.0054	2.76E+02	4.56E+03	1.2667	272757	2.81E-07
76.92	0.00973	0.0008	0.0034	0.00552	2.97E+02	4.86E+03	1.3492	303577	2.72E-07
75.92	0.00986	0.0009	0.0034	0.00564	3.20E+02	5.18E+03	1.4382	338028	2.63E-07
74.92	0.00999	0.0009	0.0034	0.00577	3.46E+02	5.52E+03	1.5343	376554	2.55E-07
73.92	0.01013	0.0009	0.0034	0.0059	3.74E+02	5.90E+03	1.638	419655	2.47E-07
72.92	0.01027	0.0009	0.0034	0.00603	4.04E+02	6.30E+03	1.7502	467892	2.40E-07
71.92	0.01041	0.0009	0.0034	0.00617	437.2435	6738.0785	1.8717	521900	2.33E-07
70.92	0.01056	0.0009	0.0034	0.00631	473.8181	7211.8967	2.0033	582391	2.26E-07
69.92	0.01071	0.0009	0.0034	0.00645	514.016	7725.9127	2.1461	650171	2.2E-07
68.92	0.01086	0.0009	0.0034	0.0066	558.2545	8284.1672	2.3012	726146	2.14E-07
67.92	0.01102	0.0009	0.0034	0.00676	607.0061	8891.1733	2.4698	811337	2.08E-07
66.92	0.01119	0.0009	0.0034	0.00692	660.8064	9551.9797	2.6533	906896	2.02E-07
65.92	0.01136	0.0009	0.0034	0.00708	720.2639	10272.244	2.8534	1014120	1.97E-07
64.92	0.01153	0.0009	0.0034	0.00725	786.0713	11058.315	3.0718	1134473	1.92E-07
63.92	0.01171	0.0009	0.0034	0.00742	859.0185	11917.333	3.3104	1269605	1.88E-07
62.92	0.0119	0.0009	0.0034	0.0076	940.0079	12857.341	3.5715	1421373	1.84E-07
61.92	0.01209	0.0009	0.0034	0.00779	1030.073	13887.414	3.8576	1591874	1.8E-07
60.92	0.01229	0.0009	0.0034	0.00798	1130.4	15017.814	4.1716	1783466	1.76E-07
59.92	0.01249	0.0009	0.0034	0.00818	1242.352	16260.166	4.5167	1998810	1.73E-07
58.92	0.01271	0.001	0.0034	0.00839	1367.501	17627.666	4.8966	2240897	1.7E-07
57.92	0.01293	0.001	0.0034	0.0086	1507.663	19135.329	5.3154	2513098	1.67E-07
56.92	0.01315	0.001	0.0034	0.00882	1664.941	20800.269	5.7779	2819202	1.64E-07
55.92	0.01339	0.001	0.0034	0.00905	1841.777	22642.047	6.2895	3163469	1.62E-07
54.92	0.01363	0.001	0.0034	0.00929	2041.014	24683.061	6.8564	3550684	1.6E-07
53.92	0.01388	0.001	0.0034	0.00954	2265.97	26949.031	7.4858	3986217	1.58E-07
52.92	0.01415	0.001	0.0034	0.00979	2520.528	29469.559	8.186	4476088	1.56E-07
51.92	0.01442	0.001	0.0034	0.01006	2809.247	32278.806	8.9663	5027035	1.55E-07
50.92	0.0147	0.001	0.0034	0.01034	3137.495	35416.301	9.8379	5646593	1.54E-07
49.92	0.015	0.001	0.0034	0.01062	3511.612	38927.912	10.813	6343170	1.54E-07
48.92	0.0153	0.001	0.0034	0.01093	3939.11	42867.022	11.908	7126129	1.54E-07
47.92	0.01562	0.001	0.0034	0.01124	4428.92	47295.942	13.138	8005879	1.54E-07
46.92	0.01596	0.001	0.0034	0.01157	4991.7	52287.643	14.524	8993950	1.54E-07

45.92	0.0163	0.001	0.0034	0.01191	5640.211	57927.854	16.091	1E+07	1.55E-07
44.92	0.01667	0.001	0.0034	0.01226	6389.794	64317.648	17.866	1.1E+07	1.56E-07
43.92	0.01705	0.001	0.0034	0.01264	7258.961	71576.608	19.882	1.3E+07	1.58E-07
42.92	0.01744	0.001	0.0034	0.01303	8270.149	79846.758	22.18	1.4E+07	1.61E-07
41.92	0.01786	0.0011	0.0034	0.01344	9450.669	89297.426	24.805	1.6E+07	1.64E-07
40.92	0.0183	0.0011	0.0034	0.01387	10833.91	100131.34	27.814	1.8E+07	1.67E-07
39.92	0.01876	0.0011	0.0034	0.01432	12460.9	112592.24	31.276	2E+07	1.72E-07
38.92	0.01924	0.0011	0.0034	0.0148	14382.29	126974.53	35.271	2.3E+07	1.77E-07
37.92	0.01974	0.0011	0.0034	0.0153	16660.96	143635.49	39.899	2.5E+07	1.83E-07
36.92	0.02028	0.0011	0.0034	0.01583	19375.37	163010.86	45.281	2.8E+07	1.9E-07
35.92	0.02084	0.0011	0.0034	0.01639	22624.04	185634.9	51.565	3.2E+07	1.99E-07
34.92	0.02144	0.0011	0.0034	0.01698	26531.39	212166.29	58.935	3.5E+07	2.09E-07
33.92	0.02207	0.0011	0.0034	0.01761	31255.59	243421.88	67.617	3.9E+07	2.21E-07
32.92	0.02274	0.0011	0.0034	0.01827	36999.12	280421	77.895	4.4E+07	2.35E-07
31.92	0.02346	0.0011	0.0034	0.01898	44022.99	324443.99	90.123	4.8E+07	2.53E-07
30.92	0.02422	0.0011	0.0034	0.01973	52666.35	377110.34	104.75	5.4E+07	2.73E-07
29.92	0.02502	0.0011	0.0034	0.02053	63373.41	440483.75	122.36	5.9E+07	2.97E-07
28.92	0.02589	0.0011	0.0034	0.02139	76731.09	517214.83	143.67	6.5E+07	3.27E-07
27.92	0.02682	0.0011	0.0034	0.02231	93522.1	610736.93	169.65	7.1E+07	3.64E-07
26.92	0.02781	0.0011	0.0034	0.0233	114800.6	725537.55	201.54	7.8E+07	4.09E-07
25.92	0.02889	0.0011	0.0034	0.02437	142001.6	867539.18	240.98	8.5E+07	4.65E-07
24.92	0.03005	0.0012	0.0034	0.02553	177100.8	1044640	290.18	9.2E+07	5.36E-07
23.92	0.0313	0.0012	0.0034	0.02678	222852.1	1267492.1	352.08	9.9E+07	6.27E-07
22.92	0.03267	0.0012	0.0034	0.02814	283145	1550637	430.73	1.1E+08	7.47E-07
21.92	0.03416	0.0012	0.0034	0.02962	363553.2	1914190.2	531.72	1.1E+08	9.05E-07
Total creep damage for one cycle									**0.001955**

Appendix-C

Creep damage calculation steps in SEF method is shown below.

Temperature	time(tr)	Stress relaxation	TR	d(tr)/TR
600	0	449.915	0.007971473	
600	0.0001	302.2045218	0.563396777	2.16576E-05
600	0.000112202	302.0748782	0.565989395	2.4189E-05
600	0.000125893	301.9301877	0.568898339	2.70017E-05
600	0.000141254	301.7688039	0.572162194	3.01236E-05
600	0.000158489	301.5889247	0.57582425	3.35842E-05
600	0.000177828	301.3885838	0.579933071	3.74152E-05
600	0.000199526	301.1656421	0.584543139	4.16494E-05
600	0.000223872	300.9177822	0.589715565	4.63215E-05
600	0.000251189	300.6425037	0.595518902	5.14671E-05
600	0.000281838	300.3371215	0.602030038	5.71225E-05
600	0.000316228	299.998768	0.609335204	6.33241E-05
600	0.000354813	299.6243985	0.617531103	7.01079E-05
600	0.000398107	299.2108029	0.626726167	7.75082E-05
600	0.000446684	298.754622	0.63704196	8.55574E-05
600	0.000501187	298.2523715	0.648614753	9.42842E-05
600	0.000562341	297.7004727	0.661597266	0.000103713
600	0.000630957	297.095292	0.676160622	0.000113861
600	0.000707946	296.4331876	0.692496518	0.000124741
600	0.000794328	295.7105649	0.710819631	0.000136353
600	0.000891251	294.9239398	0.731370305	0.000148692
600	0.001	294.0700078	0.754417523	0.000161739
600	0.001122018	293.1457182	0.780262206	0.000175463
600	0.001258925	292.1483511	0.809240871	0.000189823
600	0.001412538	291.0755935	0.84172968	0.000204764
600	0.001584893	289.9256122	0.878148926	0.00022022
600	0.001778279	288.6971195	0.918968002	0.000236116
600	0.001995262	287.3894278	0.964710894	0.000252365
600	0.002238721	286.0024908	1.015962284	0.000268873
600	0.002511886	284.5369272	1.073374303	0.000285545
600	0.002818383	282.9940262	1.137674029	0.000302279
600	0.003162278	281.3757335	1.209671817	0.000318976
600	0.003548134	279.6846178	1.29027056	0.00033554

600	0.003981072	277.9238205	1.380475996	0.000351882
600	0.004466836	276.0969889	1.481408186	0.000367918
600	0.005011872	274.2081989	1.594314313	0.000383576
600	0.005623413	272.2618693	1.720582952	0.000398795
600	0.006309573	270.2626725	1.861759998	0.000413525
600	0.007079458	268.2154446	2.019566428	0.000427728
600	0.007943282	266.1251001	2.195918142	0.000441377
600	0.008912509	263.9965526	2.392948081	0.000454456
600	0.01	261.834644	2.613030926	0.000466961
600	0.011220185	259.6440842	2.858810638	0.000478895
600	0.012589254	257.4294015	3.133231176	0.000490267
600	0.014125375	255.1949034	3.439570752	0.000501096
600	0.015848932	252.9446485	3.781480016	0.000511404
600	0.017782794	250.6824271	4.163024625	0.000521215
600	0.019952623	248.4117509	4.588732677	0.000530558
600	0.022387211	246.1358494	5.063647578	0.000539463
600	0.025118864	243.8576728	5.593386944	0.000547962
600	0.028183829	241.5798988	6.184208229	0.000556085
600	0.031622777	239.3049438	6.843081847	0.000563863
600	0.035481339	237.0349761	7.577772636	0.000571326
600	0.039810717	234.7719313	8.39693061	0.000578502
600	0.044668359	232.5175286	9.310192071	0.000585419
600	0.050118723	230.2732869	10.32829225	0.000592103
600	0.056234133	228.040542	11.46319079	0.000598577
600	0.063095734	225.8204623	12.72821155	0.000604865
600	0.070794578	223.6140647	14.13819838	0.000610986
600	0.079432823	221.4222289	15.70968858	0.000616961
600	0.089125094	219.2457119	17.46110626	0.000622807
600	0.1	217.08516	19.41297771	0.000628541
600	0.112201845	214.9411212	21.58817129	0.000634176
600	0.125892541	212.8140556	24.01216477	0.000639726
600	0.141253754	210.7043455	26.71334315	0.000645204
600	0.158489319	208.6123041	29.72333041	0.000650621
600	0.177827941	206.5381837	33.07735921	0.000655986
600	0.199526231	204.4821826	36.81468266	0.000661309
600	0.223872114	202.4444517	40.97903319	0.000666598
600	0.251188643	200.4251005	45.61913368	0.00067186
600	0.281838293	198.4242017	50.789267	0.000677101
600	0.316227766	196.4417961	56.54991045	0.000682329
600	0.354813389	194.4778965	62.96844271	0.000687547
600	0.398107171	192.5324914	70.11993135	0.000692762

600	0.446683592	190.6055481	78.08801028	0.000697977
600	0.501187234	188.6970153	86.96585728	0.000703197
600	0.562341325	186.8068258	96.85728313	0.000708424
600	0.630957344	184.9348986	107.877945	0.000713662
600	0.707945784	183.0811408	120.1566982	0.000718915
600	0.794328235	181.2454492	133.8371024	0.000724184
600	0.891250938	179.4277118	149.0790997	0.000729472
600	1	177.6278092	166.0608838	0.000734781
600	1.122018454	175.8456157	184.980983	0.000740114
600	1.258925412	174.0810001	206.0605808	0.000745471
600	1.412537545	172.3338268	229.5461008	0.000750854
600	1.584893192	170.6039564	255.7120872	0.000756265
600	1.77827941	168.8912466	284.864414	0.000761706
600	1.995262315	167.1955525	317.3438596	1.49292E-05
600	2	167.1628827	318.0081101	1.49292E-05
Total creep damage per cycle				0.036777589

Appendix-D

Creep damage calculation steps in Bilinear model is shown below.

Temp.	Step Time	time(tr)	Total Time	Misses	TR	d(tr)/TR
600	0			0		
600	0.0001	2.7778E-08	2.7778E-08	1.34618	229146611.5	1.2122E-16
600	0.0002	2.7778E-08	5.5556E-08	2.69232	240070093.9	1.1571E-16
600	0.00035	4.1667E-08	9.7222E-08	4.71149	155186229.4	2.6849E-16
600	0.000575	6.25E-08	1.5972E-07	7.7401	73937122.04	8.4531E-16
600	0.0009125	9.375E-08	2.5347E-07	12.2827	27506371.98	3.4083E-15
600	0.00141875	1.4063E-07	3.941E-07	18.4433	9073482.377	1.5498E-14
600	0.00217813	2.1094E-07	6.0504E-07	27.2371	2538998.764	8.308E-14
600	0.00331719	3.1641E-07	9.2144E-07	38.6491	679513.2204	4.6564E-13
600	0.00502578	4.7461E-07	1.3961E-06	52.9915	179569.6866	2.643E-12
600	0.00758867	7.1191E-07	2.108E-06	70.0338	49536.26933	1.4372E-11
600	0.011433	1.0679E-06	3.1758E-06	88.1315	15832.83792	6.7446E-11
600	0.0171995	1.6018E-06	4.7776E-06	106.333	5914.550726	2.7082E-10
600	0.0258493	2.4027E-06	7.1804E-06	124.961	2441.665263	9.8405E-10
600	0.0388239	3.6041E-06	1.0784E-05	146.606	982.6164127	3.6678E-09
600	0.0582859	5.4061E-06	1.6191E-05	181.349	277.2403467	1.95E-08
600	0.0874788	8.1091E-06	2.43E-05	237.131	51.52562053	1.5738E-07
600	0.131268	1.2164E-05	3.6463E-05	321.785	6.741321698	1.8043E-06
600	0.196952	1.8246E-05	5.4709E-05	340.438	4.56793468	3.9943E-06
600	0.295478	2.7368E-05	8.2077E-05	349.57	3.799046965	7.204E-06
600	0.443268	4.1053E-05	0.00012313	360.568	3.058309757	1.3423E-05
600	0.664951	6.1579E-05	0.00018471	372.906	2.412869848	2.5521E-05
600	0.997477	9.2368E-05	0.00027708	386.793	1.861683835	4.9615E-05
600	1.49627	0.00013855	0.00041563	398.688	1.499715927	9.2387E-05
600	2.24445	0.00020783	0.00062346	409.757	1.232116582	0.00016868
600	3.36672	0.00031174	0.0009352	418.229	1.063107435	0.00029324
600	5.05013	0.00046761	0.00140281	423.279	0.974728451	0.00047974
600	7.57525	0.00070142	0.00210424	398.253	1.511480451	0.00046406
600	11.3629	0.00105213	0.00315636	279.821	17.37178125	6.0565E-05
600	17.0444	0.00157819	0.00473456	69.2422	52313.8682	3.0168E-08
600	25.5667	0.00236731	0.00710186	250.607	35.98745398	6.5781E-05
600	38.3501	0.00355094	0.01065281	306.595	9.382243466	0.00037847
600	57.5252	0.00532642	0.01597922	349.888	3.775007247	0.00141097
600	76.7003	0.00532642	0.02130564	278.218	18.05100118	0.00029508

600	86.2879	0.00266322	0.02396886	227.37	67.50869308	3.945E-05
600	100.669	0.00399475	0.02796361	137.742	1407.653386	2.8379E-06
600	122.241	0.00599222	0.03395583	33.9899	1123817.722	5.332E-09
600	154.599	0.00898833	0.04294417	110.055	4912.618255	1.8296E-06
600	203.136	0.0134825	0.05642667	123.116	2652.966215	5.082E-06
600	275.942	0.02022389	0.07665056	141.489	1206.680717	1.676E-05
600	375.942	0.02777778	0.10442833	155.085	707.437862	3.9265E-05
600	475.942	0.02777778	0.13220611	162.171	543.2177836	5.1136E-05
600	575.942	0.02777778	0.15998389	166.488	464.4848058	5.9803E-05
600	675.942	0.02777778	0.18776167	169.118	422.87221	6.5688E-05
600	775.942	0.02777778	0.21553944	170.772	398.8638116	6.9642E-05
600	875.942	0.02777778	0.24331722	171.913	383.1988215	7.2489E-05
600	975.942	0.02777778	0.271095	172.717	372.5775801	7.4556E-05
600	1075.94	0.02777722	0.29887222	173.386	363.9926226	7.6313E-05
600	1175.94	0.02777778	0.32665	173.662	360.5160776	7.705E-05
600	1275.94	0.02777778	0.35442778	173.935	357.1141432	7.7784E-05
600	1375.94	0.02777778	0.38220556	174.207	353.7606564	7.8521E-05
600	1475.94	0.02777778	0.40998333	174.376	351.6949612	7.8983E-05
600	1575.94	0.02777778	0.43776111	174.465	350.612584	7.9226E-05
600	1675.94	0.02777778	0.46553889	174.555	349.5218664	7.9474E-05
600	1775.94	0.02777778	0.49331667	174.645	348.4349763	7.9722E-05
600	1875.94	0.02777778	0.52109444	174.734	347.363912	7.9967E-05
600	1975.94	0.02777778	0.54887222	174.79	346.6918883	8.0122E-05
600	2075.94	0.02777778	0.57665	174.82	346.3324793	8.0206E-05
600	2175.94	0.02777778	0.60442778	174.849	345.9854501	8.0286E-05
600	2275.94	0.02777778	0.63220556	174.879	345.6268673	8.0369E-05
600	2375.94	0.02777778	0.65998333	174.909	345.2687038	8.0453E-05
600	2475.94	0.02777778	0.68776111	174.927	345.0540067	8.0503E-05
600	2575.94	0.02777778	0.71553889	174.937	344.9347957	8.0531E-05
600	2675.94	0.02777778	0.74331667	174.947	344.8156311	8.0558E-05
600	2775.94	0.02777778	0.77109444	174.956	344.7084227	8.0583E-05
600	2875.94	0.02777778	0.79887222	174.966	344.5893464	8.0611E-05
600	2975.94	0.02777778	0.82665	174.972	344.5179229	8.0628E-05
600	3075.94	0.02777778	0.85442778	174.975	344.4822174	8.0636E-05
600	3175.94	0.02777778	0.88220556	174.979	344.4346165	8.0647E-05
600	3275.94	0.02777778	0.90998333	174.982	344.3989208	8.0656E-05
600	3375.94	0.02777778	0.93776111	174.985	344.3632292	8.0664E-05
600	3475.94	0.02777778	0.96553889	174.987	344.3394372	8.067E-05
600	3575.94	0.02777778	0.99331667	174.988	344.3275418	8.0673E-05
600	3675.94	0.02777778	1.02109444	174.989	344.3156469	8.0675E-05
600	3775.94	0.02777778	1.04887222	174.99	344.3037525	8.0678E-05

600	3875.94	0.02777778	1.07665	174.991	344.2918586	8.0681E-05
600	3975.94	0.02777778	1.10442778	174.992	344.2799651	8.0684E-05
600	4075.94	0.02777778	1.13220556	174.992	344.2799651	8.0684E-05
600	4175.94	0.02777778	1.15998333	174.992	344.2799651	8.0684E-05
600	4275.94	0.02777778	1.18776111	174.993	344.2680721	8.0686E-05
600	4375.94	0.02777778	1.21553889	174.993	344.2680721	8.0686E-05
600	4475.94	0.02777778	1.24331667	174.993	344.2680721	8.0686E-05
600	4575.94	0.02777778	1.27109444	174.993	344.2680721	8.0686E-05
600	4675.94	0.02777778	1.29887222	174.993	344.2680721	8.0686E-05
600	4775.94	0.02777778	1.32665	174.993	344.2680721	8.0686E-05
600	4875.94	0.02777778	1.35442778	174.993	344.2680721	8.0686E-05
600	4975.94	0.02777778	1.38220556	174.993	344.2680721	8.0686E-05
600	5075.94	0.02777778	1.40998333	174.993	344.2680721	8.0686E-05
600	5175.94	0.02777778	1.43776111	174.993	344.2680721	8.0686E-05
600	5275.94	0.02777778	1.46553889	174.993	344.2680721	8.0686E-05
600	5375.94	0.02777778	1.49331667	174.993	344.2680721	8.0686E-05
600	5475.94	0.02777778	1.52109444	174.993	344.2680721	8.0686E-05
600	5575.94	0.02777778	1.54887222	174.993	344.2680721	8.0686E-05
600	5675.94	0.02777778	1.57665	174.993	344.2680721	8.0686E-05
600	5775.94	0.02777778	1.60442778	174.993	344.2680721	8.0686E-05
600	5875.94	0.02777778	1.63220556	174.993	344.2680721	8.0686E-05
600	5975.94	0.02777778	1.65998333	174.993	344.2680721	8.0686E-05
600	6075.94	0.02777778	1.68776111	174.993	344.2680721	8.0686E-05
600	6175.94	0.02777778	1.71553889	174.993	344.2680721	8.0686E-05
600	6275.94	0.02777778	1.74331667	174.993	344.2680721	8.0686E-05
600	6375.94	0.02777778	1.77109444	174.993	344.2680721	8.0686E-05
600	6475.94	0.02777778	1.79887222	174.993	344.2680721	8.0686E-05
600	6575.94	0.02777778	1.82665	174.993	344.2680721	8.0686E-05
600	6675.94	0.02777778	1.85442778	174.993	344.2680721	8.0686E-05
600	6775.94	0.02777778	1.88220556	174.993	344.2680721	8.0686E-05
600	6875.94	0.02777778	1.90998333	174.993	344.2680721	8.0686E-05
600	6975.94	0.02777778	1.93776111	174.993	344.2680721	8.0686E-05
600	7075.94	0.02777778	1.96553889	174.993	344.2680721	8.0686E-05
600	7175.94	0.02777778	1.99331667	174.993	344.2680721	8.0686E-05
Total creep damage per cycle						0.00904774

Appendix-E

Creep damage calculation steps in Chaboche model is shown below.

Temp.		Time(tr)	Total Time		TR	d(tr)/TR
600	0				0	
600	0.0001	2.7778E-08	2.7778E-08	2.46381	247451069	1.12256E-16
600	0.0002	2.7778E-08	5.5556E-08	4.92753	147135098	1.88791E-16
600	0.00035	4.1667E-08	9.7222E-08	8.62296	60205135.9	6.92078E-16
600	0.00058	6.25E-08	1.5972E-07	14.1658	19119450.9	3.26892E-15
600	0.00091	9.375E-08	2.5347E-07	22.4792	4877390.29	1.92213E-14
600	0.00142	1.4063E-07	3.941E-07	33.7785	1150961.87	1.2218E-13
600	0.00218	2.1094E-07	6.0504E-07	49.9221	233337.469	9.04008E-13
600	0.00332	3.1641E-07	9.2144E-07	70.9247	46610.8164	6.78824E-12
600	0.00503	4.7461E-07	1.3961E-06	97.3678	9443.28724	5.02588E-11
600	0.00759	7.1191E-07	2.108E-06	128.757	2064.31146	3.44867E-10
600	0.01143	1.0679E-06	3.1758E-06	161.671	553.273906	1.93009E-09
600	0.0172	1.6018E-06	4.7776E-06	193.012	189.135444	8.46909E-09
600	0.02585	2.4027E-06	7.1804E-06	220.094	83.0686204	2.89245E-08
600	0.03882	3.6041E-06	1.0784E-05	239.081	48.8698855	7.3748E-08
600	0.05829	5.4061E-06	1.6191E-05	260.845	27.6767863	1.9533E-07
600	0.08748	8.1091E-06	2.43E-05	303.34	10.0880998	8.03832E-07
600	0.13127	1.2164E-05	3.6463E-05	363.019	2.91612641	4.17117E-06
600	0.19695	1.8246E-05	5.4709E-05	415.569	1.11321883	1.63899E-05
600	0.29548	2.7368E-05	8.2077E-05	453.366	0.59102393	4.63066E-05
600	0.44327	4.1053E-05	0.00012313	486.14	0.35311629	0.000116259
600	0.66495	6.1579E-05	0.00018471	509.942	0.24721532	0.000249089
600	0.99748	9.2368E-05	0.00027708	525.122	0.19833029	0.00046573
600	1.49627	0.00013855	0.00041563	533.266	0.17659793	0.000784571
600	2.24445	0.00020783	0.00062346	538.006	0.16517329	0.001258241
600	3.36672	0.00031174	0.0009352	540.941	0.15851119	0.001966686
600	5.05013	0.00046761	0.00140281	541.328	0.15765519	0.002966054
600	7.57525	0.00070142	0.00210424	502.526	0.27585019	0.002542765
600	11.3629	0.00105213	0.00315636	380.998	2.07252948	0.000507653
600	17.0444	0.00157819	0.00473456	168.972	425.068657	3.7128E-06
600	25.5667	0.00236731	0.00710186	181.894	272.215486	8.69644E-06
600	38.3501	0.00355094	0.01065281	407.039	1.29251714	0.002747309
600	41.546	0.00088775	0.01154056	438.902	0.74910753	0.001185077
600	44.7418	0.00088772	0.01242828	367.074	2.69679007	0.000329177
600	49.5356	0.00133161	0.01375989	313.442	8.07058445	0.000164996
600	56.7263	0.00199742	0.01575731	330.334	5.62763312	0.00035493
600	67.5123	0.00299611	0.01875342	348.244	3.90114545	0.000768008
600	83.6912	0.00449414	0.02324756	348.281	3.89825538	0.001152859

600	99.8702	0.00449417	0.02774172	252.389	34.3589502	0.0001308
600	116.049	0.00449411	0.03223583	171.651	386.733486	1.16207E-05
600	140.318	0.00674139	0.03897722	82.4839	22154.8474	3.04285E-07
600	176.72	0.01011167	0.04908889	45.3684	351534.357	2.87644E-08
600	231.325	0.01516806	0.06425694	128.512	2086.56243	7.2694E-06
600	313.231	0.02275167	0.08700861	187.167	228.558926	9.9544E-05
600	413.231	0.02777778	0.11478639	220.302	82.5713921	0.000336409
600	513.231	0.02777778	0.14256417	236.78	52.0206568	0.000533976
600	613.231	0.02777778	0.17034194	245.805	40.8239951	0.000680428
600	713.231	0.02777778	0.19811972	251.487	35.1726849	0.000789754
600	813.231	0.02777778	0.2258975	254.586	32.4638127	0.000855654
600	913.231	0.02777778	0.25367528	257.106	30.4329121	0.000912755
600	1013.23	0.0277775	0.28145278	258.596	29.2993106	0.00094806
600	1113.23	0.02777778	0.30923056	259.737	28.4632009	0.000975919
600	1213.23	0.02777778	0.33700833	260.331	28.0385339	0.0009907
600	1313.23	0.02777778	0.36478611	260.922	27.6230464	0.001005602
600	1413.23	0.02777778	0.39256389	261.509	27.217189	0.001020597
600	1513.23	0.02777778	0.42034167	261.734	27.063397	0.001026397
600	1613.23	0.02777778	0.44811944	261.917	26.9390308	0.001031135
600	1713.23	0.02777778	0.47589722	262.109	26.8092363	0.001036127
600	1813.23	0.02777778	0.503675	262.3	26.6808126	0.001041114
600	1913.23	0.02777778	0.53145278	262.491	26.553078	0.001046123
600	2013.23	0.02777778	0.55923056	262.565	26.5037734	0.001048069
600	2113.23	0.02777778	0.58700833	262.626	26.4632076	0.001049675
600	2213.23	0.02777778	0.61478611	262.689	26.4213849	0.001051337
600	2313.23	0.02777778	0.64256389	262.753	26.378974	0.001053027
600	2413.23	0.02777778	0.67034167	262.816	26.3373004	0.001054693
600	2513.23	0.02777778	0.69811944	262.841	26.3207836	0.001055355
600	2613.23	0.02777778	0.72589722	262.861	26.3075786	0.001055885
600	2713.23	0.02777778	0.753675	262.882	26.2937213	0.001056441
600	2813.23	0.02777778	0.78145278	262.903	26.2798722	0.001056998
600	2913.23	0.02777778	0.80923056	262.924	26.2660313	0.001057555
600	3013.23	0.02777778	0.83700833	262.932	26.2607607	0.001057767
600	3113.23	0.02777778	0.86478611	262.938	26.2568085	0.001057927
600	3213.23	0.02777778	0.89256389	262.945	26.2521985	0.001058112
600	3313.23	0.02777778	0.92034167	262.952	26.2475894	0.001058298
600	3413.23	0.02777778	0.94811944	262.959	26.2429812	0.001058484
600	3513.23	0.02777778	0.97589722	262.962	26.2410066	0.001058564
600	3613.23	0.02777778	1.003675	262.964	26.2396902	0.001058617
600	3713.23	0.02777778	1.03145278	262.966	26.2383739	0.00105867
600	3813.23	0.02777778	1.05923056	262.968	26.2370577	0.001058723
600	3913.23	0.02777778	1.08700833	262.97	26.2357416	0.001058776
600	4013.23	0.02777778	1.11478611	262.971	26.2350836	0.001058803
600	4113.23	0.02777778	1.14256389	262.972	26.2344255	0.001058829
600	4213.23	0.02777778	1.17034167	262.972	26.2344255	0.001058829
600	4313.23	0.02777778	1.19811944	262.973	26.2337675	0.001058856
600	4413.23	0.02777778	1.22589722	262.974	26.2331096	0.001058882

600	4513.23	0.02777778	1.253675	262.974	26.2331096	0.001058882
600	4613.23	0.02777778	1.28145278	262.974	26.2331096	0.001058882
600	4713.23	0.02777778	1.30923056	262.974	26.2331096	0.001058882
600	4813.23	0.02777778	1.33700833	262.974	26.2331096	0.001058882
600	4913.23	0.02777778	1.36478611	262.974	26.2331096	0.001058882
600	5013.23	0.02777778	1.39256389	262.974	26.2331096	0.001058882
600	5113.23	0.02777778	1.42034167	262.974	26.2331096	0.001058882
600	5213.23	0.02777778	1.44811944	262.974	26.2331096	0.001058882
600	5313.23	0.02777778	1.47589722	262.974	26.2331096	0.001058882
600	5413.23	0.02777778	1.503675	262.974	26.2331096	0.001058882
600	5513.23	0.02777778	1.53145278	262.974	26.2331096	0.001058882
600	5613.23	0.02777778	1.55923056	262.974	26.2331096	0.001058882
600	5713.23	0.02777778	1.58700833	262.974	26.2331096	0.001058882
600	5813.23	0.02777778	1.61478611	262.974	26.2331096	0.001058882
600	5913.23	0.02777778	1.64256389	262.974	26.2331096	0.001058882
600	6013.23	0.02777778	1.67034167	262.974	26.2331096	0.001058882
600	6113.23	0.02777778	1.69811944	262.974	26.2331096	0.001058882
600	6213.23	0.02777778	1.72589722	262.974	26.2331096	0.001058882
600	6313.23	0.02777778	1.753675	262.974	26.2331096	0.001058882
600	6413.23	0.02777778	1.78145278	262.974	26.2331096	0.001058882
600	6513.23	0.02777778	1.80923056	262.974	26.2331096	0.001058882
600	6613.23	0.02777778	1.83700833	262.974	26.2331096	0.001058882
600	6713.23	0.02777778	1.86478611	262.974	26.2331096	0.001058882
600	6813.23	0.02777778	1.89256389	262.974	26.2331096	0.001058882
600	6913.23	0.02777778	1.92034167	262.974	26.2331096	0.001058882
600	7013.23	0.02777778	1.94811944	262.974	26.2331096	0.001058882
600	7113.23	0.02777778	1.97589722	262.974	26.2331096	0.001058882
600	7213.23	0.02777778	2.003675	262.974	26.2331096	0.001058882
Total creep damage per cycle						**0.087127108**

Appendix-F

Creep damage calculation steps in Chaboche with short time hardening model is shown below.

Temp	Time(tr)		Total Time	Misses	TR	d(tr)/TR
600	0				0	
600	0.0001	2.7778E-08	2.7778E-08	2.46381	247451069	1.1226E-16
600	0.0002	2.7778E-08	5.5556E-08	4.92753	147135098	1.8879E-16
600	0.00035	4.1667E-08	9.7222E-08	8.62296	60205135.9	6.9208E-16
600	0.00058	6.25E-08	1.5972E-07	14.1658	19119450.9	3.2689E-15
600	0.00091	9.375E-08	2.5347E-07	22.4792	4877390.29	1.9221E-14
600	0.00142	1.4063E-07	3.941E-07	33.7785	1150961.87	1.2218E-13
600	0.00218	2.1094E-07	6.0504E-07	49.9221	233337.469	9.0401E-13
600	0.00332	3.1641E-07	9.2144E-07	70.9247	46610.8164	6.7882E-12
600	0.00503	4.7461E-07	1.3961E-06	97.3678	9443.28724	5.0259E-11
600	0.00759	7.1191E-07	2.108E-06	128.757	2064.31146	3.4487E-10
600	0.01143	1.0679E-06	3.1758E-06	161.671	553.273906	1.9301E-09
600	0.0172	1.6018E-06	4.7776E-06	193.012	189.135444	8.4691E-09
600	0.02585	2.4027E-06	7.1804E-06	220.094	83.0686204	2.8925E-08
600	0.03882	3.6041E-06	1.0784E-05	239.081	48.8698855	7.3748E-08
600	0.05829	5.4061E-06	1.6191E-05	260.845	27.6767863	1.9533E-07
600	0.08748	8.1091E-06	2.43E-05	303.34	10.0880998	8.0383E-07
600	0.13127	1.2164E-05	3.6463E-05	363.019	2.91612641	4.1712E-06
600	0.19695	1.8246E-05	5.4709E-05	415.569	1.11321883	1.639E-05
600	0.29548	2.7368E-05	8.2077E-05	453.366	0.59102393	4.6307E-05
600	0.44327	4.1053E-05	0.00012313	486.14	0.35311629	0.00011626
600	0.66495	6.1579E-05	0.00018471	509.942	0.24721532	0.00024909
600	0.99748	9.2368E-05	0.00027708	525.122	0.19833029	0.00046573
600	1.49627	0.00013855	0.00041563	533.266	0.17659793	0.00078457
600	2.24445	0.00020783	0.00062346	538.006	0.16517329	0.00125824
600	3.36672	0.00031174	0.0009352	540.941	0.15851119	0.00196669
600	5.05013	0.00046761	0.00140281	541.328	0.15765519	0.00296605
600	7.57525	0.00070142	0.00210424	502.526	0.27585019	0.00254277
600	11.3629	0.00105213	0.00315636	380.998	2.07252948	0.00050765
600	17.0444	0.00157819	0.00473456	168.972	425.068657	3.7128E-06
600	25.5667	0.00236731	0.00710186	181.894	272.215486	8.6964E-06
600	38.3501	0.00355094	0.01065281	407.039	1.29251714	0.00274731

600	41.546	0.00088775	0.01154056	438.902	0.74910753	0.00118508
600	44.7418	0.00088772	0.01242828	367.074	2.69679007	0.00032918
600	49.5356	0.00133161	0.01375989	313.442	8.07058445	0.000165
600	56.7263	0.00199742	0.01575731	330.334	5.62763312	0.00035493
600	67.5123	0.00299611	0.01875342	348.244	3.90114545	0.00076801
600	83.6912	0.00449414	0.02324756	348.281	3.89825538	0.00115286
600	99.8702	0.00449417	0.02774172	252.389	34.3589502	0.0001308
600	116.049	0.00449411	0.03223583	171.651	386.733486	1.1621E-05
600	140.318	0.00674139	0.03897722	82.4839	22154.8474	3.0429E-07
600	176.72	0.01011167	0.04908889	45.3684	351534.357	2.8764E-08
600	231.325	0.01516806	0.06425694	128.512	2086.56243	7.2694E-06
600	313.231	0.02275167	0.08700861	187.167	228.558926	9.9544E-05
600	413.231	0.02777778	0.11478639	220.302	82.5713921	0.00033641
600	513.231	0.02777778	0.14256417	236.78	52.0206568	0.00053398
600	613.231	0.02777778	0.17034194	245.805	40.8239951	0.00068043
600	713.231	0.02777778	0.19811972	251.487	35.1726849	0.00078975
600	813.231	0.02777778	0.2258975	254.586	32.4638127	0.00085565
600	913.231	0.02777778	0.25367528	257.106	30.4329121	0.00091275
600	1013.23	0.0277775	0.28145278	258.596	29.2993106	0.00094806
600	1113.23	0.02777778	0.30923056	259.737	28.4632009	0.00097592
600	1213.23	0.02777778	0.33700833	260.331	28.0385339	0.0009907
600	1313.23	0.02777778	0.36478611	260.922	27.6230464	0.0010056
600	1413.23	0.02777778	0.39256389	261.509	27.217189	0.0010206
600	1513.23	0.02777778	0.42034167	261.734	27.063397	0.0010264
600	1613.23	0.02777778	0.44811944	261.917	26.9390308	0.00103114
600	1713.23	0.02777778	0.47589722	262.109	26.8092363	0.00103613
600	1813.23	0.02777778	0.503675	262.3	26.6808126	0.00104111
600	1913.23	0.02777778	0.53145278	262.491	26.553078	0.00104612
600	2013.23	0.02777778	0.55923056	262.565	26.5037734	0.00104807
600	2113.23	0.02777778	0.58700833	262.626	26.4632076	0.00104968
600	2213.23	0.02777778	0.61478611	262.689	26.4213849	0.00105134
600	2313.23	0.02777778	0.64256389	262.753	26.378974	0.00105303
600	2413.23	0.02777778	0.67034167	262.816	26.3373004	0.00105469
600	2513.23	0.02777778	0.69811944	262.841	26.3207836	0.00105536
600	2613.23	0.02777778	0.72589722	262.861	26.3075786	0.00105589
600	2713.23	0.02777778	0.753675	262.882	26.2937213	0.00105644
600	2813.23	0.02777778	0.78145278	262.903	26.2798722	0.001057
600	2913.23	0.02777778	0.80923056	262.924	26.2660313	0.00105756
600	3013.23	0.02777778	0.83700833	262.932	26.2607607	0.00105777
600	3113.23	0.02777778	0.86478611	262.938	26.2568085	0.00105793
600	3213.23	0.02777778	0.89256389	262.945	26.2521985	0.00105811

600	3313.23	0.02777778	0.92034167	262.952	26.2475894	0.0010583
600	3413.23	0.02777778	0.94811944	262.959	26.2429812	0.00105848
600	3513.23	0.02777778	0.97589722	262.962	26.2410066	0.00105856
600	3613.23	0.02777778	1.003675	262.964	26.2396902	0.00105862
600	3713.23	0.02777778	1.03145278	262.966	26.2383739	0.00105867
600	3813.23	0.02777778	1.05923056	262.968	26.2370577	0.00105872
600	3913.23	0.02777778	1.08700833	262.97	26.2357416	0.00105878
600	4013.23	0.02777778	1.11478611	262.971	26.2350836	0.0010588
600	4113.23	0.02777778	1.14256389	262.972	26.2344255	0.00105883
600	4213.23	0.02777778	1.17034167	262.972	26.2344255	0.00105883
600	4313.23	0.02777778	1.19811944	262.973	26.2337675	0.00105886
600	4413.23	0.02777778	1.22589722	262.974	26.2331096	0.00105888
600	4513.23	0.02777778	1.253675	262.974	26.2331096	0.00105888
600	4613.23	0.02777778	1.28145278	262.974	26.2331096	0.00105888
600	4713.23	0.02777778	1.30923056	262.974	26.2331096	0.00105888
600	4813.23	0.02777778	1.33700833	262.974	26.2331096	0.00105888
600	4913.23	0.02777778	1.36478611	262.974	26.2331096	0.00105888
600	5013.23	0.02777778	1.39256389	262.974	26.2331096	0.00105888
600	5113.23	0.02777778	1.42034167	262.974	26.2331096	0.00105888
600	5213.23	0.02777778	1.44811944	262.974	26.2331096	0.00105888
600	5313.23	0.02777778	1.47589722	262.974	26.2331096	0.00105888
600	5413.23	0.02777778	1.503675	262.974	26.2331096	0.00105888
600	5513.23	0.02777778	1.53145278	262.974	26.2331096	0.00105888
600	5613.23	0.02777778	1.55923056	262.974	26.2331096	0.00105888
600	5713.23	0.02777778	1.58700833	262.974	26.2331096	0.00105888
600	5813.23	0.02777778	1.61478611	262.974	26.2331096	0.00105888
600	5913.23	0.02777778	1.64256389	262.974	26.2331096	0.00105888
600	6013.23	0.02777778	1.67034167	262.974	26.2331096	0.00105888
600	6113.23	0.02777778	1.69811944	262.974	26.2331096	0.00105888
600	6213.23	0.02777778	1.72589722	262.974	26.2331096	0.00105888
600	6313.23	0.02777778	1.753675	262.974	26.2331096	0.00105888
600	6413.23	0.02777778	1.78145278	262.974	26.2331096	0.00105888
600	6513.23	0.02777778	1.80923056	262.974	26.2331096	0.00105888
600	6613.23	0.02777778	1.83700833	262.974	26.2331096	0.00105888
600	6713.23	0.02777778	1.86478611	262.974	26.2331096	0.00105888
600	6813.23	0.02777778	1.89256389	262.974	26.2331096	0.00105888
600	6913.23	0.02777778	1.92034167	262.974	26.2331096	0.00105888
600	7013.23	0.02777778	1.94811944	262.974	26.2331096	0.00105888
600	7113.23	0.02777778	1.97589722	262.974	26.2331096	0.00105888
600	7213.23	0.02777778	2.003675	262.974	26.2331096	0.00105888
Total creep damage per cycle						**0.08712711**

Appendix-G

Creep damage calculation steps in Chaboche with long time hardening model is shown below.

Temp	Step time	time(tr)	Total Time	Misses	TR	d(tr)/TR
600	0			0		
600	0.001	2.7778E-07	2.7778E-07	24.6345	3594823.26	7.7272E-14
600	0.002	2.7778E-07	5.5556E-07	46.4702	317556.847	8.7473E-13
600	0.003	2.7778E-07	8.3333E-07	65.8493	66439.7817	4.1809E-12
600	0.005	5.5556E-07	1.3889E-06	97.0252	9619.67039	5.7752E-11
600	0.009	1.1111E-06	0.0000025	142.166	1173.94928	9.4647E-10
600	0.015	1.6667E-06	4.1667E-06	183.429	258.606054	6.4448E-09
600	0.024	0.0000025	6.6667E-06	215.667	94.492462	2.6457E-08
600	0.0375	0.00000375	1.0417E-05	237.554	50.9360504	7.3622E-08
600	0.05775	5.625E-06	1.6042E-05	260.161	28.1593418	1.9976E-07
600	0.08813	8.4375E-06	2.4479E-05	304.265	9.88165225	8.5386E-07
600	0.13369	1.2656E-05	3.7136E-05	365.693	2.76935317	4.5702E-06
600	0.20203	1.8984E-05	5.612E-05	418.174	1.06411781	1.784E-05
600	0.30455	2.8477E-05	8.4596E-05	455.714	0.56904677	5.0043E-05
600	0.45832	4.2715E-05	0.00012731	488.453	0.34088022	0.00012531
600	0.68898	6.4073E-05	0.00019138	511.586	0.24132406	0.0002655
600	1.03497	9.6108E-05	0.00028749	526.112	0.19553648	0.00049151
600	1.55396	0.00014416	0.00043166	533.838	0.17517385	0.00082298
600	2.33243	0.00021624	0.0006479	538.334	0.16441358	0.00131523
600	3.50015	0.00032437	0.00097226	541.157	0.15803279	0.00205253
600	5.25173	0.00048655	0.00145881	540.663	0.15912927	0.00305758
600	7.87909	0.00072982	0.00218864	494.502	0.31104694	0.00234634
600	11.8201	0.00109473	0.00328336	364.347	2.84217759	0.00038517
600	17.7317	0.00164211	0.00492547	144.917	1050.90154	1.5626E-06
600	26.5991	0.00246317	0.00738864	204.086	133.715316	1.8421E-05
600	39.9001	0.00369472	0.01108336	423.347	0.97359557	0.00379493
600	43.2253	0.00092367	0.01200703	465.699	0.48520655	0.00190366
600	46.5506	0.00092369	0.01293072	309.876	8.72614531	0.00010585
600	51.5385	0.00138553	0.01431625	322.816	6.59476971	0.00021009
600	59.0203	0.00207828	0.01639453	334.409	5.17034036	0.00040196
600	70.243	0.00311742	0.01951194	352.104	3.61212085	0.00086304

600	87.0772	0.00467617	0.02418811	306.654	9.36996912	0.00049906
600	112.328	0.00701411	0.03120222	167.64	445.713462	1.5737E-05
600	150.205	0.01052139	0.04172361	43.1494	433646.892	2.4263E-08
600	207.02	0.01578194	0.05750556	110.669	4766.64254	3.3109E-06
600	292.243	0.02367306	0.08117861	184.287	251.33418	9.419E-05
600	392.243	0.02777778	0.10895639	221.303	80.2247879	0.00034625
600	492.243	0.02777778	0.13673417	239.338	48.5314749	0.00057237
600	592.243	0.02777778	0.16451194	248.961	37.5689015	0.00073938
600	692.243	0.02777778	0.19228972	254.774	32.3071661	0.0008598
600	792.243	0.02777778	0.2200675	258.115	29.6600011	0.00093654
600	892.243	0.02777778	0.24784528	260.585	27.8591135	0.00099708
600	992.243	0.02777778	0.27562306	262.102	26.813956	0.00103594
600	1092.24	0.02777694	0.3034	263.348	25.9883163	0.00106882
600	1192.24	0.02777778	0.33117778	263.898	25.6329623	0.00108367
600	1292.24	0.02777778	0.35895556	264.451	25.2811497	0.00109875
600	1392.24	0.02777778	0.38673333	265	24.9372248	0.00111391
600	1492.24	0.02777778	0.41451111	265.279	24.7644545	0.00112168
600	1592.24	0.02777778	0.44228889	265.461	24.6524742	0.00112677
600	1692.24	0.02777778	0.47006667	265.638	24.5441141	0.00113175
600	1792.24	0.02777778	0.49784444	265.817	24.435072	0.0011368
600	1892.24	0.02777778	0.52562222	265.996	24.3265724	0.00114187
600	1992.24	0.02777778	0.5534	266.089	24.2704142	0.00114451
600	2092.24	0.02777778	0.58117778	266.147	24.2354644	0.00114616
600	2192.24	0.02777778	0.60895556	266.206	24.1999698	0.00114784
600	2292.24	0.02777778	0.63673333	266.265	24.1645334	0.00114953
600	2392.24	0.02777778	0.66451111	266.324	24.1291552	0.00115121
600	2492.24	0.02777778	0.69228889	266.355	24.1105899	0.0011521
600	2592.24	0.02777778	0.72006667	266.374	24.0992191	0.00115264
600	2692.24	0.02777778	0.74784444	266.394	24.0872563	0.00115321
600	2792.24	0.02777778	0.77562222	266.413	24.0758978	0.00115376
600	2892.24	0.02777778	0.8034	266.433	24.0639479	0.00115433
600	2992.24	0.02777778	0.83117778	266.443	24.0579755	0.00115462
600	3092.24	0.02777778	0.85895556	266.449	24.0543928	0.00115479
600	3192.24	0.02777778	0.88673333	266.456	24.0502138	0.00115499
600	3292.24	0.02777778	0.91451111	266.462	24.0466325	0.00115516
600	3392.24	0.02777778	0.94228889	266.469	24.042455	0.00115536
600	3492.24	0.02777778	0.97006667	266.472	24.0406648	0.00115545
600	3592.24	0.02777778	0.99784444	266.474	24.0394715	0.00115551
600	3692.24	0.02777778	1.02562222	266.476	24.0382783	0.00115556
600	3792.24	0.02777778	1.0534	266.478	24.0370851	0.00115562
600	3892.24	0.02777778	1.08117778	266.48	24.035892	0.00115568

600	3992.24	0.02777778	1.10895556	266.481	24.0352954	0.00115571
600	4092.24	0.02777778	1.13673333	266.482	24.0346989	0.00115574
600	4192.24	0.02777778	1.16451111	266.483	24.0341024	0.00115577
600	4292.24	0.02777778	1.19228889	266.483	24.0341024	0.00115577
600	4392.24	0.02777778	1.22006667	266.484	24.0335059	0.00115579
600	4492.24	0.02777778	1.24784444	266.484	24.0335059	0.00115579
600	4592.24	0.02777778	1.27562222	266.484	24.0335059	0.00115579
600	4692.24	0.02777778	1.3034	266.484	24.0335059	0.00115579
600	4792.24	0.02777778	1.33117778	266.484	24.0335059	0.00115579
600	4892.24	0.02777778	1.35895556	266.484	24.0335059	0.00115579
600	4992.24	0.02777778	1.38673333	266.484	24.0335059	0.00115579
600	5092.24	0.02777778	1.41451111	266.484	24.0335059	0.00115579
600	5192.24	0.02777778	1.44228889	266.484	24.0335059	0.00115579
600	5292.24	0.02777778	1.47006667	266.484	24.0335059	0.00115579
600	5392.24	0.02777778	1.49784444	266.484	24.0335059	0.00115579
600	5492.24	0.02777778	1.52562222	266.484	24.0335059	0.00115579
600	5592.24	0.02777778	1.5534	266.484	24.0335059	0.00115579
600	5692.24	0.02777778	1.58117778	266.484	24.0335059	0.00115579
600	5792.24	0.02777778	1.60895556	266.484	24.0335059	0.00115579
600	5892.24	0.02777778	1.63673333	266.484	24.0335059	0.00115579
600	5992.24	0.02777778	1.66451111	266.484	24.0335059	0.00115579
600	6092.24	0.02777778	1.69228889	266.484	24.0335059	0.00115579
600	6192.24	0.02777778	1.72006667	266.484	24.0335059	0.00115579
600	6292.24	0.02777778	1.74784444	266.484	24.0335059	0.00115579
600	6392.24	0.02777778	1.77562222	266.484	24.0335059	0.00115579
600	6492.24	0.02777778	1.8034	266.484	24.0335059	0.00115579
600	6592.24	0.02777778	1.83117778	266.484	24.0335059	0.00115579
600	6692.24	0.02777778	1.85895556	266.484	24.0335059	0.00115579
600	6792.24	0.02777778	1.88673333	266.484	24.0335059	0.00115579
600	6892.24	0.02777778	1.91451111	266.484	24.0335059	0.00115579
600	6992.24	0.02777778	1.94228889	266.484	24.0335059	0.00115579
600	7092.24	0.02777778	1.97006667	266.484	24.0335059	0.00115579
600	7192.24	0.02777778	1.99784444	266.484	24.0335059	0.00115579
600	7292.24	0.02777778	2.02562222	307.577	9.18026655	0.00302581
Total creep damage per cycle						0.09555804

Appendix-H

Creep damage calculation steps in Chaboche with viscous creep model is shown below.

Temp	Step time	time(tr)	Total Time	Missess	TR	d(tr)/TR
600	0				0	
600	0.001	2.7778E-07	2.7778E-07	24.6345	3594823.26	7.7272E-14
600	0.002	2.7778E-07	5.5556E-07	46.4702	317556.847	8.7473E-13
600	0.003	2.7778E-07	8.3333E-07	65.8493	66439.7817	4.1809E-12
600	0.005	5.5556E-07	1.3889E-06	97.0252	9619.67039	5.7752E-11
600	0.009	1.1111E-06	0.0000025	142.166	1173.94928	9.4647E-10
600	0.015	1.6667E-06	4.1667E-06	183.429	258.606054	6.4448E-09
600	0.024	0.0000025	6.6667E-06	215.667	94.492462	2.6457E-08
600	0.0375	0.00000375	1.0417E-05	237.554	50.9360504	7.3622E-08
600	0.05775	5.625E-06	1.6042E-05	260.161	28.1593418	1.9976E-07
600	0.08813	8.4375E-06	2.4479E-05	304.265	9.88165225	8.5386E-07
600	0.13369	1.2656E-05	3.7136E-05	365.693	2.76935317	4.5702E-06
600	0.20203	1.8984E-05	5.612E-05	418.174	1.06411781	1.784E-05
600	0.30455	2.8477E-05	8.4596E-05	455.714	0.56904677	5.0043E-05
600	0.45832	4.2715E-05	0.00012731	488.453	0.34088022	0.00012531
600	0.68898	6.4073E-05	0.00019138	511.586	0.24132406	0.0002655
600	1.03497	9.6108E-05	0.00028749	526.112	0.19553648	0.00049151
600	1.55396	0.00014416	0.00043166	533.838	0.17517385	0.00082298
600	2.33243	0.00021624	0.0006479	538.334	0.16441358	0.00131523
600	3.50015	0.00032437	0.00097226	541.157	0.15803279	0.00205253
600	5.25173	0.00048655	0.00145881	540.663	0.15912927	0.00305758
600	7.87909	0.00072982	0.00218864	494.502	0.31104694	0.00234634
600	11.8201	0.00109473	0.00328336	364.347	2.84217759	0.00038517
600	17.7317	0.00164211	0.00492547	144.917	1050.90154	1.5626E-06
600	26.5991	0.00246317	0.00738864	204.086	133.715316	1.8421E-05
600	39.9001	0.00369472	0.01108336	423.347	0.97359557	0.00379493
600	43.2253	0.00092367	0.01200703	465.699	0.48520655	0.00190366
600	46.5506	0.00092369	0.01293072	309.876	8.72614531	0.00010585
600	51.5385	0.00138553	0.01431625	322.816	6.59476971	0.00021009
600	59.0203	0.00207828	0.01639453	334.409	5.17034036	0.00040196
600	70.243	0.00311742	0.01951194	352.104	3.61212085	0.00086304
600	87.0772	0.00467617	0.02418811	306.654	9.36996912	0.00049906

600	112.328	0.00701411	0.03120222	167.64	445.713462	1.5737E-05
600	150.205	0.01052139	0.04172361	43.1494	433646.892	2.4263E-08
600	207.02	0.01578194	0.05750556	110.669	4766.64254	3.3109E-06
600	292.243	0.02367306	0.08117861	184.287	251.33418	9.419E-05
600	392.243	0.02777778	0.10895639	221.303	80.2247879	0.00034625
600	492.243	0.02777778	0.13673417	239.338	48.5314749	0.00057237
600	592.243	0.02777778	0.16451194	248.961	37.5689015	0.00073938
600	692.243	0.02777778	0.19228972	254.774	32.3071661	0.0008598
600	792.243	0.02777778	0.2200675	258.115	29.6600011	0.00093654
600	892.243	0.02777778	0.24784528	260.585	27.8591135	0.00099708
600	992.243	0.02777778	0.27562306	262.102	26.813956	0.00103594
600	1092.24	0.02777694	0.3034	263.348	25.9883163	0.00106882
600	1192.24	0.02777778	0.33117778	263.898	25.6329623	0.00108367
600	1292.24	0.02777778	0.35895556	264.451	25.2811497	0.00109875
600	1392.24	0.02777778	0.38673333	265	24.9372248	0.00111391
600	1492.24	0.02777778	0.41451111	265.279	24.7644545	0.00112168
600	1592.24	0.02777778	0.44228889	265.461	24.6524742	0.00112677
600	1692.24	0.02777778	0.47006667	265.638	24.5441141	0.00113175
600	1792.24	0.02777778	0.49784444	265.817	24.435072	0.0011368
600	1892.24	0.02777778	0.52562222	265.996	24.3265724	0.00114187
600	1992.24	0.02777778	0.5534	266.089	24.2704142	0.00114451
600	2092.24	0.02777778	0.58117778	266.147	24.2354644	0.00114616
600	2192.24	0.02777778	0.60895556	266.206	24.1999698	0.00114784
600	2292.24	0.02777778	0.63673333	266.265	24.1645334	0.00114953
600	2392.24	0.02777778	0.66451111	266.324	24.1291552	0.00115121
600	2492.24	0.02777778	0.69228889	266.355	24.1105899	0.0011521
600	2592.24	0.02777778	0.72006667	266.374	24.0992191	0.00115264
600	2692.24	0.02777778	0.74784444	266.394	24.0872563	0.00115321
600	2792.24	0.02777778	0.77562222	266.413	24.0758978	0.00115376
600	2892.24	0.02777778	0.8034	266.433	24.0639479	0.00115433
600	2992.24	0.02777778	0.83117778	266.443	24.0579755	0.00115462
600	3092.24	0.02777778	0.85895556	266.449	24.0543928	0.00115479
600	3192.24	0.02777778	0.88673333	266.456	24.0502138	0.00115499
600	3292.24	0.02777778	0.91451111	266.462	24.0466325	0.00115516
600	3392.24	0.02777778	0.94228889	266.469	24.042455	0.00115536
600	3492.24	0.02777778	0.97006667	266.472	24.0406648	0.00115545
600	3592.24	0.02777778	0.99784444	266.474	24.0394715	0.00115551
600	3692.24	0.02777778	1.02562222	266.476	24.0382783	0.00115556
600	3792.24	0.02777778	1.0534	266.478	24.0370851	0.00115562
600	3892.24	0.02777778	1.08117778	266.48	24.035892	0.00115568
600	3992.24	0.02777778	1.10895556	266.481	24.0352954	0.00115571

600	4092.24	0.02777778	1.13673333	266.482	24.0346989	0.00115574
600	4192.24	0.02777778	1.16451111	266.483	24.0341024	0.00115577
600	4292.24	0.02777778	1.19228889	266.483	24.0341024	0.00115577
600	4392.24	0.02777778	1.22006667	266.484	24.0335059	0.00115579
600	4492.24	0.02777778	1.24784444	266.484	24.0335059	0.00115579
600	4592.24	0.02777778	1.27562222	266.484	24.0335059	0.00115579
600	4692.24	0.02777778	1.3034	266.484	24.0335059	0.00115579
600	4792.24	0.02777778	1.33117778	266.484	24.0335059	0.00115579
600	4892.24	0.02777778	1.35895556	266.484	24.0335059	0.00115579
600	4992.24	0.02777778	1.38673333	266.484	24.0335059	0.00115579
600	5092.24	0.02777778	1.41451111	266.484	24.0335059	0.00115579
600	5192.24	0.02777778	1.44228889	266.484	24.0335059	0.00115579
600	5292.24	0.02777778	1.47006667	266.484	24.0335059	0.00115579
600	5392.24	0.02777778	1.49784444	266.484	24.0335059	0.00115579
600	5492.24	0.02777778	1.52562222	266.484	24.0335059	0.00115579
600	5592.24	0.02777778	1.5534	266.484	24.0335059	0.00115579
600	5692.24	0.02777778	1.58117778	266.484	24.0335059	0.00115579
600	5792.24	0.02777778	1.60895556	266.484	24.0335059	0.00115579
600	5892.24	0.02777778	1.63673333	266.484	24.0335059	0.00115579
600	5992.24	0.02777778	1.66451111	266.484	24.0335059	0.00115579
600	6092.24	0.02777778	1.69228889	266.484	24.0335059	0.00115579
600	6192.24	0.02777778	1.72006667	266.484	24.0335059	0.00115579
600	6292.24	0.02777778	1.74784444	266.484	24.0335059	0.00115579
600	6392.24	0.02777778	1.77562222	266.484	24.0335059	0.00115579
600	6492.24	0.02777778	1.8034	266.484	24.0335059	0.00115579
600	6592.24	0.02777778	1.83117778	266.484	24.0335059	0.00115579
600	6692.24	0.02777778	1.85895556	266.484	24.0335059	0.00115579
600	6792.24	0.02777778	1.88673333	266.484	24.0335059	0.00115579
600	6892.24	0.02777778	1.91451111	266.484	24.0335059	0.00115579
600	6992.24	0.02777778	1.94228889	266.484	24.0335059	0.00115579
600	7092.24	0.02777778	1.97006667	266.484	24.0335059	0.00115579
600	7192.24	0.02777778	1.99784444	266.484	24.0335059	0.00115579
600	7292.24	0.02777778	2.02562222	307.577	9.18026655	0.00302581
Total creep damage per cycle						**0.09555804**